FAST-Mediated Pore Expansion: Novel Roles For Annexin A1 And Plasma Membrane Architecture

by

Marta Ciechonska

Submitted in partial fulfilment of the requirements
for the degree of Doctor of Philosophy

at

Dalhousie University
Halifax, Nova Scotia
August 2013

TABLE OF CONTENTS

LIST OF FIGURES

ABSTRACT

Two approaches investigating the contribution of cellular factors to syncytium formation mediated by viral fusogens are reported in this thesis. These include the architecture of plasma membrane curvature at the site of fusion and the role of cellular annexin A1. To study the effects of plasma membrane curvature during cell-cell fusion, I completed a temporal analysis of reptilian reovirus (RRV) p14- and influenza virus hemagglutinin (HA)-mediated pore formation and pore expansion, and analyzed the effects of lysophosphatidylcholine (LPC) and chlorpromazine (CPZ) on the rates of pore formation and expansion mediated by these fusogens. While LPC did not inhibit RRV p14-mediated pore formation, it did inhibit pore expansion resulting in a reversible 'stalled pore' phenotype. By adding LPC following pore formation but prior to syncytiogenesis, I was also able to capture an HA-mediated 'stalled pore' phenotype. These results indicate that, while RRV p14-mediated fusion likely progresses through a less ordered intermediate than enveloped virus fusogens, the resolved pore structure is similar and can be maintained through the promotion of positive curvature. Resolution of negative membrane curvature in the outer leaflet ring surrounding a stable pore is thus an essential step in pore expansion leading to syncytiogenesis. In a second line of investigation, I examined the role of cellular annexin A1 (AX1) during RRV p14- and measles fusion protein (F)-mediated syncytium formation. Knockdown of AX1 in cell monolayers and chelation of intracellular calcium by BAPTA-AM both dramatically impaired p14- and F-mediated syncytiogenesis, while p14-induced pore formation was unaffected by either treatment. A direct, calcium-dependent interaction between p14 and measles F with AX1 was detected via co-immunoprecipitation, and fluorescence resonance energy transfer (FRET) confirmed this interaction with p14 inside cells. Contrary to recent reports that extracellular AX1 promotes C2C12 mouse myoblast fusion, incubation of p14-transfected C2C12 or HT1080 cells with AX1 antibody had no effect on syncytium formation. Based on these results, I conclude that intracellular AX1 plays an important role in the resolution of pores generated between fused cells by promoting pore expansion. These disparate lines of evidence suggest a converging mechanism of pore expansion irrespective of the membrane fusion event.

LIST OF ABBREVIATIONS USED

AFF	anchor cell fusion failure
AqRV	aquareovirus
ARV	avian reovirus
ATP	adenosine triphosphate
AX	annexin
BAPTA-AM	bis-aminophenoxy-ethane tetraacetic acid acetoxymethyl ester
BroV	Broome reovirus
Ca^{2+}	calcium
CeFF	*C. elegans* fusion failure
CPZ	chlorpromazine
DAG	diacylglycerol
DMEM	Dulbecco's modified Eagle's minimal essential medium
DMSO	dimethyl sulfoxide
DNM	dynamin
DOPC	dioleoyl phosphatidylcholine
Duf	dumbfounded
EFF	epithelial fusion failure
EGFR	epidermal growth factor
EGTA-AM	ethylene glycol tetraacetic acid acetoxymethyl ester
ER	endoplasmic reticulum
ERK	extracellular signal-regulated kinase
F-protein	fusion (measles)
F-actin	filamentous actin
FAST	fusion associated small transmembrane
FCM	fusion competent myoblast
Fig	factor-induced gene
FGF	fibroblast growth factor
FBS	fetal bovine serum
fMLP	formyl-Methionine-Leucine-Phenylalanine
FP	fusion peptide
FPR	formyl peptide receptor
FRET	fluorescence resonance energy transfer
Fus	fusion
GCS1	generative cell specific
GFP	green fluorescent protein
gp	glycoprotein
GTP	guanosine triphosphate
H-protein	hemagglutinin (measles)
HA	hemagglutinin (influenza)
HAP	hapless
HBSS	Hank's balanced salt solution
HEK	human epithelial kidney
HEPES	4-(2-hydroxyethyl)-1-piperazineethanesulfonic acid

HER	human epidermal growth factor receptor
HERV	human endogenous retrovirus
HGF	hepatocyte growth factor
HIV	human immunodeficiency virus
HP	hydrophobic patch
HRP	horseradish peroxidase
HSV	herpes simplex virus
HTLV	human T-cell leukemia virus
IGF	insulin-like growth factor
IL-6	interleukin 6
Irre	Irregular
Kirre	kin of Irre
LIF	leukemia inhibitory factor
LPC	lysophosphatidylcholine
MRF	myelin gene regulatory factor
MoMLV	Moloney muine leukemia virus
Myf	myogenesis factor
Myo	myogenic
NBV	Nelson Bay reovirus
NFRET	normalized FRET
NSF	*N*-ethylmaleimide sensitive factor
OA	oleic acid
Pax7	paired box 7
PBS	phosphate-buffered saline
PE	phosphatidylethanolamine
PKC	protein kinase C
PB	polybasic
PDI	protein disulfide isomerase
PLS	podosome-like structure
PP	polyproline
PtdIns	phosphatidylinositol
Prm	pheromone regulated membrane
QM5	quail muscle fibroblast
RBC	red blood cell
RPMI	Roswell park memorial institute medium
RRV	reptilian reovirus
Rst	roughest
SARS	severe acute respiratory syndrome
SC	satellite cell
SEM	scanning electron microscopy
SEV	Semliki forest virus
SIN	Sindbis
SIV	simian immunodeficiency virus
SLO	Streptolysin-O
SNAP	soluble NSF attachment protein
SNARE	SNAP receptor

Sns	Sticks and stones
SPT	spectral bleed through
Syn	Syncytin
Syt	Synaptotagmin
TBEV	tick-borne encephalitis virus
TM	transmembrane
TMD	transmembrane domain
t-SNARE	target-SNAP receptor
v-SNARE	vesicle-SNAP receptor
VSV-G	vesicular stomatitis virus glycoprotein
WASp	Wiscott-Aldrich syndrome protein

ACKNOWLEDGEMENTS

I would like to thank my family for being so supportive throughout my thesis. I am so lucky to have had access to your extra smarts and creativity (my favourite things) for my whole life!

Roy, thank you so much for accepting me into your lab and being such a terrific supervisor and role model, and for trusting me not to make too many mistakes while I got my science self-confidence. Thank you also for your constant support, for your ideas, and for listening to my ideas, which came in a jumbled format. I feel very lucky to have learned how to be a scientist from you!

Thank you to all of the members of the Duncan Lab, past and present. It has been such a privilege to be around, and learn from, such fabulous, intelligent, and hilarious people.

Thank you to all of my pals in Halifax for helping to make this city my home.

Chapter 1: Introduction

1.1 Overview

Membrane fusion is a ubiquitous process during which bilayers encasing aqueous compartments merge to allow the intermixing of their cargo. Biological membrane fusion is observed in such diverse processes as intracellular membrane trafficking, exocytosis, synaptic transmission of neurotransmitters, gamete formation during sexual reproduction, muscle and bone formation, and enveloped virus entry into host cells (Oren-Suissa and Podbilewicz, 2010). Our current understanding of fusion machinery stems from the study of enveloped virus and SNARE fusion proteins. These fusogens share many similarities, some of which include the large size of their ectodomains, partner binding on target membranes, and dramatic conformational changes during the fusion reaction (White, 2008). A structurally and functionally unusual family of membrane fusogens is encoded by non-enveloped orthoreoviruses. This fusion associated small transmembrane (FAST) protein family is responsible for the fusion of infected host cells to generate large, multinucleated syncytia (Boutilier and Duncan, 2011).

This body of work concentrates on common themes between the current fusion paradigm obtained from the study of enveloped virus fusogens and the fusion reaction mediated by FAST proteins. While many studies have concentrated on the membrane merger reaction itself, this work focuses mainly on the events following fusion and involved in expansion of fusion pores, focusing on the importance of membrane shape modulation and a novel role for the cellular host protein annexin A1.

1.2 Membrane Fusogens

The fusion of phospholipid bilayers is not a spontaneous process and is effectively suppressed by several energy barriers present at pre-fusion and merger stages in the absence of protein machinery. The obstacles to membrane merger include overcoming the hydration repulsion of negatively charged phospholipid head groups upon bilayer approach, and the disruption of lipid bilayers to influence the formation of non-bilayer lipid structures (Kozlov et al., 2010). The energy necessary to accomplish these events is

thought to be released during the refolding of fusion protein machinery from metastable pre-fusion, to stable, post-fusion protein conformations. This section discusses the similarities and differences between the fusion proteins discovered in various biological systems.

1.2.1 Enveloped virus fusion protein classes

Much of our current understanding of membrane fusion has been gleaned from the analysis of enveloped virus fusogens. All viruses containing lipid envelopes must, at some point during infection, fuse with a host membrane in order to deliver the viral core or genome into the cytoplasm of a target cell. In order to do so, enveloped viruses may fuse at the plasma membrane at neutral pH, or during receptor-mediated endocytosis at progressively lower pH characteristic of the endocytic pathway. Additionally, the fusion machinery is provided solely by the virus, with the fusion proteins falling into one of three structure-based categories termed class I-III.

Class I

The best-characterized membrane fusogen to date is the influenza virus hemagglutinnin (HA), a representative member of the class I enveloped virus fusion protein family. In addition to the *Orthomyxoviridae* virus family, class I fusogens are also found in the *Retroviridae*, such as the human immunodeficiency (HIV) gp120/gp41 env protein, as well as fusogens of related retroviruses such as simian immunodeficiency virus (SIV) gp120/gp41, Moloney murine leukemia virus (MoMLV) TM protein, and human T-cell leukemia virus (HTLV) TM protein (Harrison, 2008; Melikyan, 2008). Other examples include the S protein of severe acute respiratory syndrome (SARS) coronavirus (*Coronaviridae)*, simian virus 5 (SV5) F1 and measles virus F proteins (*Paramyxoviridae*), and the GP2 glycoprotein of ebolavirus (*Filoviridae*) (reviewed in (Skehel and Wiley 2000, Kielian and Rey 2006). The single pass transmembrane proteins comprising this family share several key ectodomain structural features. These include their pre- and post- fusion trimeric multimerization status, a characteristic alpha-helical coiled coil arrangement of the ectodomain positioned antiparallel to the membrane, as well as an N-terminally positioned fusion peptide sequence generated upon proteolysis. ‘Fusion peptides’, present in all enveloped viral fusogens, are linear motifs

consisting of approximately 20 mostly apolar amino acids, usually containing several bulky hydrophobic residues and enriched in alanines and glycines, which endow them with a degree of conformational flexibility (Tamm 2003). These sequences are responsible for the interaction with target membranes and promotion of lipid mixing during membrane merger (Epand 2003, Tamm 2003).

The representative member of class I fusogens, influenza HA, is cleaved from an HA0 precursor into two fragments, HA1 and HA2, with HA2 containing the fusion peptide sequence. Upon activation via low pH, the metastable helical bundle unfolds and the fusion peptide at the N-terminus of HA2, which is buried in the trimer interface near the base of the fiber, is projected ~100Å away from the donor membrane where it is presumed to interact with the target membrane (Fig. 1.1). In this extended structure known as the 'pre-hairpin' intermediate, HA2 is embedded in the donor membrane via its transmembrane helix and in the target membrane by the fusion peptide (Bullough, Hughson et al. 1994, Eckert and Kim 2001). A second conformational change occurs, where the donor membrane-embedded C-terminal portion of the trimer folds back in a 'jack-knife' fashion to interact in antiparallel with the N-terminal segments of the proteins. This low-energy, highly stable post-fusion conformation, termed 'trimer of hairpins', brings into proximity the transmembrane domains (TMDs) embedded in the donor membrane and the fusion peptides embedded in the target membrane, thus facilitating close membrane apposition, the initial stage of bilayer fusion (Eckert and Kim 2001, Kielian and Rey 2006).

It is believed that the dramatic conformational change of the class I fusion trimers drives the fusion reaction by providing energy to overcome the electrostatic and thermodynamic barriers to close membrane apposition and membrane merger (Carr, Chaudhry et al. 1997, Melikyan, Markosyan et al. 2000, Russell, Jardetzky et al. 2001). A variation on this model is represented by another member of the class I fusion family, the measles F protein, which is also synthesized as a precursor (F0) and is cleaved during progression through the Golgi complex to F1 and F2 that form a meta stable pre-fusion trimer. As with other paramyxovirus fusogens, one protein contains the fusion peptide and is responsible for fusion (measles virus F1) while a separate protein is responsible for receptor binding (measles hemagglutinin, H), (Dorig, Marcil et al. 1993, Tatsuo, Ono et

al. 2000, Hsu, Iorio et al. 2001). The fusion protein and receptor binding proteins of the paramyxoviruses interact with each other (as an F trimer and an H dimer for measles virus) as a complex to mediate attachment and fusion at a neutral pH.

Class II

The class II enveloped virus fusion proteins are differentiated from class I fusogens based on the secondary and tertiary structures of their pre- and post-fusion conformations. Surprisingly, they undergo remarkably similar structural rearrangements as the class I fusion proteins. Members of the class II fusion protein family include the E proteins of the flaviviruses, tick-borne encephalitis virus (TBEV) and dengue virus (*Flaviviridae*), and the E1 proteins of the alphaviruses, Semliki Forest virus (SFV) and Sindbis virus (SIN) (*Togaviridae*) (Kielian and Rey 2006). In their pre-fusion conformation, the ectodomains of class II fusogens comprise three β-sheet folds and orient themselves parallel to the membrane as dimers (Fig. 1.1). Their fusion peptides are not N-terminal, but exist as internal loops located in domain II, at the furthermost extremity of the fiber. These fusion loops are shielded from solvent at the dimer interface, and are exposed upon low pH triggering that leads to dissociation of the dimers (Kuhn, Zhang et al. 2002). The extended fusogens interact with the target membrane via the fusion loop and rearrange to form extended trimers that then fold back on themselves, similar to the class I fusogens, bringing together the TMDs and fusion loops and with them, the donor and target membranes (Gibbons, Vaney et al. 2004, Modis, Ogata et al. 2004).

Class III

The most recent addition to the groups of enveloped virus fusogens are the class III proteins, which share characteristics present in both the class I and class II fusogens. Current members of this family are the vesicular stomatitis virus (VSV) G glycoprotein (*Rhabdoviridae*), the herpes simplex virus-1 (HSV-1) glycoprotein B (*Herpesviridae*), and the baculovirus gp64 protein (*Baculoviridae*) (Kadlec et al., 2008) (Heldwein, Lou et al. 2006, Roche, Bressanelli et al. 2006, White, Delos et al. 2008). The pre-fusion structures of class III fusogens are composed of α-helical coiled coils, like class I fusogens, but, their fusion peptides are found as loops within β-strands, similarly to class II fusogens (Fig. 1.1). Interestingly, unlike all known class I and II fusogens, the

conformational changes from the metastable pre-fusion to the post-fusion conformation of both VSV-G and HSV-1 B envelope glycoprotein are reversible and dependent on the pH equilibrium, making this a hallmark distinguishing feature of this protein family (White, Delos et al. 2008, Dollery, Wright et al. 2011).

Analysis of enveloped virus fusogen structure and function reveals several common themes. Irrespective of their class, the commonalities between these fusion machines include meta-stable pre-fusion multimeric structures, dramatic conformational changes leading to the approach of lipid bilayers and the formation of stable, low-energy trimeric structures of similar shape, and the localization of the fusion peptide and TMD in close vicinity and, eventually, in the same lipid bilayer. Additionally, these fusion machines are independent catalysts necessary and sufficient for membrane merger and the transfer of viral contents into the host cytoplasm.

1.2.2 Intracellular fusion machinery

An equally extensively studied membrane fusion system involves the intracellular vesicle shuttling machinery present in the endo- and exocytosis pathways. Unlike the enveloped virus fusion proteins, components of this machinery must be present in both the donor and target membranes for effective membrane merger to occur. The proteins mediating vesicle membrane fusion belong to the SNAP [soluble NSF attachment protein] receptor (SNARE) family with v-SNARES located on the vesicle membrane and t-SNARES located in the target phospholipid bilayer. Complex formation of these proteins *in trans* is required for the onset of membrane fusion (Fig. 1.1). Characteristic SNARE proteins are present in the various vesicle trafficking pathways, and thus confer specificity to the fusion reaction and cargo delivery. The complement of all four v- and t-SNARE components has been shown to be sufficient for inducing membrane fusion when reconstituted in a liposome system or expressed on the surface of cells (Weber, Zemelman et al. 1998, Hu, Ahmed et al. 2003, Pobbati, Stein et al. 2006). However, the SNARE concentrations used in the liposome fusion assays were far above physiological levels and the fusion reaction itself was uncharacteristically leaky; it is believed that other accessory proteins, such as synaptotagmin-1, may be involved in the destabilization of

membranes during fusion *in vivo* (Dennison, Bowen et al. 2006, Martens and McMahon 2008).

Similarly to class I enveloped virus fusogens, the SNARE protein family adopts a coiled coil structure, composed of one v-SNARE and three t-SNARE helices. Zippering of the SNARE bundle has been suggested to drive membrane fusion by transferring force to the SNARE transmembrane (TM) domains (Kesavan, Borisovska et al. 2007). In the case of synaptic vesicles, it has also been postulated that fusion is inhibited by a 'clamp' protein, such as complexin and its calcium sensing regulator synaptotagmin-1 (Syt-1), which dissociate from the SNARE tetramer upon calcium stimulation, allowing for membrane fusion to ensue (Martens, Kozlov et al. 2007). Despite the controversy surrounding the details of the membrane merging reaction, it should be noted that, similarly to the viral fusogens, the SNARE protein complex comprises complex ectodomain structures that undergo dramatic structural rearrangements. This structural remodeling is required for close membrane apposition and membrane merger, where the complex adopts a low-energy, stable *cis* conformation within the same phospholipid bilayer. However, the SNARE machinery differs from the enveloped virus fusogens not only in its pre-fusion *trans* configuration, but also in the post-fusion recycling of these components. Contrary to enveloped virus entry, which needs to occur only once in order to deliver viral cargo, the SNARES can be reclaimed from fused membranes by SNAP ATPases, which convert them to pre-fusion, high-potential energy conformations that are recognized and restored to cargo-containing vesicles by specific vesicle coat budding proteins (Sollner, Bennett et al. 1993, Sollner 2004).

1.2.3 Syncytin and *C. elegans* Fusion Failure (CeFF) cell-to-cell fusion proteins

The currently known cell-to-cell fusion events include sperm-egg fusion during fertilization in mammals, *C. elegans*, protists, and plants, as well as eye lens fusion, macrophage fusion and osteoclast formation, muscle cell differentiation, trophoblast fusion, and somatic cell fusion in *C. elegans*. Despite the multitude of cell-to-cell fusion events, very little is known about the fusogens mediating this process. A key criterion of a fusogen is the ability to initiate fusion between heterologous cells. Of all the above-mentioned cell fusion events, the syncytins, responsible for trophoblast fusion during

formation of the placenta, as well as the epithelial fusion failure-1 (EFF-1) and anchor cell fusion failure-1 (AFF-1) necessary for programmed cell fusion in *C. elegans*, are the only cellular fusogens capable of fusing heterologous cells when ectopically expressed (Mi, Lee et al. 2000, Mohler, Shemer et al. 2002, Sapir, Choi et al. 2007).

The syncytin family consists of two homologs, syncytin-1 (syn-1) and syncytin-2 (syn-2), with both being able to mediate cell-to-cell fusion (Mi, Lee et al. 2000, Blaise, de Parseval et al. 2003, Malassine, Frendo et al. 2008). Isolated in a screen of secreted proteins, syn-1 is the envelope protein of the human endogenous retrovirus (HERV), and thus, is essentially a class I envelope virus fusogen which binds the type D mammalian retrovirus receptor (Mi, Lee et al. 2000, Frendo, Olivier et al. 2003). Both syn-1 and syn-2 are expressed during primary cytotrophoblast differentiation, with predominantly syn-1 driving the fusion of cytotrophoblasts leading to the formation of the syncytiotrophoblast layer of the placenta. In addition to a role in placental generation, syn-1 has also been implicated in mediating osteoclast fusion during bone resorption (Soe, Andersen et al. 2011). Surprisingly, syn-1 has also recently been found to be involved in promotion of the G1/S transition, and the subsequent proliferation of cells (Huang, Li et al. 2013). An interesting model was proposed whereby syn-1 serves a dual role in syncytiotrophoblast formation. One role involves a non-fusogenic function of syn-1 leading to the generation and replenishment of a pool of cytotrophoblasts. This was proposed upon finding that knock-down of syn-1 led to arrest of the G1/S transition phase of the cell cycle. The second role involves the fusogenic activity of syn-1 mediating merger of these cytotrophoblasts into a functional placental syncytium (Huang, Li et al. 2013). Additionally, the fusogenic activitiy of syn-1, but not syn-2, has recently been found to be partially regulated by another HERV encoded protein suppressyn, which binds to the syn-1 receptor and inhibits cell-cell fusion (Sugimoto, Sugimoto et al. 2013). This is the first known example of a mammalian cell-encoded protein that is able to negatively regulate membrane fusion.

While the syncytins appear to be cell-encoded fusogens acquired from human retroviruses, it is not clear whether the *C. elegans* fusogens EFF-1 and AFF-1 (CeFFs) have evolved independently as *bona fide* cell-cell fusogens, or like syncytin, have been adapted from endogenous viruses. Due to their ability to fuse heterologous cells when

ectopically expressed or pseudotyped onto fusion deficient VSV, the CeFFs appear to function as independent fusion machines (Podbilewicz, Leikina et al. 2006, Sapir, Choi et al. 2007, Avinoam, Fridman et al. 2011). Additionally, orthologs of the CeFFs have been found in other nematodes, two arthropods (*Calanus finmarchicus* and *Lepeophtheirus salmonis*), a ctenophore (*Pleurobrachia pileus)*, a chordate (*Branchiostoma floridae*) and a protist (*Naegleria gruberi)*, suggesting that the FFs are a family of conserved cellular fusogens (Avinoam, Fridman et al. 2011). Interestingly, it has been shown that, unlike viral fusion proteins, but similar to SNARE machinery, EFF-1 must be present in both the donor and target membranes for merger and syncytium formation to occur (Fig. 1) (Podbilewicz, Leikina et al. 2006). However, the homotypic nature of the *cis* and *trans* membrane components is unlike the heterotypic arrangement of SNARE components. Structurally, the FFs are single pass transmembrane proteins containing an N-terminal signal sequence, a large ectodomain and a relatively short endodomain, reminiscent of enveloped virus fusion proteins (Sapir, Avinoam et al. 2008). It remains to be seen whether FF-like, or syncytin-like proteins are responsible for mediating fusion in other biological systems.

1.2.4 Candidate cell-cell fusion proteins in other systems

Various proteins involved in cell-cell fusion have been identified during the fertilization event of multiple organisms including yeast, protists, fungi, plants and mammals. However, no *bona fide* fusogen that is necessary and sufficient for the merger of plasma membranes during fertilization has been identified. In the case of yeast mating, the tetra-spanning transmembrane pheromone regulated membrane-1 glycoprotein (Prm1) is required for efficient plasma membrane fusion (Heiman and Walter 2000). However, the membrane fusion reaction itself can proceed in the absence of Prm1 albeit at lower efficiency, suggesting that this protein is not essential for the fusion event (Aguilar, Engel et al. 2007, Olmo and Grote 2010). Two additional proteins have been identified as playing a role in yeast mating, Fig1 and Fus1, with Fig1 acting as a potential calcium sensor and Fus1 as a facilitator of pore stabilization and expansion (Muller, Mackin et al. 2003, Nolan, Cowan et al. 2006).

The *Arabidopsis* and protist fertilization systems, as described for *Chlamydomonas* and *Plasmodium*, require the presence of HAP2/GCS1 for membrane fusion during mating (Mori, Kuroiwa et al. 2006, Hirai, Arai et al. 2008). The HAP2 gene encodes a single pass transmembrane protein with a large ectodomain. However, this protein does not contain an identifiable canonical fusion peptide and lacks predicted coiled coil domains present in many enveloped viral fusion proteins and SNARES (Liu, Tewari et al. 2008). It will be interesting to see whether membrane fusion mediated by HAP2 in these protists proceeds analogously to that of the enveloped virus and SNARE fusion proteins. In addition, due to its essential role in mating, HAP2 may serve as an excellent target for the development of anti-malarial strategies.

Lastly, two candidate proteins that mediate mammalian fusion of sperm and egg during fertilization have been identified. The sperm component, Izumo, a member of the immunoglobulin superfamily of proteins, and the tetraspannin CD9, found in the egg, are both essential for the fusion process, with knockdown of either protein completely inhibiting fertilization (Kaji, Oda et al. 2000, Miyado, Yamada et al. 2000, Inoue, Ikawa et al. 2005). It has been demonstrated that CD9 may be involved in the creation of cell adhesion sites, or is released in vesicles that are essential for sperm-egg fusion (Miyado, Yoshida et al. 2008, Jegou, Ziyyat et al. 2011). However, it has not been definitively demonstrated that either CD9 or Izumo is the bona fide fusogen responsible for membrane merger in this system.

1.2.5 Factors affecting muscle cell fusion

Unlike enveloped virus or SNARE-mediated fusion, muscle cell differentiation and myotube formation can be divided into a series of steps requiring multiple cellular proteins for the successful development of muscle fibers. The two predominant systems employed for the study of myogenesis are *Drosophila melanogaster* muscle cell fusion and the *in vitro* tissue culture of mouse myoblast C2C12 cells. In *Drosophila*, two distinct cell populations give rise to myotubes; founder cells and the fusion-competent myoblasts (FCM). Several steps are necessary for the onset of fusion to occur, including cell migration, recognition and adhesion. Both the FCM and founder cell populations express specific proteins necessary for recognition and mutual association. These include

the immunoglobulin superfamily transmembrane proteins Kin of Irre-C/Dumbfounded (Kirre/Duf) and Roughest/Irregular Optic Chiasma-C (Rst/Irre-C) in the founder cells, and Sticks and stones (Sns) in FCMs (Bour, Chakravarti et al. 2000, Ruiz-Gomez, Coutts et al. 2000, Strunkelnberg, Bonengel et al. 2001, Abmayr and Pavlath 2012). Sns is required by FCMs for the recognition of founder cells and nascent myotubes, while Kirre, either in the membrane of founder cells or as a secreted gradient, acts as an attractant for the FCMs. The initial event necessary for the generation of new muscle fibers is the fusion of an FCM to a founder cell to form a myotube precursor, which is the 'seed' of the nascent myotube that attracts subsequent FCMs (Bate 1990, Abmayr and Pavlath 2012).

The *Drosophila* cell fusion system has been integral in highlighting the role of the actin cytoskeleton during cell-cell fusion. Actin cytoskeleton remodeling is thought to play a large role preceeding, during and after the fusion event, however, the exact roles of the factors involved remain hotly contested. The actin-nucleators SCAR/WAVE and Wiskott-Aldrich syndrome protein (WASp) have been shown to be essential to the fusion process, and while some believe that both are needed for pore formation (Kim 2007), it has also been suggested that WASp may function at a pore expansion step (Kim, Shilagardi et al. 2007, Massarwa, Carmon et al. 2007, Gildor, Massarwa et al. 2009). Additionally, actin foci and the presence of actin coated 'prefusion vesicles' have been reported at sites of myoblast fusion, the nature of which remains unknown (Kim, Shilagardi et al. 2007). The most exciting recent news in the *Drosophila* field involves the discovery of actin-rich podosome-like structures (PLS) that emanate from FCMs and are pushed into the nascent myotube prior to fusion (Sens, Zhang et al. 2010). These finger-like projections are thought to be necessary for the onset of fusion, and it has been suggested that they are responsible for close membrane apposition and membrane curvature generation, which may catalyze the fusion process. Despite the plethora of information regarding the timeline and players involved in *Drosophila* myoblast fusion, the scope of which is beyond this brief overview, a true, necessary and sufficient membrane fusogen remains to be identified.

Mammalian muscle cell fusion differs from *Drosophila* myogenesis in that it does not consist of two separate cell populations, but rather of one lineage of cells

differentiated to varying degrees. Muscle tissue is thought to consist of differentiated myotubes, as well as an undifferentiated stem cell population of myoblasts called satellite cells (SCs), which are found in the basal lamina of the muscle fibers (Sanes 2003). The myoblasts are generated from a pool of mesodermal precursors that differentiate into SCs. SCs make up a small population of single, quiescent cells, defined by the expression of Pax7, which are interspersed throughout the muscle fiber (Gayraud-Morel, Chretien et al. 2009). Upon activation by the transcription factors MyoD and Myf5, SCs divide and differentiate into elongated myocytes. The myocytes then translocate to sites of muscle injury, where they fuse with each other to generate nascent myotubes, and with the damaged myotubes to generate new tissue (Gayraud-Morel, Chretien et al. 2009, Abmayr and Pavlath 2012). The recruitment, proliferation, and migration of SCs to sites of injury is regulated by hepatocyte growth factor (HGF), fibroblast growth factor (FGF), leukemia inhibitory factor (LIF), interleukin-6 (Il-6), CD164, insulin-like growth factor (IGF) and other factors (Hawke and Garry 2001) Upon receiving a differentiation signal, SCs upregulate expression of myogenin and MRF4, two transcription factors that direct SCs to exit the cell cycle, express the muscle-specific marker sarcomeric myosin, and eventually fuse with nascent myotubes (Hawke and Garry 2001, Bizzarro, Petrella et al. 2012).

The mammalian muscle fusion system has been instrumental in understanding cellular motility and attachment during muscle tissue formation, and has identified the adhesion molecules M-cadherin, integrin, Adam12, and nephrin (the mammalian homologue of Sns) as being necessary for the recognition and adhesion of myoblasts (Zeschnigk, Kozian et al. 1995, Galliano, Huet et al. 2000, Mayer 2003, Sohn, Huang et al. 2009). Additionally, it has been found that transient exposure of phosphatidylserine (PS) at cell-cell adhesion sites is important during myotube formation (van den Eijnde, van den Hoff et al. 2001). Cholesterol-rich, transient lipid rafts also play a role in myogenesis via their role as aggregators of adhesion molecules at cell-cell contact points (Mukai, Kurisaki et al. 2009). While most studies have focused on the stages of myogenesis that precede cell-cell fusion, a recent report suggested that annexin A1 (AX1) and annexin A5 (AX5), which is known to bind PS, are involved in the actual membrane merger event (Leikina, Melikov et al. 2013). The GTPase dynamin (DNM)

and the PtdIns(4,5)P2 content in the plasma membrane of fusing C2C12 myoblasts were also shown to promote subsequent pore expansion leading to myotube formation. Several roles of the annexin protein family in membrane interactions are discussed in section 1.5. Despite the numerous studies and multiple discoveries of factors involved in mammalian myogenesis, a *bona fide* bilayer fusion protein, that is necessary and sufficient for membrane merger, has not been identified in this system.

1.3 Mechanism of biological membrane fusion: Fusion-through-hemifusion model

Biological lipid bilayers are composed of various lipids and proteins that are responsible for creating a selectively permeable barrier between aquaeous compartments, such as the cell cytoplasm and the extracellular environment. The plasma membrane components are also involved in the generation of overall membrane shape and, in the case of cells, the creation of transient microdomains such as signalling platforms or cell-cell and cell-matrix attachment sites (Chernomordik and Kozlov 2003). The lipids that comprise biological membranes can be subdivided into three categories based on their intrinsic shape. Phosphatidylcholine (PC) is cylindrically shaped, with an approximately equal radius covering the phosphate headgroup and its two hydrocarbon chains. The cylindrical shape of PC results in flat packing of lipid monolayers, and does not confer any curvature onto constraint-free membranes (Fig. 1.2) (Chernomordik and Kozlov 2008). Conversely, phosphatidylethanolamine (PE) and diacylglycerol (DAG) have relatively small headgroups but contain a complement of two acyl chains, resulting in a cone-shape that distorts membranes into bulges where the headgroups are directed to the concave side of the curve, and the tails to the convex side. This arrangement results in the generation of negative spontaneous curvature (i.e., the monolayer bends toward the lipid headgroups) (Fig. 2). Conversely, lysophosphatidylcholine (LPC) contains a large polar head group and one acyl chain, and assumes the shape of an inverted cone. Upon aggregation in lipid monolayers, LPC results in the generation of positive spontaneous curvature, with head groups oriented on the convex side of the curve and tails on the concave side (Fig. 2). Curvature-inducing lipids and fatty acids have been used to alter membrane fusion in contrived systems. For example, insertion of LPC in the outer leaflet

of bilayers induces negative curvature and impedes fusion whereas oleic acid (OA) insertion into the outer leaflet promotes positive curvature and fusion (Fig. 1.2)

It is currently believed that all biological membrane fusion reactions progress through a series of common steps (Fig. 2): (i) close membrane apposition of the phospholipid bilayers, which involves counteracting the electrostatic forces between negatively charged phospholipids, removal of the water layer and clearance of membrane resident proteins from the pre-fusion site; (ii) merger of lipids in the outer leaflets of apposed membranes via a transient, non-bilayer, high-energy intermediate (i.e. hemifusion); (iii) opening of a fusion pore able to conduct the transfer of aqueous contents between fused compartments; and lastly, (iv) expansion of the pore. Progression through these transition states is believed to involve intermediates that minimize the exposure of hydrophobic surfaces to the aqueous environment surrounding membranes. Close membrane apposition, in the context of biological fusion, has been attributed to receptor binding and membrane approach mediated by components of the membrane fusion complex. In the case of enveloped virus proteins, this process may be mediated by structural conversions between the extended pre-hairpin and hairpin conformations. For intracellular vesicle fusion, this step appears to be mediated by zippering of *cis* and *trans* SNAREs. For other cell-cell fusion events, it is unknown what mediates close membrane apposition but connections between cells appear to require the previously mentioned adhesion factors. Hemifusion and pore formation are mediated by the previously described fusogens (i.e., enveloped virus fusion proteins, SNAREs, CeFF proteins or syncytin) or presumably by unidentified fusogens in other systems. Almost nothing is known about factors involved in pore expansion needed to generate multi-nucleated cells. Recent reports indicate that the actin cytoskeleton, the GTPase dynamin, PtdIns(4,5)P2, protein kinase C (PKC) and Ca^{2+} are involved in actively expanding stable pores (Scepek, Coorssen et al. 1998, Chen, Leikina et al. 2008, Richard, Leikina et al. 2009, Leikina, Melikov et al. 2013).

The ‘black box’ of biological membrane fusion is the bilayer merger event itself. Several models describing the nature and order of lipid mixing and protein contributions have been described, and most of the known fusogens have been reported to progress via a fusion-through-hemifusion pathway (Fig. 1.2). In this model, close membrane

apposition is followed by the generation of a point-like protrusion, presumably generated by fusion protein catalysts, which is thought to minimize the energy barrier of hydration repulsion between the apposed proximal leaflets (Kozlov et al., 2010). Protrusion formation is followed by generation of a hemifusion stalk, where lipids from proximal leaflets merge but distal leaflets remain intact. Formation of the stalk intermediate generates net negative curvature, and can be inhibited by addition of LPC and promoted by addition of phosphatidylethanolamine or oleic acid. Stalk formation is thought to involve elastic deformation of membrane monoloayers, tilting of lipid molecules and splaying of their hydrophobic tails in order to decrease the energy required to generate this structure (Kozlovsky and Kozlov 2002). The stalk is then thought to expand and form a hemifusion diaphragm, the rupture of which yields a fusion pore. The progression of this fusion reaction requires increasingly more energy input at each sequential stage, with formation of a stable fusion pore being the most energy demanding step in the process. Consistent with this hypothesis, titrating the amount of fusion machines results in the arrest of membrane fusion at the hemifusion stage, prior to pore formation and pore expansion (Zaitseva, Mittal et al. 2005). As mentioned above, the energy required for this process is thought to be contributed by the conformational change of fusion proteins from a metastable pre-fusion precursor to the highly stable post-fusion conformation.

The presence of a hemifusion intermediate is indirectly supported by studies where the shape of distal leaflets of hemifused membranes was modulated by chlorpromazine (CPZ), a weak base that preferentially partitions into the distal (cytoplasmic or lumenal) leaflets of bilayers and induces positive curvature. In the presence of a hemifusion intermediate, CPZ treatment leads to rupture of the hemifusion diaphragm and an increase in pore formation (Chernomordik, Frolov et al. 1998, Melikyan, Markosyan et al. 2000, Zaitseva, Mittal et al. 2005). Whereas a stalk structure of angstrom-scale dimensions has been directly observed by X-ray diffractions in model lipid systems, neither a stalk, nor a hemifusion diaphragm, has been detected in any biological membrane fusion system (Yang and Huang 2002, Cohen and Melikyan 2004). It has also been suggested that the stalk structure may proceed directly to pore opening and bypass the hemifusion diaphragm intermediate (Kuzmin, Zimmerberg et al. 2001).

An interesting finding that does not support the existence of a stalk or lipid

intermediate prior to pore formation has been obtained via electrical capacitance measurements, where it was shown that pore opening precedes the transfer of lipids from donor to target membranes (Zimmerberg, Blumenthal et al. 1994). In addition, a disordered 'lipid-mixer' model, which bypasses the formation of an ordered stalk intermediate, has been suggested for the fusion reaction of HA (Tamm 2003). In this scenario, fusion peptides and the membrane-proximal regions of TMDs replace water molecules upon membrane approach driven by mechanical energy obtained from fusion proteins. With the thermodynamic stability of lipid membranes being conferred by the presence of headgroup interactions in the presence of water, membrane dehydration and insertion of amphipathic, bulky side chains or fusion peptides likely disrupts the lipid packing of phospholipid bilayers. By removing the ordering principles of phospholipid membranes, a disordered, lipid-mixing state may be reached that eliminates the need for a stalk structure, but is still a hemifusion lipid intermediate (Tamm 2003, Tamm, Crane et al. 2003). Alternatively, amphipathic fusion peptides may induce membrane curvature, leading to the formation of point-like protrusions that precede stalk formation. Such a scenario has been demonstrated for for synaptotagmin C2 domains, which are able to generate tubulues with highly curved, fusogenic lipid caps, reminiscent dimples or point-like protrusions (Martens, Kozlov et al. 2007, Chernomordik and Kozlov 2008).

Findings obtained via detection of lipid probe transfer in the presence of curvature inducing agents have demonstrated the existence of a membrane curvature-sensitive, lipid-based intermediates during membrane fusion of enveloped viruses, SNARES, EFF-1-mediated somatic cell fusion, and C2C12 myotube formation (Chernomordik, Frolov et al. 1998, Chernomordik and Kozlov 2005, Xu, Zhang et al. 2005, Zaitseva, Mittal et al. 2005, Podbilewicz, Leikina et al. 2006, Abdulreda, Bhalla et al. 2008, Leikina, Melikov et al. 2013). These reports suggest that membrane fusion proceeds via a lipid-merging intermediate, however, the nature of this intermediate, whether an ordered stalk, or a disordered lipid emulsion, remains to be seen in these biologically relevant systems.

1.4 FAST proteins

The non-enveloped nature of reoviruses allows them to enter cells via receptor-mediated endocytosis without the requirement for a membrane fusion protein. However,

several members of the *Reoviridae* family encode fusion-associated small transmembrane (FAST) proteins that have evolved to promote cell-cell, rather than virus-cell, membrane fusion. The FAST protein family is comprised of six members encoded by members of genera *Orthoreovirus* and *Aquareovirus*, two related genera in family *Reoviridae*: the homologous p10 proteins of avian reovirus (ARV) and Nelson Bay reovirus (NBV), the p13 protein of Broome reovirus (BroV), the p14 protein of reptilian reovirus (RRV), the p15 protein of baboon reovirus (BRV), the p16 protein of the group C aquareoviruses (AqRV-C), and the p22 protein of AqRV-A, each named according to their respective molecular masses in kDa (Fig 1.3) (Shmulevitz and Duncan 2000, Dawe and Duncan 2002, Corcoran and Duncan 2004, Racine, Hurst et al. 2009, Thalmann, Cummins et al. 2010, Ke, He et al. 2011, Guo, Sun et al. 2013).

The FAST proteins are expressed from viral RNA inside host cells and are trafficked to the plasma membrane where they mediate fusion with neighbouring cells to generate multinucleated syncytia (Shmulevitz and Duncan 2000, Corcoran and Duncan 2004, Dawe, Corcoran et al. 2005). Formation of these multinucleated structures is thought to promote viral spread without the need for cell lysis and re-entry into neighbouring cells, thus protecting the virions from being recognized by the immune system. The FAST proteins fuse at neutral pH and are not regulated by a specific trigger mechanism. The rate of syncytium formation in virus-infected cells is instead regulated by the slow accumulation of FAST proteins in the plasma membrane. All of the FAST proteins are expressed using non-optimized translation start codons (Racine and Duncan 2010), and the majority of expressed p10 FAST proteins are quickly degraded before they can exit the endoplasmic reticulum (ER) (Shmulevitz, Corcoran et al. 2004). These findings suggest that extensive cell-cell fusion may have to be delayed, possibly to allow sufficient time for assembly of progeny virions. Indirect evidence supports this conjecture. Although FAST-mediated cell-cell fusion appears to be a non-leaky process, membrane integrity is eventually compromised by the onset of apoptosis upon generation of extensive syncytium formation. These findings led to the proposal that fusogenic reoviruses initially exploit cell-cell fusion events to promote localized cell-cell spread of the infection during early viral infection of the host, followed by a second step involving the release of a large number of viral particles from leaky syncytia for systemic

dissemination (Salsman, Top et al. 2005). The virulence potential of the FAST proteins was also demonstrated in studies where the gene encoding the p14 FAST protein was cloned onto vesicular stomatitis virus (VSV). Infection of mice with the recombinant VSV resulted in increased neuropathogenicity, suggesting that FAST proteins are indeed *bona fide* virulence factors (Brown, Stephenson et al. 2009).

Although members of the FAST protein family do not display any sequence similarity, they do share many structural characteristics. These include a single-pass, type III membrane topology, indicating that their N-termini are found outside of the cell while the C-termini are internal. They are designated as type III, not type I, membrane proteins because their TMDs function as reverse signal anchors to direct membrane insertion, as opposed to type I proteins where the N-terminal signal sequence is cleaved following insertion in the ER. The FAST proteins are between 95 and 198 amino acids in length, with ectodomains of only ~19-42 residues. All members of this fusogen family are predicted to be acylated by either an N-terminal myristoyl moiety in the case of RRV p14, BRV p15, BroV p13 and AqRV-A p22, or doubly palmitoylated on cysteines located in the juxtamembranous region of ARV and NBV p10, and possibly AqRV-C p16. These modifications appear to be essential for fusion, but their exact function remains to be determined (Shmulevitz, Salsman et al. 2003, Corcoran and Duncan 2004, Dawe, Corcoran et al. 2005). All members of the FAST protein family also contain a membrane-proximal polybasic (PB) region located in their endodomains. This feature has been shown to be necessary for directing trafficking of RRVp14 via the ER/Golgi pathway to the plasma membrane (Hiren Parmar, Dalhousie University, personal communication).

The ARV and NBV p10, as well as RRV p14, contain a 'hydrophobic patch' (HP) in their ectodomains, which is thought to serve as a fusion peptide and may be analogous to the fusion peptides of class I and fusion loops of class II enveloped virus fusion proteins (Corcoran et al., 2004; Shmulevitz et al., 2004; Barry et al., 2010). Surprisingly, the HP of BRV p15 is in its endodomain, not ectodomain, where it cannot serve as a typical fusion peptide (Dawe et al., 2005). Liposome lipid-mixing assays indicate an unusual polyproline II helix in the p15 ectodomain serves as a 'fusion peptide' (Top, Read et al. 2012). Lipid-mixing mediated by the myristoylated polyproline II helix of p15

displayed an unusually long lag time prior to the onset of lipid mixing. It is possible that the internal HP of p15 may serve as an additional membrane-destabilizing motif. Indeed, generation of a chimeric p14/p15 FAST protein containing external and internal HPs increases the rate of syncytium formation (Eileen Clancy, Dalhousie University, personal communication). Furthermore, the p15 HP was shown to function as a membrane curvature sensor (Jolene Read, Dalhousie University, personal communication). This raises the intriguing possibility that an internal HP might recognize and stabilize the highly curved internal rim of a nascent fusion pore, thereby lowering the energy barrier to pore formation. Interestingly, the HPs of BroV p13, AqRV-C p16 and AqRV-A p22 are also found in their endodomains, indicating internal HPs are the preferred option for the FAST proteins and suggesting these motifs might serve a similar function as the p15 HP.

The FAST proteins function as multimers of unknown N value. For both p14 (Corcoran, Clancy et al. 2011) and p10 (Tim Key, personal communication), regions in their ectodomains dictate their multimerization status (Corcoran, Clancy et al. 2011). The RRV p14 multimers localize to cholesterol-rich, detergent-resistant microdomain, so-called lipid rafts (Corcoran, Salsman et al. 2006), and FRET analysis indicates cholesterol-dependent p10 multimerization is reversible and required for membrane fusion activity (Tim Key, personal communication). Interestingly, the NMR structure of the p14 TMD in DOPC micelles exists as a highly curved arced helix (Muzaddid Sarker, personal communication). The end-to-end length of the arced helix is just sufficient to span a dioleylphosphatidylcholine (DOPC) bilayer, but is not long enough to span the increased thickness of lipid rafts. These results suggest the p14 TMD may undergo helical transitions from a curved to a straight helix, allowing p14 to shuttle in and out of lipid rafts.

The FAST proteins can be classified as true membrane fusogens based on their ability to fuse multiple cell types when ectopically expressed, and on the ability of purified p14 to mediate liposome-cell fusion and liposome-liposome lipid mixing (Top, de Antueno et al. 2005). The FAST proteins do, however, exploit cellular factors to enhance cell-cell fusion. Atomic force microscopy measurements of p14 in liposomes indicate the 38-residue ectodomain projects <1.5 nm from the membrane surface, a distance too short to span the intercellular gap between adjacent cells (Corcoran et al.,

2006). By comparions, the HA ectodomain extends approximately 13 nm in its folded, post-fusion conformation (Wilson, Skehel et al. 1981). Furthermore, the ectodomains of the FAST proteins do not bind receptor partners on target cells (Salsman et al., 2008), and they mediate membrane merger solely from the donor membrane (Shmulevitz et al., 2004), indicating they do not form *trans*-acting homotypic interactions typical of SNAREs and CeFFs. Rather than mediating membrane binding and close apposition, the FAST proteins rely on surrogate cellular adhesion machinery, located at adherens junctions, for efficient cell-cell fusion. Cell adhesion, and particularly cadherin, engagement, at points of cell contact can bring donor and target membranes to a distance of 20-40 nm. Active actin remodeling and formation of membrane protrusions containing the FAST proteins then presumably induce close membrane apposition. (Salsman et al., 2008).

Although the FAST proteins are virally encoded fusogens, they cannot be classified in the enveloped virus fusion protein classes due to their size, structure, and biological function. (Wilson, Skehel et al. 1981) It is highly unlikely that the FAST proteins catalyze the fusion reaction in a manner analogous to the enveloped viral fusogens. Their comparatively miniscule ectodomains are unlikely to undergo the energy-generating conformational changes that are currently believed to drive membrane fusion. Instead, FAST protein-mediated membrane merger is likely dependent on the coordinated activity of all three domains (ecto-, endo- and TMD) and several motifs present in these domains. As discussed above, the ectodomains of p10, p14 and p15 all contain fusion peptide motifs and an N-terminal myristoyl moiety in p14 and p15. Reversible insertion of the myristate and shallow insertion of the bulky hydrophobic amino acids in the fusion peptides into donor and/or target membranes could alter lipid headgroup hydration and/or induce membrane curving or buckling. Mutational studies and analyses of chimeric FAST proteins also indicate the FAST protein TMDs play an active role in the fusion process, with bulky hydrophobic residues in the p15 TMD that are positioned near the outer interfacial region of the membrane being particularly important (Clancy and Duncan 2009, Clancy and Duncan 2011). In the acred-helix architecture of the p14 TMD, the corresponding residues project out toward the solvent phase (Muzaddid Sarker, personal communication) and contribute to altering lipid

headgroup packing and hydration. The combined effects of curvature and altered hydration status of the plasma membrane may generate a point-like protrusion or dimple formation, reminiscent of the pre-hemifusion membrane structure suggested for enveloped virus fusion. Alternatively, disruption of the lipid bilayer by FAST proteins could induce a less structured lipid emulsion analogous to the 'lipid mixer' model of membrane merger.

The disproportionately large size of FAST protein endodomains (almost all of the other fusogens described in preceding sections are positioned mostly external to the bilayer) suggests an important role in the fusion process. In addition to providing plasma membrane trafficking signals (i.e., the p14 PB motif), the internal HPs may promote pore formation. Interestingly, truncation and replacement analyses of the FAST proteins endodomains indicate a correlation between an intrinsically disordered structure and enhanced syncytiogenesis (Barry and Duncan 2009). Intrinsically disordered domains are a common feature of proteins that interact with multiple partners (Uversky 2011). Moreover, the endodomain of RRV p14 can also work in *trans* to augment the rate of syncytiogenesis mediated by not only the FAST proteins, but also heterologous fusogens such as influenza HA and the unidentified fusogen(s) responsible for fusion of C2C12 muscle myoblasts (Top, Barry et al. 2009). These two observations suggest the FAST protein endodomains may also indirectly promote syncytiogenesis by recruiting cellular partners involved in a common pathway central to the general process of syncytium formation. A yeast two hybrid screen with the p14 endodomain as bait identified numerous genetic interaction partners, one of which was annexin A1 (Julie Boutilier, Dalhousie University, personal communication).

1.5 Annexin A1 and the annexin superfamily

The annexin superfamily consists of 13 calcium or calcium and phospholipid-binding proteins that share approximately 40-60% sequence similarity and a conserved structure. Annexin family members are associated with numerous physiological activities involving membrane-related biological processes (Gerke, Creutz et al. 2005, Lim and Pervaiz 2007). The annexins are structurally defined as containing a highly conserved signature core comprising four, or eight in the case of annexin 6 (AX6), 70-amino acid alpha-

helical repeats that fold to form a disk-like structure (Fig 1.4). This C-terminal core region is responsible for the Ca^{2+}-binding activity of the annexin superfamily via type II, or annexin-type, Ca^{2+} binding sites (Gerke, Creutz et al. 2005). The coordination of Ca^{2+} ions via interactions with carbonyl and carboxyl groups found on the convex face of the core domain, and with the glycerol backbone of membrane phospholipids results in association of annexins with biological membranes. The concave face of the core domain is thought to face the cytoplasm and may interact with cellular partners.

The defining feature distinguishing annexins from each other is their unique N-terminal region, which is a separate domain that likely interacts with the concave surface of the core in the absence of Ca^{2+}. Upon Ca^{2+} binding, a conformational switch is induced in the C-terminal domain, which displaces the N-terminal peptide away from the core (Rosengarth and Luecke 2003). The N-termini also contain modification sites, and can interact with multiple cellular partners. The best-characterized interactions of annexins with cellular partners involve the binding of AX1 and AX2 to the EF-hand superfamily members S100A11 and S100A10, respectively. It has been shown that the N-terminal 14 amino acids form an amphiphathic helix that fits into a pocket formed by two subunits of the S100 dimer. Two annexin monomers bind to the dimer to generate heterotetramers, which are thought to be involved in bridging and aggregating membranes based on the Ca^{2+}-binding capacity of the annexins and the S100 proteins (Rety, Osterloh et al. 2000, Gerke, Creutz et al. 2005).

The annexins obtained their name due to their membrane aggregating, or 'annexing', activity, which is mediated by N- and/or C-terminal regions in a Ca^{2+}-dependent manner (Drust and Creutz 1988, Wang and Creutz 1994). The connection of two membranes resulting in aggregation has been termed the 'bivalent' activity of annexins, and has been demonstrated for AX1, AX2, AX4, AX6, and AX7 (Gerke, Creutz et al. 2005). Interestingly, whereas the core domains of AX1, AX2 and AX4 have similar Ca^{2+}-binding sensitivities, their ability to bind membranes in a Ca^{2+}-dependent manner is modulated by their N-termini. Full length AX2 is the most sensitive Ca^{2+} sensor, capable of binding membranes at micromolar concentrations of Ca^{2+}, with the affinity for Ca^{2+} incrementally decreasing for AX6, AX4 and AX1, the latter of which is the least sensitive to Ca^{2+} binding (Monastyrskaya, Babiychuk et al. 2007).

Thermodynamic analysis revealed AX1 binds Ca^{2+} ions in a cooperative fashion (Rosengarth, Rosgen et al. 2001). The differential Ca^{2+} binding affinities suggests the annexin superfamily may be a complex, cellular Ca^{2+} concentration-sensing system, conveying messages to the cell through their interacting lipid and protein partners.

In addition, several members of the annexin superfamily have been found to organize lipids into microdomains within membranes. For example, AX6 localizes to cholesterol-rich membrane regions and provides a link to the actin cytoskeleton. AX2 preferentially binds PtdIns(4,5)P2, creating sites for actin cytoskeleton attachment, and plays a role in actin comet tail formation and in the generation of actin-rich pedestals induced by enteropathogenic *E. coli* (Zobiack, Rescher et al. 2002, Hayes, Merrifield et al. 2004, Cornely, Rentero et al. 2011). Additionally, AX1 has been reported to display an affinity for ceramide platforms residing in the plasma membrane, an interaction that seems to be involved in ceramide-driven organization and internalization of membrane associated proteins (Babiychuk, Monastyrskaya et al. 2008).

While multiple annexins are present in the cytoplasm of various cell types, AX1, AX2 and AX5 are also secreted to the extracellular milieu where they exert anti-inflammatory, pro-fibrinolytic, and anti-thrombotic effects, respectively (Ling, Jacovina et al. 2004, Rand, Wu et al. 2004, D'Acquisto, Perretti et al. 2008). The annexins lack signal sequences for directing them to the secretory pathway, and it is not known precisely how they are transported to the outside of the cell (Gerke, Creutz et al. 2005). Of importance to this study, the anti-inflammatory nature of AX1 signalling is stimulated by glucocorticoids, which promotes cleavage of full length AX1 to generate an N-terminal 26 amino acid peptide that binds to the formyl peptide receptor (FPR) present on neutrophils. The FPR is a G-protein coupled receptor that recognizes bacterial formyl-Met-Leu-Phe (fMLP) peptides, which is thought to act as a chemoattractant guiding neutrophils to migrate and extravasate to sites of bacterial infection. Competitive binding of the N-terminal peptide of AX1 to FPR leads to an anti-migratory effect and a decrease in inflammation.(Perretti, Wheller et al. 1995, Walther, Riehemann et al. 2000). Additionally, AX1 knockout mice have a higher inflammatory response than wild-type mice and do not respond to glucocorticoid therapy (Roviezzo, Getting et al. 2002).

Another important membrane-centric role for annexins is membrane repair. AX5 has been shown to localize to sites of membrane rupture and form a two-dimensional lattice network (Bouter, Gounou et al. 2011). The generation of such a structure is thought to provide a physical barrier to stop further expansion of the tear. The involvement of AX1 and AX2 in membrane repair is less clear. They have both been shown to translocate to sites of muscle-cell plasma membrane tears (Lennon, Kho et al. 2003). The membrane repair response (MRR) is dependent on signalling initiated by an influx of extracellular Ca^{2+} (McNeil and Steinhardt 2003). Annexins are known to aggregate membranes in a Ca^{2+}-dependent manner, and are involved in exo- and endocytic events. In addition, AX1 and AX2 have been shown to interact with dysferlin, a C2-domain containing mediator of the membrane repair response (Lennon, Kho et al. 2003). An interesting model for the mechanism of MRR involves annexin-mediated aggregation of a pool of vesicles, which then fuse with each other and with the plasma membrane to 'patch' the bilayer disruption (Lennon, Kho et al. 2003). Interestingly, plasma membrane disruption, created by bacterial streptolysin-O (SLO) perforation, and the ensuing influx of Ca^{2+} has been shown to recruit AX1 and its binding partner S100A11 to sites of damage. Upon recruitment and sequestration of damaged plasma membrane areas, AX1 recruitment resulted in outward blebbing and removal of the injured site leading to cell survival and avoiding death of the SLO treated cell (Babiychuk, Monastyrskaya et al. 2009).

A somewhat difficult distinction between intra- and extracellular localization is posed during the analysis of lipids and proteins involved in membrane repair. All of the extracellularly found annexins (AX1, AX2 and AX5) have been implicated in membrane repair, but their exact roles in this process remain unclear (Lennon, Kho et al. 2003, McNeil, Rescher et al. 2006, Bouter, Gounou et al. 2011). While AX5 is known to bind phosphatidyl serine in the extracellular leaflet, these lipids are also present in high amounts in the cytoplasmic leaflets of the plasma membrane and are therefore found in both monolayers in areas of membrane tears (Yeung, Gilbert et al. 2008, Bouter, Gounou et al. 2011). The precise involvement of intra- and extracellular annexins in plasma membrane repair is therefore still uncertain.

In addition to plasma membrane repair, annexins are implicated in exocytic and endocytic events at the plasma membrane. The first annexin to be characterized was

termed ‘synexin’ (now AX7), and was initially believed to be a membrane fusogen that mediated merger of secretory vesicles of the adrenal medulla, called chromaffin granules. However, electron microscope studies revealed that AX7 was responsible for vesicle aggregation prior to fusion in a Ca^{2+}-dependent manner (Creutz, Pazoles et al. 1978, Creutz, Zaks et al. 1987, Gerke, Creutz et al. 2005). It is currently believed that the fusion of these vesicles is mediated by SNARE proteins and Ca^{2+}-dependent synaptotagmin, and that annexins may promote this process by aggregating vesicle membranes (Gerke, Creutz et al. 2005). Another annexin involved in exocytosis is AX2, which complexes with its partner S100A10 in a heterotetrameric conformation to promote the Ca^{2+}-dependent exocytosis of Weibel-Palade bodies in endothelial cells (Knop, Aareskjold et al. 2004).

The AX2-S100A11 complex is also involved in the endocytic pathway during the formation of endosomes and detachment of multivesicular endosomes from early endosomes, as is AX6 that associates with clathrin coated pits (Kamal, Ying et al. 1998, Mayran, Parton et al. 2003). AX1 has also been identified as playing a role in the inward vesiculation of multivesicular endosomes, where it localized to, and is phosphorylated by, the internalized epidermal growth factor receptor (EGFR) kinase. Phosphorylation of the N-terminus of AX1 renders it more susceptible to N-terminal cleavage leading to altered vesicle bending and aggregation (Futter, Felder et al. 1993, Seemann, Weber et al. 1996, White, Bailey et al. 2006, Grewal and Enrich 2009). The AX1-EGFR interaction also plays a role in signalling from EGFR located at the plasma membrane resulting in activation the ERK pathway to affect an anti-proliferative response (Alldridge and Bryant 2003). Additionally, AX8 has been shown to interact with late endosomes and couple them to the actin network to promote late endosome motility (Goebeler, Poeter et al. 2008). AX1 has also been shown to bundle actin in multiple cell lines and to interact with profilin to modulate actin dynamics (Alvarez-Martinez, Mani et al. 1996, Hayes, Rescher et al. 2004). The ability to interact with actin has also been demonstrated for AX1 during the formation of phagocytic cups, and during later stages of phagocytosis where it co-localized with transient F-actin ‘actin flashing’ (Patel, Ahmad et al. 2011).

This brief summary only touches on the complex web of regulation exerted on cells by the annexin superfamily. Their affinity for cell membranes, calcium and actin makes annexins excellent candidates for the modulation of membrane fusion dynamics.

Interestingly, two novel roles have recently been proposed for extracllular AX1, both of which are involved in the fusion of mouse muscle myoblasts. In one study, AX1 was reported to promote the migration of mouse myoblasts by signalling through formyl peptide receptors, while a second study suggests that AX1 and AX5 may be responsible for the fusion reaction itself (Bizzarro, Fontanella et al. 2012, Leikina, Melikov et al. 2013). The common theme in both studies is the extracellular nature of the mode of action of AX1 during cell fusion, with both reporting a dramatic decrease in fusion upon treatment with AX1 siRNA or with exogenously added anti-AX1 blocking antibody.

1.6 Objectives

The current membrane fusion paradigm has been derived from the study of enveloped virus fusion proteins and SNAREs. Although past studies of the FAST family have focused on their structural and functional characterization, it was not known whether they too followed this canonical pathway. One of the objectives of my Ph.D. research was therefore to determine whether FAST protein-mediated fusion progresses via a hemifusion intermediate. To this end, I employed membrane curvature agents and discovered that RRV p14-mediated fusion is not responsive to curvature agents commonly employed in the membrane fusion field. I was subsequently able to isolate a previously unidentified, membrane shape-sensitive step following the formation of stable fusion pores that is applicable not only to RRV p14-, but also to influenza HA-mediated pore expansion.

The unusually large endodomains of the FAST proteins suggest that they may be involved in recruitment of cellular host factors to the plasma membrane of fusing cells, most likely to promote pore formation or pore expansion. Based on preliminary results obtained from a yeast two-hybrid screen, I chose to investigate the role of AX1 in membrane fusion. I was able to demonstrate that AX1 does indeed interact with p14 in a Ca^{2+}-dependent manner, and that both intracellular Ca^{2+} and intracellular annexin A1 are involved in pore expansion. Furthermore, I discovered that AX1 promotes not only RRV

p14-mediated pore expansion, but also pore expansion following measles F protein-mediated fusion. This is the first demonstration that intracellular AX1 function as a generalized facilitator of pore expansion following cell-cell membrane fusion.

Although these two objectives and their findings seem unrelated, a common theme has emerged. It appears that the expansion of fusion pores during syncytium formation does not depend on the fusogen mediating membrane merger, but rather, on the architecture of the resulting membrane pore and on cellular factors that are likely involved in mediating a cellular response to membrane assault.

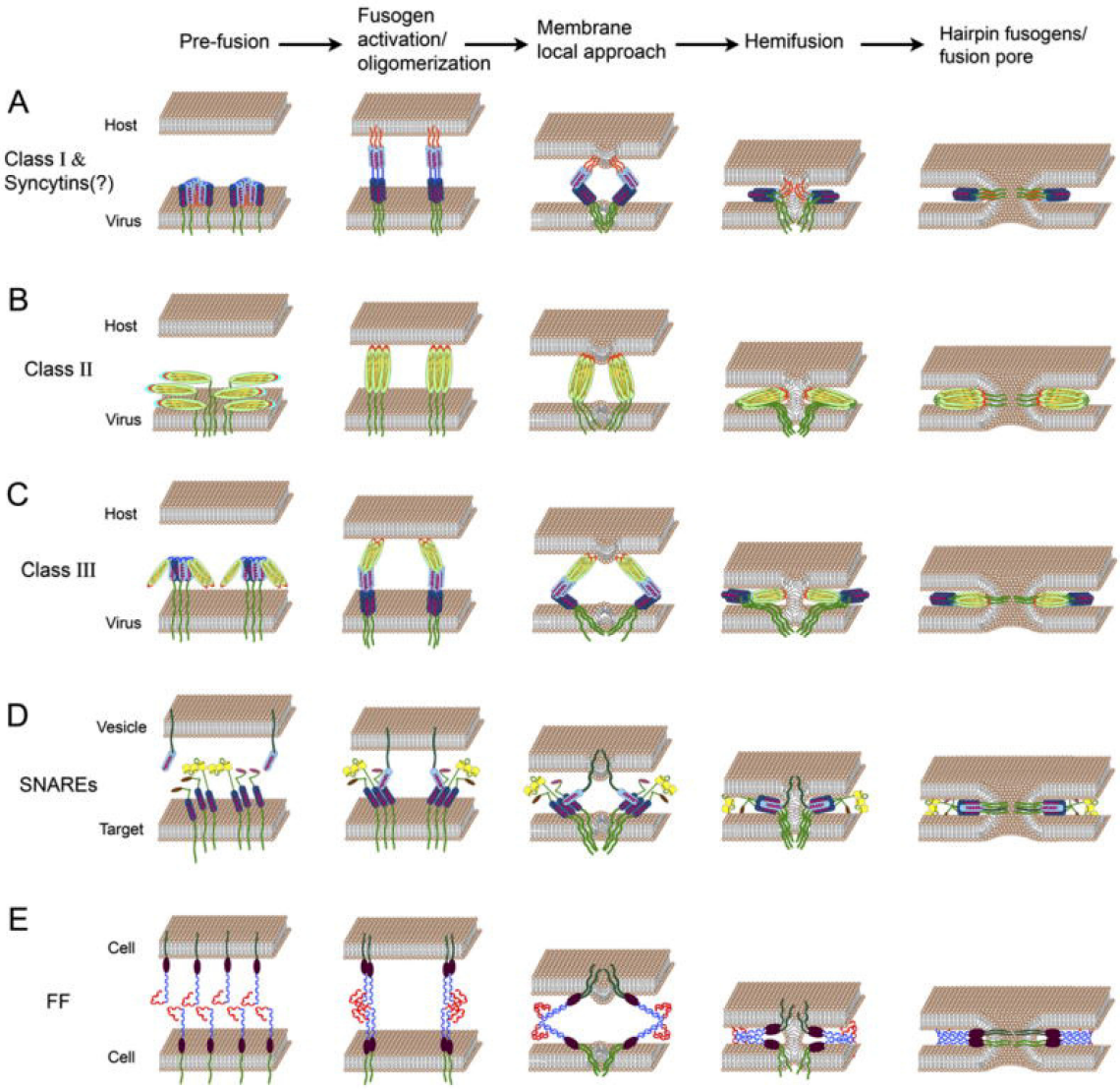
Pre-fusion
Fusogen activation/ oligomerization
Membrane local approach
Hemifusion
Hairpin fusogens/ fusion pore
A
Host
Class I & Syncytins(?)
Virus
B
Host
Class II
Virus
C
Host
Class III
Virus
D
Vesicle
SNAREs
Target
E
Cell
FF
Cell

Figure 1.1 **Current models of membrane merger mediated by enveloped virus class I, II, III proteins, SNARE proteins, and the EFF-1 developmental fusogen.** Adapted from Sapir *et al.* (Sapir, Avinoam et al. 2008). (A) The class I enveloped virus fusogen pre-fusion structure is composed of two α-helical domains containing a buried N-terminal fusion peptide. Activation of the protein leads to the formation of coiled coil domains and exposure of the fusion peptide. Interaction with the host membrane, and folding back of the fusion protein lead to close membrane apposition and lipid mixing. (B) The class II enveloped virus fusogen pre-fusion structure consists of β-sheets oriented tangentially to the plasma membrane, with internal fusion loops at the apex of each monomer. Upon activation and exposure of the fusion loops, the fusion proteins trimerize, interact with the host membrane, and fold back to bring membranes into close membrane apposition. (C) Class III enveloped virus fusogens contain fusion loops similar to class II fusogens but these are attached to α-helices, rather than embedded in β-sheets. (D) SNARE-mediated vesicle fusion mechanism. Binding of three t-SNARE α-helices with a v-SNARE α-helix leads to the zippering of these domains, bringing vesicle and target membranes into close contact. (E) Hypothetical model of FF family-mediated fusion. The FF proteins are thought to dimerize in *cis* membranes, which is followed by *trans* multimerization with FF proteins in adjacent cell membranes. Membrane approach is thought to be mediated by tight zippering of the *trans* FF proteins analogous to SNARE-mediated fusion.

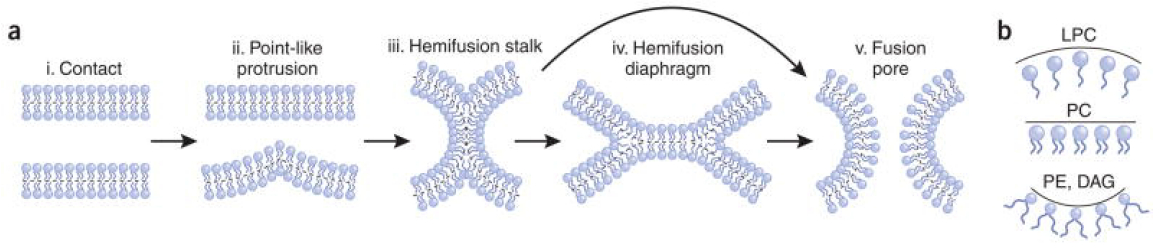

Figure 1.2 **Fusion-through-hemifusion model.** Adapted from Chernomordik *et al.* (Chernomordik and Kozlov 2008). (a) (i) Close membrane apposition leading to membrane approach and (ii) point-like protrusion, or dimples, generated by curvature inducing components of the fusion machinery result in (iii) the formation of a stalk intermediate between donor and target membranes. The stalk is thought to expand laterally to generate (iv) a hemifusion diaphragm, which then ruptures to generate (v) a fusion pore. It is also possible that the stalk structure transitions directly to a fusion pore, as signified by the arrow. (b) Lipid curvature diagram. Positive membrane curvature inducing, cone-shaped agent lysophosphatidylcholine LPC (top), neutral curvature, cylindrically shaped phosphatidylcholine (PC) (middle), and negative curvature inducing, inverse cone-shaped phosphatidylethanolamine (PE) and diacylglycerol (DAG).

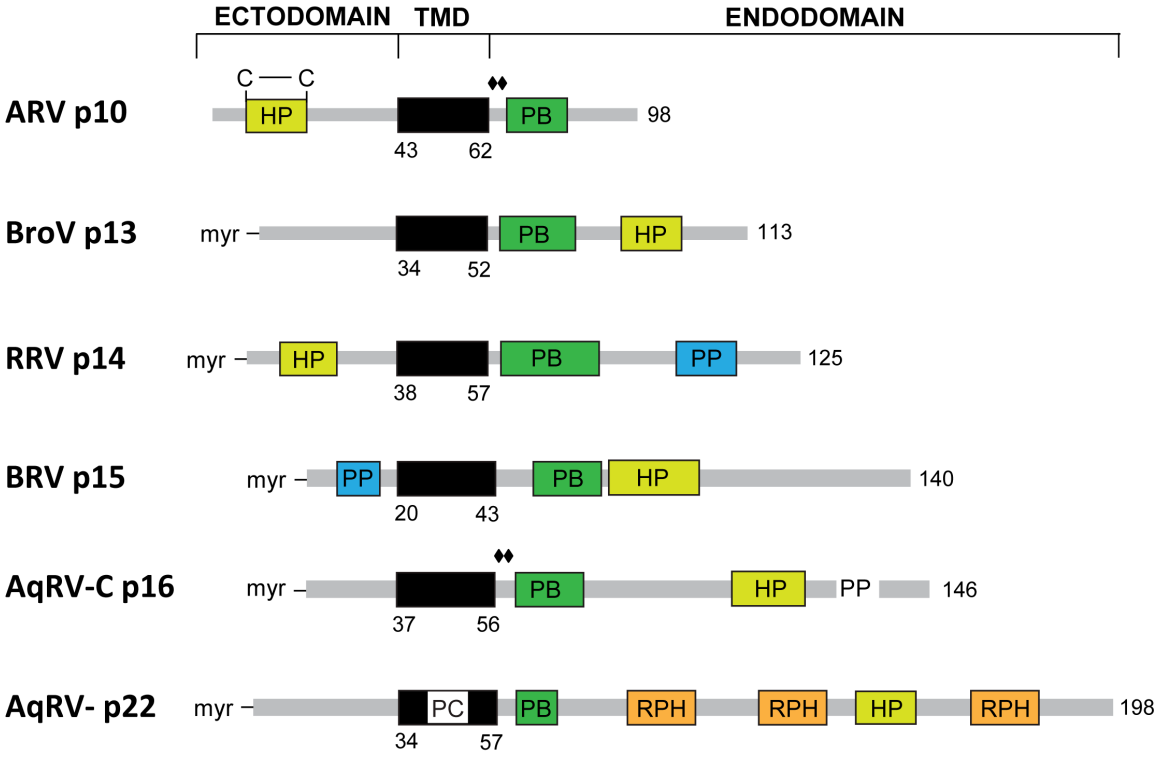

Figure 1.3 **The orthoreovirus-encoded fusion associated small transmembrane (FAST) protein family.** Adapted from Boutilier and Duncan (Boutilier and Duncan 2011). The FAST proteins contain a single transmembrane domain (TMD) spanning amino residues denoted underneath. The avian and Nelson Bay reovirus (ARV and NBV) p10, Broome reovirus (BroV) p13, reptilian reovirus (RRV) p14 and baboon reovirus (BRV) p15, and group-C Aquareovirus (AqRV-C) p16 and group-A Aquareovirus (AqRV) p22 contain a polybasic (PB) region, denoted in green and a hydrophobic patch (HP) denoted in yellow. RRV p14 encodes a poly-proline (PP) helix, denoted in blue, in its endodomain, whereas in BRV p15, it is located in the ectodomain. All FAST proteins are acylated, either by an N-terminal myristic acid (myr), in the case of RRV p14, BRV p15, and AtRV p22, or by two palmitic moieties (diamonds) in the juxtamembranous region of the endodomain of ARV and NBV p10. Additionally, AtRV p22 contains three regions enriched in arginine, proline, and histidine (RPH), denoted in orange. The length of each protein is denoted at the right of each member.

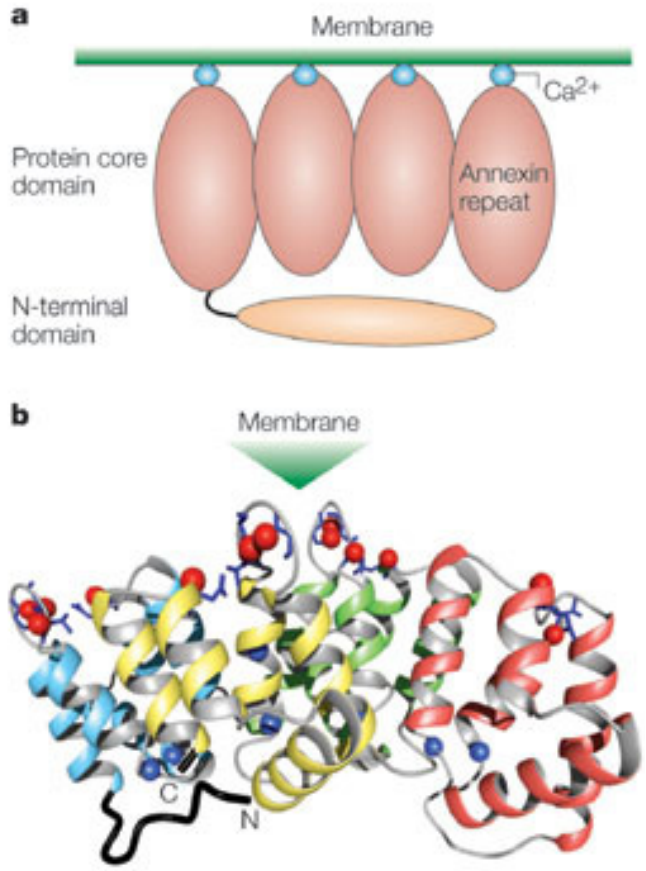

Figure 1.4 **(a) Schematic diagram of Ca^{2+}-bound Annexin A1. (b) Structural model of the annexin core in a Ca^{2+}-bound conformation.** The four annexin repeats are differently coloured, with each containing five α-helices. N and C-termini are coloured in black. Red spheres represent oxygens involved in forming type II Ca^{2+}-binding sites. Blue spheres represent nitrogen atoms of highly conserved residues. Figure adapted from Gerke et *al.* (Gerke, Creutz et al. 2005).

Chapter 2: Materials and Methods

2.1 Cells and antibodies

Cells were grown to 80% confluency and subcultured at a ratio of 1:5 every two days, with the exception of C2C12 mouse muscle myoblasts, which were grown to a confluency of 60% and subcultured 1:20 every two days. All cells were incubated at 37°C and 5% CO_2. Quail muscle fibroblast (QM5) cells were grown in 199 medium containing Earle's salts (Invitrogen) and supplemented with 10% heat-inactivated fetal bovine serum (FBS) (Invitrogen). Vero cells were grown in 199 medium containing Earle's salts and 5% FBS. HT1080 and HEK cells were grown in Dulbecco's modified Eagle medium (DMEM) containing 10% FBS and 25 mM HEPES.

Primary antibodies: Polyclonal anti-RRV p14 rabbit antiserum was described previously (Corcoran and Duncan, 2004). Polyclonal rabbit anti-p14 ecto peptide antibody (amino acids 1-36) was prepared by New England Peptide. Monoclonal anti-annexin A1 antibody was obtained from Santa Cruz Biotechnology, and used in all immunoprecipitation/western blotting experiments. Monoclonal anti-annexin A1 (AX1) and anti-PDI antibody, obtained from Abcam, was used in antibody blocking experiments. Monoclonal anti-FLAG M2 antibody was purchased from Invitrogen. Polyclonal anti-green fluorescent protein (GFP) antibody was purchased from Clonetech. Polyclonal rabbit anti-F anti-COOH #29 and anti-H (eluted) antibodies were obtained from Dr. Ryan Noyce and Dr. Chris Richardson, Dalhousie University. Polyclonal rabbit anti-HER2 antibody was obtained from Dr. Graham Dellaire, Dalhousie University. Secondary antibodies: Polyclonal anti-rabbit HRP and anti-mouse HRP were purchased from Santa Cruz Biotechnologies. Polyclonal anti-rabbit Alexa 647 antibody was purchased from Invitrogen.

2.2 Cloning

Plasmid constructs containing RRV p14, p14 G2A, p14C105, p14C78, p14Δ30, p14Δ36 and BRV p15 have previously been described (Dawe and Duncan 2002, Corcoran and Duncan 2004, Noyce, Taylor et al. 2011). With the exception of measles-

Edmonston strain F and H expressing plasmids, donated by Dr. Ryan Noyce and Dr. Chris Richardson (Dalhousie University), and the HER2 expressing plasmid donated by Dr. Graham Dellaire (Dalhousie University), all translation initiation sites were optimized using a Kozak consensus sequence and cloned into the pcDNA3 expression vector (Invitrogen). The p14 polyproline mutant was generated by cloning of a gene-block generated by IDT Technologies, containing p14 with alanine substitutions of all five prolines in the polyproline region. The p14 alanine substitution mutants (Ala17 and Ala18) were generated by Dr. Deniz Top (presently at Rockefeller University), the p14 polybasic (PB) mutant was generated by Dr. Christopher Barry (currently at University of Wisconsin, Madison), and FLAG-zyxin and FLAG-14-3-3 constructs were generated by Dr. FuiBoon Kai (Dalhousie University). AX1 was cloned from a PC3 human prostate cancer cell line RNA library and cloned into pcDNA3 by Cameron Landry (currently at University of Toronto) and N-terminally tagged with a triple FLAG epitope. Site directed mutagenesis using the Quick Change (Stratagene) method was performed to generate the triple negative FLAG-AX1-DN mutant, which was previously characterized by (McNeil, Rescher et al. 2006). Wild type AX1 was used as a template to generate AX1 N-terminal deletion mutants Δ13, Δ26, and Δ4, where numbers indicate residues deleted from the N-terminus. The FRET pair RRV p14-mCherry and EGFP-AX1 were cloned into pcDNA3 by Tim Key (Dalhousie University). Influenza virus hemagglutinin (HA) and HA G1S and HA G1V mutants were donated by Dr. Judith White (University of Virginia), and re-cloned into pcDNA3 by Dr. Deniz Top.

2.3 Transfections and syncytial indexing

All syncytial indexing studies reported in Chapter 3 were performed in QM5 cells. Cells were seeded in 12-well cluster plates and transfected with 1µg DNA and 3µl Lipofectamine (Invitrogen) per well. Transfection mixes were added to cells in serum-free 199 medium, which was replaced by 199 medium supplemented with 10% FBS at 4 hrs post-transfection. Cells were fixed with methanol and stained using the Wright-Giemsa stain, according to the manufacturer's protocol. Syncytial nuclei were counted in five fields of each well at 20X magnification, and an average count per field was calculated. Images were captured under bright field using a Zeiss Axiovert 200 inverted

microscope and Axiovision software or a Nikon Diaphot TMD microscope. Syncytial indexing studies reported in Chapter 4 were performed in HT1080 and C2C12 cells. HT1080 cells were transfected with 1 ug DNA and 1.5 μl Lipofectamine LTX (Invitrogen) in DMEM supplemented with 10% FBS and 25mM HEPES buffer. Cells were fixed and stained as above. C2C12 cell monolayers grown in 48-well cluster plates were transfected with 0.5 μg DNA and 1.5ul Lipofectamine LTX (Invitrogen) in OptiMEM media (Invitrogen) and the transfection mixes were added to cells growing in DMEM supplemented with 10% FBS and 25 mM HEPES. Cells were fixed and stained as above. HT1080 cell monolayers transfected with RRV p14 were fixed at 12 hrs post-transfection, and those co-transfected with measles H and F were fixed at 22 hrs post-transfection. In experiments where AX1 or dysferlin was knocked down, all DNA transfections were performed at 24 or 36 hrs post-siRNA transfection, as indicated for each experiment. All siRNA sequences employed in this study were composed of four ON-TARGETplus SMARTpool siRNAs purchased from Dharmacon-Thermo Scientific and diluted to stock concentrations of 20 μM. For siRNA transfection, HT1080 cells were seeded in 12-well cluster plates and transfected with 5 μl of siRNA and 2.5 μl DharmaFECT1 in OptiMEM media (Invitrogen), which was added to cells incubated with DMEM growth media supplemented with 10% FBS and 25 mM HEPES. All DNA constructs transfected in co-immunoprecipitation experiments and during stable cell line generation were performed using 1 μl of DNA per 3 μl of polyethyleneimine in serum free DMEM, which was replaced by supplemented growth medium at 6 hrs post transfection.

2.4 Influenza HA activation

QM5 cells transfected with influenza type A HA or HA mutant constructs were incubated for 24 hrs. HA was trypsin cleaved by incubating transfected cells with 10 μg/ml of trypsin in PBS for 1 to 3 min at room temperature. Cells were washed three times with PBS and allowed to recover in growth medium for 5 to 20 min at 37°C, and washed with PBS. Fusion was induced by washing cells with HA activation media, which was composed of medium 199 with Earle's salts, pH 4.8, followed by an incubation period of 1-3 min in activation media at room temperature. The cells were

then washed three times with HBSS and incubated under regular growth conditions to allow for fusion.

2.5 Red-blood cell assay

Fresh human red blood cells (RBCs) were labeled with octadecyl rhodamine B (R18) according to a previously published method (Qiao, Armstrong et al. 1999). Freshly collected RBCs were labeled in 1.75 μg/ml R18 in RPMI media (Invitrogen) (1% hematocrit) for 15 min at room temperature. The labeled cells were then washed with RPMI containing 10% FBS for 20 min at room temperature, and these washes were followed by three quick washes with RPMI containing 10% FBS followed by unsupplemented RPMI. QM5 cells were transfected with HA, HA G1S or HA G1V and activated at 24 hrs post-transfection according to the protocols described above. Labeled RBCs were added to QM5 cells expressing HA, HA mutants, or HA plus RRV p14 and incubated for 10 minutes to allow for attachment. HA fusion (except in cells expressing HA + RRV p14, where HA was used as a binding surrogate) was triggered as described above. Fusion was captured using a Zeiss Axiovert 200 inverted microscope under 40X magnification at 30 min after HA triggering or 4 hrs after the addition of RBCs to p14-expressing cells.

2.6 Pore formation

In Chapter 3, a heterotypic pore formation assay was performed between QM5 cells transfected with GFP and one of RRV p14, BRV p15 or influenza HA, and Vero cells labeled with calcein Red-Orange (Invitrogen) according to the manufacturer's protocol. QM5 cells grown in 6-well cluster plates to a confluency of approximately 15% were co-transfected with GFP and one of the above-mentioned constructs, and incubated for 4 hrs in the case of RRV p14, 6 hrs in the case of BRV p15, and 24 hrs in the case of HA. Confluent T-175 flasks of Vero cells were washed three times with HBSS and labeled with 12.5 μg/ml CellTrace calcein red-orange AM, initially resuspended in 50 μl DMSO then in 8 ml HBSS, then added to flasks and incubated for 30 min at 37°C. Labeled cells were washed three times with HBSS, and regular growth media was added during cell recovery lasting between 2 and 6 hrs. At the times

mentioned above for each fusogen, Vero cells were digested with trypsin and resuspended in 9 ml of medium 199 supplemented with Earle's salts and 10% FBS. Donor QM5 cells were overseeded with labeled target Vero cells by adding 1 ml of the Vero cell suspension to each well. Cells were co-cultured for up to 4 hrs for RRV p14 and 6 hrs for BRV p15, or until the detection of small syncytia containing 4-6 nuclei. In the case of HA-expressing donor cells, target Vero cells were co-cultured for 1 hr and HA activation was performed as described above. Following low-pH treatment, cells were incubated for up to 1 hr prior to fixation, based on the differing kinetics of small syncytium formation between experiments. Co-cultured cells were treated with 0.1% trypsin, resuspended in 250 µl of PBS, and added to 250 µl of 7.4% formaldehyde. Co-fluorescence was detected by flow cytometry using a FACSCalibur apparatus (Becton-Dickinson), and pore formation was scored as the presence of GFP and calcein in a single event, signifying transfer of soluble contents. Each sample was assessed by counting 10 000 events and analyzed using Cell Quest and FCS Express V3 software. In Figure 3.5, and Figure 4.19, the pore formation assay described above was adapted to a homotypic assay employing HT1080 cells. HT1080 cells target cells were added to donor, fusogen-containing HT1080 cells at 4 hrs post-transfection and cells were fixed as described above for flow cytometry. Donor cells were grown either in 6-well plates, as described above for flow cytometry experiments, or on coverslips in 6-well plates for examination of dye transfer by fluorescence microscopy. Methanol-fixed cells grown on coverslips were washed two times with PBS and mounted on microscope slides with ProLong Gold antifade mounting medium (Invitrogen).

2.7 Lysophosphatidylcholine (LPC) and chlorpromazine (CPZ) treatments

Stably transfected HA-expressing QM5 cells were transfected with GFP. Vero cells were added at 6 hrs post transfection and allowed to adhere and spread for 1 hr. A freshly prepared stock of 100 mM myristoyl -lysophosphatidylcholine (LPC) in PBS (Avanti Polar Lipids) was diluted to 100 µM in growth medium supplemented with 5%FBS and added to the heterogeneous cell monolayer for 30 min at 37°C. HA fusion was activated in the presence of 100 µM LPC in 199 growth medium supplemented with Earle's salts and 5% FBS. Cells were recovered in growth medium supplemented with

the lysolipid for 30 min to allow for fusion and syncytium formation. QM5 cells co-transfected with p14 and GFP were treated with 100 μM LPC either prior to the addition of Vero cells, at the time of co-culture, or at 30 and 60 min after the addition of Vero cells in the heterotypic pore formation assay.

In the homotypic HT1080 pore formation assay in Figure 3.5, 100 μM LPC in DMEM growth medium supplemented with 5% FBS and 25 mM HEPES was added to cells at the time of co-culture. In the case of BRV p15 pore expansion arrest, the heterotypic QM5-Vero pore formation assay was employed. Target cells were overseeded onto BRV p15 expressing cells at 6 hrs post-transfection and LPC was added at 1 hr after co-culture. Cells were fixed either at 1 hr or 6 hrs following co-culture and pore formation was analyzed by flow cytometry as described above.

To assess the effects of LPC on syncytium formation, QM5 cells were seeded in 12-well cluster plates and transfected with RRV p14 or influenza HA. In the case of p14-mediated fusion in QM5 cell monolayers, growth medium containing 100 μM LPC was added at 4 hrs post-transfection and cells were fixed at 1 hr intervals for 5 hrs after the addition of lysolipid. In the case of influenza HA-mediated fusion, monolayers of QM5 cells were transfected and fusion was triggered as described above. Growth medium supplemented with 5% FBS and containing 100 μM LPC was added to cells at 10 min after treatment with activation medium, cells were fixed at 30 min following activation. Removal of LPC from treated cells in Figure 3.8 and 3.11 was accomplished by washing cells two times with PBS and adding 199 growth medium to allow for cell recovery.

Chlorpromazine (CPZ) (Sigma) was freshly prepared in PBS to a working concentration of 0. 5μM. In the case of RRV p14 fusion, cells were washed two times with PBS and treated with CPZ for 1 min at room temperature. Cells were then washed two times with PBS and incubated in growth medium supplemented with 10% FBS for 2-4 hrs prior to fixing and syncytial nuclei detection. The effects of CPZ on RRV p14 pore formation were assessed via the heterotypic QM5-Vero assay. Target Vero cells were added to donor p14-expressing QM5 cells at 3 hrs post-transfection and the co-cultured cells were treated with CPZ as described above 1 hr after the addition of Vero cells. In experiments of HA-mediated pore formation, QM5 donor cells were transfected with HA and target Vero cells were added at 24 hrs post-transfection. The co-culture was treated

with activation medium and with CPZ at 4 min after triggering of HA. Fusion was allowed to proceed for 30 min prior to fixation. To assess the effects of CPZ on HA-mediated syncytium formation, QM5 cell monolayers were transfected for 24 hrs, fusion was triggered as above and cells were treated with CPZ at 4 min following the onset of fusion. Syncytia were allowed to progress for 30 min prior to fixation.

To assess the effects of oleic acid (OA) (Sigma) treatment on RRV p14-mediated fusion of QM5 cell monolayers, an OA stock was prepared to a concentration of 100 mM and diluted in growth medium supplemented with 5% FBS to 10 μM and 200 μM concentrations. QM5 cell monolayers were transfected with RRV p14 and treated with OA at 4 hrs post-transfection. Cells were fixed at 8 hrs post-transfection and syncytial nuclei were quantified as described above.

2.8 Fluorescence microscopy

Effects of AX1 siRNA treatment (Figure 4.19) and BAPTA treatment (Figure 4.20) on pore formation were analyzed by fluorescence microscopy via a homotypic HT1080 and Vero assay, respectively. The pore formation assay was performed as described above and transfection protocol volumes were doubled to accommodate the 6-well format. In the case of AX1 knockdown, donor HT1080 cells, grown on coverslips in 6-well cluster plates, were transfected with AX1 siRNA and with RRV p14 and GFP DNA constructs at 24 hrs post-siRNA transfection. Target, untransfected, HT1080 cells were overseeded on top of donor cells at 4 hrs and fixed at 12 hrs post-DNA transfection. Coverslips were mounted as described above and imaged using a Zeiss Axiovert 200 inverted microscope and Axiovision software. In the case of intracellular Ca^{2+} chelation, donor Vero cells, grown on coverslips in 6-well cluster plates, were transfected with RRV p14 and GFP. Donor and target cells were treated separately with BAPTA-AM (Invitrogen) at 4 hrs post-transfection as described below according to the manufacturer's instructions. Briefly, BAPTA-AM was resuspended in DMSO to a 13 mM stock concentration, and further diluted in HBSS to a working concentrations of 20-100 μM. Cells were washed three times in HBSS and incubated with 8 mL of BAPTA-AM at 37°C for 30 min. Cells were then washed three times with HBSS and allowed to recover in standard growth medium. BAPTA-AM-treated target cells were overseeded on top of

donor cells at 5 hrs post transfection, fixed at 10 hrs post-transfection, and analyzed by fluorescence microscopy as above.

2.9 Fluorescence Resonance Energy Transfer (FRET)

HT1080 cell monolayers were seeded on coverslips and co-transfected with C-terminally EGFP-tagged annexin-A1 and C-terminally mCherry-tagged p14. Formaldehyde-fixed cells were imaged at 100x using the Zeiss LSM 510 Meta confocal microscope. The PixFRET Image-J plug-in was used to calculate donor and acceptor spectral bleed-through (SBT) values, as well as normalized FRET (NFRET) levels in each pixel.

Spectral Bleed-Through Determination: Donor and acceptor SBT were determined by acquiring one stack of two images (the FRET and the donor/acceptor images) of cells expressing either only EGFP or mCherry. For each stack, the SBT ratios were mathematically modeled after background subtraction. Donor and acceptor SBT ratios were modeled using exponential relationships with fluorophore intensity after exclusion of aberrant background values at low intensities and the application of a Gaussian blur.

Normalized FRET Calculation: With the SBT values determined, the NFRET for the p14/annexin interaction was calculated. A stack of three images was acquired for each cell imaged: (1) The sensitized emission FRET image (donor excitation, acceptor emission); (2) the donor image (donor excitation, donor emission), and (3) the acceptor image (acceptor excitation, acceptor emission). Background subtraction and Gaussian blur of the donor, acceptor and FRET channels were performed on each image of the stack prior to analysis. The FRET signal was normalized to the square root of the product of the donor and acceptor fluorescence intensities for each pixel of each image. This normalization controlled for variations in fluorophore expression levels between images and provided a quantification of FRET intensity that is comparable between different samples.

NFRET Quantification: Pixel amplitude distributions of the 8-bit NFRET images generated by the PixFRET software were summarized as histograms using a bin width of 0.03906 NFRET units. Each histogram was fit with four Gaussian distributions, and that

with the highest calculated R2 value was used for further analysis. Ten images were acquired for each condition in duplicate (a total of twenty images). The mean NFRET (mNFRET) was determined for each image from the best-fit Gaussian distribution. The grey box highlights the standard deviation of mNFRETs, the + indicates the mean mNFRET, the line is the median mNFRET and the wisker ends indicate the absolute min and max mNFRETs for each condition. The Gaussian-fitted NFRET histograms were also used to calculate the average pixel amplitude from each condition. Error bars represent standard error propagated within and across experiments.

2.10 Scanning electron microscopy

The effects of LPC on cell morphology during RRV p14 mediated fusion were analyzed by scanning electron microscopy (SEM). QM5 cells were grown on coverslips in 12-well cluster plates, and the pore formation assay was performed as above. Coverslips were washed with 0.1 M sodium cacodylate buffer and fixed in 2.5% gluteraldehyde 4 hrs after the addition of target cells. The coverslips were then washed five times with 0.1M sodium cacodylate and incubated in 1% osmium tetroxide in 0.1 M sodium cacodylate for 30 min. The coverslips were again washed five times in 0.1 M sodium cacodylate and dehydrated by sequential 10 min washes in 50, 75, 95, and two 100% ethanol washes. The coverslips were dried using a Polaron E3000 Critical Point Dryer (Quorum Technologies), mounted onto stubs and coated with gold using a Polaron SC7620 Mini Sputter Coater (Quorum Technologies) using double sided carbon tape. The samples were analyzed using a Hitachi S-4700 FEG scanning electron microscope (Hitachi High Technologies).

2.11 Surface expression

HT1080 cells were seeded in 24-well cluster plates and sequentially transfected with AX1 siRNA and RRV p14 G2A at 24 hrs following siRNA transfection. Cells were incubated for 24 hrs at 37°C, washed in cold HBSS blocking buffer containing 1% BSA, and incubated in blocking buffer for 30 min at 4°C. Cells were then incubated with 300 µl of a 1:1000 dilution of anti-p14-ecto antibody diluted in blocking buffer for 1 hr at 4°C, and washed six times with blocking buffer. Cells were then incubated with goat

anti-rabbit Alexa 647 secondary antibody for 1 hr at 4°C in the dark, and washed six times with blocking buffer, followed by two washes with PBS. Antibody-labeled cells were treated with 10 mM EDTA in PBS for 1 min at room temperature and resuspended in 150 μl of cold PBS. The cell suspension was fixed in 150 μl of 7.4% formaldehyde in PBS. Surface expression was assessed by detecting fluorescent cells by flow cytometry using a FACSCalibur (Becton-Dickinson) and analyzed using Cell Quest and FCSExpress software.

2.12 shRNA cell lines

The AX1 gene silencing target sequences were GGTGACCGATCTGAGGACTTT for AX1-sh1, as previously published by Babiychuk et *al*. 2008, as well as CAACTTCGCAGAGTGTTTCAGAAATACA for AX1-sh2**,** ACAGAGAGGAACTGAAGAGAGAT for AX1-sh3 generated by analysis of the AX1 sequence via software available online from Dr. Gregory Hannon, Cold Spring Harbour Laboratories http://cancan.cshl.edu/RNAi_central/RNAi.cgi?type=shRNA (Babiychuk, Monastyrskaya et al. 2008). These sequences were cloned into the Phoenix retroviral expression vector. Phoenix cells were seeded in 10 cm dishes and transfected with shRNA-containing constructs with PEI, as described above. Growth medium was replaced at 24 hrs post-transfection and collected in 15 mL tubes at 48 hrs post-transfection to harvest virus. The samples were centrifuged at 2000xg for 5 min to pellet cell debris. The viral supernatant was filtered using a 0.45 μm filter to remove debris. Polybrene was added to a final concentration of 4 μg/ml, and 1 ml of the virus-containing medium was added to HT1080 cells seeded in 6-well cluster plates. The virus was removed from cells after 24 hrs and transduced cells were treated with media containing 1 ug/ml neomycin (Invitrogen) at 24 hrs after the removal of virus-containing media. Cells were grown under these selective conditions for three days, with periodic replacement of the medium.

2.13 Co-immunoprecipitation

HEK cells were seeded in 10 cm dishes and co-transfected with FLAG-AX1 and RRV p14 or measles H and F constructs as described above. Cells were harvested by

scraping at 12-16 hrs post-transfection and centrifuged at 2000xg. Cell pellets were treated with 1 ml of lysis buffer containing 20 mM Tris-HCl, 137 mM NaCl, 10% glycerol, 1% NP-40, 5 mM $CaCl_2$ and a protease inhibitor cocktail. $CaCl_2$ concentrations were decreased in titration experiments and NP-40 concentration was increased to 2% in Figure 4.14. Cells were subjected to mechanical lysis by 10 passages through a 30 gauge needle and incubated at 4°C for 30 min. The samples were then centrifuged at 14 000 RPM at 4°C using a benchtop Eppendorf centrifuge to remove remaining cellular debris. The supernatants were transferred to chilled tubes and incubated with 2 μl of anti-FLAG antibody at 4°C for 12-14 hrs. Samples used in Figure 4.14 were further centrifuged at 100 000xg, transferred to fresh tubes and treated with 2 μl of anti-FLAG antibody at 4°C for 12-14 hrs in an end-over-end rotator. Dynabeads (Invitrogen) were washed in lysis buffer and 10 ul of 50% bead-containing slurry in lysis buffer was added to each sample and incubated in an end-over-end rotator. Beads were subjected to five washes with 1 ml of cold lysis buffer, transferred to new tubes, eluted with 60 μl boiling sample buffer and analyzed by Western blotting.

2.14 Intracellular Ca^{2+} modulation

The effects of Ca^{2+} chelators BAPTA-AM and EGTA-AM were assessed by fluorescence microscopy, as described above, as well as via a standard syncytial indexing assay in HT1080 cells and a homotypic Vero cell pore formation assay. HT1080 cells were seeded in 12-well cluster plates and transfected with RRV p14 or measles F and H. BAPTA-AM was prepared as described above. HT1080 cells were washed twice with HBSS and incubated with 20-100 μM BAPTA-AM in HBSS for 30 min at 37°C. Cells were washed with HBSS and incubated in standard growth medium for 4 hrs in the case of RRV p14, and 20 hrs in the case of measles F and H, after the addition of BAPTA. Cells were fixed and syncytial nuclei were indexed as described above. In FRET analysis of calcium chelation effects on AX1 and RRV p14 interaction, HT1080 cells were seeded on coverslips and transfected with RRV p14-GFP and AX1-mCherry constructs and BAPTA-AM was added as above, cells were fixed at 24 hrs post-transfection, mounted for fluorescence microscopy as above, and analyzed by confocal microscopy on a LSM Meta 510 microscope. RRV p14-mediated pore formation was detected in a homotypic

Vero pore forming assay as described above. Donor and target Vero cells were treated with BAPTA-AM prior to transfer of target cells to donor cells, as described in section 2.8. Target cells were overseeded on top of p14-expressing donor cells at 5 hrs post-transfection and processed for flow cytometry analysis at 10 hrs post-transfection. EGTA-AM (Invitrogen) was resuspended to a stock concentration of 100 mM and diluted to 10-200 μM in HBSS. HT1080 cells were seeded in 12-well cluster plates and transfected with RRV p14. At 4 hrs post-transfection, cells were washed three times with HBSS and incubated with the above-mentioned concentrations of EGTA-AM at 37°C for 30 min. The cells were then washed three times with HBSS and incubated with standard growth medium and fixed at 12 hrs post-transfection.

HT1080 cell monolayers were seeded, transfected with RRV p14, and treated with BAPTA-AM as above. Ionomycin (Invitrogen) was resuspended in PBS to a 0.5 M stock concentration, and diluted in HBSS to 1 mM. At 8 hrs post-transfection, cells were washed twice with PBS and incubated with 1 mM ionomycin in standard growth medium. Cells were fixed at 14 hrs post-transfection.

2.15 Antibody inhibition

HT1080 cells and C2C12 cells were seeded in 48-well cluster plates and transfected with RRV p14. At 2 hrs post-transfection, transfected cells were treated with 250 μl of 1:10 (100 μg/ml), 1:25 (40 μg/ml), and 1:50 (20 μg/ml) anti-AX1 or anti PDI antibody in growth medium. Cell monolayers were fixed at 14 hrs post-transfection in the case of HT1080 and 12 hrs post-transfection in the case of C2C12 cells, and syncytial nuclei were indexed as described above. In the case of antibody inhibition of differentiating C2C12 cells, the experiment was performed according to a previously published protocol (Leikina, Melikov et al. 2013). Briefly, cells were seeded in 48-well cluster plates and differentiation was induced by incubating cells with DMEM supplemented with 5% horse serum at 24 hrs post-seeding. Differentiation medium containing 100 μg/ml anti-AX1 or anti-PDI antibody was added to cells at 51 hrs after the onset of differentiation. Cells were incubated with 250 μl of the antibody-containing media for 16 hrs, fixed and syncytial nuclei were indexed as described above.

CHAPTER 3: Effects of plasma membrane curvature on viral fusogen-mediated syncytium formation

3.1 Introduction

Membrane fusion is involved in a vast array of biological processes ranging from fertilization and tissue formation, to intracellular membrane trafficking and virus entry into host cells (Jahn, Lang et al. 2003, Chernomordik and Kozlov 2005, Earp, Delos et al. 2005, Hernandez, Stein et al. 2012). In spite of the abundance of biological fusion processes, little is known about the cellular fusion machinery mediating this process, and most of our current understanding of membrane merger is derived from the study of enveloped virus fusion proteins. It is generally accepted that membrane fusion involves the mixing of lipids and resident protein components of two bilayers undergoing fusion, as well as the mixing of volumes originally bound by the separate membranes (Chernomordik and Kozlov 2005). The nature and order of intermediate steps linking these events has been the subject of multiple studies, which have attempted to delineate a general pathway based mostly on the study of enveloped virus fusogens. This canonical membrane fusion model has been defined as the 'fusion-through-hemifusion pathway'. The first step of this process involves the merger and free transfer of lipids between the outer phospholipid monolayers of apposed membrane bilayers resulting in the formation of a fusion stalk structure; this initial step is termed hemifusion, and is the least energy intensive step during the reaction. The lipid stalk is thought to elongate into a hemifusion diaphragm, which bursts, thus allowing for the intermixing of lipids found in the distal leaflets of the bilayers, as well as for the transfer of soluble contents through a nascent fusion pore (Chernomordik and Kozlov 2005). Pore formation is believed to be the most energy-demanding step during the entire fusion reaction. Small, transient fusion pores may be reversible but pore expansion generates a stable pore (Chernomordik and Kozlov 2003).

The fusion-through-hemifusion hypothesis has been derived from mathematical modeling of phospholipid membrane merger, experimental evidence based on the manipulation of outer and/or inner leaflet shape, and studies comparing the movement of

lipid probes in the presence of wild type and mutant fusogens such as influenza hemagglutinin (HA) (Chernomordik, Leikina et al. 1997, Chernomordik, Frolov et al. 1998, Russell, Jardetzky et al. 2001, Jahn and Grubmuller 2002, Reese and Mayer 2005, Risselada and Grubmuller 2012). Insertion of membrane bending compounds such as chlorpromazine (CPZ), lysophosphatidylcholine (LPC), or oleic acid (OA) have been used to investigate the pathway of membrane fusion. The inverse cone shape of LPC, a lipid composed of a large polar head group and a single hydrocarbon chain, has made it an attractive tool for alterating lipid bilayer curvature. When inserted into the outer membrane of a lipid bilayer, LPC promotes positive curvature, and is thought to inhibit the formation of a fusion stalk; conversely, when inserted into the inner, lumenal leaflet, the presence of LPC promotes the resolution of a hemifusion diaphragm and subsequent pore formation. This compound has been employed in studies dissecting the fusion reaction of enveloped viruses with both liposomes and red blood cells (RBCs), RBCs to cells with ectopically expressed viral fusogens, SNARE-mediated vesicle fusion, and the formation of mouse muscle myotubes (Melikyan, White et al. 1995, Chernomordik, Leikina et al. 1997, Reese and Mayer 2005, Leikina, Melikov et al. 2013). CPZ is a cationic amphipath that preferentially inserts into negatively charged inner leaflets of plasma membranes (similar to LPC inserted in the inner leaflet), to generate a micelle-like curvature and break the hemifusion diaphragm, thus promoting pore formation and expansion (Melikyan, Brener et al. 1997, Qiao, Armstrong et al. 1999, Zaitseva, Mittal et al. 2005). Lastly, OA acts in a manner opposite to LPC when inserted into outer bilayer leaflets, and is thought to promote negative curvature and expedite the rupture of hemifusion diaphragm structures (Leikina and Chernomordik 2000, Stiasny and Heinz 2004).

The non-enveloped orthoreovirus fusion-associated small transmembrane (FAST) proteins are the smallest known membrane fusion proteins, ranging from 10 to 22 kDa in size. Unlike other known viral fusion proteins, the FAST proteins are non-structural and therefore not involved in virus entry but rather in cell-to-cell fusion and syncytium formation following infection or transfection. The ectodomains of the FAST proteins are unusually small, ranging from 20 to 40 amino acids and both RRV p14 and BRV p15 are N-terminally modified by a myristoyl moiety (Corcoran and Duncan 2004, Dawe,

Corcoran et al. 2005). Most fusion processes are thought to progress through the paradigmatic hemifusion stalk and are driven by mechanical energy derived from dramatic conformational changes of the multimeric fusion machines. The currently available hemifusion assays, which have been used to study the transfer of lipidic dyes from donor to target membranes, have not been amenable to detecting this hemifusion intermediate during RRV p14-mediated membrane merger (Clancy, Barry et al. 2010). This has been largely due to the differences in the timing of the onset of fusion, where the inability to trigger FAST fusion results in a delay in membrane merger and subsequent redistribution of lipidic dyes to all cellular membranes (Clancy, Barry et al. 2010).

To investigate whether, like all other known fusion processes, the FAST protein-mediated membrane fusion progresses via a hemifusion intermediate, I employed the above-mentioned assays including RBC to donor cell fusion, as well as treatment of fusing cells with LPC, CPZ, and OA. I was able to show that, while HA readily fuses target RBCs to donor cells as previously reported, RRV p14 does not fuse membranes in this system. Furthermore, I was able to demonstrate that manipulation of membrane curvature with the above-mentioned reagents (LPC, CPZ and OA) had no effect on RRV p14-mediated membrane fusion and stable pore formation, suggesting that a hemifusion intermediate is either too unstable to be detected, or that the RRV p14-mediated lipid mixing stage does not involve such a highly ordered lipid structure. Interestingly, treatment of cells expressing BRV p15 with LPC, resulted in a clear abrogation of soluble dye transfer, indicating that fusion mediated by this member of the FAST protein family does include a lysolipid-sensitive stage and may proceed via a hemifusion intermediate that may be similar to that of enveloped virus- and SNARE-mediated membrane merger. In addition, I completed a temporal analysis of FAST protein- as well as HA-mediated pore formation (soluble dye transfer) and pore expansion (syncytium formation), and subsequently analyzed the role of LPC on the rates of pore expansion during RRV p14- and HA-mediated fusion. While LPC did not inhibit FAST protein mediated pore formation, it did inhibit pore expansion resulting in a reversible ‘stalled pore’ phenotype. By adding LPC following the completion of pore formation but prior to syncytiogenesis, I was also able to capture an HA-mediated ‘stalled pore’ phenotype. These results suggest that while RRV p14-mediated fusion may progress through a less ordered

intermediate than that suggested for type I and II fusion proteins, the resolved pore structure is likely similar and can be maintained through the promotion of positive curvature. These results further suggest that the resolution of a negative membrane curvature in the outer leaflet ring that surrounds a stable pore is an essential step in pore expansion leading to syncytiogenesis.

3.2 Results

3.2.1 RRV p14 does not promote membrane fusion with RBCs.

In light of the paradigmatic fusion-through-hemifusion model, derived mainly through the study of enveloped virus fusogens and SNARE proteins, we undertook a comprehensive approach to determine whether the FAST protein family-mediated membrane fusion proceeds via the same pathway. Several key findings that have been the cornerstones of this model have emerged from tracking the transfer of labeled lipids during fusion of enveloped viruses to target red blood cells (RBCs), or through the fusion of RBCs to donor transfected cells (Melikyan, White et al. 1995, Qiao, Armstrong et al. 1999).

Mirroring canonical studies that employed labeled RBCs to detect hemifusion, I transfected donor quail muscle fibroblasts (QM5) with the FAST fusogen RRV p14, EGFP, and a binding surrogate HA0. The influenza virus HA0 protein retains receptor-binding activity, but in the absence of trypsin cleavage to generate HA1 and HA2 is non-fusogenic (Qiao, Armstrong et al. 1999). Since the FAST proteins lack receptor-binding activity (Salsman, Top et al. 2008), the uncleaved HA0 was included to ensure efficient binding of RBCs to p14-expressing donor cells. These donor cells were co-cultured with target RBCs labeled with R18 lipid dye. As a positive control for dye transfer, I used the well characterized, trypsin-activated wild type HA1/2, as well as HA G1S, a hemifusion permissive but pore formation deficient mutant, and HA G1V, where the mutation from glycine to valine at position one renders the protein incapable of mediating lipid mixing (Qiao, Armstrong et al. 1999).

As expected, membrane fusion, visualized as transfer of red lipidic dye, pore formation, visualized by transfer of GFP to fused cells cells, and syncytiogenesis were detected when the wild type HA construct was used to mediate the reaction (Fig. 3.1). In

addition, I detected the expected phenotype for the HA G1S mutant, which was capable of inducing the transfer of the lipidic dye, but not pore formation or expansion; and the HA G1V mutant, which remained fusion-dead, with no transfer of fluorescent markers detected. To my surprise, although p14 has been reported to fuse multiple cell types, it was not able to induce lipid transfer between transfected donor cells and RBCs (Fig. 3.1). Due to the relatively small size of the p14 ectodomain, I hypothesized that the distance between the fusion peptide of p14 and the target RBC membrane is too great to induce lipid mixing. To eliminate this possibility, I co-transfected p14 with HA G1V as a surrogate binding partner. The close apposition of membranes was induced by low pH triggering a conformational change of G1V; in this scenario, RRV p14 was, in theory, much closer to the target membrane. As in the previous case, no fusion was detected between the donor QM5 cells and target RBCs (data not shown).

3.2.2 Chlorpromazine does not detect a hemifusion intermediate during RRV p14-mediated cell-cell fusion.

An indirect method often employed in exploring the lipid mixing and pore formation steps during membrane fusion takes advantage of the pharmacological reagent chlorpromazine (CPZ). With a preferential affinity for the negative charge of inner plasma membrane leaflets, CPZ readily crosses lipid bilayers, inserts into the inner monolayer, and promotes negative curvature of the cytoplasm-facing membrane. The introduction of negative curvature to the inner leaflet of a bilayer that is undergoing hemifusion is thought to drive the reaction to favour pore formation.

Based on previous reports of CPZ treatment during HA-mediated membrane fusion, I hypothesized that if RRV p14 orchestrates membrane merger via a hemifusion intermediate, addition of CPZ would enhance the transition from a hemifused state to pore formation. To detect pore formation, I used a heterotypic fusion assay based on the transfer of fluorescent dye from donor to target cells to generate doubly labeled fused cells, that are readily detected by flow cytometry. Analogous to the RBC experiment, wild type HA, HA G1S and HA G1V were used as positive controls. As expected, CPZ treatment of HA and HA G1S-transfected cells resulted in an increase in syncytium formation, as seen via Giemsa staining in Fig. 3.2A. An increase in pore formation

mediated by HA and HA G1S was also detected by FACS as seen in the scatter plots in Fig. 3.2B. Surprisingly, RRV p14-mediated pore formation, or the subsequent formation of syncytia did not increase in the presence of CPZ, suggesting that p14-mediated membrane merger is not sensitive to membrane deformation caused by CPZ addition.

It has previously been reported that membrane fusion can be arrested at the sequential steps of hemifusion or pore formation by titration of the fusion protein mediating the merger (Danieli, Pelletier et al. 1996, Zaitseva, Mittal et al. 2005). To eliminate the possibility that CPZ had no effect in our p14 cell-to-cell fusion system due to fusogen oversaturation, we titrated the amount of transfected HA or p14 prior to CPZ treatment. This experiment was performed by Eileen Clancy. It was clear that CPZ addition to cells expressing wild type HA nearly doubled the extent of pore formation as seen in the scatter plots in Fig. 3.3A and corresponding graph in Fig. 3.3B. Conversely, at all concentrations of transfected RRV p14, CPZ treatment had no detectable effect on the extent of pore formation, as seen in Fig. 3.3C and D.

3.2.3 Lysophosphatidylcholine does not affect p14-mediated pore formation.

In addition to CPZ treatment, much of our understanding of fusion intermediates has been gained through the manipulation of outer leaflet bilayer shape by treatment of enveloped viruses, liposomes, or donor cells expressing enveloped virus fusogens, with lysophosphatidylcholine (LPC) (Chernomordik, Leikina et al. 1997, Chernomordik, Frolov et al. 1998). Similarly to CPZ, LPC also induces negative curvature, however, it preferentially inserts into the outer leaflet of the plasma membrane bilayer. Effectively, CPZ and LPC incorporation have opposite effects on membrane shape, and on the progression of membrane fusion. Whereas CPZ promotes rupture of the hemifusion pore, LPC incorporation into outer leaflets prevents the formation of a fusion stalk, and has been reported to effectively block hemifusion. In this study, using the canonical influenza HA fusogen as a control, I examined the effects of LPC treatment on RRV p14 mediated fusion in an effort to isolate an LPC-sensitive, pre-pore formation, stage of membrane fusion.

Our group reported that assays employing fluorescent lipid markers are not amenable to the study of RRV p14-mediated fusion reaction due to the confounding

effects of plasma membrane endocytosis during the relatively long fusion time frame of these non-triggered proteins (Clancy, Barry et al. 2010). In the absence of a robust and reliable hemifusion assay, we assessed the effects of LPC treatment on RRV p14-mediated fusion by examining the extent of pore formation in the presence and absence of LPC. To do so, I initially set out to determine the time frame of the onset of pore formation in the heterotypic QM5-Vero cell-to-cell fusion assay. Donor QM5 cells were transfected with GFP and p14, whereas target Vero cells were labeled with the fluorescent cytoplasmic marker calcein. At 4 hrs post-transfection, Vero cells were lifted and co-cultured with the donor cells. Pore formation was assessed using flow cytometry to detect the transfer of calcein to GFP-expressing cells at one hour-post transfer of Vero cells and then at one hour intervals until four hours post-seeding (Fig. 3.4A). I found that fairly extensive pore formation occurred during the first hour of co-culture, with an average 15-20% increase per hour during the following intervals. To test whether treatment of cells with LPC was able to inhibit pore formation, I pre-incubated both cell populations with 100 μM myristoyl LPC, which was present at time of addition of target to donor cells (0 min), or LPC was added 30 or 60 min after the addition of target cells. Pore formation was assessed after 4 hrs of co-culture. Pore formation was decreased by ~30% when cells were pre-treated with LPC prior to and during, co-incubation (Fig. 3.4B). However, it should be noted that some cytotoxicity occurred when trypsinized target Vero cells were treated with LPC prior to attachment, and that the seeded cells did not attach as well as those seeded prior to LPC treatment (Fig. 3.4B). A slight reduction in pore formation (~25%) was also observed when LPC was added 30 min after addition of target cells, but no significant difference was detected if LPC addition was delayed until 60 min after target cell addition (Fig. 3.4B). Overall, these results suggest that LPC treatment of cell membranes does not inhibit RRV p14-mediated membrane merger or pore formation.

To ensure that LPC did indeed inhibit membrane fusion mediated by an alternate fusogen, this assay was replicated using HA as the cell-to-cell fusion protein. Treating cells with LPC prior to triggering membrane fusion inhibited HA-mediated pore formation by ~80%, while similar treatment of p14-transfected cells had no effect on p14-mediated pore formation (Fig. 3.4C). The lack of LPC-mediated fusion arrest

observed during RRV p14 cell-to-cell fusion was therefore not due to deficiencies in the LPC inhibition assay. Similar to the previously described CPZ treatment controls, Eileen Clancy also titrated the amount of p14 in order to avoid oversaturation effects. Treatment with LPC did not inhibit p14-mediated pore formation when cells were transfected with as little as 0.05 μg of DNA (Fig. 3.4C). These results suggested that the p14-mediated membrane fusion pathway may not involve a hemifusion intermediate, or conversely, that this intermediate does not conform to the geometry of an LPC-sensitive stalk or is too short-lived for LPC to exert an observable effect.

Finally, I developed a homotypic pore formation assay to directly image the transfer of cytoplasmic markers in the presence and absence of LPC by fluorescence microscopy. Donor HT1080 cells, co-transfected with p14 and GFP, fused with the HT1080 target cell population labeled with calcein, and formed syncytia in the absence of LPC (Fig. 3.5). LPC had no effect on the transfer of fluorescent cytoplasmic markers between cells, confirming the FACS data that LPC does not inhibit p14-mediated pore formation. Surprisingly, the co-fluorescent cells (yellow cells in Fig. 3.5) were mono-nucleated cells, either immediately adjacent to each other or connected by long, thin cytoplasmic extensions, but not syncytia. This finding suggested that, although p14-mediated pore formation occurs irrespective of the presence or absence of LPC, pore expansion may be blocked in the presence of the lysolipid.

Despite the many similarities that tie the reovirus FAST proteins into one family, these fusogens also greatly differ from each other in the topological arrangement of their structural motifs. For example, whereas the HP of RRV p14 is found in its ectodomain, this motif is located in the cytoplasm of BRV p15. Conversely, whereas a polyproline region is internal in the case of RRV p14, it is found on the outside of the cells in the case of BRV p15. In addition, unlike RRV p14, the polyproline fusion peptide of BRV p15 has been shown to exhibit a substantial lag time prior to lipid mixing in a liposome-to-liposome lipid-mixing assay (Top, Read et al. 2012). Although an RRV p14 hemifusion intermediate could not be detected following CPZ or LPC treatment, I hypothesized that the long BRV p15-induced lag phase prior to membrane fusion may allow for the isolation of a pre-fusion intermediate by means of bilayer deformation. I therefore analyzed the pore formation kinetics of BRV p15 in the presence and absence of LPC,

added at the time of addition of target Vero cells. BRV p15 is a less robust fusogen than RRV p14, therefore, the pore formation experiment was extended from four to six hours post-addition of target cells. A small difference in soluble content transfer was detected after one hour of co-incubation, and a much larger LPC-induced decrease was observed after six hours (Fig. 3.6). This surprising result suggested that, unlike RRV p14, but similar to all other known membrane fusogens, p15 pore formation could be arrested at a pre pore-formation stage during membrane fusion.

3.2.4 Lysophosphadtidylcholine reversibly inhibits RRV p14-mediated pore expansion.

The unexpected finding that LPC treatment does not arrest RRV p14-mediated fusion at a pre pore-formation stage, but seems to abrogate the pore expansion needed to generate syncytia (Fig. 3.5), warranted further investigation. As previously determined in Fig. 3.4, p14 pore formation is substantial within 1 hr after the addition of target Vero cells to donor, fusogen-transfected, QM5 cells, and continues to gradually increase over four or more hrs. Few if any syncytia are evident within 1 hr, but begin to appear shortly thereafter as pore formation continues. Taking advantage of this finding, LPC was introduced to donor and target cells at 1 hr of co-culture and the extent of syncytiogenesis was assessed at 60 min increments for five hours. As seen in Fig. 3.7B, the presence of LPC abrogated syncytium formation for the duration of the experiment. The effects of differing levels of RRV p14 expression on the sensitivity to LPC pore expansion block were also examined by titrating transfected RRV p14 DNA amounts. Addition of the lysolipid inhibited pore expansion at all DNA concentrations tested, indicating a robust pore expansion arrest at saturating levels of fusogen expression (Fig. 3.7A).

Previous studies have reported that myristoyl LPC-mediated hemifusion arrest is reversible, with full fusion ensuing upon removal of the lysolipid from the culture medium. In this study, I was able to replicate these results in the context of RRV p14-mediated pore expansion. LPC was added to cells at 4 hrs post-transfection, a time point at which pore formation is well established but syncytia have not yet appeared, cells were then incubated with LPC for 4 hrs at which time the LPC was removed and cells were incubated for an additional 6 hrs to see if syncytium formation occurred (Fig. 3.8A).

Interestingly, the extent of RRV p14-mediated syncytium formation was equivalent after 6 hrs, whether cells were previously treated with LPC or not (Fig. 3.8A).

To further characterize this finding, I performed a time course analysis of syncytium formation in the presence and absence of LPC. In this experiment monolayers of QM5 cells were transfected, LPC was added at 4 hrs post-transfection, and syncytium formation was monitored at hourly intervals for the next 4 hrs. To assess the rate of syncytium formation after an LPC-induced pore expansion arrest, I removed the lysolipid from the culture medium after 3 hrs of incubation. As previously observed (Fig. 3.7), the presence of LPC eliminated syncytium formation (Fig. 3.8B). Interestingly, following removal of LPC the rate of syncytiogenesis was much more rapid than in cells not treated with LPC. Within 1 hr after LPC removal, the extent of syncytium formation was equivalent with that observed in untreated cells (Fig. 3.8B). This finding suggests that when cells were allowed to continue to form pores under expansion-limiting conditions, subsequent removal of the pore expansion block results in rapid pore expansion and pore merger to generate syncytia.

3.2.5 Oleic acid has no effect on p14-mediated syncytium formation.

Several studies have reported that treatment of membranes with oleic acid can be employed to counteract the effects of LPC on membrane deformation, and, in some cases, to expedite the membrane fusion reaction (Chernomordik, Leikina et al. 1997, Stiasny and Heinz 2004). I adapted this approach to the present study by either pre-treating RRV p14-expressing cells with oleic acid prior to adding LPC, or by adding both LPC and oleic acid to cells at the same time. A range of oleic acid concentrations was tested, with the lowest and highest treatments reported in Fig. 3.9. In my study, oleic acid at concentrations between 10 and 200 μM had no effect on either increasing syncytium formation when used alone, or on counteracting the LPC effect of pore expansion arrest.

3.2.6 Lysophosphadtidylcholine has dramatic effects on cell morphology.

The abrogation of hemifusion via LPC treatment is most effective at concentrations that approach cytotoxic levels (personal communication, Evgenia Leikina, National Institute of Health, USA). This was also the case with RRV p14-mediated pore expansion arrest observed in this study. In addition, LPC treatment has generally been

employed in studies of enveloped viruses, liposomes, or SNARE vesicles and synthetic lipid bilayers, and its effects on live cell membranes have not been well characterized. To explore the effects of lysolipid on cellular plasma membranes in our study, I analyzed LPC-treated cells by using the standard pore formation protocol and analyzing cell structures by scanning electron microscopy (SEM). LPC was added to cells 1 hr after addition of the target cells. Comparison of cell membranes in the presence and absence of the lysolipid revealed striking differences in local membrane morphology, as well as overall cell shape (Fig 3.10). Cell monolayers treated with LPC had lots of rounded cells, and the flattened cells exhibited multiple membrane projections from the cell body. I assume that LPC treatment prevented many of the target Vero cells from spreading following attachment and fusion with donor QM5 cells, and that the flattened cells with membrane protrusions were most likely the adhered donor QM5 cells.

3.2.7 Lysophosphadtidylcholine reversibly inhibits influenza HA-mediated pore expansion.

Lastly, to determine whether the effect of LPC-mediated pore expansion arrest was an RRV p14-specific phenomenon, or whether we had isolated a general, post-fusion, membrane shape-sensitive intermediate during syncytium formation, I investigated the role of LPC in the context of influenza HA-mediated syncytium formation. Analogous to the RRV p14 study, a comprehensive analysis of HA-mediated pore formation was undertaken. FACS analysis of soluble dye transfer between donor and target cells revealed that pore formation was detectable as early as 5 min after triggering fusion with low pH, and continued to increase for the duration of the assay (40 min) (Fig. 3.11A). Due to the onset of syncytiogenesis at approximately 15 min post-pH treatment, I chose to add LPC 10 min after triggering HA-mediated membrane fusion to ensure that a significant level of pore formation had taken place with no visible syncytia present. The addition of lysolipid at this time resulted in the inhibition of HA-mediated pore expansion and syncytium formation (Fig 3.11B). In addition, and similar to the LPC-induced p14 pore expansion arrest induced by LPC, the inhibition of pore expansion following HA-mediated membrane fusion was also shown to be reversible, with

syncytium formation rapidly returning to untreated cell levels after removal of LPC from the medium (Fig. 3.11C).

3.3 Discussion

3.3.1 The stability of the FAST-mediated membrane fusion lipid intermediate may be dependent on the specific protein family member.

The 'fusion-through-hemifusion' model is currently thought to represent a universal pathway initiated and catalyzed by all known fusogenic protein machinery. Enveloped virus fusogens, as well as the SNARE machinery and even the cellular EFF-1 and AFF-1 membrane fusion proteins are complex, multimeric structures that are thought to initiate membrane apposition and merger via the transfer of mechanical energy generated by drastic conformational changes during the membrane fusion reaction (Jahn, Lang et al. 2003, Sapir, Choi et al. 2007, Martens and McMahon 2008). With an estimated size of ~13 nm, the ectodomain of the canonical fusogen, the influenza HA trimer, shares much more similarity with the above mentioned fusogens, than with the miniscule 1.5 nm ectodomain of RRV p14 (Corcoran, Syvitski et al. 2004). With their diminutive ectodomains, the size of the FAST proteins greatly differs from all known fusogens. Interestingly, the FAST proteins also differ extensively from each other with respect to the distribution of their functional motifs across the plasma membrane. In addition, the lack of receptor binding activity and the absence of a fusion trigger further distinguish the FAST proteins from other known fusion machinery. Due to the extremely unusual characteristics of the FAST family, we were very keen to apply the 'hemifusion toolbox' to analyze their membrane merging capacity.

The existence of a hemifusion intermediate has been suggested based on observations of lipidic marker transfer between viruses or SNARE containing-vesicles and liposomes or RBCs, and between RBCs and donor cell membranes. Unfortunately, the application of this well-established assay to our system did not result in RRV p14 mediated fusion of donor cells to RBCs. One possible explanation for the lack of lipid transfer in the presence of the FAST fusogen involves the distance between the RBC and the donor QM5 cell containing RRV p14. Despite the co-transfection of HA0 as the

surrogate receptor binding protein that compensated for the lack of receptor binding activity of RRV p14, the intermembrane distance to be traversed was likely too great for the 1.5 nm ectodomains of this FAST family member. To simulate close membrane apposition in the presence of RRV p14, I triggered the conformational change of the surrogate binding HA G1V, a mutant incapable of lipid mixing. The lack of lipid mixing in the presence of the triggered surrogate binding protein suggested that crossing the intermembrane distance was not the only barrier that RRV p14 must overcome to fuse RBCs. Another explanation for the lack of fusion activity may involve the unusual composition of the RBC phospholipid membrane. Although p14 has been reported to be a promiscuous fusogen, capable of inducing syncytium formation in multiple cell lines, it is not able to fuse *Spodoptera frugiperda* Sf21 cells. It is also possible that p14 and HA may not co-localize in the plasma membrane in close enough proximity for p14 to take advantage of HA-mediated close membrane apposition.

The unexpected finding that neither CPZ nor LPC treatment had any effect on RRV p14-mediated fusion provided evidence that progression of fusion through a stable hemifusion structure, such as a hemifusion stalk, is unlikely in the case of this particular fusogen. The mode of action of these two compounds vastly differs, with CPZ inserting into the inner monolayer to promote fusion, while LPC inserts into the outer monolayer to prevent lipid mixing. The inability of both compounds to exert any detectable effects on pore formation provides corroborating evidence for the lack of a stable hemifusion intermediate.

There is no known trigger for the FAST proteins, which means cell-cell fusion occurs over time as FAST protein expression and trafficking to the plasma membrane reaches some critical threshold level for fusion to proceed. Due to the untriggered nature of FAST protein-mediated fusion, we were unable to employ lipidic markers to track hemifusion since these lipid markers are rapidly internalized by endocytosis. To detect the presence of a hemifusion intermediate via indirect methods, I adapted a pore formation assay to assess effects of CPZ and LPC treatment during membrane fusion by quantifying soluble dye transfer in the presence and absence of these compounds. Additionally, CPZ enhancement of membrane fusion by disruption of hemifusion diaphragms was also detected by observing the extent of syncytium formation. By

employing HA along with HA G1S and HA G1V fusion mutants as controls during the treatments, I was able to show that our assays could reproduce previously obtained results. The existence of a lipid mixing intermediate could be detected via increases in pore formation in the presence of CPZ and a decrease in pore formation in the presence of LPC. I also excluded the possiblity that LPC effects on RRV p14-mediated membrane fusion are not detectable due to LPC normalization across the membrane due to long incubations, based on reports that trans-bilayer translocation of this lysolipid begins to take place after approximately 10 hr, a time scale that was not reached in my experiments (Sprong, van der Sluijs et al. 2001).

With no change in the extent of pore formation mediated by RRV p14 in the presence of pore-promoting CPZ or pore-formation preventing LPC, I was able to conclude that, if a hemifusion stalk structure does exist during RRV p14-meidated membrane fusion, it is extremely short lived and cannot be captured by the currently available methods. Alternatively, it is also possible that RRV p14-mediated membrane fusion progresses via a less ordered fusion intermediate. Such a scenario of membrane fusion has been proposed and is termed the 'lipid mixer model', where water between the apposed membranes is displaced by the amphipathic, boomerang shaped, fusion peptides present in the ectodomains of the fusion machines, which are then responsible for facilitating the mixing together of the outer leaflets of apposing bilayers (Tamm, Crane et al. 2003). If so, the introduction of curvature inducing agents would not be expected to exert an effect on the disordered inner and outer leaflets. Alternatively, it has also been suggested that, at least in the case of LPC, it is not the stalk that is directly influenced by addition of the lysolipid, but that binding of LPC to the hydrophobic fusion peptide itself is the reason for the arrest in lipid mixing driven by enveloped virus fusogens (Gunther-Ausborn, Praetor et al. 1995, Gunther-Ausborn and Stegmann 1997). However, if this scenario were indeed the case for LPC-induced hemifusion arrest, then RRV p14-mediated fusion should also be abrogated, as this fusogen also possesses an amphipathic fusion peptide in its ectodomain (Corcoran et al., 2004).

The finding that RRV p14-mediated membrane fusion may proceed via less structured lipid intermediates is plausible based on the many fundamental differences between this fusogen and all other well characterized enveloped virus fusogens.

However, to my great surprise, another member of the FAST family, BRV p15, was not able to induce stable pore formation in the presence of LPC. The ectodomain of BRV p15 is even smaller than that of RRV p14, and contains a type II polyproline helix, in place of a typical fusion peptide. Interestingly, a myristoylated p15 ectodomain peptide containing the polyproline helix exhibits an unusual lag phase prior to the onset of lipid mixing between liposomes (Top et al., 2012), as opposed to the more traditional lipid mixing profile seen in the case of lipid mixing induced by the RRV p14 peptide. (Corcoran, Syvitski et al. 2004, Top, Read et al. 2012). The authors suggest that the lag phase is necessary for the aggregation of p15 fusion machinery prior to the onset of lipid mixing (Top, Read et al. 2012). It is tempting to speculate that LPC may insert into the membrane of p15-containing donor cells and inhibit the aggregation of this fusogen. In this scenario, LPC would not inhibit the formation of stalk structures, but rather the functionality of BRV p15 multimers thus affecting membrane merger at an earlier step. An interesting experiment that may resolve this controversy would involve the treatment of cells transfected with BRV p15 with CPZ. If the presence of CPZ enhanced syncytium formation during BRV p15-mediated membrane fusion, it would indicate that this fusogen does indeed mediate fusion via an ordered, hemifusion stalk. Alternatively, if CPZ treatment had no effect on the rate of syncytiogenesis, this would suggest that p15-meidated membrane merger was analogous to that of RRV p14 and proceeded via a less structured intermediate.

3.3.2 Pore expansion: converging pathways.

While the membrane fusion reaction leading to nanometer-sized pores has been characterized in multiple systems, very few studies have investigated events following the formation of stable pores. This is not surprising, as most studies have used fusion assays with enveloped viruses or synaptic vesicles. Fusion assays with these small membrane spheres do not need to expand pores to great lengths to complete their task. Recently, several studies have explored the events following membrane merger of adjacent cells that lead to expansion of stable pores into micrometer sized lumenal openings and the eventual generation of syncytia. In these studies, baculovirus gp64 and influenza virus HA were employed to initiate fusion and their dependency on pH

triggering allowed for the synchronization of fusion and subsequent pore expansion (Chen, Leikina et al. 2008, Richard, Leikina et al. 2009). Both studies concluded that pore expansion between donor and target cells required ATP hydrolysis. Dissolution of the actin network at the fusion site also promotes the rate of pore expansion, at least in the case of gp64 (Chen, Leikina et al. 2008). The effects of actin polymer stability during HA-mediated syncytium formation could not be assessed due to dissolution of the network upon pH treatment (Richard, Leikina et al. 2009). Parainfluenza virus (PIV5) F protein does not require a low pH trigger, which allowed the demonstration that pore expansion is promoted by disruption of the actin cytoskeleton (Wurth, Schowalter et al. 2010). The reports that actin dissolution promotes pore expansion are in stark contrast to previous reports from Drosophila myoblast studies, which state that actin cytoskeleton polymerization drives the resolution of fusion pores (Massarwa, Carmon et al. 2007, Gildor, Massarwa et al. 2009). The role of actin dynamics in pore expansion may therefore depend on the nature of the fusion reaction. Our group previously showed that inhibiting actin dynamics inhibits p14-mediated cell fusion (Salsman et al., 2008). However, these effects were attributed to disruption of adherens junctions needed for close membrane apposition prior to membrane fusion. It may be possible to exploit my pore-trapping assay to assess the role of actin remodeling in pore expansion following p14-mediated cell-cell fusion. By allowing pore formation to occur in the presence of LPC, we could specifically analyze the effects of actin disruption or stabilization on events that occur downstream of membrane fusion.

In addition to the limited number of studies examining the role of actin and ATP in pore expansion, several membrane curvature-inducing domains have been reported to augment the rate of syncytium formation. These curvature-inducing domains include the BAR (Bar/amphiphysin/Rvs) domain of GRAF1 (GTPase regulator associated with foal adhesion kinase 1), F-BAR domain of FCHo2 (FCH-domain only protein 2), as well as the GTPase dynamin (Richard, Leikina et al. 2011, Leikina, Melikov et al. 2013). The curvature inducing domains mentioned above preferentially bind to membranes enriched in PtdIns(4,5)P_2. The role of this phospholipid was investigated in the context of pore expansion, revealing that the extent of syncytium formation decreased with reduced levels of PtdIns(4,5)P_2 (Richard, Leikina et al. 2011, Leikina, Melikov et al. 2013). The

requirement of this lipid during pore expansion was postulated to involve PtdIns(4,5)P_2 signalling pathways that recruit membrane curvature inducing- or stabilizing proteins, rather than any influence of PtdIns(4,5)P_2 itself on membrane shape. Another plasma membrane lipid reported to be involved in pore expansion is phosphatidylserine (PS), the externalization of which has been found to be essential for myotube formation and exogenous antibody blocking of this phospholipid reduced myogenesis (van den Eijnde, van den Hoff et al. 2001). Interestingly, although PS exposure occurred at myoblast cell-cell contact sites, it was hypothesized that the presence of PS is involved in either cell-cell recognition or in downstream intracellular signalling, rather than in influencing the curvature of the fusing bilayers. In my opinion, the role of these lipids and curvature-inducing domains in pore expansion remains unclear.

In this study, I was able to identify a lysolipid-sensitive, post pore-formation stage during syncytiogenesis. The effects of LPC on pore expansion were not due to the potential toxic effects of LPC since the inhibitory effect was rapidly reversible. My results further support the concept that bilayer curvature modulation is important not only prior to and during membrane fusion, but also during pore resolution. Moreover, despite the above-mentioned differences in the effects of LPC on FAST protein- and HA-mediated membrane merger, lysolipid treatment of cells connected by a fused pore resulted in a reversible expansion arrest, irrespective of the fusogen used to mediate membrane merger. This report provides direct evidence that this post-fusion step is independent of the fusogen, and suggests pore expansion and syncycytiogenesis may be a universal cellular response to pore formation between neighbouring cells.

As mentioned above, it is becoming clear that pore expansion requires an energy-demanding cellular event, such as actin remodeling and ATP hydrolysis, to drive the expansion process. Additionally, the highly curved bilayer architecture of the pore rim, and possibly the presence of specific lipids such as PtdIns(4,5)P_2, could recruit curvature sensing and/or inducing proteins including dynamin and proteins containing BAR, F-BAR, or ENTH domains (Richard, Leikina et al. 2011). However, these factors would exert an influence on the inner leaflet of the membrane pore while LPC must be exerting its effects on the outer leaflet.

How might LPC, functioning from the outer leaflet of the membrane bilayer to inhibit pore expansion? LPC insertion and promotion of positive curvature is thought to prevent the formation of stable hemifusion stalks. Since the outer rim of a fusion pore has a high negative curvature, LPC insertion in the outer leaflet could prevent lateral propagation of this negative curvature and inhibit pore expansion. The scanning electron microscopy (SEM) results provide a clue to an alternate possible mechanism of pore expansion arrest in the presence of LPC. As shown, lysolipid treatment of live cells induces dramatic plasma membrane rearrangements, somewhat reminiscent of nanotube formation (Gurke, Barroso et al. 2008) The formation of these tubules near sites of pore formation might serve as a physical barrier to pore expansion. Alternatively, these tubules could sequester plasma membrane needed for pore expansion or induce membrane tension that impedes pore expansion. Irrespective of the mode of action of LPC-mediated pore expansion arrest, the reversibility of this process has resulted in the development of a useful pore expansion synchronization assay for both RRV p14 and HA. It will be interesting to explore the functional roles of curvature sensing cellular machinery, as well as the effects of the actin cytoskeleton on pore expansion following virus fusogen-mediated membrane merger. Additionally, LPC treatment of fused cells may prove useful in teasing out the differences and similarities between cellular mechanisms involved in viral fusogen-mediated syncytium formation and myogenesis.

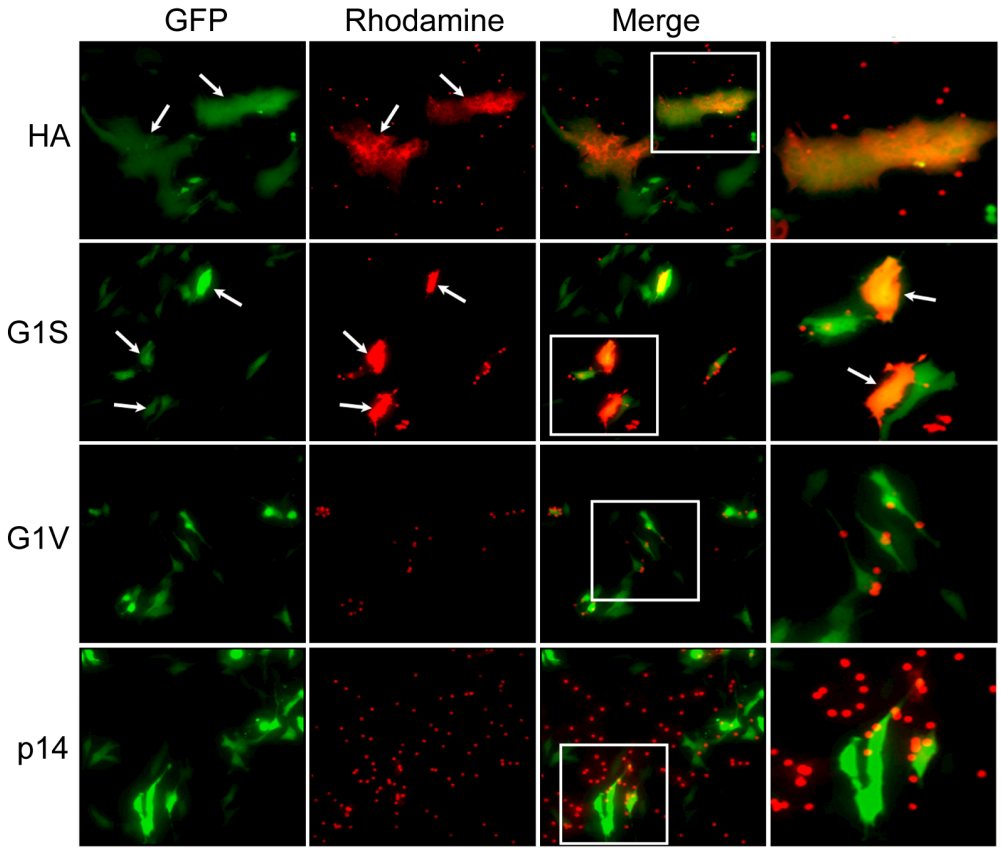

Figure 3.1 **RRV p14 does not fuse red blood cell membranes.** QM5 cells were co-transfected with plasmids expressing EGFP and either HA, G1S or GIV, or with EGFP, p14, and HA. Following transfection, cells were overlaid with RBCs labelled with the red lipidic dye R18. In the cells expressing HA or the HA mutants, the fusion activity of HA was activated and triggered by treatment with trypsin and low pH. HA was trypsin-activated but fusion was not triggered with low pH in the cells co-transfected with p14 (HA in these cells served as a surrogate RBC adhesin). Following incubation at 37 °C to allow cell–RBC fusion to proceed, cells were fixed and fluorescent images were captured by confocal microscopy. Arrows indicate co-transfected cells (G1S row) or syncytia (HA row) expressing the fusogen and GFP that acquired the red lipid dye from RBCs, as indicated by the yellow color in the merged images. The right hand column shows a higher magnification of the boxed regions from the merged images to more clearly indicate the presence of bound RBCs and co-fluorescent cells.

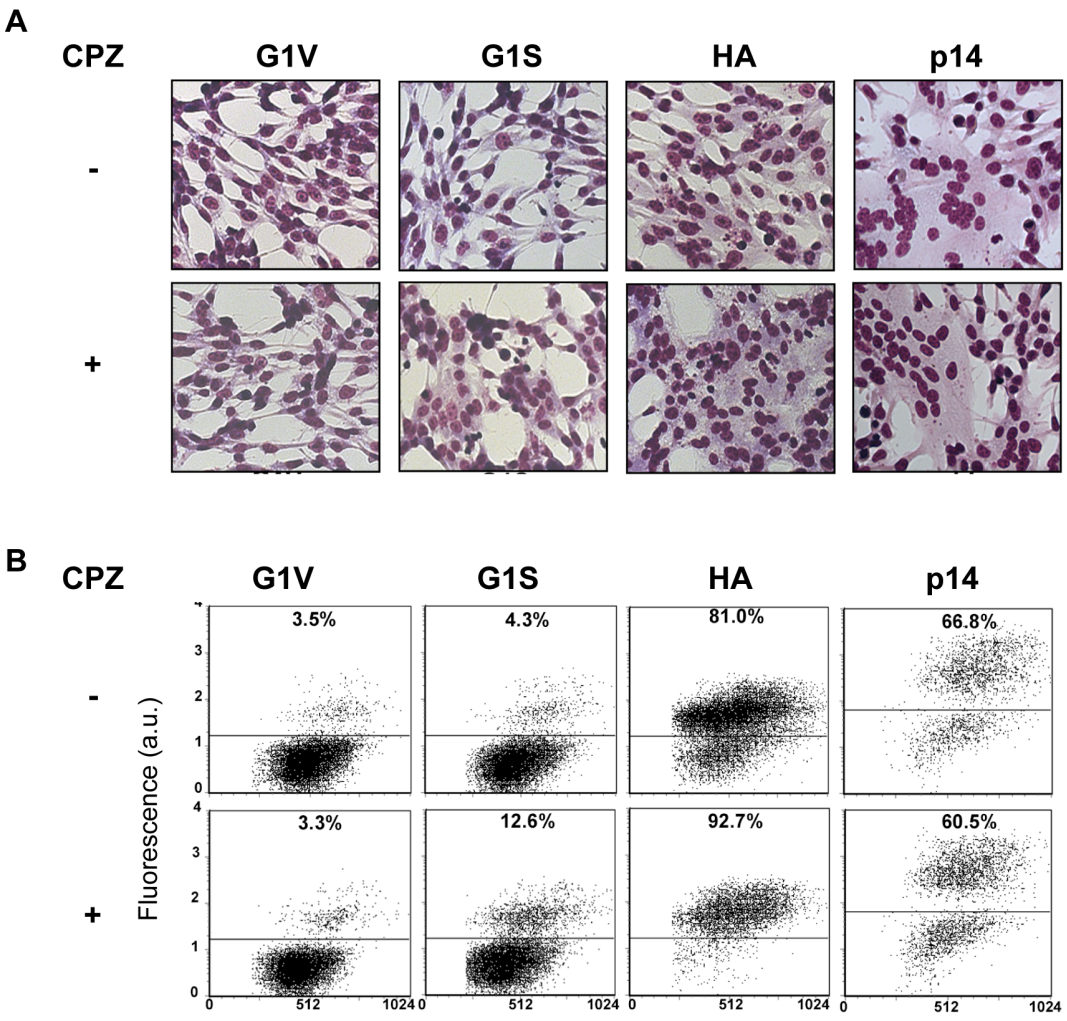

Figure 3.2 **Chlorpromazine treatment has differential effects on RRV p14- and influenza HA-mediated pore formation.** (A) QM5 cells were transfected with p14, HA, G1S or G1V and HA fusion was activated by trypsin and low pH treatment. Cells were either treated with 0.5 μM CPZ for 1 min or left untreated, then incubated for 30 min or 2 hrs for HA- or p14-transfected cells, respectively, to allow fusion to proceed. Cells were fixed and Giemsa stained, and light microscopy images were captured at 200× magnification. (B) The extent of pore formation was measured by adding calcein red-labelled Vero cells to QM5 cells co-transfected with EGFP and HA, G1S, G1V or p14 for 4 hrs, then CPZ treated as in (A). Pore formation was quantified by analyzing the percentage of the gated EGFP-expressing cells that acquired calcein red from the target Vero cells, plotted against the forward scatter (FSC).

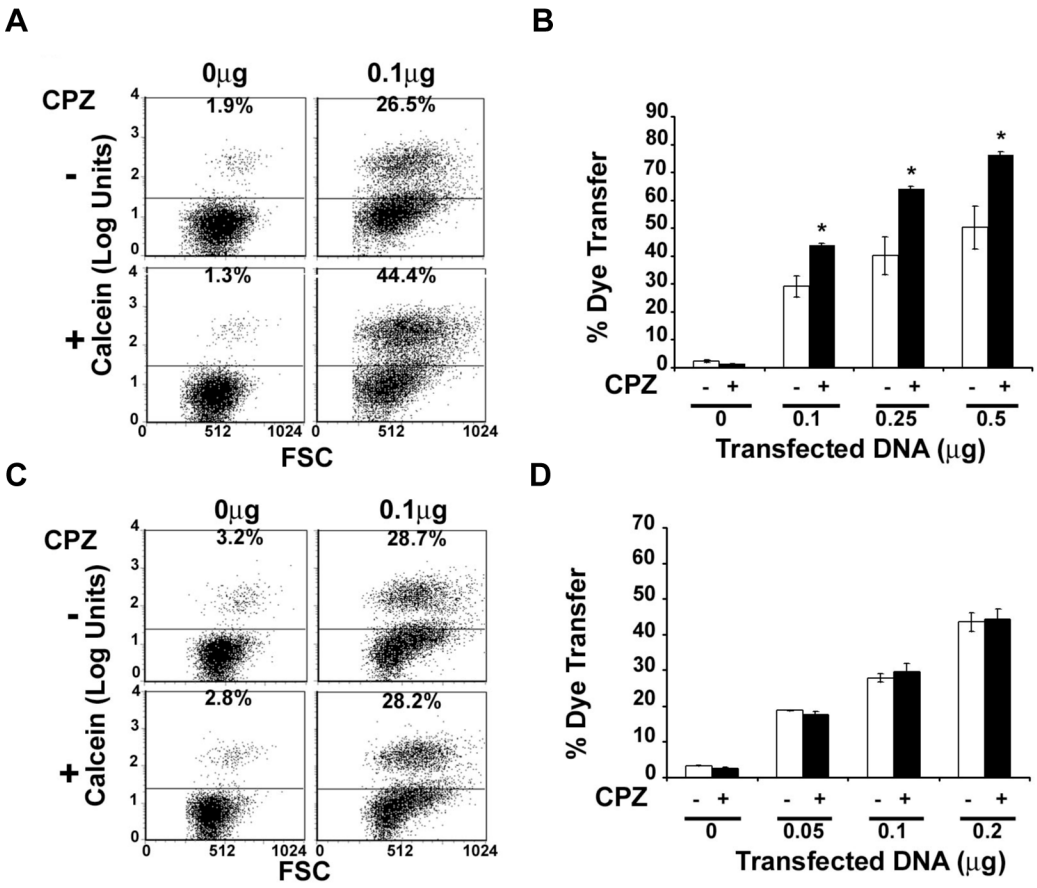

Figure 3.3 **The chlorpromazine insensitivity of RRV p14 is not due to fusogen oversaturation.** (A) Representative dot plot showing the percentage of pore forming cells transfected with 0.1 μg of HA plasmid DNA with (+) or without (-) CPZ treatment. Calcein red labelled Vero cells were added to QM5 cells that were transfected with HA, and incubated for 4 hrs. HA fusion was triggered with low pH then 0.5 μM CPZ was added for 1 min. Following a 30 min incubation, cells were fixed with 3.7% formaldehyde and measured for dual staining by FACS with gating for GFP positive cells, to show extent of pore formation. (B) Quantification of the pore formation assay described above with cells transfected with the indicated amounts of HA expressing plasmid, and co-incubated with labelled Vero cells for 4 hrs. 10 000 gated cells were counted. Results are the mean ± SD of triplicate samples from a representative experiment (n=3). (C) Representative dot plot showing the percentage of pore forming cells transfected with 0.1 μg of p14 plasmid DNA in the presence or absence of CPZ. (D) Pore formation with or without CPZ treatment was determined for cells transfected with p14 plasmid at the indicated amounts, as described above. Experiments were performed by Marta Ciechonska and Eileen Clancy.

A

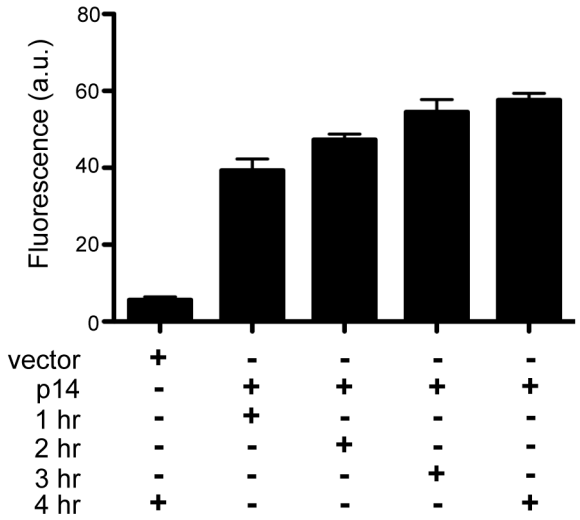
Fluorescence (a.u.)
80
60
40
20
0
vector + - - - -
p14 - + + + +
1 hr - + - - -
2 hr - - + - -
3 hr - - - + -
4 hr + - - - +

B

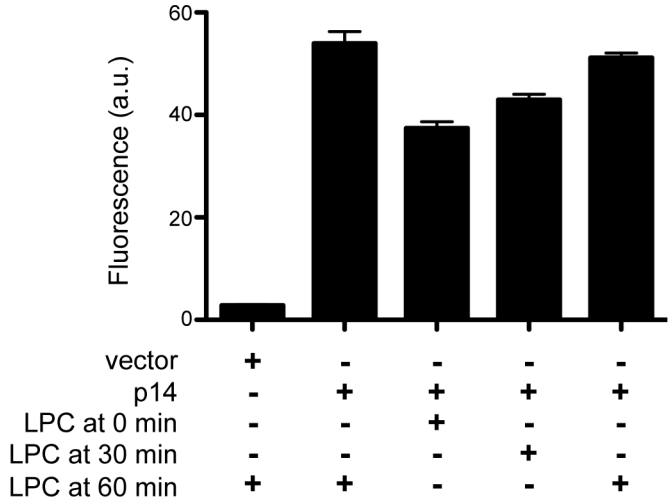
Fluorescence (a.u.)
60
40
20
0
vector + - - - -
p14 - + + + +
LPC at 0 min - - + - -
LPC at 30 min - - - + -
LPC at 60 min + + - - +

C

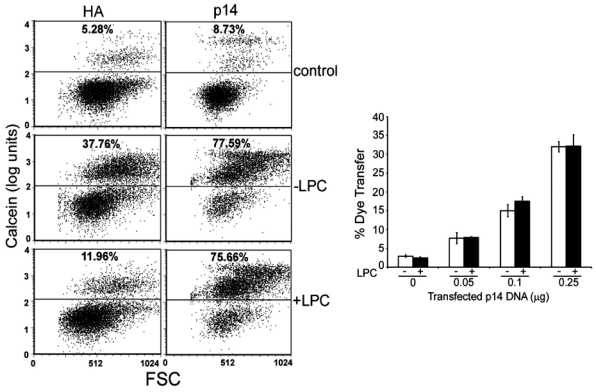
HA
p14
5.28%
8.73%
control
37.76%
77.59%
-LPC
11.96%
75.66%
+LPC
Calcein (log units)
FSC
0
512
1024
% Dye Transfer
LPC
0
0.05
0.1
0.25
Transfected p14 DNA (μg)

Figure 3.4 **Lysophosphatidylcholine treatment does not arrest RRV p14-mediated membrane fusion at a pre-pore formation step.** (A) QM5 cells were co-transfected with p14 and GFP, and Vero cells were labeled with calcein Red-Orange . Vero cells were trypsinized and co-cultured with QM5 cells at 4 hrs post-transfection. Cells were resuspended in EDTA and fixed with formaldehyde at 1, 2, 3, and 4 hrs of co-culture, and the extent of pore formation was quantified by FACS. Results are the mean ± SD of triplicate samples from a representative experiment (n=3). (B) The pore formation assay was performed as above. 100 μM myristoyl lysophosphatidylcholine was added to Vero cells at the time of addition to QM5 cells (0 min), or at 30 or 60 min after the transfer of Vero cells to QM5 cells. Results are the mean ± SD of triplicate samples from a representative experiment (n=2). (C) QM5 cells stably expressing influenza HA were transiently transfected with EGFP, treated with trypsin and low pH, then co-cultured for 30 min with calcein red-labelled Vero cells in the presence or absence of 100 μM LPC. QM5 cells were also transiently transfected with p14 and co-cultured for 5 h with calcein red-labelled Vero cells, for the last 4 h in the presence or absence of 100 μM LPC. Results are a representative dot plot quantifying the percent of gated EGFP-expressing cells that acquired calcein red from the target Vero cells as a result of pore formation, plotted against the forward scatter (FSC). Controls were either non-activated HA (HA panels) or pcDNA3 (p14 panels). The percentage of gated donor cells transfected with the indicated doses of p14 plasmid DNA that acquired calcein red from target Vero cells due to pore formation in the presence (black bars) or absence (white bars) of LPC was quantified as described in (A). Results are the mean ± SD of a single experiment done in triplicate. The p14 DNA titration experiment was performed by Eileen Clancy, and all others were performed by Marta Ciechonska.

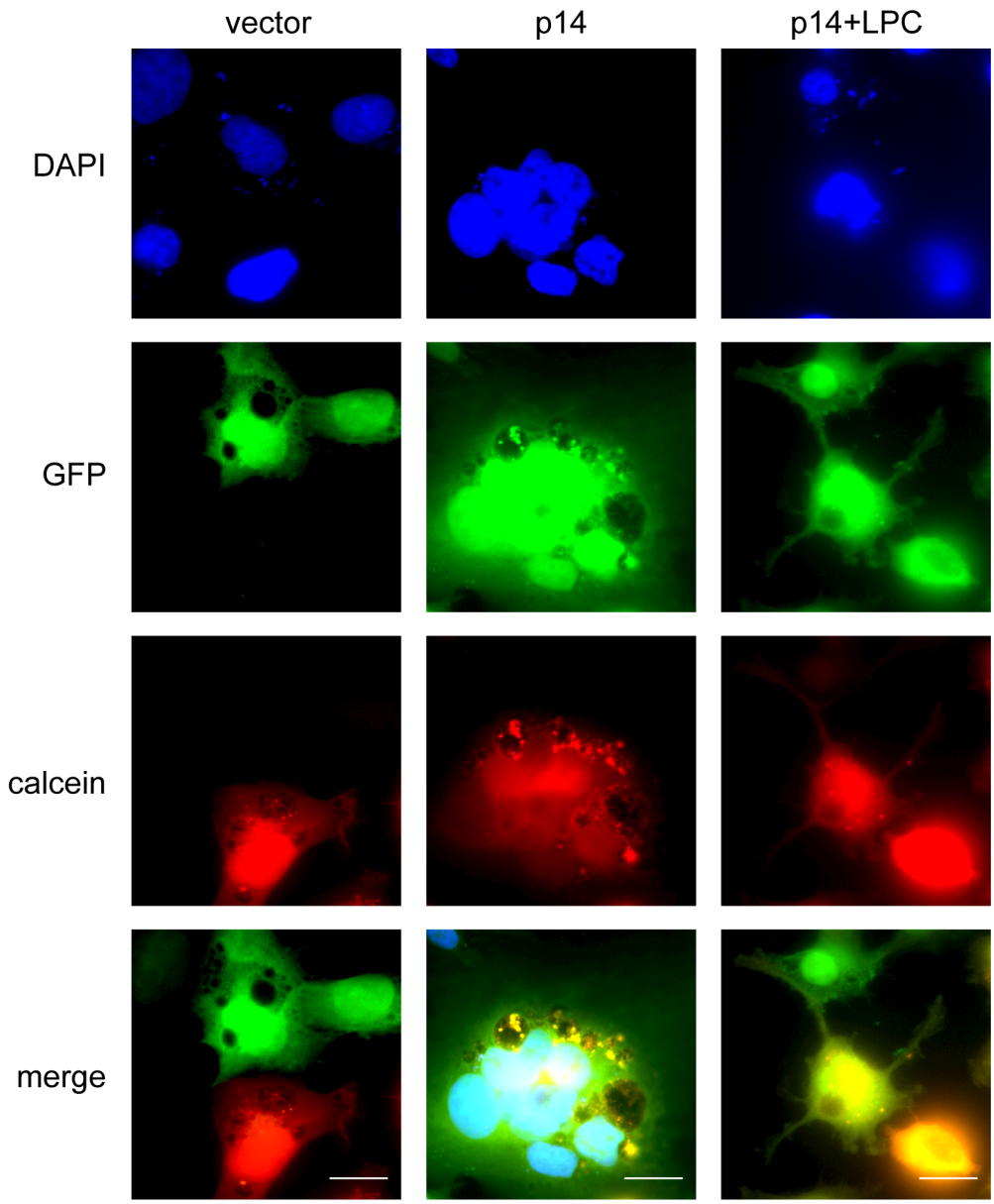

Figure 3.5 **Lysophosphatidylcholine does not inhibit RRV p14-mediated pore formation.** A homotypic pore formation assay was performed to assess the extent of p14-mediated pore formation by fluorescence microscopy. Donor HT1080 cells were co-transfected with p14 and GFP, while target HT1080 cells were labeled with calcein Red-Orange. The calcein labeled cells were trypsinized and seeded on top of donor cells at 4 hrs post-transfection. Cells were fixed at 12 hrs post-transfection and imaged by fluorescence microscopy.

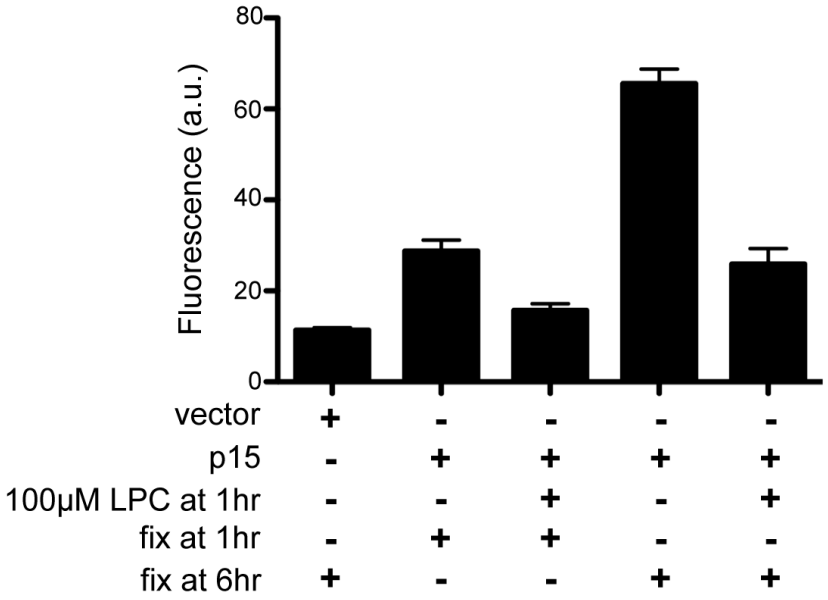

Figure 3.6 **Lysophosphatidylcholine treatment arrests BRV p15-mediated fusion at a pre-pore formation step.** The extent of p15-mediated pore formation in a heterotypic quail muscle fibroblast (QM5) to Vero assay was quantified by flow cytometry. QM5 cells were co-transfected with p15 and GFP, while Vero cells were labeled with Calcein Red-Orange. Vero cells were trypsin lifted and overseeded on top of QM5 cells at 4 hrs post-transfection. LPC was added at 1 hr after co-culture of donor and target cells. Cells were fixed at 1 hr of co-culture and at 6 hrs of co-culture. Cells were lifted and fixed with formaldehyde at 1, 2, 3, and 4 hrs of co-culture and the extent of pore formation was quantified by FACS. The experiment was completed in triplicate (n=4) with 10 000 events counted per sample.

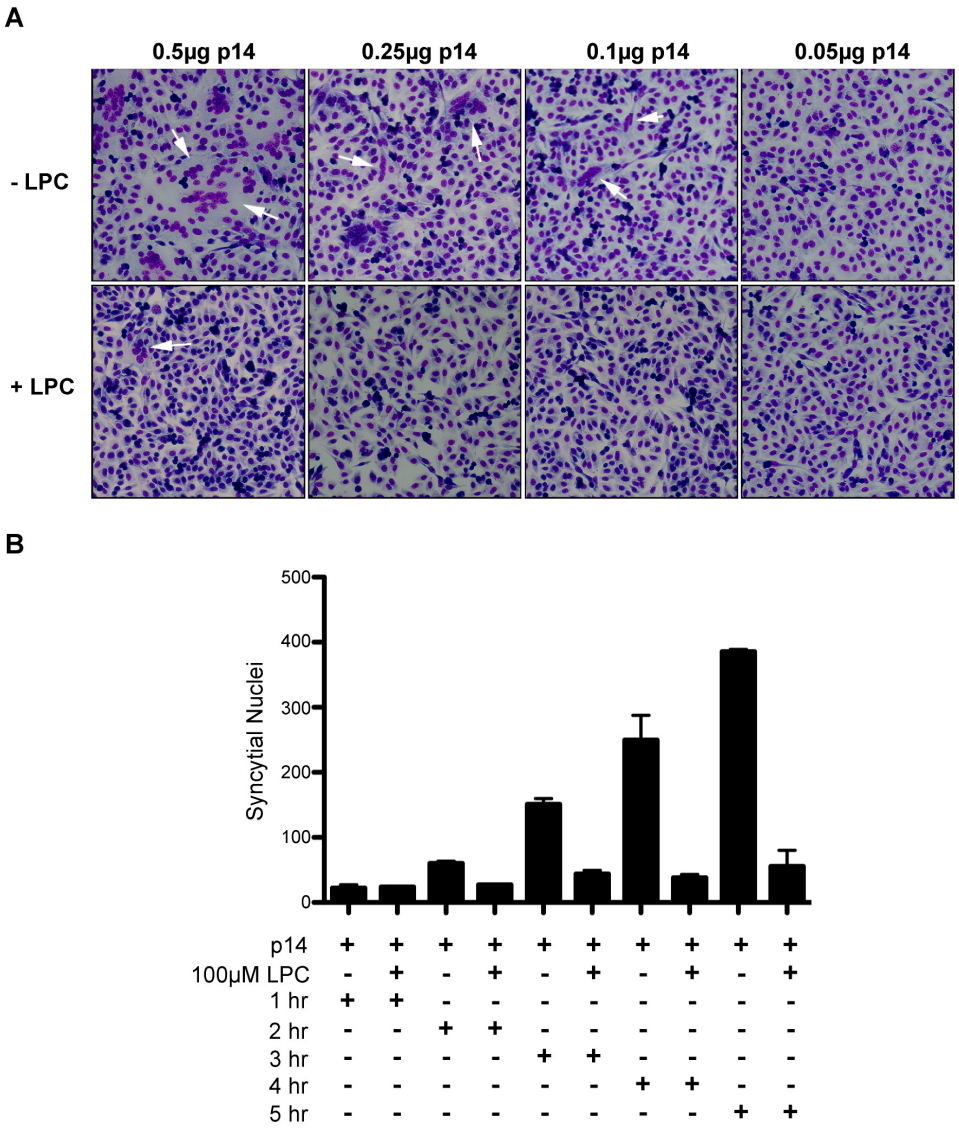

Figure 3.7 **Lysophosphatidylcholine arrests RRV p14-mediated syncytium formation at a post-pore formation step.** (A) QM5 monolayers were transfected with decreasing amounts of RRV p14, treated with 100 µM myristoyl LPC at 4 hrs post-transfection, and fixed at 8 hrs post-transfection. Syncytial nuclei were visualized by Giemsa staining. (B) QM5 cells were treated as in (A) and monolayers were fixed at 1, 2, 3, 4 or 5 hrs after LPC addition. Syncytial indexing was performed by determining the average number of syncytial nuclei in five random microscopic fields. Results are the mean ± SD of triplicate samples from a representative experiment (n=2).

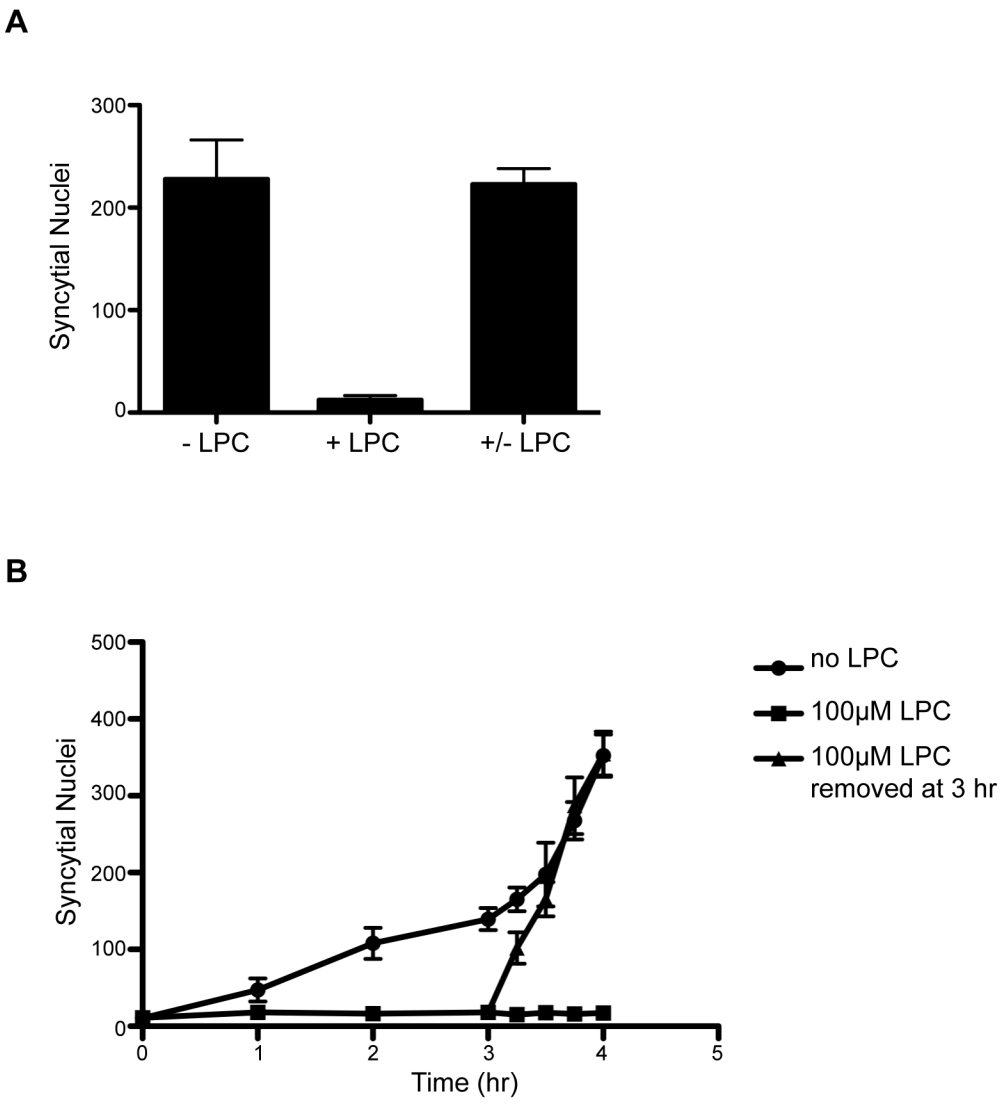

Figure 3.8 **RRV p14-mediated pore expansion LPC-arrest is reversible.** (A) QM5 monolayers were transfected with 0.1 μg RRV p14, treated with 100 μM myristoyl LPC at 4 hrs post-transfection, and fixed at 10 hrs post transfection. In one sample, LPC was removed after 3 hrs of incubation (indicated as (+/-LPC). Syncytial nuclei were visualized by Giemsa staining and syncytial indexing was performed by determining the average number of syncyital nuclei in five random microscopic fields. Results are the mean ± SD of triplicate samples from a representative experiment (n=2). (B) QM5 monolayers were transfected with decreasing amounts of RRV p14, treated with 100 μM myristoyl LPC at 4 hrs post-transfection, and removed from culture medium after 3 hrs of incubation. Monolayers were fixed at 1, 2, , or 4 hrs after LPC addition and at 15 min increments after the removal of LPC. Syncytial indexing was performed by determining the average number of syncytial nuclei in five random microscopic fields. Results are the mean ± SD of triplicate samples from a representative experiment (n=2).

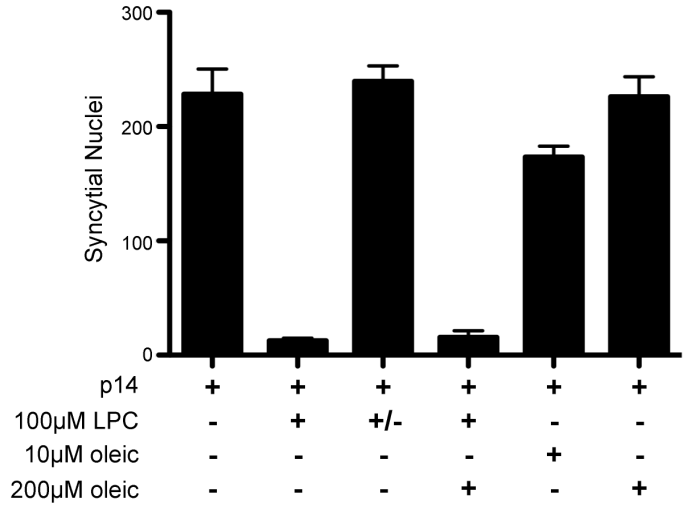

Figure 3.9 **Oleic acid has no effect on RRV p14-mediated fusion and does not reverse the effects of lysophosphatidylcholine during pore expansion.** QM5 monolayers were transfected with 0.1 μg RRV p14, and treated with 100 μM myristoyl LPC alone or with 200 μM oleic acid, or with 10 or 200 μM oleic acid alone at 4 hrs post-transfection, and fixed at 8 hrs post transfection. Syncytial indexing was performed by determining the average number of syncyital nuclei in five random microscopic fields. Results are the mean ± SD of triplicate samples from a representative experiment (n=2).

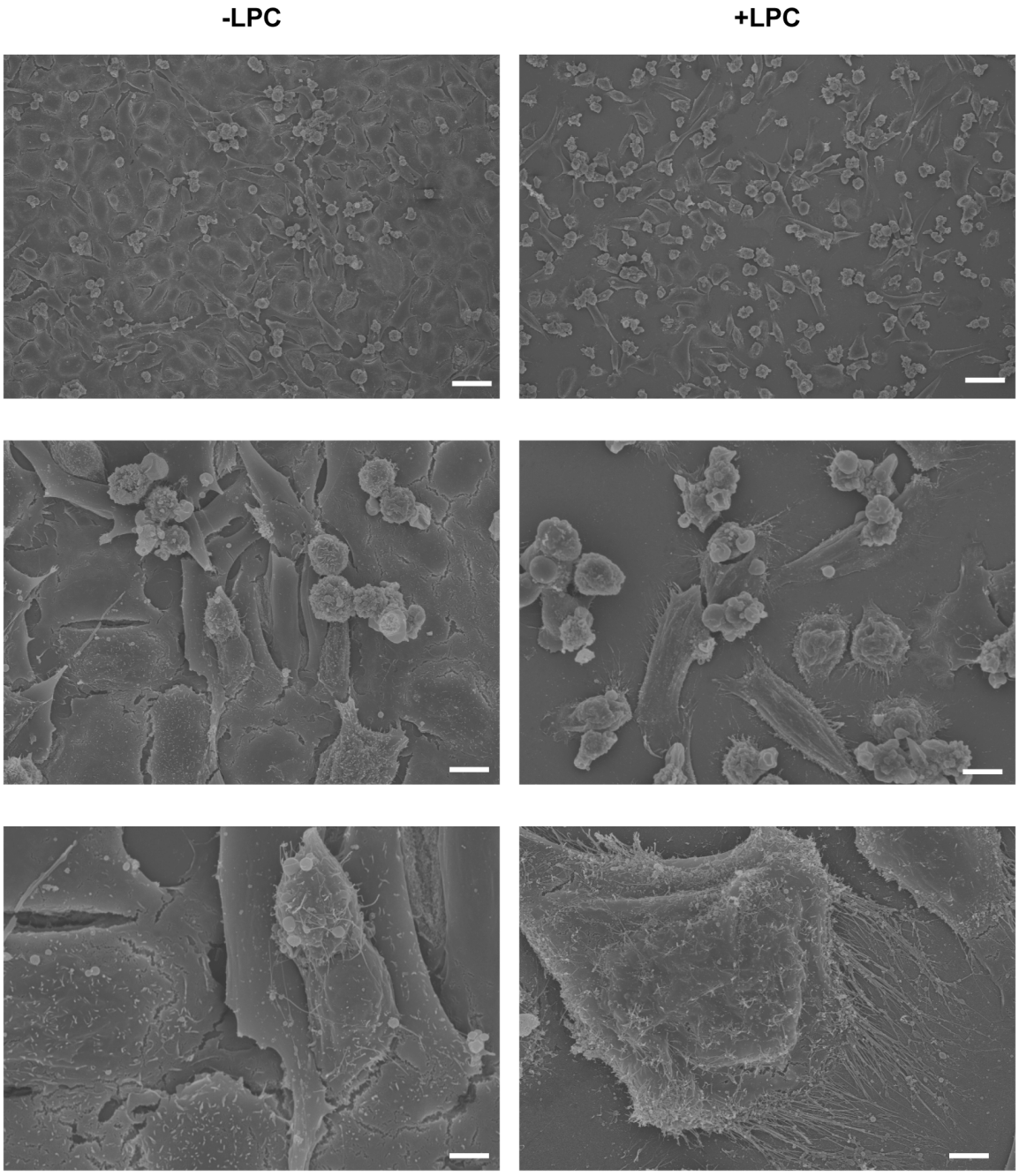

Figure 3.10 **Lysophosphatidylcholine treatment induces tubulation of cellular membranes.** QM5 cells were co-transfected with p14 and GFP and Vero cells were trypsin lifted and co-cultured with QM5 cells at 4 hrs post-transfection. Cells were fixed with formaldehyde after 4 hrs of co-culture and slides were prepared for scanning electron microscopy. Bars indicate 40 μm (top), 10 μm (middle), and 4 μm (bottom).

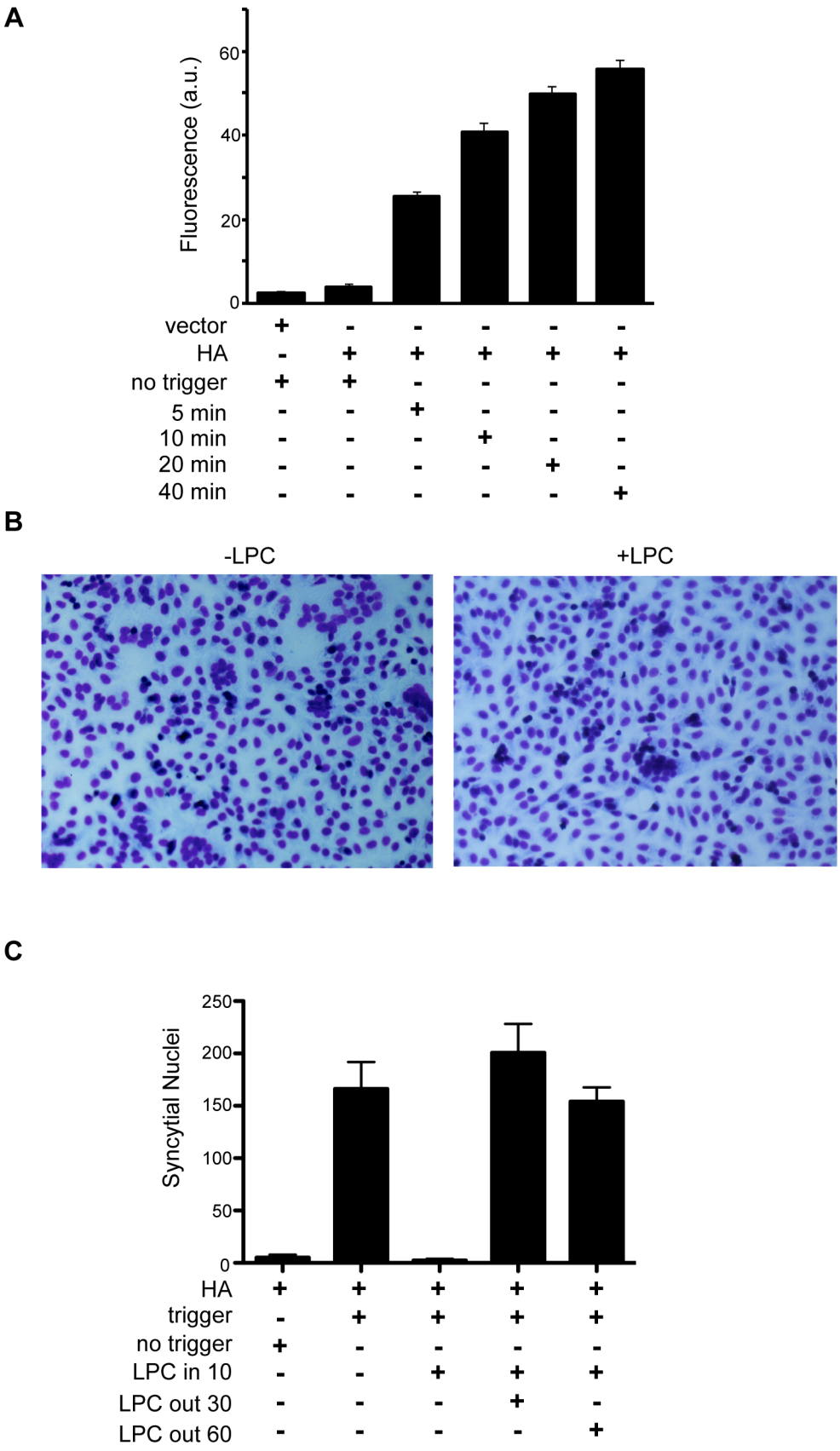
A
Fluorescence (a.u.)
60
40
20
0
vector + - - - - -
HA - + + + + +
no trigger + + - - - -
5 min - - + - - -
10 min - - - + - -
20 min - - - - + -
40 min - - - - - +
B
-LPC
+LPC
C
Syncytial Nuclei
250
200
150
100
50
0
HA + + + + +
trigger - + + + +
no trigger + - - - -
LPC in 10 - - + + +
LPC out 30 - - - + -
LPC out 60 - - - - +

Figure 3.11 **Influenza HA-mediated syncytiogenesis is sensitive to lysophosphatidylcholine-dependent pore expansion arrest.** (A) Donor QM5 cells were co-transfected with HA and GFP plasmid DNA. Target Vero cells were labeled with calcein Red-Orange and added to the QM5 cells expressing HA. The co-cultured cells were treated with trypsin and low pH, fixed after 5, 10, 20, or 40 min of incubation, and soluble content transfer was detected by FACS. Results are the mean ± SD of triplicate samples from a representative experiment (n=2). (B) Monolayers of QM5 cells were transfected with HA plasmid DNA and fusion was triggered by trypsin and low pH treatment. LPC was added at 10 min post-fusion triggering, and the cells were fixed and Giemsa stained at 30 min following pH treatment. (C) QM5 cells were treated as in (B) and LPC was washed out at 30 and 60 min following trypsin and pH treatment. Cells were fixed at 2 hrs after the onset of fusion. Syncytial indexing was performed by determining the average number of syncyital nuclei in five random microscopic fields. Results are the mean ± SD of triplicate samples from a representative experiment (n=2).

CHAPTER 4: Roles of Annexin A1 in viral fusogen-mediated fusion

4.1 Introduction

Members of the fusion-associated small transmembrane (FAST) protein family greatly differ from all known fusion proteins in their size, bulk distribution across biological membranes, and their primary objective in initiating cell-cell membrane fusion. While fusion proteins encoded by enveloped viruses have evolved to deliver viral cargo to host cells, the FAST proteins are non-structural viral proteins, and their sole known function is to fuse neighbouring cells to generate multinucleated syncytia. RRV p14, the most robust fusogen of the known FAST proteins, exhibits a type III membrane topology, with a short, 36-residue, extracellular N-terminal domain, and a much longer, 68-residue C-terminal endodomain (Corcoran and Duncan 2004, Corcoran, Syvitski et al. 2004). The ectodomain of p14 is N-terminally myristoylated, and contains a multimerization motif that is essential for the onset of p14-mediated syncytiogenesis (Corcoran, Clancy et al. 2011). The cytoplasmic endodomain contains two characteristic regions; a juxtamembranous stretch of six basic residues, as well as a C-terminus proximal poly-proline tract. Although the last 20 residues of the cytoplasmic domain are responsible for the enhancement of, but are not necessary for, syncytium formation, truncation of 47 residues results in complete fusion arrest (Corcoran and Duncan 2004, Barry and Duncan 2009). In addition, the entire cytoplasmic region of p14 can be cleaved by unknown cellular proteases to generate a soluble p14 endodomain, which, when co-expressed with wild type fusogens, is responsible for significant enhancement of not only p14-mediated syncytium formation, but also influenza hemeagglutinin-mediated cell-to-cell fusion and mouse C2C12 myoblast fusion into myotubes (Top, Barry et al. 2009). It has been suggested that the generic enhancing effect of the p14 endodomain points to the exploitation of a common cellular pathway during syncytium formation.

Although muscle cell fusion and myotube formation have been extensively studied, and the currently identified cellular proteins involved in this process are known to be responsible for pre-and post-fusion steps; the *bona fide* cellular fusogen (or fusogens) responsible for membrane merger remains unknown (Richardson, Nowak et al.

2008, Sens, Zhang et al. 2010, Abmayr and Pavlath 2012, Gruenbaum-Cohen, Harel et al. 2012). Studies of global proteome signature changes during myogenesis have identified a vast array of cellular factors that are differentially expressed during this process. Among many candidate proteins, the expression of annexin A1 (AX1) and annexin A5 (AX5) was found to be upregulated (Tannu, Rao et al. 2004, Kislinger, Gramolini et al. 2005, Gonnet, Bouazza et al. 2008). Very recent studies, published while the present studies were underway, indicated that both AX1 and AX5 play a role in myogenesis, in the context of primary- and C2C12- muscle cell fusion. However, whereas Leikina et al. (2013) suggest that the annexins themselves are involved in membrane apposition and membrane merger, Bizzaro et al. (2012) reported that AX1 is involved in cell migration, a step preceding membrane fusion (Bizzarro, Belvedere et al. 2012, Leikina, Melikov et al. 2013). The precise role(s) of annexins in cell-cell membrane fusion are, therefore, still unclear.

Members of the Annexin protein family are characterized by their ability to interact with phospholipid membranes in a calcium-dependent manner via a highly conserved C-terminal core domain composed of four or eight 70-residue repeats. Variation between individual members of the family is thought to be imposed by the N-terminal domain, a region containing protein modification and interaction sites (Gerke, Creutz et al. 2005). AX1 and AX5 are found in the cytoplasm, as well as secreted to the outside of the cell (Gerke, Creutz et al. 2005, Arnoys and Wang 2007). In addition, calcium signalling and binding to AX1 and AX5 are essential for their mobilization as well as for differential interaction with phospholipid bilayers and cellular partners (Mailliard, Haigler et al. 1996, Lee, Na et al. 1999, Radke, Austermann et al. 2004, Gerke, Creutz et al. 2005, Potez, Luginbuhl et al. 2011). Among their many actions in a diversity of cellular processes, including inflammation, coagulation, endocytosis, and apoptosis, AX1 and AX5 have been implicated in plasma membrane repair, via a mechanism of vesicle fusion (Gerke, Creutz et al. 2005, McNeil, Rescher et al. 2006, Bouter, Gounou et al. 2011, Potez, Luginbuhl et al. 2011). In addition to its role in aggregation and/or delivery of membrane repair vesicles, AX1 has also been reported to interact with dysferlin, a protein involved in vesicle trafficking and fusion during membrane repair (Lennon, Kho et al. 2003).

Several viral proteins have been reported to interact with members of the Annexin family in a calcium-dependent manner. Annexin 2 (AX2) interacts with HIV Gag in multilamellar vesicles of monocyte-derived macrophages, becoming packaged into HIV virions, and can also act extracellularly as an infection cofactor by simultaneously binding to phosphatidylserine (PS) present in the HIV envelope and to the macrophage secretory leukocyte protease inhibitor (SLPI) receptor in cell membranes (Ma, Greenwell-Wild et al. 2004, Ryzhova, Vos et al. 2006, Rai, Mosoian et al. 2010). The AX2-S11A100 tetramer, described in Chapter 1, has been reported to interact with the human papillomavirus L2 minor capsid protein during virus binding to host cells (Woodham, Da Silva et al. 2012, Raff, Woodham et al. 2013). AX2 has also been reported to interact with cytomegalovirus (CMV) and enterovirus particles (Wright, Kurosky et al. 1994) to enhance infectivity by bridging the viral membrane to the host cell (Raynor, Wright et al. 1999, Yang, Chou et al. 2011). In addition, annexin A5 (AX5) has been reported to act as a bridge between the host plasma membrane and the small hepatitis B surface antigen (SHBsAg) as well as with PS located in the viral envelope (De Meyer, Gong et al. 1999). Notably, neither AX2 nor AX5 has been reported to participate directly in virus-mediated membrane fusion or in steps immediately following the fusion reaction.

The involvement of AX1 and AX5 during murine myogenesis, as well as their significant role in membrane repair, suggest that these proteins likely localize to sites of plasma membrane fusion or disruption. The calcium-dependent involvement of annexins in virus infection raises the important question of whether annexins are involved not only in virus-mediated entry, but also in viral fusogen-mediated syncytium formation. Support for the latter conjecture was obtained using a yeast two-hybrid screen that identified the first 90 residues of AX1 as a genetic interaction partner of the RRV p14 endodomain (Julie Boutilier, personal communication). This finding seeded the hypothesis that AX1 is involved in p14-mediated cell-to-cell fusion. In addition, the ability of the p14 endodomain to enhance cell-cell fusion mediated by diverse viral and cellular fusogens at a post-pore formation stage in the fusion reaction (i.e. fusion pore expansion) suggests the involvement of a common cellular pathway, or set of pathways, in resolving membrane pores to generate multinucleated syncytia.

In the present study, I investigated the role of AX1 in non-enveloped reovirus RRV p14-mediated syncytium formation. Co-immunoprecipitation and FRET analysis revealed that AX1 interacts with RRVp14 in a calcium-dependent manner. In addition, siRNA knockdown of AX1 and AX5 greatly reduced p14-mediated syncytium formation, as did depletion of intracellular calcium. These results were recapitulated when the function of p14 was substituted with the measles F protein. Furthermore, microscopy and FACS analysis of fluorescent dye transfer between fused cells indicated that both AX1 and intracellular calcium are involved in a post-fusion, pore expansion step during syncytium formation. These results point to a novel intracellular role for AX1, and potentially AX5, during virus-mediated syncytiogenesis, and suggest that a general cellular response is involved in resolving intercellular membrane merger and pore formation.

4.2 Results

4.2.1 Annexin A1 and Annexin A5 are necessary for RRV p14-mediated syncytium formation

AX1 was identified as a potential p14-interacting partner in a yeast two-hybrid screen executed using a human cDNA library as prey and the endodomain of p14 as bait (Julie Boutilier, personal communication). This candidate 'hit' was promising, as the Annexin family of proteins has been implicated in a wide range of membrane-related cellular events (Gerke, Creutz et al. 2005). In order to investigate the role, if any, that AX1 and AX5 play in RRV p14-mediated membrane fusion, p14 was transfected into HT1080 cells previously treated with control, AX1, or AX5 siRNA. Monolayers of cells containing the control siRNA fused at an appreciable rate, as indicated by the presence of multinucleated syncytia observed in Giemsa-stained monolayers (Fig. 4.1A). In contrast, treatment of cells with AX1 or AX5 siRNA dramatically impaired syncytium formation (Fig 4.1A). The extent of syncytium formation was quantified by determining the mean number of syncytial nuclei per microscopic field, as described in Materials and Methods. Both AX1 and AX5 siRNA treatment dramatically decreased p14-mediated syncytium formation (Fig. 4.1A), with AX1 or AX5 knockdown decreasing syncytium formation by ~93% or ~67%, respectively (Fig 4.1B).

To determine whether syncytium formation could be rescued after AX1 siRNA treatment, plasmid DNA expressing AX1, at two different plasmid DNA concentrations (0.9 μg or 0.5 μg), was co-transfected with the plasmid expressing p14. As indicated (Fig. 4.1B), 0.9 μg of AX1 plasmid DNA partially compensated for the inhibitory effects of AX1 siRNA, restoring p14-induced syncytiogenesis to ~57% of the level obtained in cells treated with control siRNA. The 0.5 μg dose of AX1 plasmid DNA had no such restorative effect on syncytiogenesis (Fig. 4.1B). Cellular levels of AX1 were analyzed by Western blotting, which demonstrated a robust knockdown after siRNA treatment, and a subsequent increase in expression following the transfection of 0.9 μg of AX1 DNA (Fig 4.1C), suggesting the inhibitory effects of AX1 siRNA were specific for AX1. However, subsequent repetition of this experiment, using 0.9 μg of AX1 plasmid DNA, failed to restore syncytiogenesis (Fig. 4.2). Since western blot analysis of AX1 expression was not performed in these experiments, it is not certain that AX1 levels had indeed been restored.

AX1 has been implicated in membrane protein trafficking and endocytosis (Futter, Felder et al. 1993, Tcatchoff, Andersson et al. 2012). In order to eliminate the possibility that the knockdown of AX1 and AX5 resulted in p14 trafficking defects to the plasma membrane leading to a decrease in syncytium formation, the cell surface expression of p14 was assessed. Due to the rapid generation of wild-type p14-mediated syncytia, a previously characterized mutant incapable of mediating fusion, p14 G2A, was used. This was necessary to allow enough time for sufficient surface expression of p14 for detection by FACS analysis without the generation of large syncytia, which cannot be processed by flow cytometry. FACS analysis of siRNA-treated cells expressing p14 revealed that decreased AX1 or AX5 expression does not impact the cell surface localization of p14 (Fig. 4.1D) Overton subtraction values, a relative comparison of surface expression of p14, were 69%, 76% and 67% for cells treated with control, AX1 or AX5 siRNAs, respectively.

At this point, I chose to concentrate on AX1, as its depletion resulted in a more pronounced syncytiogenesis defect, and because only AX1 was identified in the yeast two-hybrid screen. In order to compliment the siRNA study, and to eliminate the possibility of 'off-target effects' of this technique, three AX1 shRNA cell lines were

generated using a retroviral transduction system. A previously validated AX1 shRNA sequence (Babiychuk, Monastyrskaya et al. 2011), and two shRNA sequences targeting AX1, generated using RNAi Central software, were employed to generate the AX1 shRNA cell lines. While a decrease in p14-mediated syncytium formation was observed in cells transduced with the previously reported AX1 shRNA construct (AX1-sh1 in this study), no difference in fusion was seen between cells transduced with control siRNA or the other two AX1 shRNA constructs (AX1-sh2 and -sh3) (Fig 4.3A). Analysis of AX1 expression in the shRNA-expressing cell lines demonstrated a substantial decrease in the AX1-sh1 cell line, but not in the AX1-sh2 or AX1-sh3 cell lines, corroborating the reduced syncytium formation phenotype induced by AX1-sh1 (Fig 4.3B).

4.2.2 Annexin A1 interacts with RRV p14 in a calcium-dependent manner

The RNAi results implicated AX1 in p14-indcued syncytiogenesis, and the yeast two-hybrid screen suggested AX1 interacts with the p14 endodomain. To determine whether p14-AX1 interaction can occur in a physiologically relevant, mammalian tissue culture system, co-immunoprecipitation experiments were performed using full-length p14 and N-terminally FLAG-tagged AX1. Anti-FLAG antibody was used to immunoprecipitate full length AX1 and the presence of p14 in the immunoprecipitate was detected by western blot analysis using polyclonal anti-p14 antiserum. Western blot analysis of the cell lysates confirmed expression of both p14 and AX1 (Fig. 4.4). Most notably, p14 was only detected in the immunoprecipitates when cells were co-expressing AX1 (Fig. 4.4, lane 1 vs. lane 6), and only when the immunoprecipitation was performed in the presence of 5 mM calcium (Fig. 4.4, lane 6 vs. lane 7). Thus, p14 interacts with AX1 in a calcium-dependent manner.

The N-terminal domain of AX1, which comprises amino acids 1 to 45 (Rosengarth and Luecke 2003), is able to interact with several cellular partners (Mailliard, Haigler et al. 1996, Lennon, Kho et al. 2003, Herbert, Odell et al. 2007, Poeter, Radke et al. 2012). The AX1 N-terminal domain is also proteolytically cleaved at positions 12 and 26, thus eliminating an interaction site for the AX1 binding partner S100A11 and generating a formyl peptide receptor signalling peptide respectively (Walther, Riehemann et al. 2000, Sakaguchi, Murata et al. 2007). In addition, the

segment of AX1 found to interact with p14 in the yeast two-hybrid system was composed of the N-terminal 90 amino acids. I therefore generated N-terminal deletion mutants at positions 13, 26, and 45 (Fig 4.4A) to determine if, and where, p14 interacts with the N-terminal domain of AX1. As before, anti-FLAG antibody was used to immunoprecipitate the truncated AX1 constructs and p14 was detected in the immunoprecipitates by western blotting using anti-p14 antiserum. Surprisingly, all three deletion constructs were equally capable of interacting with p14 as full-length AX1, and this interaction was calcium-dependent (Fig 4.4B), indicating the AX1 N-terminal is not the site of p14 interaction.

One of the most prominent features of the Annexin protein family is their ability to interact with membranes and cellular partners in a Ca^{2+}-dependent manner (Seemann, Weber et al. 1996, Hayes, Rescher et al. 2004, Monastyrskaya, Babiychuk et al. 2007). To determine whether the AX1 interaction with p14 was dependent on physiological levels of Ca^{2+}, co-immunoprecipitation experiments were performed using immunoprecipitation buffer containing a range of Ca^{2+} concentrations. As shown (Fig 4.5), p14 co-precipitated with AX1 in a Ca^{2+} concentration-dependent manner, showing decreasing levels of interaction between 100 μM and 25 μM Ca^{2+} that was lost at Ca^{2+} concentrations of 10 μM or less. Intracellular Ca^{2+} concentrations are maintained at around 200 nM under normal physiological conditions but increase to low micromolar concentrations following triggered release of intracellular Ca^{2+} stores (Marambaud, Dreses-Werringloer et al. 2009). Thus, p14-AX1 interactions occur at Ca^{2+} levels anticipated in cells with activated calcium signaling pathways. Furthermore, experiments conducted using a similar range of Mg^{2+} concentrations indicated only low levels of p14-AX1 interaction, and only at 1 mM Mg^{2+} (Fig. 4.6), indicating these interactions are Ca^{2+}-specific and not satisfied just by divalent cations.

4.2.3 FRET analysis indicates AX1 interacts with p14 at an intracellular membrane compartment

To further validate the p14-AX1 interaction under physiologically relevant conditions (i.e. inside vertebrate cells), I collaborated with another graduate student in the lab (Tim Key) to use fluorescence resonance energy transfer (FRET) experiments. This approach is widely applied to detect *in vivo* protein-protein interactions that occur over

distances of <10 nm (Schultz, Jaryszak et al. 1986). HT1080 cells were co-transfected with C-terminally GFP-tagged p14 and N-terminally mCherry-tagged AX1. Sensitized emission was used to quantify FRET efficiency, using the PixFRET ImageJplug-in, as described in Materials and Methods. Co-transfection of soluble EGFP and mCherry-tagged p14 constructs indicated no interaction between the fluors (Fig. 4.7, bottom row) and served as a baseline for background fluorescence. The same situation applied in cells co-transfected with soluble mCherry and EGFP-tagged AX1 (data not shown). Cells transfected with a construct expressing a chimeric protein comprising EGFP directly linked to mCherry by a flexible linker sequence revealed strong FRET (Fig. 4.5 A, top row) and served as a positive control for maximal FRET efficiency. Generation of a FRET signal was readily detected in cells co-transfected with EGFP-tagged- and mCherry-tagged-p14 constructs (Fig 4.7A, second row), confirming recent results obtained using co-immunoprecipitation indicating p14 forms homomultimers during transit to the plasma membrane (Corcoran, Clancy et al. 2011). To determine whether AX1 and p14 were directly interacting, formaldehyde-fixed cells expressing EGFP-tagged AX1 and mCherry-tagged p14, were imaged at 100x using the Zeiss LSM 510 Meta confocal microscope. The PixFRET Image-J plug-in was used to calculate donor and acceptor spectral bleed-through (SBT) values, as well as normalized FRET (NFRET) levels in each pixel. Although FRET efficiency was low compared to the theoretical maximum (i.e., the chimeric EGFP-mCherry construct), there was a clear FRET signal obtained between p14 and AX1 (Fig. 4.5B, third row) whose efficiency was ~50% of that obtained for homomultimerization of p14 (Fig. 4.7C). Interestingly, the FRET signal that was detected was localized intracellularly, not at the plasma membrane, suggesting p14 and AX1 interact at some intracellular membrane compartment.

4.2.4 Co-immunoprecipitation indicates the ectodomain of p14 is required for interaction with AX1

With the interaction between AX1 and full-length p14 confirmed, I attempted to map the location of the presumed p14 endodomain motif responsible for AX1 interaction. The p14 endodomain contains a membrane-proximal polybasic region (Fig. 4.8A). In addition to being involved in export of p14 from the Golgi complex to the plasma membrane

(Hiren Parmar, Dalhousie University, personal communication), the polybasic motif also influences p14 association with exosomes (Jolene Read, Dalhousie University, personal communication). To determine whether this functionally important endodomain motif contributes to p14-AX1 interactions, HEK cells were co-transfected with AX1 and either a wild-type p14 or a p14 polybasic region alanine substitution construct generously provided by Hiren Parmar, Dalhousie University (Fig 4.8A). Co-immunoprecipitation of FLAG-tagged AX1 revealed that both the wild-type p14 and the p14 polybasic construct were able to form complexes with AX1 with equal efficiency, indicating this motif is not necessary for p14-AX1 interaction (Fig 4.8B).

A second noticeable motif in the p14 endodomain is a proline-rich region near the C-terminus that includes a stretch of five consecutive proline residues (Fig. 4.9A). Previous results indicate a C-terminal deletion that includes removal of the penta-proline motif results in decreased syncytium formation (Corcoran and Duncan 2004). A triple alanine scan of the endodomain, where groups of three adjacent residues are replaced by alanine within the context of full-length p14, also revealed that substitutions within the polyproline tract results in decreased syncytiogenesis (Jolene Read, personal communication). To investigate whether this region may be mediating the interaction with p14, co-immunoprecipitation experiments were conducted with p14 constructs where alanine residues replaced the first (p14Ala17), last (p14Ala19), or all five (p14PPKO) proline residues of the penta-proline sequence (Fig 4.9A). Probing western blots of the immunoprecipitates with polyclonal antiserum raised against full-length p14 detected interactions between AX1 and full-length p14 or p14Ala19 construct, but not between AX1 and the p14Ala17 or p14PPKO constructs (Fig. 4.9B). However, probing western blots of cell lysates revealed the antiserum raised against full-length p14 had greatly diminished ability to recognize the alanine substitution constructs compared to an antiserum raised against the p14 ectodomain (Fig 4.9B). Presumably, the penta-proline motif represents a dominant epitope recognized by the anti-full length p14 antiserum. Using the anti-ectodomain antiserum to probe western blots of immunoprecipitates indicated all three alanine constructs interacted with AX1 at levels similar to those observed for full-length p14 (Fig. 4.9B). The penta-proline motif, therefore, does not contribute to p14 interaction with AX1.

Having eliminated the two obvious linear motifs in the p14 endodomain as sites for AX1 interaction, I used a series of four well-characterized p14 endodomain or ectodomain truncation constructs (Figs. 4.10A and 4.11A). The p14Δ105construct is missing the C-terminal 20 residues of p14 and is able to mediate syncytium formation, but at a slower rate than wild-type p14, while p14Δ78 is missing 47 residues of the ~68-residue endodomain and is fusion-dead (Corcoran and Duncan 2004, Barry and Duncan 2009). The ectodomain deletion constructs are missing the N-terminal 30 (p14Δecto30) or 36 residues (p14Δecto36) of the ~38-residue p14 ectodomain, and both of these constructs are fusion-dead (Noyce, Taylor et al. 2011). Co-immunoprecipitation analysis was performed to analyze the interaction profile of these constructs with AX1, using ectodomain or endodomain-specific antisera to detect the endodomain or ectodomain truncation constructs, respectively. Surprisingly, both the C105 and C78 deletion mutants were able to efficiently interact with AX1 (Fig 4.10B) whereas neither of the N-terminal ectodomain truncation constructs co-precipitated with AX1 (Fig 4.11B).

4.2.5 Annexin interactions by co-immunoprecipitation are specific for p14.

The endodomain truncation results were unexpected since the endodomain was used to identify AX1 as a p14 interaction partner in the yeast two-hybrid experiments. These results raised concerns regarding the specificity of the co-immunoprecipitation assay. I therefore conducted several control experiments to test the validity of the p14-AX1 interaction. To eliminate the possibility that p14 was merely binding to the FLAG tag used in the co-immunoprecipitations, constructs expressing the FLAG-tag fused to two intracellular proteins, zyxin and 14-3-3, were used in place of FLAG-AX1. These constructs were generously provided by Dr. Fui Boon Kai.

Co-immunoprecipitation experiments revealed that neither FLAG-zyxin nor FLAG-14-3-3 complexed with p14 (Fig 4.12). FLAG-tagged zyxin and 14-3-3 were only weakly detected in cell lysates, suggesting expression issues might have contributed to the inability to detect these proteins in the immunoprecipitates. To ensure AX1 was not interacting with p14 solely because of gross overexpression of the protein, a soluble protein, GFP, and a membrane protein, HER2, were used in place of p14. The HER2 construct and antibody was generously provided by Dr. Graham Dellaire, Dalhousie

University. Both GFP and HER2 were readily detected in cell lysates, but neither protein co-immunoprecipitated with FLAG-AX1 (Fig 4.13). Interestingly, co-immunoprecipitation of p14 was also detected with an AX1 construct containing point substitutions that mutate three core domain Ca^{2+}-binding sites (McNeil, Rescher et al. 2006). In addition, wild type AX1 was also able to interact with a fusion-defective p14-G2A construct in a calcium-dependent manner (Fig 4.12), implying p14 membrane fusion activity is not required for AX1 interactions.

To ensure that cellular membranes were fully solubilized upon cell lysis, and that AX1 was not co-precipitating p14 by interacting with plasma membrane vesicles containing p14 instead of directly with p14, cells were subjected to lysis in 2% NP-40. Co-immunoprecipitation analysis confirmed that p14 was still capable of interaction with AX1 (Fig 4.14). Lastly, HEK cell lysates co-transfected with p14 and FLAG-AX1 in the presence of 100 μM Ca^{2+} were subjected to centrifugation at 100 000xg to ensure that p14 and AX1 were not contained in residual membrane fractions within the supernatant. The vast majority of p14 was present in the supernatant fraction after ultracentrifugation, with only trace amounts detected in the pellet (Fig 4.14), implying p14 was fully solubilized by the standard detergent lysis protocol. Under these conditions, p14 was still co-precipitated with AX1 from the supernatant obtained following the ultracentrifugation step, and in the presence of either high (5 mM) or low (100 μM) concentrations of Ca^{2+} (Fig 4.14). These finding suggest that the p14-AX1 interaction is not based on indiscriminate calcium-dependent binding of AX1 to membranes containing p14.

4.2.6 Annexin A1 is required for efficient measles F-mediated syncytium formation

To determine whether the involvement of AX1 in syncytium formation was specific to p14 or was a more general cellular response to virus mediated cell-to-cell fusion, I investigated the role of AX1 in measles fusion (F) protein-mediated syncytiogenesis. The measles F protein was chosen to represent a canonical viral fusogen, which greatly differs in size and mode of action from the FAST proteins. In addition, the measles F-protein does not require a low pH trigger, and its syncytial kinetics in HT1080 were similar to those of p14 allowing for easy detection of impaired cell fusion and for comparison with p14-mediated syncytium formation.

The requirement for AX1 and AX5 during measles F-mediated cell-to-cell fusion was tested in a manner analogous to that of p14 in Fig 1. HT1080 cells were sequentially transfected with control or AX1 siRNA, followed by transfection with measles F and hemagglutinin (H) proteins, for which the constructs and antibodies were generously provided by Dr. Ryan Noyce. To induce F-mediated cellular fusion, both the F and H proteins of measles virus must be transfected to form heterodimers, with H responsible for receptor binding and activation of F, and F for mediating the fusion reaction (Wild, Malvoisin et al. 1991, Corey and Iorio 2007). HT1080 cells, where AX1 expression was abrogated by siRNA, were found to fuse approximately 50% less efficiently than those treated with control siRNA (Fig 4.15A). Syncytium formation was quantified at 14, 18, and 22 hrs post-transfection and the 50% difference in cell-to-cell fusion was maintained throughout the time course (Fig 4.15B). Low (0.1 μg DNA/well) and high (0.5 μg DNA/well) concentrations of F and H proteins were transfected in order to analyze the effect of fusion protein concentration on syncytium formation in the presence and absence of AX1 or AX5. As expected, transfecting lower amounts of DNA resulted in less fusion, with almost no syncytia appearing in cells treated with AX1 and AX5 siRNA (Fig 4.15C). Interestingly, high fusion protein expression conditions were able to partially overcome the inhibitory effect of AX1 siRNA treatment (Fig 4.15C). For the purpose of a direct comparison, AX1 and AX5 siRNA-treated HT1080 cells were also transfected with p14 within the same experiment. The extent of syncytium generation in the presence or absence of AX1 and AX5 (Fig 4.15C) was consistent with previous results (Fig. 4.1).

To further investigate whether the involvement of AX1 in measles F-mediated syncytium formation mirrored p14-mediated syncytiogenesis, co-immunoprecipitation experiments of AX1 with F and H were performed. Surprisingly, even under stringent conditions of 2% NP40 treatment, immunoprecipitation of FLAG-tagged AX1 yielded complexes with both F and with H, when cells were expressing both proteins or expressing either protein alone (Fig 4.16). These results suggest that both F and H proteins of measles virus were able to independently interact with AX1.

4.2.7 Intacellular calcium is involved in RRV p14- and measles F-mediated syncytium formation

Having determined that the presence of Ca^{2+} is essential in the maintenance of p14-AX1, I chose to investigate the role that intracellular Ca^{2+} itself may play during virus-mediated syncytium formation. To this end, I used 1,2-Bis(2-aminophenoxy)ethane-N,N,N′,N′-tetraacetic acid tetrakis(acetoxymethyl ester) (BAPTA-AM), which has been widely used as an intracellular Ca^{2+} chelator in studies of intracellular Ca2+ release and neurotransmitter signalling (Dargan and Parker 2003, Bird, DeHaven et al. 2008, Vyleta and Smith 2011) . Monolayers of quail muscle fibroblast (QM5) cells were transfected with p14 and treated with commonly reported concentrations of BAPTA-AM ranging from 0 to 40 μM (Megeath and Fallon 1998, Bijlenga, Liu et al. 2000, Worrall and Olefsky 2002). Syncytium formation was greatly reduced following treatment with 20 μM BAPTA-AM and was nearly abrogated in the presence of 40 μM BAPTA-AM (Fig 4.17A). The requirement for intracellular Ca^{2+} during p14-mediated syncytium formation was not cell-type specific, as similar results were obtained by treating p14-transfected HT1080 cells with BAPTA-AM (Fig 4.17.B). In addition, when HT1080 cells transfected with a FRET pair of p14-GFP and mCherry-AX1 were treated with BAPTA-AM, the FRET efficiency was reduced by ~70% in the presence of 20 μM BAPTA-AM and by >90% in the presence of 40 μM BAPTA-AM (Fig 4.17C). BAPTA treatment of HT1080 cells co-transfected with measles F and H proteins also resulted in a significant decrease in syncytium formation, although it required 50 μM BAPTA-AM to reduce syncytiogenesis by ~60% (Fig 4.17D). No further decrease in measles F protein-mediated syncytium formation was seen following treatment with 100 μM BAPTA-AM (Fig 4.17D).

The involvement of Ca^{2+} during p14 fusion was also investigated by chelating the cation with EGTA-AM (ethylene glycol tetra(acetoxymethyl ester)) in HT1080 cells. Cells were transfected with p14 and treated with EGTA-AM at 4 hrs post-transfection, which paralleled the BAPTA-AM studies. However, only a modest decrease in p14-mediated syncytium formation was detected following treatment with 100-200 μM EGTA-AM, the highest concentrations of the chelator that did not result in cytotoxicity (Fig 4.18A).

In an effort to determine whether the inhibitory effects of BAPTA-AM-could be overcome by releasing intracellular Ca^{2+} stores, cells expressing p14 were treated with the ionophore ionomycin. The efficacy of 1 mM ionomycin to increase intracellular Ca^{2+} concentrations was confirmed by detection of a spike in fluorescence in cells loaded with the calcium indicator Fluo-4 AM (data not shown). HT1080 cells transfected with p14 and treated with BAPTA-AM at 4 hrs post-transfection were treated with 1 mM ionomycin at 5 and 6 hrs post-transfection, with the ionophore remaining in the culture medium until fixation at 12 hrs post-transfection. No significant difference in p14-mediated syncytiogenesis was detected between cells treated with BAPTA-AM and those treated with BAPTA-AM and 1 mM ionomycin (Fig 4.18B).

4.2.8 Annexin A1 and intracellular calcium are necessary for RRV p14-mediated pore expansion but not pore formation

Although our studies clearly demonstrated that AX1 plays a role in p14-mediated syncytiogenesis, it remained unclear whether AX1 is necessary for efficient lipid mixing and/or pore formation during the cell-to-cell fusion reaction, or whether it is involved in a post-fusion, pore expansion step. I developed a fluorescent, dual colour, homotypic pore formation assay to determine where in the p14-mediated cell-cell membrane fusion reaction AX1 exerts its effects. Sparsely seeded HT1080 cells ($1x10^5$ cells per well) were transfected with control or AX1 siRNA, and after 36 hrs were co-transfected with plasmids expressing p14 and GFP. The GFP plasmid served as a marker to identify cells expressing p14. Target HT1080 cells were labeled with the soluble cytoplasmic fluor calcein Red-Orange-AM, cells were overseeded on the donor cell monolayers 6 hrs after plasmid transfection, and donor and target cells were co-cultured for 6 hrs. Flow cytometry was employed to quantify the number of cells expressing GFP and p14 that also contained calcein, indicative of pore formation between donor and target cells. As shown, (Fig. 4.19B), the extent of fluorescent marker transfer was equal when donor cells contained normal or decreased levels of AX1, indicating that AX1 in the donor, fusogen containing cell is not necessary for pore formation (Fig 4.19A and B).

Interestingly, fluorescence microscopy detected small syncytia present in this homotypic pore formation assay, indicated by co-localization of green and red fluorescent

markers in multinucleated cells, irrespective of whether cells were treated with control or AX1 siRNA (Fig 4.19A). This result markedly contrasted with the dramatic reduction in syncytia formation induced by AX1 siRNA and shRNA in the syncytiogenesis assays (Figs. 4.1 and 4.3). It is notable that the syncytiogenesis assay involves treatment of the entire monolayer with AX1 siRNA. In the pore formation assay, only donor cells are treated with AX1 siRNA; the large number of target cells employed in this assay make it unfeasible to treat target cells by siRNA transfection.

Similar to AX1 depletion, the chelation of intracellular Ca^{2+} by BAPTA-AM was also found to dramatically decrease p14-mediated syncytium formation. To investigate whether intracellular Ca^{2+} is necessary for membrane fusion or for the subsequent pore enlargement step, a modified version of the pore formation experiment described above was performed. While donor Vero cells were co-transfected with p14 and GFP plasmids, target Vero cells were labeled with calcein Red-Orange-AM, and both donor and target cells were treated with BAPTA-AM prior to co-culturing the two populations. Co-localization of GFP and calcein by both fluorescence microscopy and flow cytometry analysis revealed that the two concentrations of BAPTA-AM that substantially impaired p14-induced syncytium formation (Fig. 4.17) had no effect on pore formation (Fig. 4.20B), indicating intracellular Ca^{2+} concentrations do not affect pore formation. The FACS results were supported by analysis of the same homotypic pore formation assay using fluorescence microscopy. When intracellular Ca^{2+} was chelated by BAPTA-AM treatment of both the donor and target cell populations, syncytiogenesis was inhibited (i.e. no syncytia were detected), the same as it was in the previously described syncytiogenesis assay. However, numerous mononucleated cells containing both fluorescent markers were observed in the presence or absence of 40 μM BAPTA-AM (Fig. 4.20A, arrows), indicating pore formation was unaffected by chelating intracellular Ca^{2+} (Fig 4.20A).

4.2.9 Extracellular annexin A1 is necessary for C2C12 myotube formation but not for RRV-p14 mediated syncytium formation

Recent reports of studies with mouse muscle myoblast C2C12 cells have suggested that extracellular AX1 is involved in cell-to cell fusion leading to myotube formation

(Bizzarro, Belvedere et al. 2012, Leikina, Melikov et al. 2013). A key finding leading to these conclusions derived from studies of antibody inhibition of extracellular AX1 during C2C12 differentiation. To assess whether the role of AX1 during p14-mediated syncytium formation was analogous to that in myoblast fusion, I performed antibody-blocking experiments in HT1080 cells expressing p14. To eliminate the possibility of the onset of syncytium formation in the absence of blocking antibody, p14-transfected cells were treated with anti-AX1 antibody as early as 2 hrs post-transfection (syncytium formation first appears in p14-transfected HT1080 cells at approximately 8 hrs post-transfection). Quantification of syncytia revealed that the presence of extracellular AX1 antibody had no effect on p14-mediated syncytium formation in HT1080 cells at all antibody dilutions tested (Fig 4.21A and B).

To ensure the anti-AX1 antibody was capable of inhibiting AX1-dependent cell-cell fusion, I replicated the previously reported findings in C2C12 cells. C2C12 myoblasts proliferate in the presence of FBS, but when FBS is replaced by 2% horse serum undergo differentiation-dependent cell-cell fusion to create multinucleated myotubes. When C2C12 cells were induced to differentiate in the presence of anti-AX1 antibody, myotube formation was inhibited by ~55% (Fig 4.22A and B). In addition to validating the previously published antibody inhibition assay, the C2C12 system provided an excellent avenue for evaluating whether cell-type differences between HT1080 cells and C2C12 cells contributed to the different effects of anti-AX1 antibody on C2C12 myotube formation during myogenesis versus p14-induced cell-cell fusion. C2C12 cells were transfected with p14 and treated with anti-AX1 antibody under growth conditions (i.e., in the presence of FBS rather than horse serum). Unlike C2C12 myogenesis, p14-mediated C2C12 syncytium formation was insensitive to treatment of cells with extracellular anti-AX1 antibody (Fig 4.22 C and D). Thus, AX1 appears to exert very different effects on p14-mediated syncytium formation versus C2C12 cell-to-cell fusion during myogenesis.

4.3 Discussion

Previous studies have compared members of the FAST protein family to enveloped viral fusogens and have effectively demonstrated the many contrasts in their size, distribution across membranes, and their likely modes of action. The present investigation into the role of AX1 and AX5, in the context of p14- and measles F-mediated cell-to-cell fusion yielded several surprising discoveries. We found that, not only do AX1 and AX5 play a role in p14-mediated pore expansion, but AX1 is also a factor in measles F-mediated syncytiogenesis. AX1 was found to interact with both proteins by co-immunoprecipitation, and to do so intracellularly in the case of p14, as demonstrated by FRET. Antibody inhibition of extracellular AX1 had no effect on p14-mediated syncytium formation in HT1080 cells, thus strengthening our hypothesis that the enhancing role of AX1 occurred in an intracellular capacity. Furthermore, the p14-AX1 interaction was shown to be Ca^{2+}-dependent, and chelation of intracellular Ca^{2+} was able to drastically reduce both p14- and F-mediated syncytium formation. Additional investigation into the role of AX1, employing fluorescence microscopy and FACS analysis, clearly revealed AX1 is involved in a post-pore formation, pore expansion event. This finding has provided some insight into potential similarities between viral fusogen-induced pore expansion, which occurs downstream of membrane merger and pore formation events. Surprisingly, while we uncovered a commonality during syncytiogenesis mediated by extremely diverse viral fusogens, we also found a startling difference between the role of AX1 in p14- and C2C12 myoblast fusion. As previously reported by Leikina et al. 2013, AX1 antibody inhibition was effective in hindering C2C12 myotube formation, however, no effect on fusion kinetics was detected during p14-mediated fusion of undifferentiated C2C12 cells (Leikina, Melikov et al. 2013). Thus, AX1 is a multifunctional cellular fusion factor that can function extracellularly to enhance the pre-fusion and/or fusion stages of syncytium formation, and intracellularly to promote post-fusion pore expansion. It remains to be seen whether these diverse roles of AX1 reflect common or distinctive pathways of virus and myoblast-fusogen induced syncytium formation.

4.3.1 Annexin A1 is involved in syncytium formation mediated by p14 and measles virus F and H proteins.

Downregulation of AX1 expression by siRNA or shRNA has been a fundamental tool in uncovering the multifunctional role of this protein in various cellular processes including phagocytosis, endocytosis, cellular proliferation, blebbing and myoblast fusion (Bizzarro, Fontanella et al. 2010, Babiychuk, Monastyrskaya et al. 2011, Khau, Langenbach et al. 2011, Patel, Ahmad et al. 2011, Tcatchoff, Andersson et al. 2012). In order to ensure that off-target effects were not responsible for the decrease in 14-mediated syncytium formation in this study, cellular AX1 was depleted via treatment with siRNA or shRNA, targeting different sequences of AX1. One of the shRNAs was based on a previously published and validated shRNA sequence (Babiychuk, Monastyrskaya et al. 2011) (Fig 4.1 and Fig 4.3). As I showed, knockdown of AX1 expression using siRNA or shRNA inhibited p14-mediated syncytiogenesis. Interestingly, only the validated AX1 shRNA was able to knockdown the expression of AX1, however, less efficiently than siRNA treatment. This difference in knock-down may be due to treatment of cells with a pool of four siRNAs versus one shRNA sequence, potentially resulting in a more robust silencing phenotype. Having validated the relevance of siRNA knock down of AX1 during p14-induced syncytium formation, I repeated this experiment in the context of an AX5-deficient background. Indeed, the knock-down of AX5 also decreased p14-induced syncytium formation, mirroring the finding that depletion of AX5 leads to reduced myoblast fusion (Leikina, Melikov et al. 2013).

Both AX1 and AX5 are implicated in plasma membrane repair (McNeil, Rescher et al. 2006, Bouter, Gounou et al. 2011). Based on the idea that plasma membrane remodeling and fusion events occur during membrane repair, we hypothesized that this cellular process might also be involved during virus-mediated syncytium formation. A previous report indicates dysferlin, a calcium-binding protein, interacts with AX1 and plays a major role during vesicle fusion-mediated membrane repair (Lennon, Kho et al. 2003). To investigate whether dysferlin also plays a role in virus-mediated syncytium formation, the expression of this repair factor was knocked down via siRNA and p14- as well as measles F-mediated fusion of HT1080 cells was assessed. Quantification of syncytial nuclei indicated that the presence of dysferlin was not required by either viral

fusogen for syncytium formation in this cell line (Fig 4.23 A and B). This result does not eliminate the possibility that membrane repair is involved in viral fusogen-mediated syncytium formation. However, it does suggest that this process, if it is involved in syncytium formation, proceeds via dysferlin-independent pathways.

The discovery that AX1 could modulate cell fusion during C2C12 differentiation suggested p14 has evolved to access this cellular pathway in its role as a dedicated cell-to-cell fusogen. AX1-dependence could be restricted to dedicated cell-cell fusogens, such as the FAST proteins and the unidentified fusogens involved in C2C12 differentiation-dependent fusion, or it could reflect a more general cellular response to membrane assault, such as during membrane blebbing, endocytosis, membrane repair or cell-cell fusion mediated by enveloped virus fusogens (McNeil, Rescher et al. 2006, Idone, Tam et al. 2008, Babiychuk, Monastyrskaya et al. 2011). To differentiate between these possibilities, a canonical enveloped virus fusogen complex, the measles F and H heterodimer, was employed in a syncytiogenesis assay in cells treated with AX1 siRNA. Surprisingly, depletion of AX1 resulted in a marked decrease in measles F-mediated fusion of cell monolayers. The well characterized measles virus fusion complex has evolved to function from the viral membrane to mediate virus-cell fusion, independently mediating the entire fusion reaction. My finding that AX1 also influences measles virus-induced syncytiogenesis suggested AX1 is likely involved in a general cellular response to membrane fusion or perhaps membrane perturbation, functioning to resolve intercellular pores via pore expansion.

Having determined that depletion of AX1 is detrimental to viral fusogen-mediated syncytiogenesis, I attempted to rescue p14-mediated syncytium formation in the AX1 deficient cells by supplementing them with AX1 plasmid DNA. Surprisingly, increased syncytium formation was seen upon AX1 DNA transfection in only one experiment (Fig 4.1), and in three subsequent experiments neither control nor AX1 siRNA treated cells formed syncytia when wild type AX1 was overexpressed with p14 (Fig 4.2). This intriguing finding suggested that a highly specific cellular concentration of AX1 may be necessary for the onset of syncytium formation, and that excess amounts of AX1 may block or interfere with the fusion site or signaling pathways involved in cellular rearrangements. Alternatively, transfection of AX1 may modulate alternative cellular

pathways that conflict with cell fusion. For example, overexpression of AX1 results in increased caspase-3 activation leading to apoptosis, the onset of which may interfere with p14-mediated syncytiogenesis (Solito, de Coupade et al. 2001, Hsiang, Tunoda et al. 2006). In contrast, it is known that caspase-3 activation and the onset of apoptosis is essential for the efficient differentiation and fusion of myoblasts during myotube formation (Fernando, Kelly et al. 2002). Interestingly, a recent report indicates that apoptotic cells themselves do not fuse, but that phosphatidyl serine (PS) exposed on the extracellular leaflet of the plasma membrane seems to promote the differentiation and fusion between healthy muscle cells via the PS receptor BAI1 and its effector ELMO/Dock 180/Rac-1 proteins (Hochreiter-Hufford, Lee et al. 2013). It is possible that, in the context of p14-mediated cell fusion, overexpression of AX1 may lead to the activation of the cellular apoptotic machinery. However, since apoptotic cells themselves, at least in the context of myoblast fusion, do not seem to undergo cell fusion, overexpression of AX1 in monolayers may effectively render all cells to become non-fusogenic. Additional evidence suggesting such a scenario comes from co-transfection studies of soluble GFP and p14 constructs, where the overexpression of GFP essentially abrogates syncytium formation (Cameron Landry, personal communication). Further analysis of the apoptotic state of co-transfected cells is necessary to corroborate this theory. However, this finding does caution that studies employing protein overexpression to investigate cell fusion may lead to erroneous conclusions.

4.3.2 Annexin A1 interacts with p14 and measles virus F and H proteins.

Co-immunoprecipitation studies were undertaken in an effort to further investigate the role that AX1 plays during syncytium formation. While it was predicted that AX1 would bind to p14, based on the preliminary yeast-two-hybrid results, the interaction of AX1 with not only measles F but also H proteins, when expressed together or separately, was quite unexpected. Interestingly, the cytoplasmic tails of both F and H proteins can separately bind to the measles matrix (M) protein. This interaction is necessary for the efficient targeting of the viral glycoproteins to the apical side of polarized cells, for control of cell-to-cell fusion, and for efficient virion release (Cathomen, Naim et al. 1998, Naim, Ehler et al. 2000, Runkler, Dietzel et al. 2008). A

sequence alignment of the cytoplasmic tails of H, F and p14 did not identify any obvious sequence similarity (data not shown). However, it is possible that these cytoplasmic tails could interact with the same cellular partner via a secondary structure that is assumed upon binding.

Interestingly, measles F and H proteins have somewhat longer cytoplasmic tails (33 residues for F and 34 residues for H) than many other enveloped virus glycoproteins (e.g 11 residues for influenza HA) (Jin, Leser et al. 1994, Moll, Klenk et al. 2002). It would be interesting to determine whether other enveloped virus fusogens with shorter cytoplasmic tails also interact with AX1.

Co-immunoprecipitation is a standard technique for detecting protein-protein interactions. However, meaningful results can only be obtained when coupled with stringent controls. In this study, a battery of control experiments was undertaken to eliminate the possibility of detecting false positive, artifactual interactions. Firstly, I eliminated the possibility that p14 was preferentially binding to the magnetic immunoprecipitation beads or to the FLAG tag of AX1. Secondly, I rejected the notion that AX1 was promiscuously binding to any overexpressed soluble (GFP) or transmembrane (HER2) proteins. Interestingly, while AX1 binds EGFR, it does not interact with another member of the EGFR family, HER2, further pointing to its high interaction specificity (Radke, Austermann et al. 2004). Thirdly, I ensured that cell lysis conditions and solubilization of membranes were not leading to the precipitation of membrane vesicles containing p14 and phospholipid-bound AX1. Previously employed ultracentrifugation protocols and high detergent conditions (Mathias, Lim et al. 2009, Gyorgy, Szabo et al. 2011) revealed the supernatants I used for co-immunoprecipitation were cleared of any residual plasma membrane complexes .

Most notably, my co-immunoprecipitation results implying p14-AX1 interactions were confirmed *in vivo* under physiological conditions by the detection of FRET pairing upon p14 and AX1 co-transfection . FRET signals are inversely proportional to the gap between donor and acceptor proteins. With a scale that is the inverse sixth power of the distance, only interactions between proteins less than 10 nm apart can produce a detectable energy transfer signal, implying a direct protein-protein interaction event (Wouters, Verveer et al. 2001, Gell, Grant et al. 2012). These results gave us confidence

that AX1 does indeed interact with RRV p14. Similar FRET studies should be performed to confirm AX1 interaction with measles F and H proteins. The approach used to detect FRET was very stringent. Under these conditions, we detected a direct p14-AX1 interaction occurring at what is a presumably an intracellular membrane compartment. Determining the identity of this intracellular interaction compartment would be challenging using co-immunofluorescence with membrane compartment markers due to spectral overlap, but should be attempted. Since, the p14-AX1 FRET interactions are an underestimate and only detect the strongest interactions, we also cannot exclude that p14-AX1 interactions may also be occurring at the plasma membrane.

4.3.3 Annexin A1 interacts with p14 and measles virus F and H proteins in a calcium-dependent manner.

AX1 interacts with multiple cellular partners in a calcium-dependent manner, as in the case of S100A11, dysferlin, F-actin, EGFR, and cPLA2, or in a calcium-independent manner, as in the case of profilin (Glenney, Tack et al. 1987, Alvarez-Martinez, Mani et al. 1996, Kim, Rhee et al. 2001, Lennon, Kho et al. 2003, Hayes, Rescher et al. 2004, Radke, Austermann et al. 2004, Herbert, Odell et al. 2007). Due to the characteristic calcium binding nature of AX1, I investigated whether the AX1 and p14 interaction is also calcium-dependent. As shown, calcium-dependent interactions were detected between AX1 and p14, as well as between AX1 and measles F and H proteins. Numerous studies report interactions between members of the AX1 family and cellular proteins at millimolar concentrations of calcium (Mailliard, Haigler et al. 1996, de Coupade, Solito et al. 2003, Wang, Chintagari et al. 2007). In the present study, initial co-immunoprecipitation experiments were conducted at high $CaCl_2$ concentrations (i.e 5 mM). The preliminary finding that AX1-p14 interaction is calcium-dependent was subsequently confirmed at physiologically relevant calcium concentrations by co-immunoporecipitation and FRET analysis. The resting state intracellular calcium concentration of non-excitable cells is on the order of 10-100 nM, and can rise to several micromolar upon stimulation (Bootman and Berridge 1995). To simulate intracellular calcium signaling conditions and demonstrate a physiologically relevant AX1-p14 interaction in an *in vitro* system, I determined that p14-AX1 interactions occur even when

the calcium concentration of the immunoprecipitation buffer was titrated to micromolar levels. This result mirrored one obtained by Ryzhova et al. (2006) who reported an enhancement of interaction of HIV Gag with AX2 in the presence of 100 μM calcium, without increasing non-specific binding (Ryzhova, Vos et al. 2006). In addition, increasing the extracellular concentration of calcium ions from 100 μM to 10 mM increases fusion mediated by HIV envelope protein (env) bound to its receptor CD4 and enhances syncytium formation at a post-binding step (Dimitrov, Broder et al. 1993).

My results also revealed p14-AX1 interactions at physiologically relevant calcium concentrations, but not with similar concentrations of magnesium. Interestingly, replacing calcium with magnesium did not have the same effect, and did not increase syncytiogenesis mediated by HIV env, thus demonstrating a specific requirement for calcium during HIV env-mediated syncytium formation (Dimitrov, Broder et al. 1993). Magnesium supplementation also has no effect on the binding dose response of the calcium sensor otoferlin, which directly influences SNARE-mediated synaptic vesicle fusion to plasma membranes during exocytosis (Johnson and Chapman 2010). The lack of interaction between AX1 and p14 at micromolar levels of magnesium in my study also suggests that calcium specificity plays an important role during this binding event, and that calcium may play an important role during p14-AX1 interaction and p14-mediated syncytium formation.

The calcium dependency of the p14-AX1 interaction was also probed by examining the ability of a non-calcium-binding AX1 construct. This dominant-negative mutant has been reported to decrease the AX1-dependent membrane resealing process due to its inability to bind calcium (McNeil, Rescher et al. 2006). Interestingly, the core domain calcium-binding sites mutated in this construct are involved in calcium-dependent binding of AX1 to endosomal membranes and multivesicular bodies (Futter, Felder et al. 1993, Rescher, Zobiack et al. 2000). However, the association of AX1 with membranes can be calcium-dependent and -independent, with dependency being conferred via phosphorylation of AX1 by EGFR residing in the multivesicular bodies (Futter, Felder et al. 1993). It is likely that the p14-AX1 interaction reported in our study does not require the binding of AX1 to a specific phospholipid membrane, and that the

calcium-dependency, as observed by co-immunoprecipitation and FRET, is necessary for bridging of the two proteins via alternate binding sites.

4.3.4 The N-terminal tail of annexin A1 is not required for interaction with p14.

While members of the Annexin protein family share a high degree of sequence conservation in their core phospholipid-binding domain, their N-terminal tails are highly variable and are the site of modification, they mediate differential calcium-binding sensitivity, and they interact with cellular partners such as the well-characterized interaction of AX1 with S100A11 (Seemann, Weber et al. 1996, Gerke and Moss 2002, Gerke, Creutz et al. 2005, Monastyrskaya, Babiychuk et al. 2007). However, several reports have shown that the core domain of AX1 can also serve as an interaction site for cellular partners. The plasma membrane-resident EGFR not only phosphorylates AX1 on Tyr 21, but also interacts with the core region of this protein at the plasma membrane and within endosomes in a calcium-dependent manner (Radke, Austermann et al. 2004). Additionally, the 72 C-terminal residues of the AX1 core domain mediates interaction with cellular phospholipase A2α (PLA2α) (Kim, Rhee et al. 2001). In my study, full truncation of the AX1 N-terminus had no effect on the binding of p14, thus indicating that the association is likely mediated by the core domain of AX1. Given that the N-terminal 90 residues of AX1 were employed in the yeast two-hybrid screen, and that deletion of the 45 residue N-terminal domain had no effect on binding, it is likely that the first repeat of the core domain may be the p14-interacting region of AX1.

4.3.5 Multimerization of p14 may be required for interaction with annexin A1.

The soluble p14 endodomain was previously implicated in enhancing syncytium formation mediated by various fusogens, suggesting that it may interact with cellular partners that participate in a common pore expansion pathway (Top, Barry et al. 2009). The p14 endodomain was used as the bait protein in the above-mentioned yeast-two hybrid system where AX1 was identified as a partner. The present study suggests that neither the C-terminal 47 resides nor the ensuing polybasic region of the p14 endodomain are responsible for AX1 interaction. A remaining region of ten amino acids between the polybasic stretch and the C78 deletion mutant, as well as four amino acids that reside between the transmembrane domain and polybasic region, remain to be evaluated as

potential AX1 interaction sites. The surprising finding that p14 mutants lacking the ectodomain do not interact with AX1 via co-immunoprecipitation invokes two possibilities; that AX1 interacts with the N-terminal 30 amino acids of p14, or that the p14 ectodomain may be responsible for the location and aggregation of p14 and membrane destabilization. Previous reports indicate the p14 ectodomain contains the multimerization motif necessary for oligomerization of this fusogen during transit through the Er-Golgi trafficking pathway, and that ectodomain deletion mutants do not elicit any measurable effects on target cell membranes (Corcoran, Clancy et al. 2011, Noyce, Taylor et al. 2011). It is possible that AX1 may only interact with an intact p14 multimer, or that membrane perturbation, even in the absence of full fusion may be required for AX1 binding. This hypothesis is further substantiated by the detection of an interaction between AX1 and p14-G2A, a fusion-incompetent mutant lacking an N-terminal myristoylation sequence due to a single mutation at the N-terminal glycine residue. This construct presumably contains the correct multimerization signal, and has been shown to influence membrane perturbation resulting in the activation of intracellular immunity pathways (Ryan Noyce, personal communication).

4.3.6 Intracellular calcium is essential for efficient syncytiogenesis during p14- and measles F-mediated membrane fusion.

A separate line of evidence for the dependence of viral fusogen-mediated syncytium formation on intracellular calcium was obtained via the chelation of intracellular Ca^{2+} ions with BAPTA-AM. Several previously reported studies have employed BAPTA-AM in efforts to identify a role for intracellular calcium in vesicle fusion. The fusion of membranous organelles to the plasma membrane during *C. elegans* spermatogenesis requires the presence of FER-1, a member of the ferlin family, characterized by the presence of four to seven C2-calcium binding domains. Chelation of intracellular Ca^{2+} by BAPTA-AM effectively abrogates membranous organelle fusion, while the presence or absence of extracellular calcium has no effect on this process as demonstrated by treatment with EGTA (Washington and Ward 2006). Similarly, the requirement for intracellular calcium during exosome release has also been shown via treatment of cells with BAPTA-AM (Savina, Furlan et al. 2003). Chelation of

intracellular calcium was used to demonstrate that intracellular calcium signaling is responsible for converting synaptotagmin, a C2 domain-containing protein, from a clamp which assembles the SNARE complex to a trigger for exocytosis (Chicka, Hui et al. 2008).

In the present study, I found that chelation of intracellular calcium by BAPTA-AM dramatically decreased p14-mediated syncytiogenesis. EGTA-AM was also employed in a manner similar to that of BAPTA-AM, however, no decrease in fusion was noted. While both chelators are able to bind calcium with similar affinity, the kinetics of binding differ between BAPTA, with an on rate of ~100-1000 $\mu M^{-1}s^{-1}$, and EGTA with an on rate of ~3-10 $\mu M^{-1}s^{-1}$; this difference in calcium binding kinetics differentially regulates intracellular calcium signaling (Dargan and Parker 2003). It is possible that a differential calcium buffering capacity may also be involved in regulating syncytium formation induced by viral fusogens. While measles F-mediated fusion also decreased in the absence of calcium, a complete fusion-block was not achieved. Interestingly, these results mirrored those obtained upon AX1 knockdown. Upon further investigation, FRET analysis revealed that BAPTA treatment also resulted in the loss of AX1 and p14 interaction. This result corroborated our previous results that the presence of calcium was essential for p14-AX1 interaction, as well as substantiated the previous results that intracellular calcium is involved in p14-mediated syncytiogenesis.

4.3.7 Annexin A1 and intracellular calcium act downstream of membrane fusion to facilitate efficient pore expansion during syncytiogenesis.

Intracellular calcium has been implicated in fusion pore expansion events during vesicle exocytosis of secretory granules as well as during neurotransmitter release, stimulating faster expansion and a shift from kiss-and-run fusion to more efficient pore resolution respectively (Scepek, Coorssen et al. 1998, Haller, Dietl et al. 2001, Elhamdani, Azizi et al. 2006). In addition, spikes in intracellular calcium at the site of lamellar body fusion in rat type II pneumocytes occur 200-500 ms following pore formation. This fusion-associated Ca^{2+} entry (FACE) mechanism was shown to be mediated by vesicle-associated P2X4 purinergic receptors, and the influx of calcium was shown to facilitate fusion pore dilation and surfactant release (Haller, Dietl et al. 2001,

Miklavc, Frick et al. 2010, Miklavc, Mair et al. 2011). In the present study, chelation of intracellular calcium with BAPTA-AM also resulted in a dramatic decrease in pore expansion, but had no discernable effect on pore formation. This novel finding may suggest that, similar to its role during exocytic vesicle fusion and content release, intracellular calcium concentration may be involved in controlling the rate of dilation of cell-cell membrane fusion pores.

Scepek et al. (1998) also report that activation of protein kinase C (PKC) promotes the rate of pore expansion of exocytic vesicles fused with the plasma membrane (Scepek, Coorssen et al. 1998). Conversely, it has been reported that PKC negatively regulates HA-mediated pore expansion between fused cells (Richard, Leikina et al. 2009). AX1 has also been shown to translocate across plasma membranes upon calcium-dependent PKC-mediated phosphorylation (John, Cover et al. 2002, Solito, Mulla et al. 2003). I found that knockdown of AX1 expression in p14-transfected donor cells does not affect efficient pore formation. Furthermore, depleting intracellular calcium in both donor and target cells had no effect on pore formation when assessed by either flow cytometry (Fig. 4.19B) or fluorescence microscopy (Fig. 4.19A). The role of AX1 in p14-mediated cell-cell fusion is therefore downstream of pore formation. Since AX1 knockdown and BAPTA-AM treatment both severely impaired p14-mediated syncytiogenesis (Figs. 4.1 and 4.17), I infer that AX1 is required for efficient pore expansion following p14-mediated pore formation.

Interestingly, fluorescence microscopy indicated small syncytia can form when donor cells treated with AX1 siRNA were used during the pore formation assay (Fig. 4.19A). In contrast to our syncytiogenesis assay, where all cells are treated with siRNA and subsequently transfected with fusogens, the target population used in the pore formation assay contained a full complement of wild type AX1. I therefore hypothesize that AX1 present in these target cells is sufficient to promote pore expansion and syncytium formation. AX1 could exert its pore expansion role from only the target cells, or following AX1-independent pore formation, AX1 could enter donor cells to exert an effect from both the target and donor cells, resolving intercellular pores to multinucleated syncytia.

4.3.8 A novel role for annexin A1 and its implications in viral fusion protein-mediated syncytium formation

Extracellular AX1 was recently reported to be involved in mouse myoblast differentiation and myotube formation (Bizzarro, Fontanella et al. 2010, Leikina, Melikov et al. 2013). Leikina et al. (2013) report that the involvement of AX1 in differentiation is linked to the presence of extracelluar calcium and phosphatidylserine in the outer leaflet of the plasma membrane, and that AX1 itself is involved at an early, membrane merger stage of myoblast fusion. Bizzarro et al. (2012) report that AX1 is not the fusogen, but is involved in signaling via formyl peptide receptors (FPRs) and effecting the migration of myoblasts at a pre-fusion step in myogenesis (Bizzarro, Belvedere et al. 2012, Bizzarro, Fontanella et al. 2012). Despite the divergent conclusions of these two groups, a common experimental approach employing antibody inhibition revealed a decrease in cell fusion in the presence of anti-AX1 antibody, implicating extracellular AX1 in C2C12 fusion. The abrogation of p14 fusion via antibody inhibition has previously been reported using an antibody targeted to the fusogen itself, thus validating that this experimental method is capable of abolishing p14-mediated fusion (Salsman, Top et al. 2005). Results obtained in the present study suggest p14-mediated fusion is not affected by the presence of extracellular anti-AX1 antibody, implying extracellular AX1 is not necessary for a pre-fusion cell-migration step, the cell fusion reaction itself or the ensuing pore expansion and syncytiogenesis. However, our results point to a calcium-dependent role of intracellular AX1 at a post-fusion step during RRV p14 and measles F-mediated syncytium formation. Interestingly, Leikina et al. (2013) report that extracellular annexin A5 is also involved in myoblast fusion, our preliminary results suggest that knockdown of AX5 also inhibits p14-mediated syncytium formation. It is very intriguing that the vastly differing fusion systems of differentiating myotubes and viral fusogen-mediated cell-to-cell fusion have incorporated these proteins at different stages of syncytium formation. These studies are the first to characterize specific roles of the annexins during cell-to-cell fusion, and future research is necessary to determine whether any similar pathways, such as the involvement of AX1 during pore expansion, are utilized by both systems.

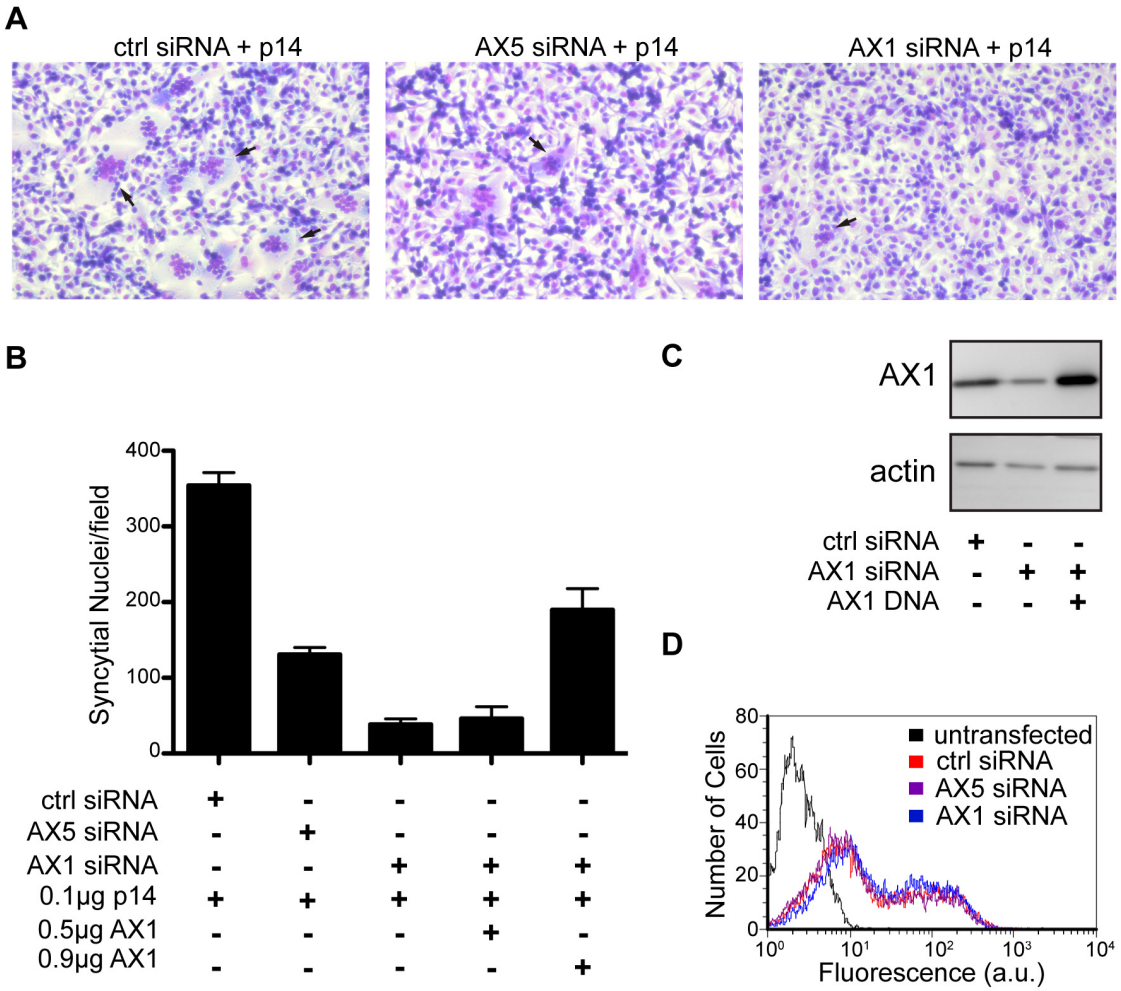
A
ctrl siRNA + p14
AX5 siRNA + p14
AX1 siRNA + p14
B
Syncytial Nuclei/field
400
300
200
100
0
ctrl siRNA + - - - -
AX5 siRNA - + - - -
AX1 siRNA - - + + +
0.1µg p14 + + + + +
0.5µg AX1 - - - + -
0.9µg AX1 - - - - +
C
AX1
actin
ctrl siRNA + - -
AX1 siRNA - + +
AX1 DNA - - +
D
Number of Cells
80
60
40
20
0
untransfected
ctrl siRNA
AX5 siRNA
AX1 siRNA
10⁰
10¹
10²
10³
10⁴
Fluorescence (a.u.)

Figure 4.1 **Cellular annexin A1 and annexin A5 are necessary for efficient RRV p14-mediated syncytium formation.** (A) HT1080 cells were transfected with control, annexin A1 (AX1) or annexin A5 (AX5) siRNA. At 36 hrs post-siRNA transfection, cells were transfected with p14 DNA, fixed at 12 hrs post-DNA transfection, and stained with Giemsa to visualize syncytia. Arrows indicate syncytia. (B) Cells were transfected with indicated siRNAs, then co-transfected with indicated plasmid DNAs expressing p14 or AX1, fixed and stained at 12 hrs. The extent of syncytium formation was quantified by determining the average number of syncytial nuclei per field from five random fields in triplicate. The results are expressed as a mean ± standard deviation of a representative experiment (n=3). AX1 A1 DNA, at 0.5 μg and 0.9 μg per well, was co-transfected with p14 in order to conteract the effect of siRNA knockdown. (C) The AX1 siRNA knockdown was verified by SDS-PAGE and immunoblotting with monoclonal anti-annexin A1 antibody. In addition, the knockdown was reconstituted by transfecting AX1 DNA at 36 hrs post-siRNA transfection, and analyzing AX1 expression at 12 hrs post-DNA transfection. Actin expression was used as a loading control and was detected by SDS-PAGE and immunoblotting with polyclonal anti-actin antibody. (D) The effect of siRNA knockdown of AX1 and AX5 on p14 surface expression was determined by sequentially transfecting AX1 or AX5 siRNA and fusion incompetent p14-G2A DNA. Live cells were stained at 24 hrs post-DNA transfection with anti-ectodomain p14 antibody (1:1000) followed by secondary Alexa 647 antibody (1:2000). Cells were fixed, and analyzed by flow cytometry. Experiments were performend twice in quadruplicate, 10 000 cells were counted per sample.

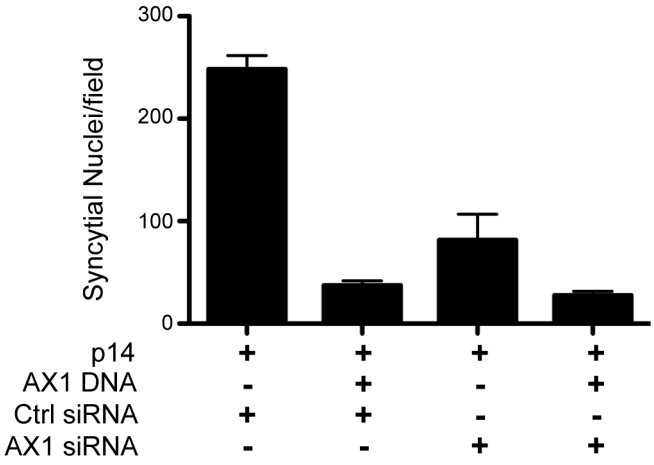

Figure 4.2 **Overexpression of annexin A1 or the RRV p14 endodomain does not rescue the siRNA knockdown phenotype.** HT1080 cells were transfected with control, AX1 siRNA. At 36 hrs post-siRNA transfection, cells were co-transfected with p14 DNA and either empty vector, p14 endodomain, or AX1 DNA. Cells were fixed at 12 hrs post-DNA transfection, and stained with Giemsa to visualize syncytia. The extent of syncytium formation was quantified by determining the average number of syncytial nuclei per field from five random fields in triplicate. The results are expressed as a mean ± standard deviation of a representative experiment (n=3).

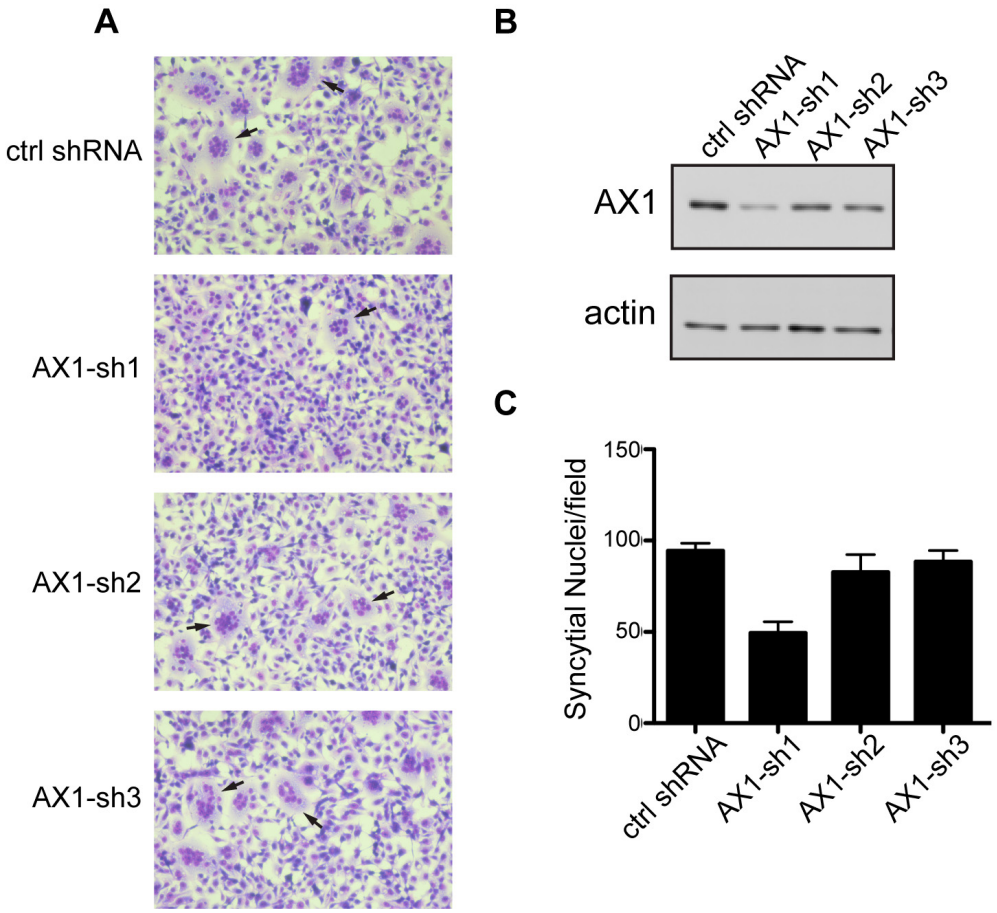

Figure 4.3 **Knockdown of annexin A1 by shRNA impairs RRV p14-mediated syncytium formation.** (A) The Phoenix retroviral expression system was used to generate three HT1080 cell lines carrying anti-AX1 shRNA. The cell lines expressing AX1 shRNA were transfected with RRV p14 DNA, fixed at 12 hrs post-transfection, and stained with Giemsa for visualization of syncytia, which are indicated by arrows. (B) Annexin A1 expression in all three shRNA-expressing cell lines, as well as a control shRNA-expressing cell line, was assayed by SDS-PAGE and immunoblotting with anti-AX1 monoclonal antibody. Actin expression was used as a loading control and was detected by SDS-PAGE and immunoblotting with polyclonal anti-Actin antibody. (C) The extent of p14-mediated syncytium formation in cell lines expressing control or AX1 shRNA was quantified by determining the average number of syncytial nuclei per field from five random fields in triplicate, and results are expressed as a mean ± standard deviation from a single experiment.

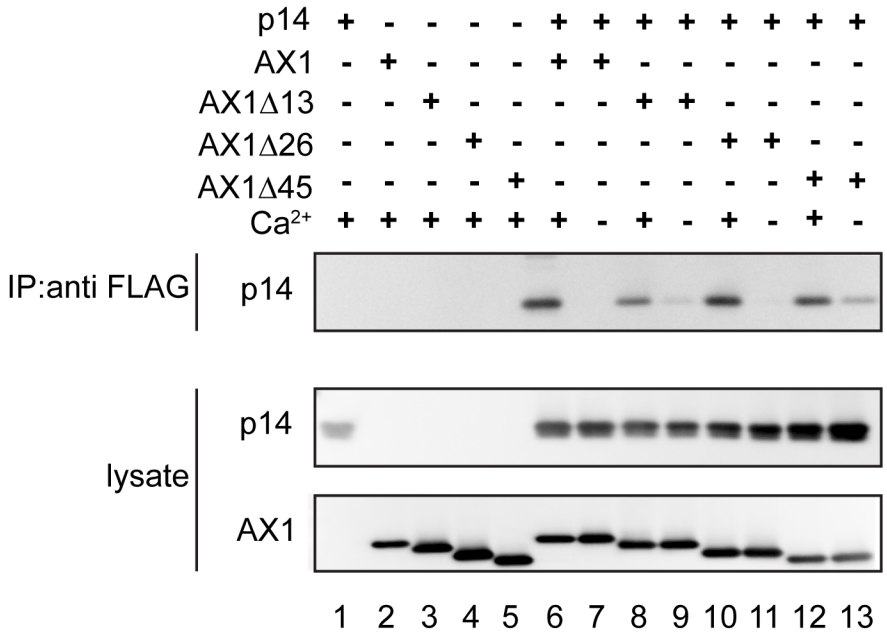

Figure 4.4 **Annexin A1 interaction with p14 does not require the annexin N-terminus and is calcium-dependent.** HEK cells were co-transfected with p14 and one of the indicated FLAG-tagged full-length or N-terminally truncated AX1 constructs. Truncation mutants were named to indicate the number of amino acids deleted from the N-terminus. Lysates were harvested at 14 hrs post-transfection and immunoprecipitated with anti-FLAG antibody. Immunoprecipitates were analyzed for the presence of p14 by SDS-PAGE and immunoblotting with polyclonal anti-p14 full-length antibody. The presence of AX1 in the cell lysates was detected by immunoblotting with a monoclonal anti-AX1 antibody. Immunoprecipitation was performed in the presence and absence of 5 mM calcium.

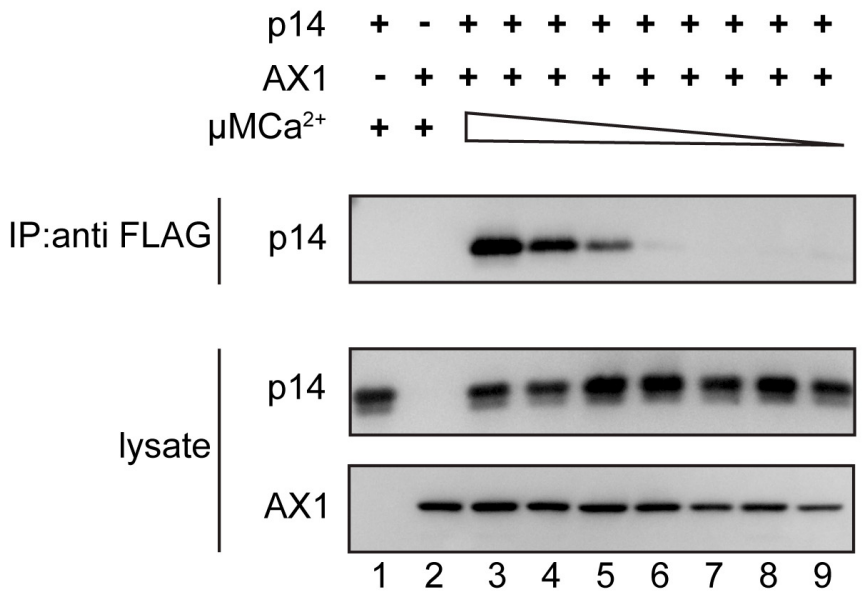

Figure 4.5 **Annexin A1 and RRV p14 interaction is dependent on physiological levels of calcium.** HEK cells were co-transfected with N-terminally FLAG-tagged AX1 and wild type RRV p14. Cells were lysed in buffer containing the following Ca^{2+} concentrations (numbers indicate loading lanes): 5 mM (1,2), 100 μM (3), 50 μM (4), 25 μM (5), 10 μM (6), 1 μM (7), 0.5 μM (8) and 0 μM (9). Lysates were harvested at 14 hrs post-transfection and immunoprecipitated with anti-FLAG antibody. Immunoprecipitates were analyzed for the presence of p14 by SDS-PAGE and immunoblotting with polyclonal anti-p14 full-length antibody. The presence of annexin A1 in the cell lysates was detected by immunoblotting with a monoclonal anti-AX1 antibody.

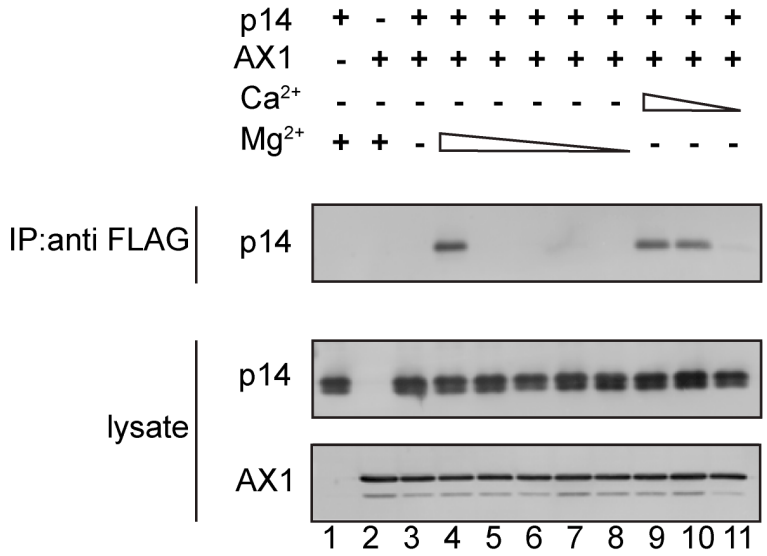

Figure 4.6 **Annexin A1 and RRV p14 interaction is preferentially mediated by calcium.** HEK cells were co-transfected with N-terminally FLAG-tagged AX1 and wild type RRV p14. Cells were lysed in buffer containing decreasing concentrations of Mg^{2+} including (numbers indicate loading lanes): 5 mM (1,2), 1 mM (4), 100 µM (5), 25 µM (6), 10 µM (7), and 0 µM (8), and the following Ca^{2+} concentrations: 100 µM (9), 50 µM (10) or 25 µM (11). Buffer used to lyse cells in lane (3) did not contain Ca^{2+} or Mg^{2+}. Lysates were harvested at 14 hrs post-transfection and immunoprecipitated with anti-FLAG antibody. Immunoprecipitates were analyzed for the presence of p14 by SDS-PAGE and immunoblotting with polyclonal anti-p14 full-length antibody. The presence of annexin A1 in the cell lysates was detected by immunoblotting with a monoclonal anti-AX1 antibody.

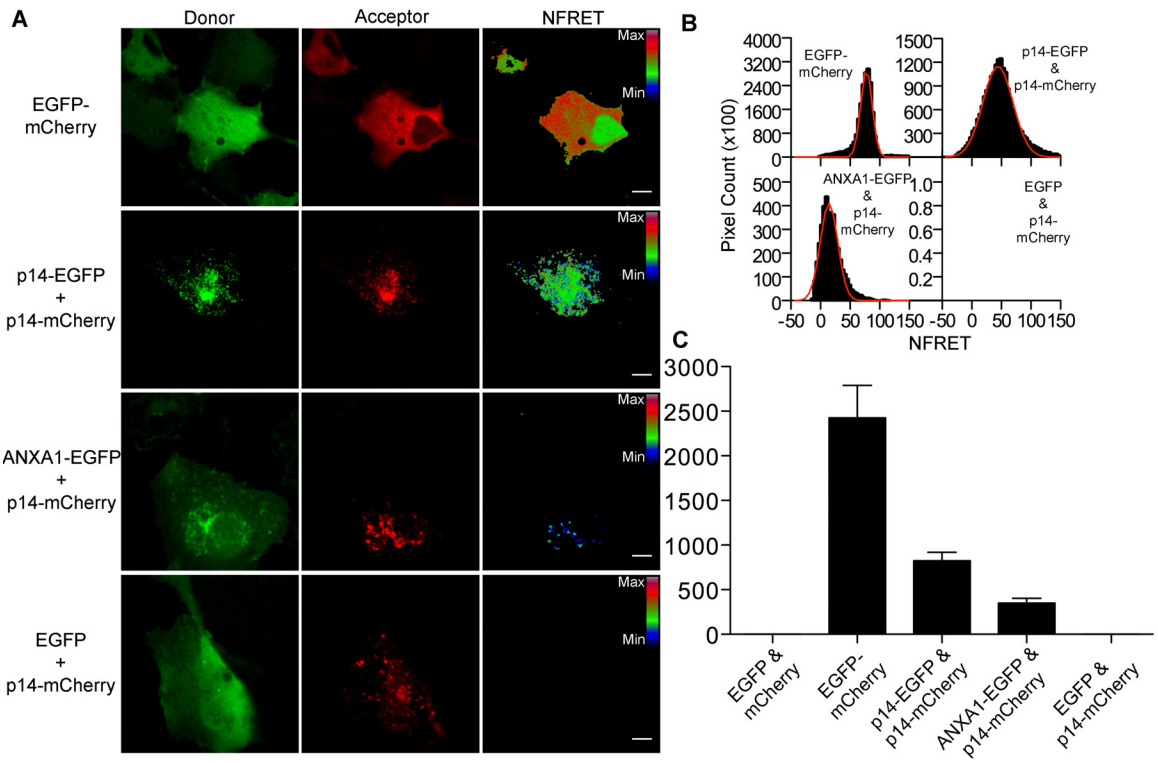

Figure 4.7 **Annexin A1 interacts with RRV p14 in the cytoplasm as determined by fluorescence resonance energy transfer.** HT1080 monolayers were co-transfected with C-terminally EGFP-tagged AX1 and C-terminally mCherry tagged RRV p14 for 10 hrs, then fixed using formaldehyde. (A) Cells were imaged using the Zeiss LSM 510 Meta confocal microscope to detect Fluorescence Resonance Energy Transfer (FRET) generated from AX1-p14 protein-protein interactions. The PixFRET Image-J plug-in was used to calculate donor and acceptor spectral bleed-through (SBT) values, as well as normalized FRET (NFRET) levels in each pixel. (B) Pixel distributions of the 8-bit NFRET images generated by the PixFRET software were summarized as histograms using a bin width of 0.03906 NFRET units. Each histogram was fitted with a Gaussian distribution to eliminate anomalous pixel values. Ten images were acquired for each condition in duplicate (twenty images total). (C) The Gaussian-fitted NFRET histograms were used to calculate the average pixel amplitude from each condition. Error bars represent standard error propagated within and across experiments. Data generated by Timothy Key.

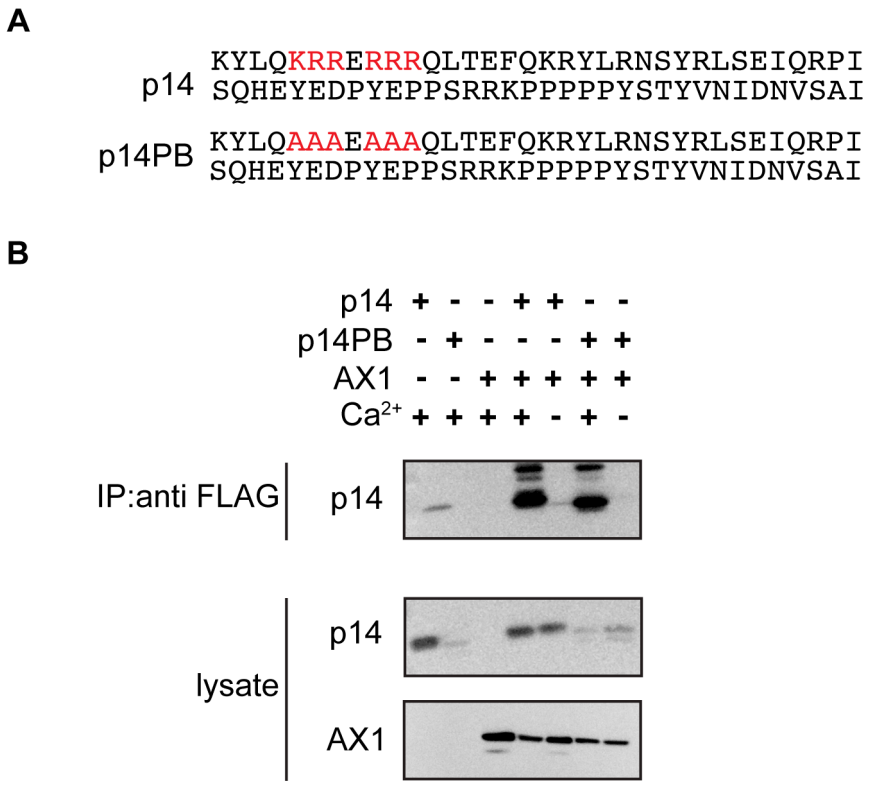

Figure 4.8 **The polybasic region of p14 is not essential for the interaction with Annexin A1.** (A) Schematic representation of the RRV p14 and RRV p14 polybasic mutant (PB) sequences. (B) HEK cells were co-transfected with N-terminally FLAG-tagged AX1 and wild type or PB-substitution p14 construct. Lysates were harvested at 14 hrs post-transfection and immunoprecipitated with anti-FLAG antibody. Immunoprecipitates were analyzed for the presence of p14 by SDS-PAGE and immunoblotting with polyclonal anti-p14 full-length antibody. The presence of AX1 in the cell lysates was detected by immunoblotting with a monoclonal anti-AX1 antibody. Immunoprecipitation was performed in the presence and absence of 5mM calcium.

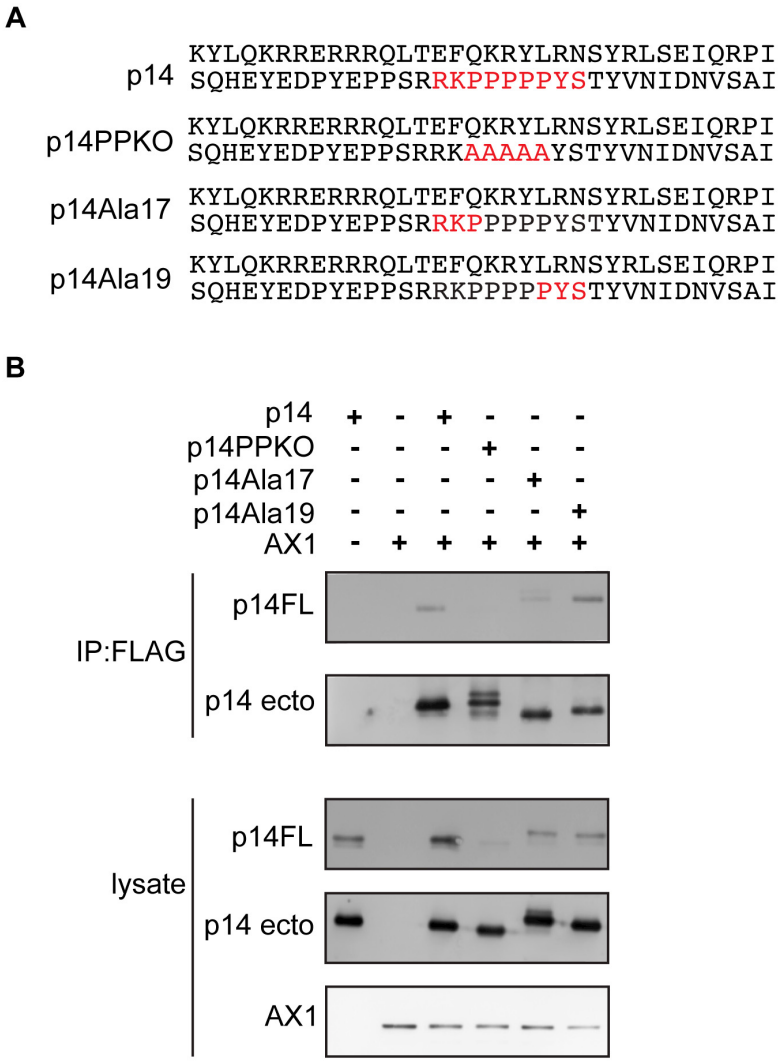

Figure 4.9 **The poly-proline region of the p14 endodomain is not essential for the interaction with annexin A1.** (A) Schematic representation of RRV p14 poly-proline region and alanine substitution mutants as denoted in red (Ala17 and Ala 19), or a fully substituted poly-proline tract construct (PPKO). (B) HEK cells were co-transfected with N-terminally FLAG-tagged AX1 and either wild type RRV p14 or one of the alanine substitution mutants Ala17, Ala19, or PPKO. Lysates were harvested at 14 hrs post-transfection and immunoprecipitated with anti-FLAG antibody. Immunoprecipitates were analyzed for the presence of p14 by SDS-PAGE and immunoblotting with polyclonal anti-p14 full-length antibody or polyclonal anti-p14 ectodomain antibody. The presence of AX1 in the cell lysates was detected by immunoblotting with a monoclonal anti-AX1 antibody. Immunoprecipitation was performed in the presence and absence of 5 mM calcium.

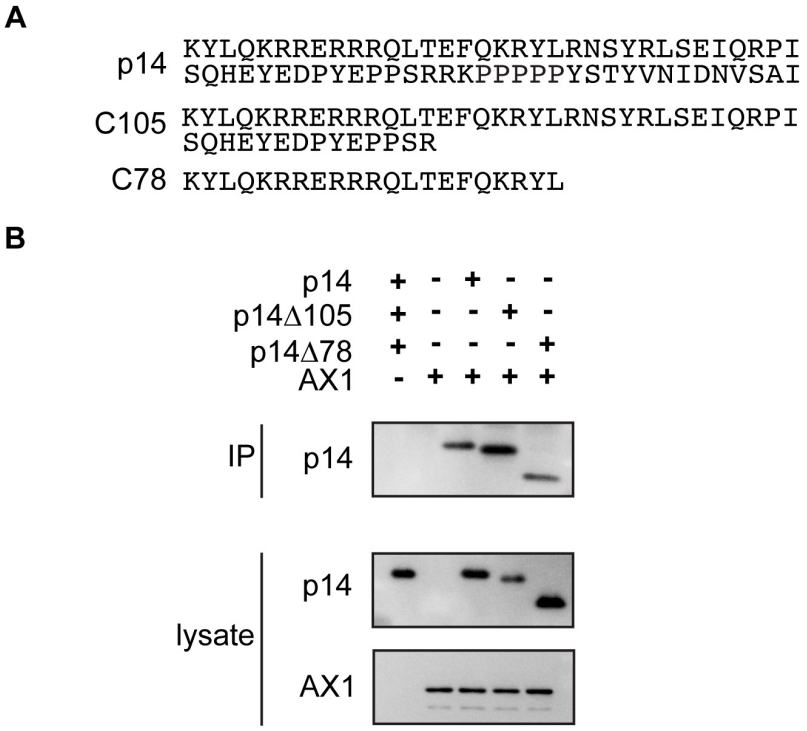

Figure 4.10 **The RRV p14 endodomain region between amino acid residues 78 and 125 does not interact with annexin A1.** (A) Schematic representation of the RRV p14 endodomain and C-terminal RRV-p14 amino acid deletions C105 and C78. (B) HEK cells were co-transfected with N-terminally FLAG-tagged AX1 and either wild type RRV p14, or one of the C-terminal deletion mutants (C78 and C105). Lysates were harvested at 14 hrs post-transfection and immunoprecipitated with anti-FLAG antibody. Immunoprecipitates were analyzed for the presence of p14 by SDS-PAGE and immunoblotting with polyclonal anti-p14 ectodomain antibody. The presence of AX1 was detected by immunoblotting with a monoclonal anti-AX1 antibody. Immunoprecipitation was performed in the presence of 5 mM calcium.

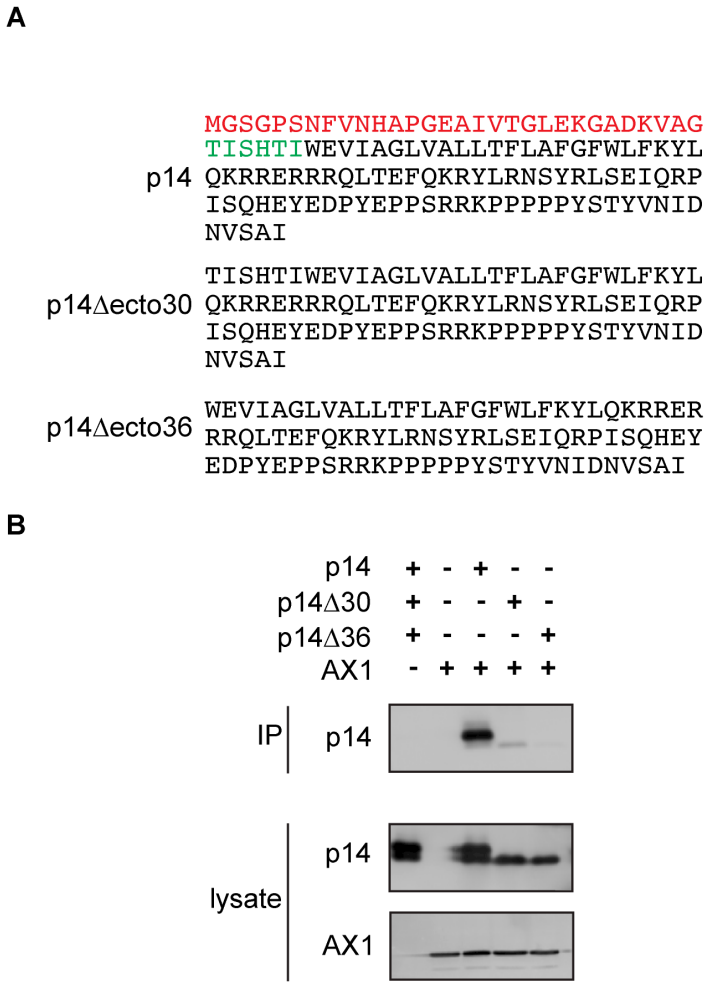

Figure 4.11 **The ectodomain of RRV p14 is essential for interaction with Annexin A1.** (A) Schematic representation of RRV p14 and N-terminal RRV-p14 amino acid deletions (p14Δecto30 (red) and p14Δecto36 (red+green)). (B) HEK cells were co-transfected with N-terminally FLAG-tagged AX1 and either wild type RRV p14, or one of the N-terminal deletion mutants. Lysates were harvested at 14 hrs post-transfection and immunoprecipitated with anti-FLAG antibody. Immunoprecipitates were analyzed for the presence of p14 by SDS-PAGE and immunoblotting with polyclonal anti-p14 full-length antibody. The presence of Annexin A1 was detected by immunoblotting with a monoclonal anti-AX1 antibody. Immunoprecipitation was performed in the presence of 5mM calcium.

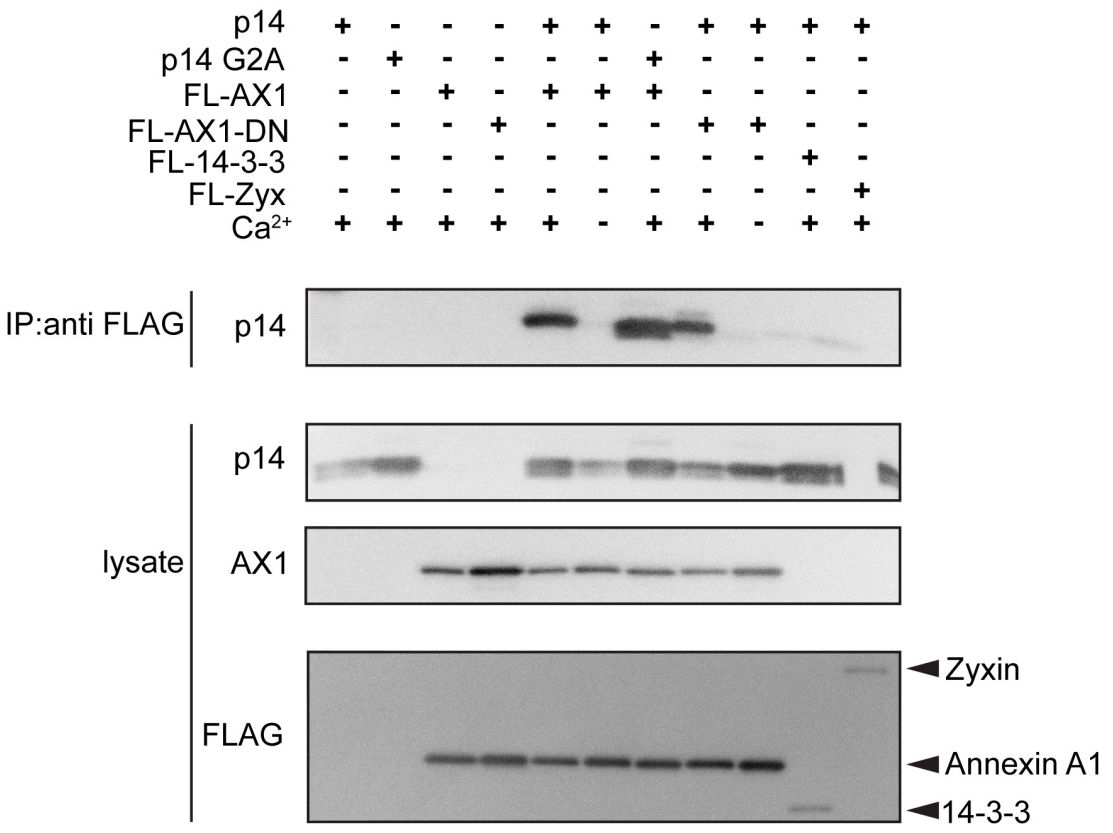

Figure 4.12 **Annexin A1 interaction with RRVp14 does not involve the known annexin A1 calcium-binding site and is independent of the generation of syncytia by RRV p14.** HEK cells were co-transfected with N-terminally FLAG-tagged AX1 and one of wild type p14, a non-fusogenic p14 mutant (G2A), or a non-calcium binding AX1 mutant (AX1-DN). FLAG-tagged zyxin or 14-3-3 were co-transfected with wild type RRV p14 as immunoprecipitation controls. Lysates were harvested at 14 hrs post-transfection and immunoprecipitated with anti-FLAG antibody. Immunoprecipitates were analyzed for the presence of p14 by SDS-PAGE and immunoblotting with polyclonal anti-p14 full-length antibody. The presence of AX1 was detected by immunoblotting with a monoclonal anti-AX1 antibody and the presence of FLAG tagged AX1, zyxin, and 14-3-3 was detected by immunoblotting with a monoclonal anti-FLAG antibody.

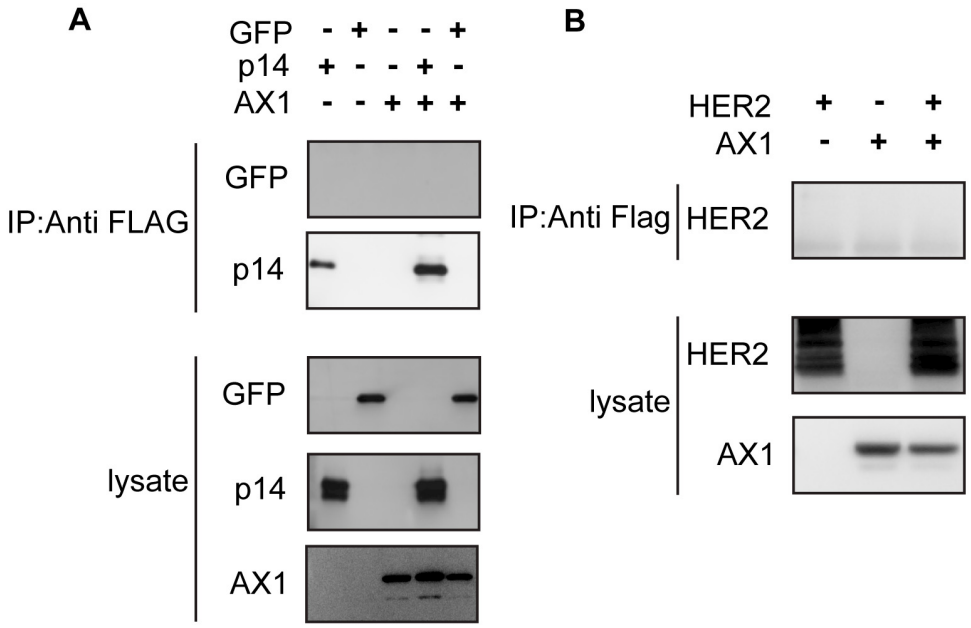

Figure 4.13 **The interaction between N-terminally tagged Annexin A1 and RRV p14 is protein-specific.** HEK cells were co-transfected with N-terminally FLAG-tagged AX1 and plasmids expressing (A) soluble GFP or wild type p14, or (B) the membrane integral protein HER2. Lysates were harvested at 14 hrs post-transfection and immunoprecipitated with anti-FLAG antibody. Immunoprecipitates were analyzed for the presence of p14 by SDS-PAGE and immunoblotting with polyclonal anti-p14 full-length antibody. The presence of GFP (A) was detected by immunoblotting with a polyclonal anti-GFP antibody and the presence of HER2 (B) was detected by immunoblotting with a polyclonal anti-HER2 antibody.

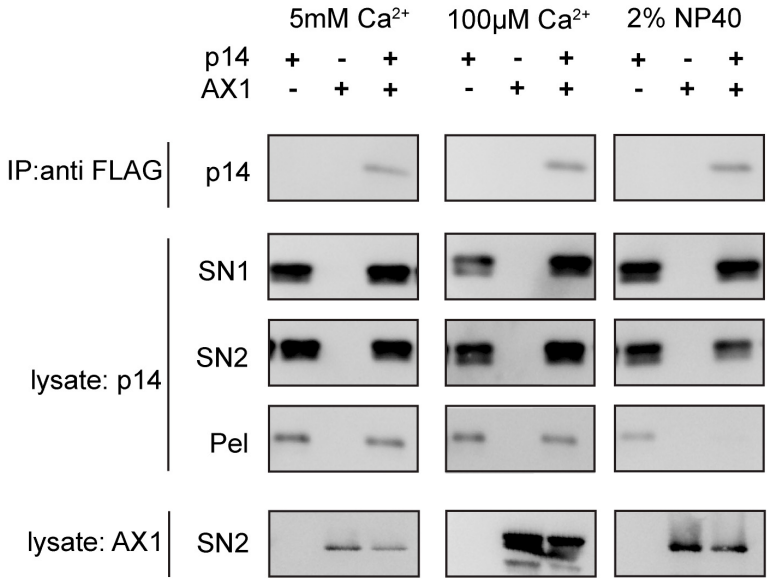

Figure 4.14 **The interaction between N-terminally tagged Annexin A1 and RRV p14 is maintained in high detergent or physiological calcium concentration coupled with stringent differential centrifugation conditions.** HEK cells were co-transfected with N-terminally FLAG-tagged AX1 and wild type RRV p14. Cells were lysed in control 1% NP40 and 5mM Ca^{2+}, 1% NP-40 and 100µM Ca^{2+}, or 2% NP-40 and 5mM Ca^{2+}, and centrifuged at 14000xg. The supernatant (SN1) was then centrifuged at 100 000xg and the resulting soluble (SN2) and pellet (Pel) fractions were collected and analyzed for presence of RRV p14 and AX1 by Western-blotting, SN and PEL fractions were diluted to ensure equal sample loading. SN2 fractions were immunoprecipitated with anti-FLAG antibody. Immunoprecipitates were analyzed for the presence of p14 by SDS-PAGE and immunoblotting with polyclonal anti-p14 full-length antibody. The presence of Annexin A1 was detected by immunoblotting with a monoclonal anti-AX1 antibody.

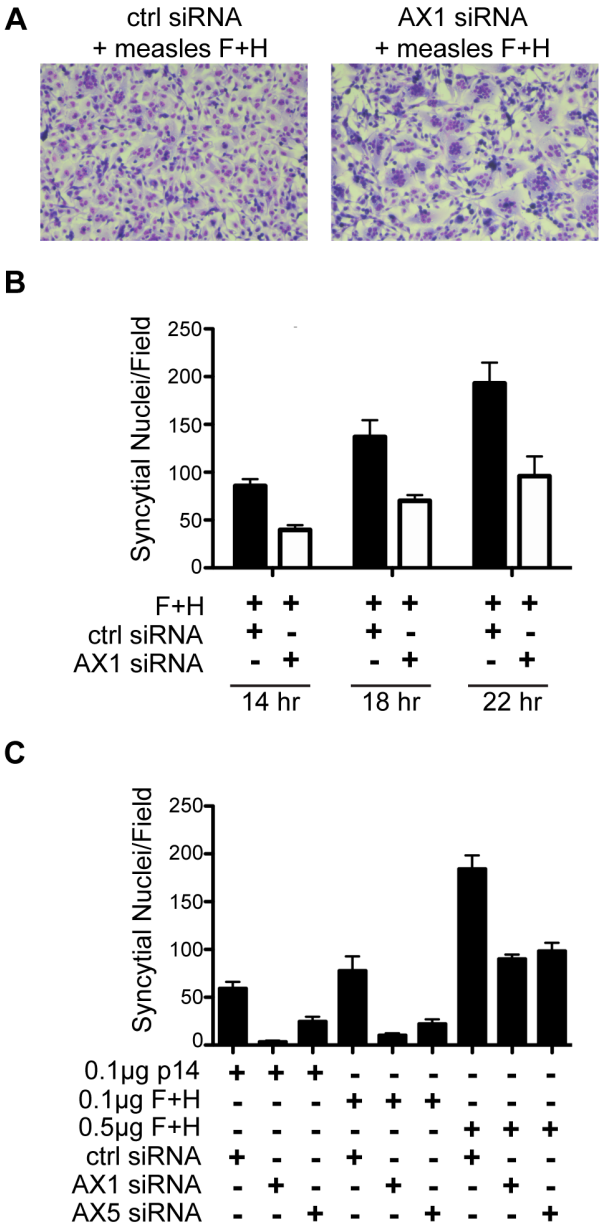

Figure 4.15 **Annexin A1 is necessary for efficient measles F-mediated syncytium formation.** (A) HT1080 cells were transfected with control, AX1 or AX5 siRNA. At 36 hrs post-siRNA transfection, cells were transfected with measles F and H DNA, fixed at 22 hrs post-DNA transfection, and stained with Giemsa to visualize syncytia. (B) A time course of the extent of syncytium formation was quantified by determining the average number of syncytial nuclei per field from five random fields in triplicate at 14, 18, and 22 hrs post-transfection. The results are expressed as a mean ± standard deviation of a single experiment. (C) The experiment was performed as in (B) and included a p14 control. The p14 expressing cells were fixed at 12 hrs post-transfection, while the H and F expressing cells were fixed at 18 hrs post-transfection. The results are expressed as a mean ± standard deviation (n=2).

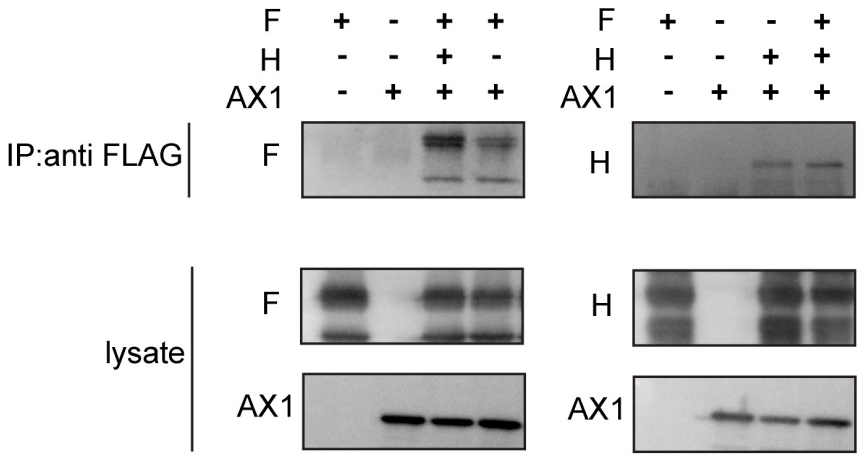

Figure 4.16 **Annexin A1 interacts with measles F and H proteins.** HEK cells were co-transfected with N-terminally FLAG-tagged AX1 and either both the measles F and H proteins, or individually with F or H. Cells were lysed in buffer supplemented with 2% NP40. Lysates were immunoprecipitated with anti-FLAG antibody. Immunoprecipitates were analyzed for the presence of F and H by SDS-PAGE and immunoblotting with polyclonal anti-F and anti-H antibodies. The presence of AX1 was detected by immunoblotting with a monoclonal anti-AX1 antibody. Immunoprecipitation was performed in the presence of 5mM calcium and 2% NP-40.

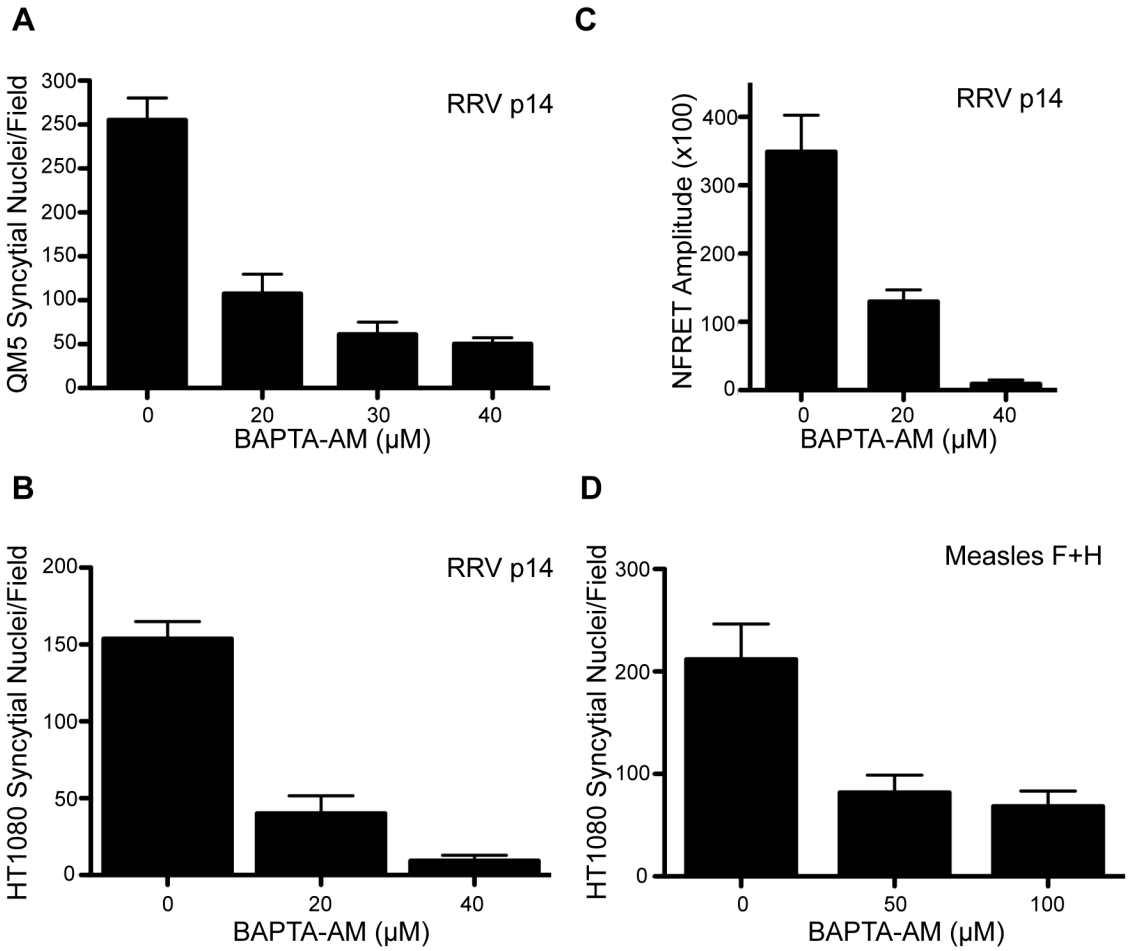

Figure 4.17 **Depletion of intracellular calcium by BAPTA inhibits RRV p14-mediated syncytium formation.** (A) Quail muscle fibroblast (QM5) cells were transfected with p14 and treated with increasing concentrations of BAPTA-AM at 4 hrs post-transfection. Cell monolayers were fixed and Giemsa stained at 8 hrs post-transfection. The extent of syncytium formation was quantified by determining the average number of syncytial nuclei per field from five random fields in triplicate. The results are expressed as a mean ± standard deviation of a representative experiment, (n=2). (B) HT1080 cells were transfected with p14 and treated with BAPTA-AM at 4 hrs post-transfection. Cells were fixed at 12 hrs post-transfection and syncytium formation was quantified as in (A). (C) HT1080 monolayers were co-transfected with C-terminally EGFP-tagged AX1 and C-terminally mCherry tagged RRV p14 treated with BAPTA at 4 hrs, fixed at 10 hrs post-transfection using formaldehyde, and analyzed by confocal microscopy. The PixFRET Image-J plug-in was used to calculate donor and acceptor spectral bleed-through (SBT) values, as well as normalized FRET (NFRET) levels in each pixel. Gaussian-fitted NFRET histograms were used to calculate the average pixel amplitude from each condition. Graph contributed by Timothy Key. (D) HT1080 cells were transfected with measles F and H proteins and treated with BAPTA-AM at 4 hrs post-transfection. Cells were fixed at 24 hrs post-transfection. Experiments in (B) and (C) are expressed as a mean ± standard error, (n=3)

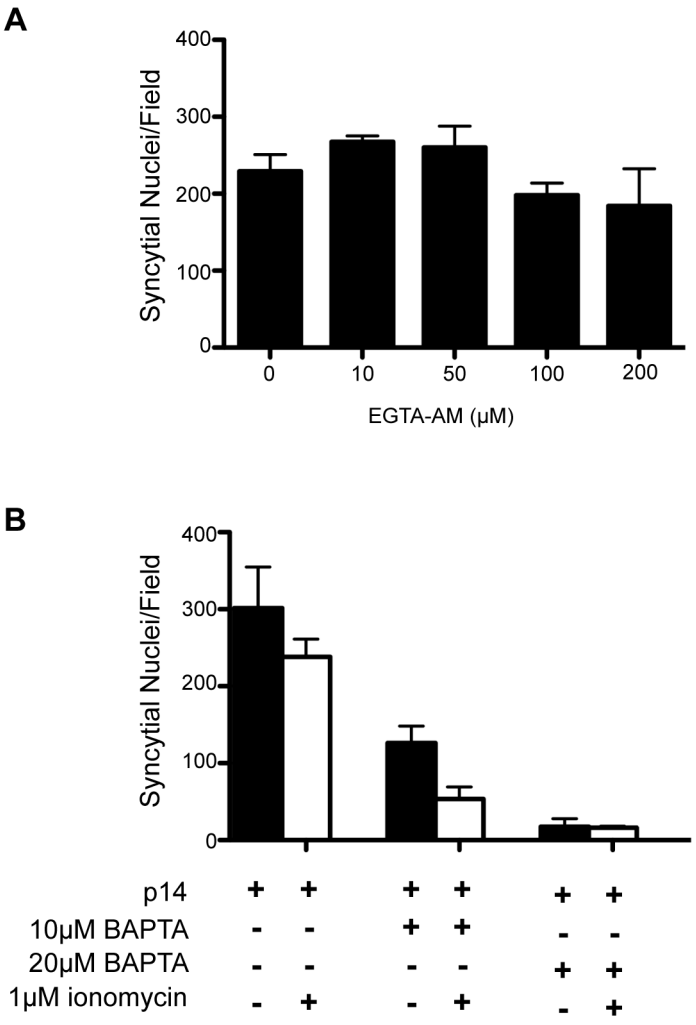

Figure 4.18 **EGTA-mediated intracellular calcium depletion and ionomycin-dependent intracellular calcium supplementation have no effect on RRV p14 mediated syncytium formation.** (A) HT1080 cells were transfected with p14 and treated with various concentrations of EGTA-AM at 4 hrs post-transfection. Monolayers of cells were fixed, Giemsa stained, and assayed for syncytia as previously. The results are expressed as a mean ± standard deviation of a representative experiment, (n=2). (B) HT1080 cells were transfected with p14 and treated with BAPTA-AM at 4 hrs post transfection. Monolayers were treated with 1 mM ionomycin at 8 hrs post-transfection and fixed at 14 hrs post-transfection. The results are expressed as a mean ± standard deviation of a representative experiment, (n=2).

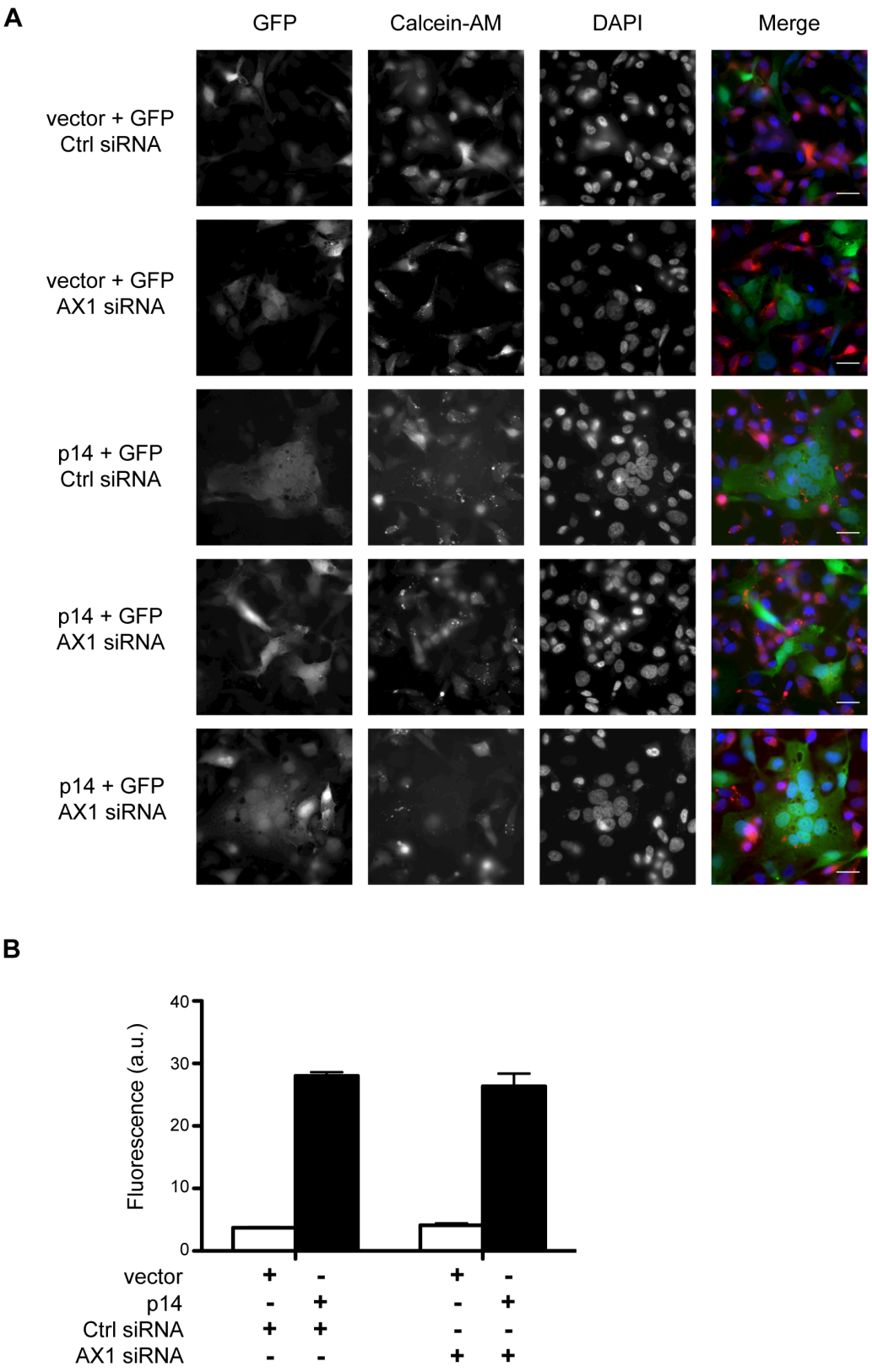
A
GFP
Calcein-AM
DAPI
Merge
vector + GFP
Ctrl siRNA
vector + GFP
AX1 siRNA
p14 + GFP
Ctrl siRNA
p14 + GFP
AX1 siRNA
p14 + GFP
AX1 siRNA
B
Fluorescence (a.u.)
40
30
20
10
0
vector + - + -
p14 - + - +
Ctrl siRNA + + - -
AX1 siRNA - - + +

Figure 4.19 **The presence of annexin A1 in donor, fusogen-containing cells is not essential for pore formation.** (A) A homotypic, dual-colour pore formation assay was performed in HT1080 cells. Donor cells were transfected with control or AX1 siRNA. At 36 hrs post-transfection, cells were transfected with either p14 and GFP or a vector control and GFP. Target HT1080 cells were labeled with CellTrace Calcein Orange-AM, and overlaid onto donor cells at 4 hrs post-transfection. Cells were fixed at 12 hrs post-transfection and soluble dye transfer was detected by fluorescence microscopy. Bar, 10 μm. (B) Cells were treated as in (A), but were removed from wells prior to fixation, and transfer of fluorescent markers was assayed by flow cytometry. Cells were gated for the expression of GFP and the extent of calcein acquisition due to pore formation was detected as an increase in fluorescence in arbitrary units (au). 10 000 events were counted in triplicate in each experiment. The results are expressed as a mean ± standard error (n=3).

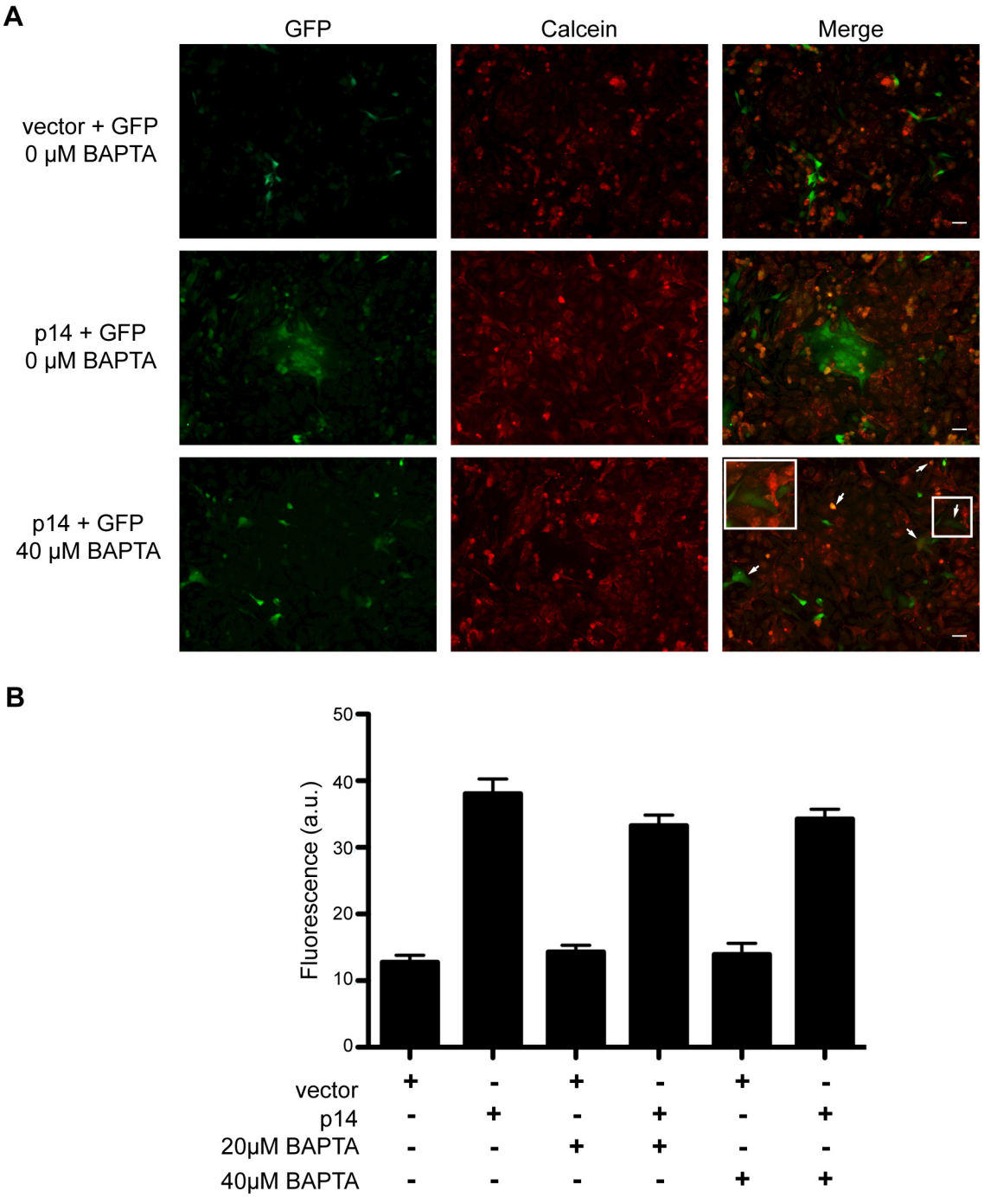
A
GFP
Calcein
Merge
vector + GFP
0 μM BAPTA
p14 + GFP
0 μM BAPTA
p14 + GFP
40 μM BAPTA
B
Fluorescence (a.u.)
50
40
30
20
10
0
vector
p14
20μM BAPTA
40μM BAPTA

Figure 4.20 **Intracellular calcium is not necessary for RRVp14 mediated pore formation.** (A) A homotypic, dual-colour pore formation assay was performed in Vero cells. Donor cells were transfected with either p14 and GFP or a vector control and GFP. Target Vero cells were labeled with CellTrace Calcein Orange-AM. Both donor and target cells were treated with BAPTA-AM at 4 hrs post-transfection. Target cells were overlaid onto donor cells at 5 hrs post-transfection and fixed at 10 hrs post-transfection. Soluble dye transfer was visualized by fluorescence microscopy, Bar, 50 μm. (B) Cells were treated as in (A), but were removed from wells prior to fixation. Transfer of calcein to GFP expressing cells was assayed by flow cytometry. Cells were gated for the expression of GFP and the extent of calcein acquisition due to pore formation was detected as an increase in fluorescence in arbitrary units (au). 5 000 events were counted in triplicate in each experiment. The results are expressed as a mean ± standard deviation of a representative experiment (n=2).

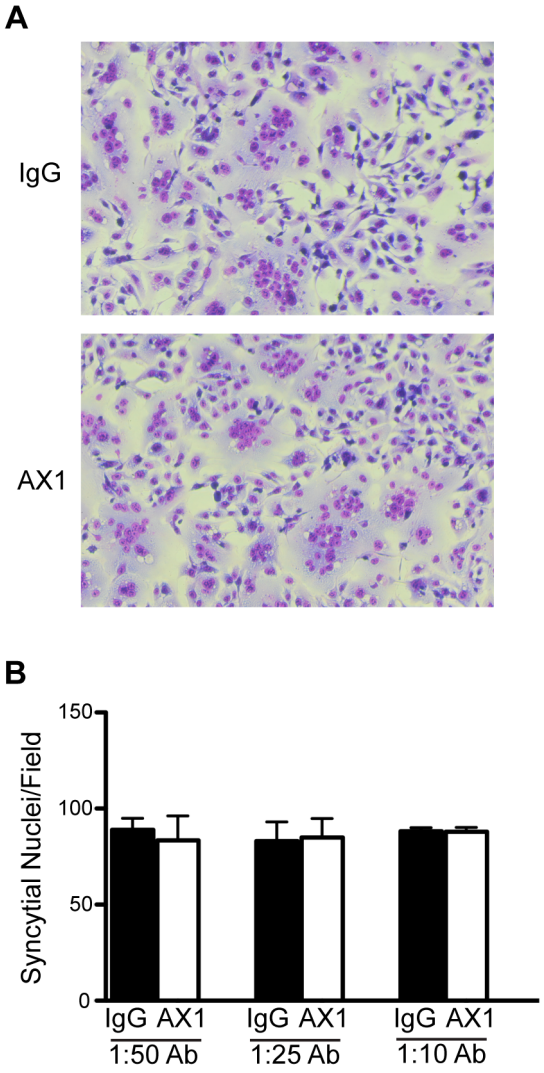

Figure 4.21 **Antibody inhibition of annexin A1 does not effect RRV p14-mediated fusion in HT1080 cells.** (A) HT1080 cells were transfected with RRV p14. Media supplemented with AX1 antibody at a 1:10 dilution was added to the cell monolayers at 2 hrs post-transfection. Cells were fixed and Giemsa stained at 14 hrs post-transfection. (B) HT1080 cells, transfected with p14 were treated with AX1 antibody at dilutions of 1:50, 1:25, and 1:10. The extent of syncytium formation was quantified by determining the average number of syncytial nuclei per field from five random fields. The results are expressed as a mean ± standard error (n=3).

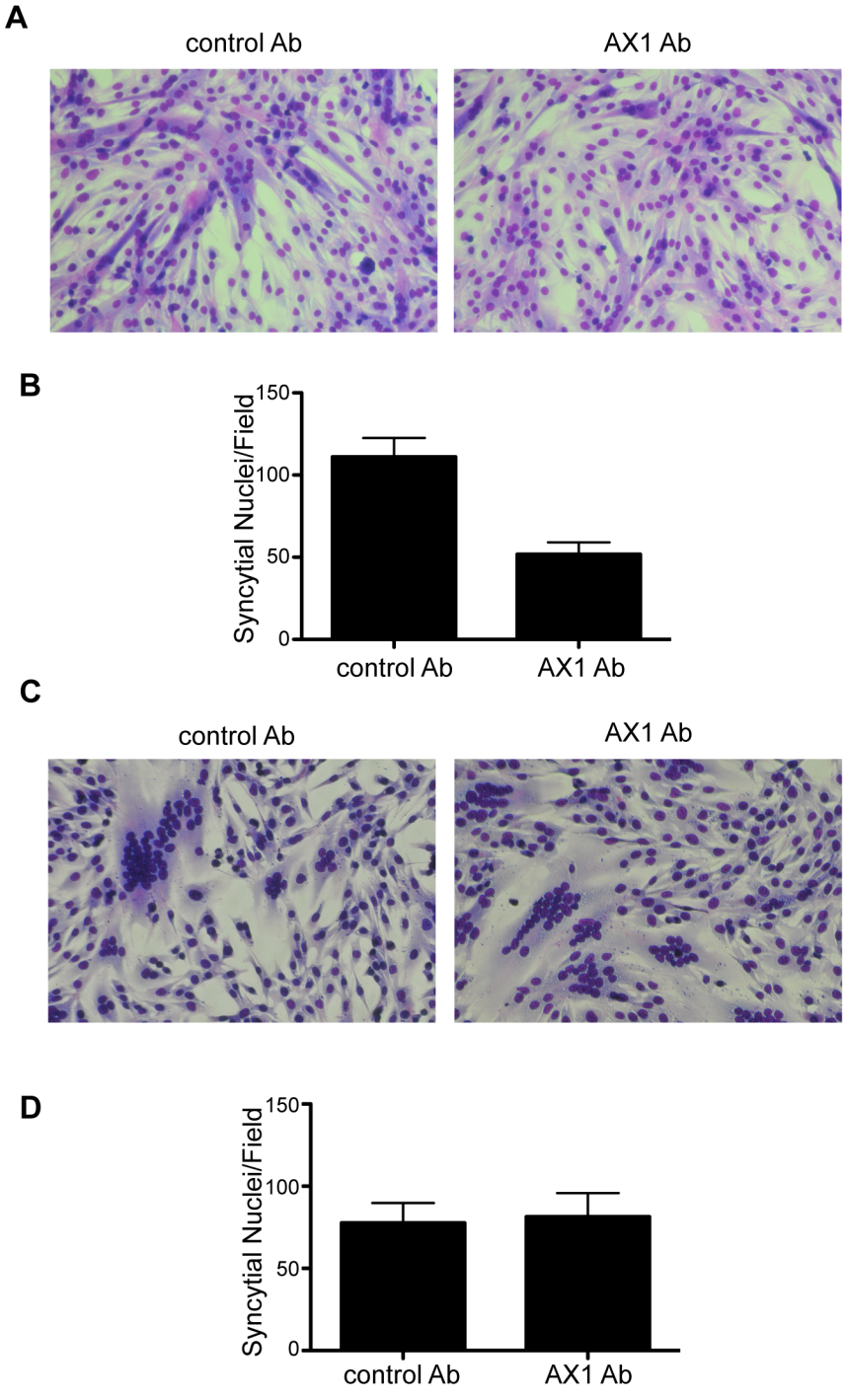
A
control Ab
AX1 Ab
B
Syncytial Nuclei/Field
150
100
50
0
control Ab
AX1 Ab
C
control Ab
AX1 Ab
D
Syncytial Nuclei/Field
150
100
50
0
control Ab
AX1 Ab

Figure 4.22 **Antibody inhibition of annexin A1 can arrest C2C12 muscle cell fusion during differentiation, but not p14-mediated fusion of C2C12 cells.** (A) C2C12 muscle cell differentiation was induced by addition of horse serum. Media supplemented with AX1 antibody at a 1:10 dilution was added to the cell monolayers at 51 hrs following the initiation of differentiation. Cells were fixed and Giemsa stained after 16 hrs of incubation with the AX1 antibody. (B) The extent of myotube formation in (A) was quantified by counting syncytial nuclei in five random fields of a single well, and is represented as a mean ± standard error (n=3). (C) C2C12 cell monolayers were transfected with p14 and treated with a 1:10 dilution of AX1 antibody at 2 hrs post-transfection. Cells were fixed and Giemsa stained at 12 hrs post-transfection. (D) The extent of syncytium formation in (C) was quantified by counting syncytial nuclei in five random fields of a single well, and is represented as a mean ± standard error (n=3).

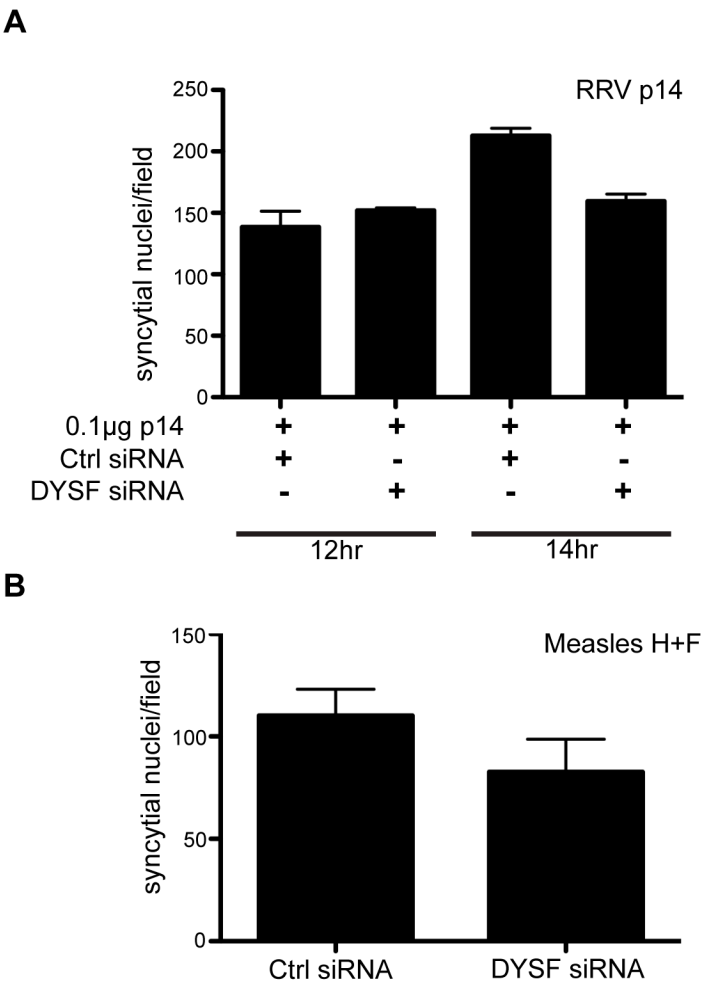

Figure 4.23 **Dysferlin is not involved in RRV- p14 or measles F-mediated syncytium formation.** (A) HT1080 cells were transfected with control or dysferlin siRNA. At 36 hrs post-siRNA transfection, cells were transfected with p14 DNA, fixed at 12 hrs post-DNA transfection, and stained with Giemsa to visualize syncytia. The extent of syncytium formation was quantified by determining the average number of syncytial nuclei per field from five random fields in triplicate. The results are expressed as a mean ± standard error (n=3). (B) HT1080 cells were transfected with control or dysferlin siRNA. At 36 hrs post-siRNA transfection, cells were transfected with measles F and H DNA, fixed at 24 hours post-DNA transfection, and stained with Giemsa to visualize syncytia. The extent of syncytium formation was quantified by determining the average number of syncytial nuclei per field from five random fields in triplicate. The results are expressed as a mean ± standard deviation, from a single experiment.

Chapter 5: Discussion

5.1 FAST protein membrane fusion intermediates

The present work contains a comprehensive analysis of the kinetics of RRV p14-mediated pore formation and syncytiogenesis. Addition of target cells to donor cells allowed for the establishment of a trigger-like mechanism and, thus, the partial synchronization of RRV-p14-mediated membrane fusion. With this tool, I was able to show that pre-treatment of membranes with bilayer deforming agents, which are known to abrogate or promote enveloped virus-mediated membrane merger, is ineffective in the case of RRV p14-mediated cell-cell fusion. The inability of both CPZ and LPC to influence a putative hemifusion intermediate leads to the conclusion that such an ordered structure is not invoked during RRV p14-mediated membrane merger. Interestingly, this was not the case for BRV p15, where pore-formation was entirely abrogated in the presence of LPC. It is therefore likely that fusion mediated by these proteins progresses via differing intermediates and/or kinetics.

It is unclear whether the RRV p14 and BRV p15 FAST proteins evolved from a common ancestor or two separate gain-of-function events. BRV p15 and RRV p14 do not contain any sequence similarity, and they have a different arrangement of structural motifs. For example, the HP and polyproline motifs of RRV p14 and BRV p15 are inverted across the plasma membrane. The reversed location of these motifs suggests that they may not serve similar functions during the fusion process. RRV and BRV also have different coding strategies for their FAST proteins; RRV p14 is endoded on the bicistronic S1 genome segment that also encodes the viral fiber protein, whereas BRV p15 is encoded on the bicistronic S4 genome segment that also encodes a small non-structural protein of undefined function (Corcoran and Duncan, 2004; Dawe and Duncan, 2002). The above considerations suggest two separate gain-of-function events, and possibly two distinct mechanisms of action of p14 and p15. Contrary to this, the FAST proteins are modular fusogens. For instance, an RRV p14 construct containing its native ectoplasmic HP and an internal BRV p15 HP results in the most robust FAST fusogen observed to date. Similarly, the p15 endodomain or TMD can functionally replace the corresponding p14 domains (Clancy and Duncan, 2009; Clancy, Ph.D. thesis), suggesting

these domains serve similar functions in the fusion reaction and that p14 and p15 evolved from a common ancestor. Interestingly, the reciprocal domain swaps are not functional; the p14 endodomain or TMD are not functional in a p15 backbone (Clancy and Duncan, 2011; Eileen Clancy, Ph.D. thesis). The combinatorial specificity of chimeric FAST proteins suggests the three fusion domains work in a cooperative manner to mediate membrane fusion, with the specific function of a given domain dictating whether it can cooperate with the other domains present in the protein. As an example, BRV p15 and RRV p14 can use either an ectodomain polyproline helix or a HP, respectively, as fusion peptides to promote lipid mixing. If the polyproline fusion peptide is less efficient than a HP fusion peptide, then additional requirements may be needed in the TMD or endodomain to promote membrane merger, and pre-emptive modification of the outer leaflet by LPC treatment may prove to render the polyproline peptide insufficient to induce lipid mixing.

The serendipitous observation that addition of LPC abrogates pore expansion immediately following the onset of pore formation led to the isolation of a novel membrane shape-sensitive stage of syncytium formation. This stage was observed during RRV p14- and influenza HA-mediated pore expansion, two vastly different fusogens that seem to mediate membrane merger via different intermediates. In both cases, pore expansion was sensitive to treatment with lysolipid. This suggests a convergence of events following pore formation, and a diminishing role for the fusion protein. Furthermore, LPC inhibited pore expansion in several cell lines, indicating that resolution of intermembrane pores may be a universal cellular response to plasma membrane attack.

Currently, two studies of eukaryotic cell fusogens, the *C. elegans* EFF-1 and the unknown mouse muscle fusion protein, reported the existence of a hemifusion intermediate in cell-cell fusion that can be trapped via LPC treatment (Podbilewicz, Leikina et al. 2006, Leikina, Melikov et al. 2013). In the EFF-1 study, the authors report that transfer of fluorescent membrane dye (DiI), without transfer of a cytoplasmic dye (CMAC), occurs in 12% of cell pairs, and LPC was shown to inhibit the formation of multinucleated cells in a reversible manner (Podbilewicz, Leikina et al. 2006). Based on these two lines of evidence, the authors concluded EFF-1 fuses through a hemifusion intermediate. However, CMAC is a mildly thiol-reactive compound that reacts with

intracellular components once it crosses the membrane, which is why it stays entrapped inside cells. The absence of CMAC transfer is therefore not indicative of the absence of pore formation, merely the absence of a large enough pore to allow transfer of CMAC-protein complexes. Similarly, in the LPC assay, hemifusion was scored as membrane dye transfer between mononucleated cell pairs. As I have now shown, LPC can inhibit pore expansion while having no effects on pore formation, which would appear in the above assays as membrane dye transfer without transfer of CMAC or formation of a multinucleated cell. Similar to the FAST proteins, lack of an EFF-1 fusion trigger necessitates a temporal analysis of pore versus syncytium formation that would ensure addition of LPC at a pre-fusion step. Additionally, the authors report that the LPC-sensitive stage is reversible, and that syncytium formation rapidly progresses after LPC removal, which mirrors my results during post-fusion pore expansion arrest. These results suggest that EFF-1-mediated fusion likely proceeds via a lipid intermediate followed by content mixing, however, the results do not prove the existence of a canonical, highly structured 'hemifusion' architecture and the conclusion that EFF-1 induces hemifusion is overstated.

In the second, very recent, study Leikina et *al.* report that differentiation-induced C2C12 mouse myoblast fusion is sensitive to LPC treatment and thus proceeds via a hemifusion intermediate. These conclusions are based on the use of the same fluorescent lipidic and cytoplasmic dyes as in the previous study, and dye transfer was analyzed at 16 and 24 hrs after the addition of differentiation media. Studies in the Duncan lab have demonstrated that long incubations of cells with the lipid probe DiI lead to extensive internalization of the dye by endocytosis and also low, but detectable, levels of fusion-independent dye redistribution to neighbouring cells (Clancy, Barry et al. 2010). This was also reported by Leikina et *al.*, where fusion was scored at a time when the fluorescent lipids were mostly found in internalized intracellular membranes. In our experience, detection of lipid transfer between plasma membranes becomes increasingly more difficult to interpret at stages where most of the probe is internalized. Interestingly, LPC addition to the differentiating cells did not inhibit myogenic differentiation, and upon removal of the lysolipid, pore expansion proceeded at an expedited rate, similar to that of FAST protein-and HA-mediated expansion reported in the present study.

The possibility of convergence in pore expansion pathways following fusion mediated by EFF-1, influenza HA and the FAST proteins and in differentiating mouse myoblasts is an exciting proposition. The recent interest in cellular contributions during syncytium formation will likely identify many factors involved in this process. It will be interesting to see whether the same cellular factors are involved in restructuring the cellular architecture upon membrane merger induced by such differing mechanisms. The post-fusion LPC arrest can be used to stall cells prior to pore expansion in order to detect any accumulation of effector proteins at fusion pores. Additionally, scanning electron microscopy studies and temporal analysis of pore formation during LPC-arrested intermediates of EFF-1 and mouse muscle fusion should shed more light on the effects of lysolipid treatment during cell-to-cell fusion in these systems. It may also be possible to use EM tomography to map the architecture of the fusion pore and underlying actin cytoskeleton, something that has been impossible to do up until now due to the transient nature of fusion pores.

5.2 Pore expansion: cellular solutions to virus-mediated intermembrane merger

AX1 has been implicated in cell-to-cell fusion of C2C12 and primary muscle myoblasts. In these systems, AX1 is reported to be involved in a pre-fusion step during differentiating myoblast migration (Bizzarro, Belvedere et al. 2012), or alternatively to mediate the membrane fusion reaction itself (Leikina, Melikov et al. 2013). Both reports focus on the role of extracellular AX1, either in the context of the whole protein (Leikina et al. 2013) or an N-terminal peptide Ac2-26, which signals through formyl peptide receptors (Bizzarro et al. 2012) (Bizzarro, Fontanella et al. 2012, Leikina, Melikov et al. 2013). In this study, I found a clear difference in AX1 function between virus-mediated syncytium formation and myotube formation. While the downregulation of AX1 expression decreases fusion mediated by endogenous muscle cell fusogens, as well as by RRV p14 and measles virus F protein, AX1 antibody inhibition abrogates myotube formation but has no effect on fusion mediated by RRV p14. I show that intracellular AX1 can interact with viral fusion proteins themselves, and that the presence of AX1 is necessary at a post-fusion, pore expansion step during viral fusogen induced syncytiogenesis. In addition, the role of intracellualar calcium has been implicated in

mitochondrial and SNARE-mediated vesicle fusion (de Brito and Scorrano 2008, Martens 2010), but it has not been investigated during cell-to-cell fusion. In this study, I found that intracellular calcium is not essential for the RRV-p14 mediated fusion reaction, but is required for the interaction of RRV-p14 with AX1, and is also required for efficient pore expansion and syncytium formation mediated by both RRV-p14 and measles virus F protein. These findings point to the existence of a common cellular response to cell membrane perturbation during virus-mediated fusion, and suggest a novel role for intracellular AX1.

In the present study, I identified AX1 as directly interacting with fusion machines to direct the expansion process. AX1 is involved in multiple cellular processes, including membrane repair, endocytosis, and actin bundling during phagocytosis (Gerke, Creutz et al. 2005, Patel, Ahmad et al. 2011). The membrane- and actin-binding activity of this protein suggests that it is an excellent canditate for playing a role during pore expansion of fused pores. It is highly likely that such a process requires a plethora of cellular signalling events leading to the reorganization of cellular architecture. Recent reports that the GTPase dynamin and PtdIns(4,5)P2 are both involved in nascent pore expansion hints at the recruitment of membrane curvature sensing and/or inducing proteins (Leikina, Melikov et al. 2013). Dynamin has also been implicated in HIV-Env entry, however, it is not known whether it is via its ability to associate with membrane-bending proteins or via regulation of actin dynamics (Miyauchi, Kim et al. 2009).

Fusion protein signalling has been reported during HIV Env-mediated virus entry (Pontow, Heyden et al. 2004). However, in this case, it is the binding of Env to its co-receptros CCR5 and CXCR4 that initiates signalling cascades controlled by these cellular membrane proteins (Pontow, Heyden et al. 2004). Some of the effectors of the Env-receptor binding signalling pathway include the mobilization of intracellular Ca^{2+} and the activation of Rac GTPase, which stimulates the formation of ruffles and lamellipodia (Harmon and Ratner 2008). Effectors of Rac include Ser/Thr kinases, lipid kinases, actin-binding proteins and adaptor scaffold molecules (Burridge and Wennerberg 2004). Specifically, two fusion-specific effectors of Rac that are responsible for actin cytoskeletal rearrangements involved in virus entry and infection have been identified; the Wave2 signalling complex and its effector Arp 2/3 as well as Abl kinase (Harmon,

Campbell et al. 2010). Interestingly, these effects are virus-receptor specific, as VSV-G and AMLV Env-mediated infection do not require these elements.

It is tempting to speculate that the endodomains of the FAST proteins are able to bypass the need for co-receptor binding and modulation of intracellular signalling by interacting with celluar proteins, such as AX1, themselves. This hypothesis is supported by the findings that the soluble endodomain of RRVp14 is able to enhance syncytium formation kinetics when co-expressed with a membrane fusogen. However, unlike the above-mentioned virus specific activation of Wave2 and Arp 2/3, the role of AX1 seems to be more conserved, as two vastly different fusogens, RRV p14 and measles F, require the presence of this effector. In addition, a recent report suggests that AX1 acts extracellularly via FPR receptors to initiate a signalling cascade leading to the migration of C2C12 myoblasts prior to fusion (Bizzarro, Fontanella et al. 2012). The lack of extracellular AX1 activity during RRV p14 fusion implies that, if motility is required, p14 alone may recruit proteins involved in actin-restructuring proteins restructuring via its interaction with the actin-bundling AX1.

AX1 associates with, and is phosphorylated by, EGFR present in late endosomes and multivesicular bodies. FRET analysis of the RRV p14-AX1 interaction reported in this study suggests that the detectable bulk of these complexes localizes to distinct intracellular puncta. It remains to be seen whether these are late endosomes or other vesicular bodies. Additionally, lack of a FRET signal at the membrane surface does not indicate that complexes are not present in this location, as we employed very stringent conditions during our analysis, which may eliminate weak signals.

5.3 Future Directions

The findings reported in the present study set the stage for a new avenue of research, not only in the field of FAST protein-mediated fusion, but also in the general area of cell-to-cell fusion directed by diverse fusogens. The discovery that AX1 directly interacts with viral fusogens poses the question of whether this is a common trend among fusion proteins or whether it is specific to the two fusion machines employed in this study. Several unexplored avenues with respect to this interaction involve the location and timing of association of RRV p14 or measles F and AX1, and whether other fusogens

access AX1 to play a role during pore expansion. In addition, we need to investigate whether other interacting partners of AX1, such as actin, EGFR, and S100A11, and the association of AX1-S100A11 tetramers with cPLA2 in endosomes, play a role during cell-to-cell fusion and generation of multinucleated syncytia. Complex formation is a common occurrence during cellular signalling events, and it is therefore highly possible that a juxtamembranous signalosome structure initiated by the fusion protein accumulates to orchestrate the resolution of fusion pores.

Another interesting avenue of investigation relates to the role of Ca^{2+} during membrane fusion and pore expansion. Currently, no concrete proof exists that cell-cell fusion is not a leaky process, as it can be masked by a rapid resealing response initiated by the influx of extracellular Ca^{2+}. It will be crucial to determine whether intracellular Ca^{2+} flux occurs during cell-cell fusion and syncytium formation, and the specific microenvironments where this event may occur. Additionally, determination of the source of Ca^{2+} signalling will prove to be informative as to the particular signalling pathways employed during syncytium formation. Another question arising from this study pertains to the differentiation between processes involved in cell-to-cell fusion mediated by cellular or virally encoded fusogens, versus virus entry into cells during infection. It is likely that the signalling pathways involved in these fusion events will vastly differ, given the disparate phenotypes resulting from each type of fusion.

5.4 Conclusion

A converging theme of the present work pertains to differentiating membrane fusion ending with stable pore formation and the expansion of these pores to generate multinucleated syncytia. The act of membrane merger is an event mediated by the fusogen, and likely proceeds via lipid mixing followed by content exchange between fusing partners. The architecture of merging lipid bilayers may include either highly structured or lipid emulsion intermediates, which resolve into intermembranous pores. At this point, the nature of the system employed becomes crucial, as lipid bilayers, liposomes, red blood cells, and viruses are vastly different from the plasma membranes and the complex array of contents and structures found in eukaryotic cells. Findings reported in this work suggest that the resolution of these intermembranous pores is a

cellular response to membrane perturbation by fusion machines. And while so little is known, many opportunities for great discoveries linking various cellular fusion events have emerged.

BIBLIOGRAPHY

Abdulreda, M. H., A. Bhalla, E. R. Chapman and V. T. Moy (2008). "Atomic force microscope spectroscopy reveals a hemifusion intermediate during soluble N-ethylmaleimide-sensitive factor-attachment protein receptors-mediated membrane fusion." Biophys J **94**(2): 648-655.

Abmayr, S. M. and G. K. Pavlath (2012). "Myoblast fusion: lessons from flies and mice." Development **139**(4): 641-656.

Aguilar, P. S., A. Engel and P. Walter (2007). "The plasma membrane proteins Prm1 and Fig1 ascertain fidelity of membrane fusion during yeast mating." Mol Biol Cell **18**(2): 547-556.

Alldridge, L. C. and C. E. Bryant (2003). "Annexin 1 regulates cell proliferation by disruption of cell morphology and inhibition of cyclin D1 expression through sustained activation of the ERK1/2 MAPK signal." Exp Cell Res **290**(1): 93-107.

Alvarez-Martinez, M. T., J. C. Mani, F. Porte, C. Faivre-Sarrailh, J. P. Liautard and J. Sri Widada (1996). "Characterization of the interaction between annexin I and profilin." Eur J Biochem **238**(3): 777-784.

Arnoys, E. J. and J. L. Wang (2007). "Dual localization: proteins in extracellular and intracellular compartments." Acta Histochem **109**(2): 89-110.

Avinoam, O., K. Fridman, C. Valansi, I. Abutbul, T. Zeev-Ben-Mordehai, U. E. Maurer, A. Sapir, D. Danino, K. Grunewald, J. M. White and B. Podbilewicz (2011). "Conserved eukaryotic fusogens can fuse viral envelopes to cells." Science **332**(6029): 589-592.

Babiychuk, E. B., K. Monastyrskaya and A. Draeger (2008). "Fluorescent annexin A1 reveals dynamics of ceramide platforms in living cells." Traffic **9**(10): 1757-1775.

Babiychuk, E. B., K. Monastyrskaya, S. Potez and A. Draeger (2009). "Intracellular Ca(2+) operates a switch between repair and lysis of streptolysin O-perforated cells." Cell Death Differ **16**(8): 1126-1134.

Babiychuk, E. B., K. Monastyrskaya, S. Potez and A. Draeger (2011). "Blebbing confers resistance against cell lysis." Cell Death Differ **18**(1): 80-89.

Barry, C. and R. Duncan (2009). "Multifaceted sequence-dependent and -independent roles for reovirus FAST protein cytoplasmic tails in fusion pore formation and syncytiogenesis." J Virol **83**(23): 12185-12195.

Bate, M. (1990). "The embryonic development of larval muscles in Drosophila." Development **110**(3): 791-804.

Bijlenga, P., J. H. Liu, E. Espinos, C. A. Haenggeli, J. Fischer-Lougheed, C. R. Bader and L. Bernheim (2000). "T-type alpha 1H Ca2+ channels are involved in Ca2+ signaling during terminal differentiation (fusion) of human myoblasts." Proc Natl Acad Sci U S A **97**(13): 7627-7632.

Bird, G. S., W. I. DeHaven, J. T. Smyth and J. W. Putney, Jr. (2008). "Methods for studying store-operated calcium entry." Methods **46**(3): 204-212.

Bizzarro, V., R. Belvedere, F. Dal Piaz, L. Parente and A. Petrella (2012). "Annexin A1 induces skeletal muscle cell migration acting through formyl peptide receptors." PLoS One **7**(10): e48246.

Bizzarro, V., B. Fontanella, A. Carratu, R. Belvedere, R. Marfella, L. Parente and A. Petrella (2012). "Annexin A1 N-terminal derived peptide Ac2-26 stimulates fibroblast migration in high glucose conditions." PLoS One **7**(9): e45639.
Bizzarro, V., B. Fontanella, S. Franceschelli, M. Pirozzi, H. Christian, L. Parente and A. Petrella (2010). "Role of Annexin A1 in mouse myoblast cell differentiation." J Cell Physiol **224**(3): 757-765.
Bizzarro, V., A. Petrella and L. Parente (2012). "Annexin A1: novel roles in skeletal muscle biology." J Cell Physiol **227**(8): 3007-3015.
Blaise, S., N. de Parseval, L. Benit and T. Heidmann (2003). "Genomewide screening for fusogenic human endogenous retrovirus envelopes identifies syncytin 2, a gene conserved on primate evolution." Proc Natl Acad Sci U S A **100**(22): 13013-13018.
Bootman, M. D. and M. J. Berridge (1995). "The elemental principles of calcium signaling." Cell **83**(5): 675-678.
Bour, B. A., M. Chakravarti, J. M. West and S. M. Abmayr (2000). "Drosophila SNS, a member of the immunoglobulin superfamily that is essential for myoblast fusion." Genes Dev **14**(12): 1498-1511.
Bouter, A., C. Gounou, R. Berat, S. Tan, B. Gallois, T. Granier, B. L. d'Estaintot, E. Poschl, B. Brachvogel and A. R. Brisson (2011). "Annexin-A5 assembled into two-dimensional arrays promotes cell membrane repair." Nat Commun **2**: 270.
Boutilier, J. and R. Duncan (2011). "The reovirus fusion-associated small transmembrane (FAST) proteins: virus-encoded cellular fusogens." Curr Top Membr **68**: 107-140.
Brown, C. W., K. B. Stephenson, S. Hanson, M. Kucharczyk, R. Duncan, J. C. Bell and B. D. Lichty (2009). "The p14 FAST protein of reptilian reovirus increases vesicular stomatitis virus neuropathogenesis." J Virol **83**(2): 552-561.
Bullough, P. A., F. M. Hughson, J. J. Skehel and D. C. Wiley (1994). "Structure of influenza haemagglutinin at the pH of membrane fusion." Nature **371**(6492): 37-43.
Burridge, K. and K. Wennerberg (2004). "Rho and Rac take center stage." Cell **116**(2): 167-179.
Carr, C. M., C. Chaudhry and P. S. Kim (1997). "Influenza hemagglutinin is spring-loaded by a metastable native conformation." Proc Natl Acad Sci U S A **94**(26): 14306-14313.
Cathomen, T., H. Y. Naim and R. Cattaneo (1998). "Measles viruses with altered envelope protein cytoplasmic tails gain cell fusion competence." J Virol **72**(2): 1224-1234.
Chen, A., E. Leikina, K. Melikov, B. Podbilewicz, M. M. Kozlov and L. V. Chernomordik (2008). "Fusion-pore expansion during syncytium formation is restricted by an actin network." J Cell Sci **121**(Pt 21): 3619-3628.
Chernomordik, L. V., V. A. Frolov, E. Leikina, P. Bronk and J. Zimmerberg (1998). "The pathway of membrane fusion catalyzed by influenza hemagglutinin: restriction of lipids, hemifusion, and lipidic fusion pore formation." J Cell Biol **140**(6): 1369-1382.
Chernomordik, L. V. and M. M. Kozlov (2003). "Protein-lipid interplay in fusion and fission of biological membranes." Annu Rev Biochem **72**: 175-207.
Chernomordik, L. V. and M. M. Kozlov (2005). "Membrane hemifusion: crossing a chasm in two leaps." Cell **123**(3): 375-382.
Chernomordik, L. V. and M. M. Kozlov (2008). "Mechanics of membrane fusion." Nat Struct Mol Biol **15**(7): 675-683.

Chernomordik, L. V., E. Leikina, V. Frolov, P. Bronk and J. Zimmerberg (1997). "An early stage of membrane fusion mediated by the low pH conformation of influenza hemagglutinin depends upon membrane lipids." J Cell Biol **136**(1): 81-93.
Chicka, M. C., E. Hui, H. Liu and E. R. Chapman (2008). "Synaptotagmin arrests the SNARE complex before triggering fast, efficient membrane fusion in response to Ca2+." Nat Struct Mol Biol **15**(8): 827-835.
Clancy, E. K., C. Barry, M. Ciechonska and R. Duncan (2010). "Different activities of the reovirus FAST proteins and influenza hemagglutinin in cell-cell fusion assays and in response to membrane curvature agents." Virology **397**(1): 119-129.
Clancy, E. K. and R. Duncan (2009). "Reovirus FAST protein transmembrane domains function in a modular, primary sequence-independent manner to mediate cell-cell membrane fusion." J Virol **83**(7): 2941-2950.
Clancy, E. K. and R. Duncan (2011). "Helix-destabilizing, beta-branched, and polar residues in the baboon reovirus p15 transmembrane domain influence the modularity of FAST proteins." J Virol **85**(10): 4707-4719.
Cohen, F. S. and G. B. Melikyan (2004). "The energetics of membrane fusion from binding, through hemifusion, pore formation, and pore enlargement." J Membr Biol **199**(1): 1-14.
Corcoran, J. A., E. K. Clancy and R. Duncan (2011). "Homomultimerization of the reovirus p14 fusion-associated small transmembrane protein during transit through the ER-Golgi complex secretory pathway." J Gen Virol **92**(Pt 1): 162-166.
Corcoran, J. A. and R. Duncan (2004). "Reptilian reovirus utilizes a small type III protein with an external myristylated amino terminus to mediate cell-cell fusion." J Virol **78**(8): 4342-4351.
Corcoran, J. A., J. Salsman, R. de Antueno, A. Touhami, M. H. Jericho, E. K. Clancy and R. Duncan (2006). "The p14 fusion-associated small transmembrane (FAST) protein effects membrane fusion from a subset of membrane microdomains." J Biol Chem **281**(42): 31778-31789.
Corcoran, J. A., R. Syvitski, D. Top, R. M. Epand, R. F. Epand, D. Jakeman and R. Duncan (2004). "Myristoylation, a protruding loop, and structural plasticity are essential features of a nonenveloped virus fusion peptide motif." J Biol Chem **279**(49): 51386-51394.
Corey, E. A. and R. M. Iorio (2007). "Mutations in the stalk of the measles virus hemagglutinin protein decrease fusion but do not interfere with virus-specific interaction with the homologous fusion protein." J Virol **81**(18): 9900-9910.
Cornely, R., C. Rentero, C. Enrich, T. Grewal and K. Gaus (2011). "Annexin A6 is an organizer of membrane microdomains to regulate receptor localization and signalling." IUBMB Life **63**(11): 1009-1017.
Creutz, C. E., C. J. Pazoles and H. B. Pollard (1978). "Identification and purification of an adrenal medullary protein (synexin) that causes calcium-dependent aggregation of isolated chromaffin granules." J Biol Chem **253**(8): 2858-2866.
Creutz, C. E., W. J. Zaks, H. C. Hamman, S. Crane, W. H. Martin, K. L. Gould, K. M. Oddie and S. J. Parsons (1987). "Identification of chromaffin granule-binding proteins. Relationship of the chromobindins to calelectrin, synhibin, and the tyrosine kinase substrates p35 and p36." J Biol Chem **262**(4): 1860-1868.

D'Acquisto, F., M. Perretti and R. J. Flower (2008). "Annexin-A1: a pivotal regulator of the innate and adaptive immune systems." Br J Pharmacol **155**(2): 152-169.
Danieli, T., S. L. Pelletier, Y. I. Henis and J. M. White (1996). "Membrane fusion mediated by the influenza virus hemagglutinin requires the concerted action of at least three hemagglutinin trimers." J Cell Biol **133**(3): 559-569.
Dargan, S. L. and I. Parker (2003). "Buffer kinetics shape the spatiotemporal patterns of IP3-evoked Ca2+ signals." J Physiol **553**(Pt 3): 775-788.
Dawe, S., J. A. Corcoran, E. K. Clancy, J. Salsman and R. Duncan (2005). "Unusual topological arrangement of structural motifs in the baboon reovirus fusion-associated small transmembrane protein." J Virol **79**(10): 6216-6226.
Dawe, S. and R. Duncan (2002). "The S4 genome segment of baboon reovirus is bicistronic and encodes a novel fusion-associated small transmembrane protein." J Virol **76**(5): 2131-2140.
de Brito, O. M. and L. Scorrano (2008). "Mitofusin 2 tethers endoplasmic reticulum to mitochondria." Nature **456**(7222): 605-610.
de Coupade, C., E. Solito and J. D. Levine (2003). "Dexamethasone enhances interaction of endogenous annexin 1 with L-selectin and triggers shedding of L-selectin in the monocytic cell line U-937." Br J Pharmacol **140**(1): 133-145.
De Meyer, S., Z. Gong, E. Depla, G. Maertens and S. H. Yap (1999). "Involvement of phosphatidylserine and non-phospholipid components of the hepatitis B virus envelope in human Annexin V binding and in HBV infection in vitro." J Hepatol **31**(5): 783-790.
Dennison, S. M., M. E. Bowen, A. T. Brunger and B. R. Lentz (2006). "Neuronal SNAREs do not trigger fusion between synthetic membranes but do promote PEG-mediated membrane fusion." Biophys J **90**(5): 1661-1675.
Dimitrov, D. S., C. C. Broder, E. A. Berger and R. Blumenthal (1993). "Calcium ions are required for cell fusion mediated by the CD4-human immunodeficiency virus type 1 envelope glycoprotein interaction." J Virol **67**(3): 1647-1652.
Dollery, S. J., C. C. Wright, D. C. Johnson and A. V. Nicola (2011). "Low-pH-dependent changes in the conformation and oligomeric state of the prefusion form of herpes simplex virus glycoprotein B are separable from fusion activity." J Virol **85**(19): 9964-9973.
Dorig, R. E., A. Marcil, A. Chopra and C. D. Richardson (1993). "The human CD46 molecule is a receptor for measles virus (Edmonston strain)." Cell **75**(2): 295-305.
Drust, D. S. and C. E. Creutz (1988). "Aggregation of chromaffin granules by calpactin at micromolar levels of calcium." Nature **331**(6151): 88-91.
Earp, L. J., S. E. Delos, H. E. Park and J. M. White (2005). "The many mechanisms of viral membrane fusion proteins." Curr Top Microbiol Immunol **285**: 25-66.
Eckert, D. M. and P. S. Kim (2001). "Mechanisms of viral membrane fusion and its inhibition." Annu Rev Biochem **70**: 777-810.
Elhamdani, A., F. Azizi and C. R. Artalejo (2006). "Double patch clamp reveals that transient fusion (kiss-and-run) is a major mechanism of secretion in calf adrenal chromaffin cells: high calcium shifts the mechanism from kiss-and-run to complete fusion." J Neurosci **26**(11): 3030-3036.
Epand, R. M. (2003). "Fusion peptides and the mechanism of viral fusion." Biochim Biophys Acta **1614**(1): 116-121.

Fernando, P., J. F. Kelly, K. Balazsi, R. S. Slack and L. A. Megeney (2002). "Caspase 3 activity is required for skeletal muscle differentiation." Proc Natl Acad Sci U S A **99**(17): 11025-11030.
Frendo, J. L., D. Olivier, V. Cheynet, J. L. Blond, O. Bouton, M. Vidaud, M. Rabreau, D. Evain-Brion and F. Mallet (2003). "Direct involvement of HERV-W Env glycoprotein in human trophoblast cell fusion and differentiation." Mol Cell Biol **23**(10): 3566-3574.
Futter, C. E., S. Felder, J. Schlessinger, A. Ullrich and C. R. Hopkins (1993). "Annexin I is phosphorylated in the multivesicular body during the processing of the epidermal growth factor receptor." J Cell Biol **120**(1): 77-83.
Galliano, M. F., C. Huet, J. Frygelius, A. Polgren, U. M. Wewer and E. Engvall (2000). "Binding of ADAM12, a marker of skeletal muscle regeneration, to the muscle-specific actin-binding protein, alpha -actinin-2, is required for myoblast fusion." J Biol Chem **275**(18): 13933-13939.
Gayraud-Morel, B., F. Chretien and S. Tajbakhsh (2009). "Skeletal muscle as a paradigm for regenerative biology and medicine." Regen Med **4**(2): 293-319.
Gell, D. A., R. P. Grant and J. P. Mackay (2012). "The detection and quantitation of protein oligomerization." Adv Exp Med Biol **747**: 19-41.
Gerke, V., C. E. Creutz and S. E. Moss (2005). "Annexins: linking Ca2+ signalling to membrane dynamics." Nat Rev Mol Cell Biol **6**(6): 449-461.
Gerke, V. and S. E. Moss (2002). "Annexins: from structure to function." Physiol Rev **82**(2): 331-371.
Gibbons, D. L., M. C. Vaney, A. Roussel, A. Vigouroux, B. Reilly, J. Lepault, M. Kielian and F. A. Rey (2004). "Conformational change and protein-protein interactions of the fusion protein of Semliki Forest virus." Nature **427**(6972): 320-325.
Gildor, B., R. Massarwa, B. Z. Shilo and E. D. Schejter (2009). "The SCAR and WASp nucleation-promoting factors act sequentially to mediate Drosophila myoblast fusion." EMBO Rep **10**(9): 1043-1050.
Glenney, J. R., Jr., B. Tack and M. A. Powell (1987). "Calpactins: two distinct Ca++-regulated phospholipid- and actin-binding proteins isolated from lung and placenta." J Cell Biol **104**(3): 503-511.
Goebeler, V., M. Poeter, D. Zeuschner, V. Gerke and U. Rescher (2008). "Annexin A8 regulates late endosome organization and function." Mol Biol Cell **19**(12): 5267-5278.
Gonnet, F., B. Bouazza, G. A. Millot, S. Ziaei, L. Garcia, G. S. Butler-Browne, V. Mouly, J. Tortajada, O. Danos and F. Svinartchouk (2008). "Proteome analysis of differentiating human myoblasts by dialysis-assisted two-dimensional gel electrophoresis (DAGE)." Proteomics **8**(2): 264-278.
Grewal, T. and C. Enrich (2009). "Annexins--modulators of EGF receptor signalling and trafficking." Cell Signal **21**(6): 847-858.
Gruenbaum-Cohen, Y., I. Harel, K. B. Umansky, E. Tzahor, S. B. Snapper, B. Z. Shilo and E. D. Schejter (2012). "The actin regulator N-WASp is required for muscle-cell fusion in mice." Proc Natl Acad Sci U S A **109**(28): 11211-11216.
Gunther-Ausborn, S., A. Praetor and T. Stegmann (1995). "Inhibition of influenza-induced membrane fusion by lysophosphatidylcholine." J Biol Chem **270**(49): 29279-29285.

Gunther-Ausborn, S. and T. Stegmann (1997). "How lysophosphatidylcholine inhibits cell-cell fusion mediated by the envelope glycoprotein of human immunodeficiency virus." Virology **235**(2): 201-208.
Guo, H., X. Sun, L. Yan, L. Shao and Q. Fang (2013). "The NS16 protein of aquareovirus-C is a fusion-associated small transmembrane (FAST) protein, and its activity can be enhanced by the nonstructural protein NS26." Virus Res **171**(1): 129-137.
Gurke, S., J. F. Barroso and H. H. Gerdes (2008). "The art of cellular communication: tunneling nanotubes bridge the divide." Histochem Cell Biol **129**(5): 539-550.
Gyorgy, B., T. G. Szabo, M. Pasztoi, Z. Pal, P. Misjak, B. Aradi, V. Laszlo, E. Pallinger, E. Pap, A. Kittel, G. Nagy, A. Falus and E. I. Buzas (2011). "Membrane vesicles, current state-of-the-art: emerging role of extracellular vesicles." Cell Mol Life Sci **68**(16): 2667-2688.
Haller, T., P. Dietl, K. Pfaller, M. Frick, N. Mair, M. Paulmichl, M. W. Hess, J. Furst and K. Maly (2001). "Fusion pore expansion is a slow, discontinuous, and Ca2+-dependent process regulating secretion from alveolar type II cells." J Cell Biol **155**(2): 279-289.
Harmon, B., N. Campbell and L. Ratner (2010). "Role of Abl kinase and the Wave2 signaling complex in HIV-1 entry at a post-hemifusion step." PLoS Pathog **6**(6): e1000956.
Harmon, B. and L. Ratner (2008). "Induction of the Galpha(q) signaling cascade by the human immunodeficiency virus envelope is required for virus entry." J Virol **82**(18): 9191-9205.
Hawke, T. J. and D. J. Garry (2001). "Myogenic satellite cells: physiology to molecular biology." J Appl Physiol **91**(2): 534-551.
Hayes, M. J., C. J. Merrifield, D. Shao, J. Ayala-Sanmartin, C. D. Schorey, T. P. Levine, J. Proust, J. Curran, M. Bailly and S. E. Moss (2004). "Annexin 2 binding to phosphatidylinositol 4,5-bisphosphate on endocytic vesicles is regulated by the stress response pathway." J Biol Chem **279**(14): 14157-14164.
Hayes, M. J., U. Rescher, V. Gerke and S. E. Moss (2004). "Annexin-actin interactions." Traffic **5**(8): 571-576.
Heiman, M. G. and P. Walter (2000). "Prm1p, a pheromone-regulated multispanning membrane protein, facilitates plasma membrane fusion during yeast mating." J Cell Biol **151**(3): 719-730.
Heldwein, E. E., H. Lou, F. C. Bender, G. H. Cohen, R. J. Eisenberg and S. C. Harrison (2006). "Crystal structure of glycoprotein B from herpes simplex virus 1." Science **313**(5784): 217-220.
Herbert, S. P., A. F. Odell, S. Ponnambalam and J. H. Walker (2007). "The confluence-dependent interaction of cytosolic phospholipase A2-alpha with annexin A1 regulates endothelial cell prostaglandin E2 generation." J Biol Chem **282**(47): 34468-34478.
Hernandez, J. M., A. Stein, E. Behrmann, D. Riedel, A. Cypionka, Z. Farsi, P. J. Walla, S. Raunser and R. Jahn (2012). "Membrane fusion intermediates via directional and full assembly of the SNARE complex." Science **336**(6088): 1581-1584.
Hirai, M., M. Arai, T. Mori, S. Y. Miyagishima, S. Kawai, K. Kita, T. Kuroiwa, O. Terenius and H. Matsuoka (2008). "Male fertility of malaria parasites is determined by GCS1, a plant-type reproduction factor." Curr Biol **18**(8): 607-613.
Hochreiter-Hufford, A. E., C. S. Lee, J. M. Kinchen, J. D. Sokolowski, S. Arandjelovic, J. A. Call, A. L. Klibanov, Z. Yan, J. W. Mandell and K. S. Ravichandran (2013).

"Phosphatidylserine receptor BAI1 and apoptotic cells as new promoters of myoblast fusion." Nature **497**(7448): 263-267.
Hsiang, C. H., T. Tunoda, Y. E. Whang, D. R. Tyson and D. K. Ornstein (2006). "The impact of altered annexin I protein levels on apoptosis and signal transduction pathways in prostate cancer cells." Prostate **66**(13): 1413-1424.
Hsu, E. C., C. Iorio, F. Sarangi, A. A. Khine and C. D. Richardson (2001). "CDw150(SLAM) is a receptor for a lymphotropic strain of measles virus and may account for the immunosuppressive properties of this virus." Virology **279**(1): 9-21.
Hu, C., M. Ahmed, T. J. Melia, T. H. Sollner, T. Mayer and J. E. Rothman (2003). "Fusion of cells by flipped SNAREs." Science **300**(5626): 1745-1749.
Huang, Q., J. Li, F. Wang, M. T. Oliver, T. Tipton, Y. Gao and S. W. Jiang (2013). "Syncytin-1 modulates placental trophoblast cell proliferation by promoting G1/S transition." Cell Signal **25**(4): 1027-1035.
Idone, V., C. Tam, J. W. Goss, D. Toomre, M. Pypaert and N. W. Andrews (2008). "Repair of injured plasma membrane by rapid Ca2+-dependent endocytosis." J Cell Biol **180**(5): 905-914.
Inoue, N., M. Ikawa, A. Isotani and M. Okabe (2005). "The immunoglobulin superfamily protein Izumo is required for sperm to fuse with eggs." Nature **434**(7030): 234-238.
Jahn, R. and H. Grubmuller (2002). "Membrane fusion." Curr Opin Cell Biol **14**(4): 488-495.
Jahn, R., T. Lang and T. C. Sudhof (2003). "Membrane fusion." Cell **112**(4): 519-533.
Jegou, A., A. Ziyyat, V. Barraud-Lange, E. Perez, J. P. Wolf, F. Pincet and C. Gourier (2011). "CD9 tetraspanin generates fusion competent sites on the egg membrane for mammalian fertilization." Proc Natl Acad Sci U S A **108**(27): 10946-10951.
Jin, H., G. P. Leser and R. A. Lamb (1994). "The influenza virus hemagglutinin cytoplasmic tail is not essential for virus assembly or infectivity." EMBO J **13**(22): 5504-5515.
John, C., P. Cover, E. Solito, J. Morris, H. Christian, R. Flower and J. Buckingham (2002). "Annexin 1-dependent actions of glucocorticoids in the anterior pituitary gland: roles of the N-terminal domain and protein kinase C." Endocrinology **143**(8): 3060-3070.
Johnson, C. P. and E. R. Chapman (2010). "Otoferlin is a calcium sensor that directly regulates SNARE-mediated membrane fusion." J Cell Biol **191**(1): 187-197.
Kaji, K., S. Oda, T. Shikano, T. Ohnuki, Y. Uematsu, J. Sakagami, N. Tada, S. Miyazaki and A. Kudo (2000). "The gamete fusion process is defective in eggs of Cd9-deficient mice." Nat Genet **24**(3): 279-282.
Kamal, A., Y. Ying and R. G. Anderson (1998). "Annexin VI-mediated loss of spectrin during coated pit budding is coupled to delivery of LDL to lysosomes." J Cell Biol **142**(4): 937-947.
Ke, F., L. B. He, C. Pei and Q. Y. Zhang (2011). "Turbot reovirus (SMReV) genome encoding a FAST protein with a non-AUG start site." BMC Genomics **12**: 323.
Kesavan, J., M. Borisovska and D. Bruns (2007). "v-SNARE actions during Ca(2+)-triggered exocytosis." Cell **131**(2): 351-363.
Khau, T., S. Y. Langenbach, M. Schuliga, T. Harris, C. N. Johnstone, R. L. Anderson and A. G. Stewart (2011). "Annexin-1 signals mitogen-stimulated breast tumor cell proliferation by activation of the formyl peptide receptors (FPRs) 1 and 2." FASEB J **25**(2): 483-496.

Kielian, M. and F. A. Rey (2006). "Virus membrane-fusion proteins: more than one way to make a hairpin." Nat Rev Microbiol **4**(1): 67-76.
Kim, S., K. Shilagardi, S. Zhang, S. N. Hong, K. L. Sens, J. Bo, G. A. Gonzalez and E. H. Chen (2007). "A critical function for the actin cytoskeleton in targeted exocytosis of prefusion vesicles during myoblast fusion." Dev Cell **12**(4): 571-586.
Kim, S. W., H. J. Rhee, J. Ko, Y. J. Kim, H. G. Kim, J. M. Yang, E. C. Choi and D. S. Na (2001). "Inhibition of cytosolic phospholipase A2 by annexin I. Specific interaction model and mapping of the interaction site." J Biol Chem **276**(19): 15712-15719.
Kislinger, T., A. O. Gramolini, Y. Pan, K. Rahman, D. H. MacLennan and A. Emili (2005). "Proteome dynamics during C2C12 myoblast differentiation." Mol Cell Proteomics **4**(7): 887-901.
Knop, M., E. Aareskjold, G. Bode and V. Gerke (2004). "Rab3D and annexin A2 play a role in regulated secretion of vWF, but not tPA, from endothelial cells." EMBO J **23**(15): 2982-2992.
Kozlovsky, Y. and M. M. Kozlov (2002). "Stalk model of membrane fusion: solution of energy crisis." Biophys J **82**(2): 882-895.
Kuhn, R. J., W. Zhang, M. G. Rossmann, S. V. Pletnev, J. Corver, E. Lenches, C. T. Jones, S. Mukhopadhyay, P. R. Chipman, E. G. Strauss, T. S. Baker and J. H. Strauss (2002). "Structure of dengue virus: implications for flavivirus organization, maturation, and fusion." Cell **108**(5): 717-725.
Kuzmin, P. I., J. Zimmerberg, Y. A. Chizmadzhev and F. S. Cohen (2001). "A quantitative model for membrane fusion based on low-energy intermediates." Proc Natl Acad Sci U S A **98**(13): 7235-7240.
Lee, K. H., D. S. Na and J. W. Kim (1999). "Calcium-dependent interaction of annexin I with annexin II and mapping of the interaction sites." FEBS Lett **442**(2-3): 143-146.
Leikina, E. and L. V. Chernomordik (2000). "Reversible merger of membranes at the early stage of influenza hemagglutinin-mediated fusion." Mol Biol Cell **11**(7): 2359-2371.
Leikina, E., K. Melikov, S. Sanyal, S. K. Verma, B. Eun, C. Gebert, K. Pfeifer, V. A. Lizunov, M. M. Kozlov and L. V. Chernomordik (2013). "Extracellular annexins and dynamin are important for sequential steps in myoblast fusion." J Cell Biol **200**(1): 109-123.
Lennon, N. J., A. Kho, B. J. Bacskai, S. L. Perlmutter, B. T. Hyman and R. H. Brown, Jr. (2003). "Dysferlin interacts with annexins A1 and A2 and mediates sarcolemmal wound-healing." J Biol Chem **278**(50): 50466-50473.
Lim, L. H. and S. Pervaiz (2007). "Annexin 1: the new face of an old molecule." FASEB J **21**(4): 968-975.
Ling, Q., A. T. Jacovina, A. Deora, M. Febbraio, R. Simantov, R. L. Silverstein, B. Hempstead, W. H. Mark and K. A. Hajjar (2004). "Annexin II regulates fibrin homeostasis and neoangiogenesis in vivo." J Clin Invest **113**(1): 38-48.
Liu, Y., R. Tewari, J. Ning, A. M. Blagborough, S. Garbom, J. Pei, N. V. Grishin, R. E. Steele, R. E. Sinden, W. J. Snell and O. Billker (2008). "The conserved plant sterility gene HAP2 functions after attachment of fusogenic membranes in Chlamydomonas and Plasmodium gametes." Genes Dev **22**(8): 1051-1068.

Ma, G., T. Greenwell-Wild, K. Lei, W. Jin, J. Swisher, N. Hardegen, C. T. Wild and S. M. Wahl (2004). "Secretory leukocyte protease inhibitor binds to annexin II, a cofactor for macrophage HIV-1 infection." J Exp Med **200**(10): 1337-1346.
Mailliard, W. S., H. T. Haigler and D. D. Schlaepfer (1996). "Calcium-dependent binding of S100C to the N-terminal domain of annexin I." J Biol Chem **271**(2): 719-725.
Malassine, A., J. L. Frendo, S. Blaise, K. Handschuh, P. Gerbaud, V. Tsatsaris, T. Heidmann and D. Evain-Brion (2008). "Human endogenous retrovirus-FRD envelope protein (syncytin 2) expression in normal and trisomy 21-affected placenta." Retrovirology **5**: 6.
Marambaud, P., U. Dreses-Werringloer and V. Vingtdeux (2009). "Calcium signaling in neurodegeneration." Mol Neurodegener **4**: 20.
Martens, S. (2010). "Role of C2 domain proteins during synaptic vesicle exocytosis." Biochem Soc Trans **38**(Pt 1): 213-216.
Martens, S., M. M. Kozlov and H. T. McMahon (2007). "How synaptotagmin promotes membrane fusion." Science **316**(5828): 1205-1208.
Martens, S. and H. T. McMahon (2008). "Mechanisms of membrane fusion: disparate players and common principles." Nat Rev Mol Cell Biol **9**(7): 543-556.
Massarwa, R., S. Carmon, B. Z. Shilo and E. D. Schejter (2007). "WIP/WASp-based actin-polymerization machinery is essential for myoblast fusion in Drosophila." Dev Cell **12**(4): 557-569.
Mathias, R. A., J. W. Lim, H. Ji and R. J. Simpson (2009). "Isolation of extracellular membranous vesicles for proteomic analysis." Methods Mol Biol **528**: 227-242.
Mayer, U. (2003). "Integrins: redundant or important players in skeletal muscle?" J Biol Chem **278**(17): 14587-14590.
Mayran, N., R. G. Parton and J. Gruenberg (2003). "Annexin II regulates multivesicular endosome biogenesis in the degradation pathway of animal cells." EMBO J **22**(13): 3242-3253.
McNeil, A. K., U. Rescher, V. Gerke and P. L. McNeil (2006). "Requirement for annexin A1 in plasma membrane repair." J Biol Chem **281**(46): 35202-35207.
McNeil, P. L. and R. A. Steinhardt (2003). "Plasma membrane disruption: repair, prevention, adaptation." Annu Rev Cell Dev Biol **19**: 697-731.
Megeath, L. J. and J. R. Fallon (1998). "Intracellular calcium regulates agrin-induced acetylcholine receptor clustering." J Neurosci **18**(2): 672-678.
Melikyan, G. B., S. A. Brener, D. C. Ok and F. S. Cohen (1997). "Inner but not outer membrane leaflets control the transition from glycosylphosphatidylinositol-anchored influenza hemagglutinin-induced hemifusion to full fusion." J Cell Biol **136**(5): 995-1005.
Melikyan, G. B., R. M. Markosyan, H. Hemmati, M. K. Delmedico, D. M. Lambert and F. S. Cohen (2000). "Evidence that the transition of HIV-1 gp41 into a six-helix bundle, not the bundle configuration, induces membrane fusion." J Cell Biol **151**(2): 413-423.
Melikyan, G. B., J. M. White and F. S. Cohen (1995). "GPI-anchored influenza hemagglutinin induces hemifusion to both red blood cell and planar bilayer membranes." J Cell Biol **131**(3): 679-691.
Mi, S., X. Lee, X. Li, G. M. Veldman, H. Finnerty, L. Racie, E. LaVallie, X. Y. Tang, P. Edouard, S. Howes, J. C. Keith, Jr. and J. M. McCoy (2000). "Syncytin is a captive

retroviral envelope protein involved in human placental morphogenesis." Nature **403**(6771): 785-789.
Miklavc, P., M. Frick, O. H. Wittekindt, T. Haller and P. Dietl (2010). "Fusion-activated Ca(2+) entry: an "active zone" of elevated Ca(2+) during the postfusion stage of lamellar body exocytosis in rat type II pneumocytes." PLoS One **5**(6): e10982.
Miklavc, P., N. Mair, O. H. Wittekindt, T. Haller, P. Dietl, E. Felder, M. Timmler and M. Frick (2011). "Fusion-activated Ca2+ entry via vesicular P2X4 receptors promotes fusion pore opening and exocytotic content release in pneumocytes." Proc Natl Acad Sci U S A **108**(35): 14503-14508.
Miyado, K., G. Yamada, S. Yamada, H. Hasuwa, Y. Nakamura, F. Ryu, K. Suzuki, K. Kosai, K. Inoue, A. Ogura, M. Okabe and E. Mekada (2000). "Requirement of CD9 on the egg plasma membrane for fertilization." Science **287**(5451): 321-324.
Miyado, K., K. Yoshida, K. Yamagata, K. Sakakibara, M. Okabe, X. Wang, K. Miyamoto, H. Akutsu, T. Kondo, Y. Takahashi, T. Ban, C. Ito, K. Toshimori, A. Nakamura, M. Ito, M. Miyado, E. Mekada and A. Umezawa (2008). "The fusing ability of sperm is bestowed by CD9-containing vesicles released from eggs in mice." Proc Natl Acad Sci U S A **105**(35): 12921-12926.
Miyauchi, K., Y. Kim, O. Latinovic, V. Morozov and G. B. Melikyan (2009). "HIV enters cells via endocytosis and dynamin-dependent fusion with endosomes." Cell **137**(3): 433-444.
Modis, Y., S. Ogata, D. Clements and S. C. Harrison (2004). "Structure of the dengue virus envelope protein after membrane fusion." Nature **427**(6972): 313-319.
Mohler, W. A., G. Shemer, J. J. del Campo, C. Valansi, E. Opoku-Serebuoh, V. Scranton, N. Assaf, J. G. White and B. Podbilewicz (2002). "The type I membrane protein EFF-1 is essential for developmental cell fusion." Dev Cell **2**(3): 355-362.
Moll, M., H. D. Klenk and A. Maisner (2002). "Importance of the cytoplasmic tails of the measles virus glycoproteins for fusogenic activity and the generation of recombinant measles viruses." J Virol **76**(14): 7174-7186.
Monastyrskaya, K., E. B. Babiychuk, A. Hostettler, U. Rescher and A. Draeger (2007). "Annexins as intracellular calcium sensors." Cell Calcium **41**(3): 207-219.
Mori, T., H. Kuroiwa, T. Higashiyama and T. Kuroiwa (2006). "GENERATIVE CELL SPECIFIC 1 is essential for angiosperm fertilization." Nat Cell Biol **8**(1): 64-71.
Mukai, A., T. Kurisaki, S. B. Sato, T. Kobayashi, G. Kondoh and N. Hashimoto (2009). "Dynamic clustering and dispersion of lipid rafts contribute to fusion competence of myogenic cells." Exp Cell Res **315**(17): 3052-3063.
Muller, E. M., N. A. Mackin, S. E. Erdman and K. W. Cunningham (2003). "Fig1p facilitates Ca2+ influx and cell fusion during mating of Saccharomyces cerevisiae." J Biol Chem **278**(40): 38461-38469.
Naim, H. Y., E. Ehler and M. A. Billeter (2000). "Measles virus matrix protein specifies apical virus release and glycoprotein sorting in epithelial cells." EMBO J **19**(14): 3576-3585.
Nolan, S., A. E. Cowan, D. E. Koppel, H. Jin and E. Grote (2006). "FUS1 regulates the opening and expansion of fusion pores between mating yeast." Mol Biol Cell **17**(5): 2439-2450.

Noyce, R. S., K. Taylor, M. Ciechonska, S. E. Collins, R. Duncan and K. L. Mossman (2011). "Membrane perturbation elicits an IRF3-dependent, interferon-independent antiviral response." J Virol **85**(20): 10926-10931.
Olmo, V. N. and E. Grote (2010). "Prm1 targeting to contact sites enhances fusion during mating in Saccharomyces cerevisiae." Eukaryot Cell **9**(10): 1538-1548.
Patel, D. M., S. F. Ahmad, D. G. Weiss, V. Gerke and S. A. Kuznetsov (2011). "Annexin A1 is a new functional linker between actin filaments and phagosomes during phagocytosis." J Cell Sci **124**(Pt 4): 578-588.
Perretti, M., S. K. Wheller, Q. Choudhury, J. D. Croxtall and R. J. Flower (1995). "Selective inhibition of neutrophil function by a peptide derived from lipocortin 1 N-terminus." Biochem Pharmacol **50**(7): 1037-1042.
Pobbati, A. V., A. Stein and D. Fasshauer (2006). "N- to C-terminal SNARE complex assembly promotes rapid membrane fusion." Science **313**(5787): 673-676.
Podbilewicz, B., E. Leikina, A. Sapir, C. Valansi, M. Suissa, G. Shemer and L. V. Chernomordik (2006). "The C. elegans developmental fusogen EFF-1 mediates homotypic fusion in heterologous cells and in vivo." Dev Cell **11**(4): 471-481.
Poeter, M., S. Radke, M. Koese, F. Hessner, A. Hegemann, A. Musiol, V. Gerke, T. Grewal and U. Rescher (2012). "Disruption of the annexin A1/S100A11 complex increases the migration and clonogenic growth by dysregulating epithelial growth factor (EGF) signaling." Biochim Biophys Acta.
Pontow, S. E., N. V. Heyden, S. Wei and L. Ratner (2004). "Actin cytoskeletal reorganizations and coreceptor-mediated activation of rac during human immunodeficiency virus-induced cell fusion." J Virol **78**(13): 7138-7147.
Potez, S., M. Luginbuhl, K. Monastyrskaya, A. Hostettler, A. Draeger and E. B. Babiychuk (2011). "Tailored protection against plasmalemmal injury by annexins with different Ca2+ sensitivities." J Biol Chem **286**(20): 17982-17991.
Qiao, H., R. T. Armstrong, G. B. Melikyan, F. S. Cohen and J. M. White (1999). "A specific point mutant at position 1 of the influenza hemagglutinin fusion peptide displays a hemifusion phenotype." Mol Biol Cell **10**(8): 2759-2769.
Racine, T. and R. Duncan (2010). "Facilitated leaky scanning and atypical ribosome shunting direct downstream translation initiation on the tricistronic S1 mRNA of avian reovirus." Nucleic Acids Res **38**(20): 7260-7272.
Racine, T., T. Hurst, C. Barry, J. Shou, F. Kibenge and R. Duncan (2009). "Aquareovirus effects syncytiogenesis by using a novel member of the FAST protein family translated from a noncanonical translation start site." J Virol **83**(11): 5951-5955.
Radke, S., J. Austermann, F. Russo-Marie, V. Gerke and U. Rescher (2004). "Specific association of annexin 1 with plasma membrane-resident and internalized EGF receptors mediated through the protein core domain." FEBS Lett **578**(1-2): 95-98.
Raff, A. B., A. W. Woodham, L. M. Raff, J. G. Skeate, L. Yan, D. M. Da Silva, M. Schelhaas and W. M. Kast (2013). "The evolving field of human papillomavirus receptor research: a review of binding and entry." J Virol **87**(11): 6062-6072.
Rai, T., A. Mosoian and M. D. Resh (2010). "Annexin 2 is not required for human immunodeficiency virus type 1 particle production but plays a cell type-dependent role in regulating infectivity." J Virol **84**(19): 9783-9792.
Rand, J. H., X. X. Wu, R. Lapinski, W. L. van Heerde, C. P. Reutelingsperger, P. P. Chen and T. L. Ortel (2004). "Detection of antibody-mediated reduction of annexin A5

anticoagulant activity in plasmas of patients with the antiphospholipid syndrome." Blood **104**(9): 2783-2790.
Raynor, C. M., J. F. Wright, D. M. Waisman and E. L. Pryzdial (1999). "Annexin II enhances cytomegalovirus binding and fusion to phospholipid membranes." Biochemistry **38**(16): 5089-5095.
Reese, C. and A. Mayer (2005). "Transition from hemifusion to pore opening is rate limiting for vacuole membrane fusion." J Cell Biol **171**(6): 981-990.
Rescher, U., N. Zobiack and V. Gerke (2000). "Intact Ca(2+)-binding sites are required for targeting of annexin 1 to endosomal membranes in living HeLa cells." J Cell Sci **113 (Pt 22)**: 3931-3938.
Rety, S., D. Osterloh, J. P. Arie, S. Tabaries, J. Seeman, F. Russo-Marie, V. Gerke and A. Lewit-Bentley (2000). "Structural basis of the Ca(2+)-dependent association between S100C (S100A11) and its target, the N-terminal part of annexin I." Structure **8**(2): 175-184.
Richard, J. P., E. Leikina and L. V. Chernomordik (2009). "Cytoskeleton reorganization in influenza hemagglutinin-initiated syncytium formation." Biochim Biophys Acta **1788**(2): 450-457.
Richard, J. P., E. Leikina, R. Langen, W. M. Henne, M. Popova, T. Balla, H. T. McMahon, M. M. Kozlov and L. V. Chernomordik (2011). "Intracellular curvature-generating proteins in cell-to-cell fusion." Biochem J **440**(2): 185-193.
Richardson, B. E., S. J. Nowak and M. K. Baylies (2008). "Myoblast fusion in fly and vertebrates: new genes, new processes and new perspectives." Traffic **9**(7): 1050-1059.
Risselada, H. J. and H. Grubmuller (2012). "How SNARE molecules mediate membrane fusion: recent insights from molecular simulations." Curr Opin Struct Biol **22**(2): 187-196.
Roche, S., S. Bressanelli, F. A. Rey and Y. Gaudin (2006). "Crystal structure of the low-pH form of the vesicular stomatitis virus glycoprotein G." Science **313**(5784): 187-191.
Rosengarth, A. and H. Luecke (2003). "A calcium-driven conformational switch of the N-terminal and core domains of annexin A1." J Mol Biol **326**(5): 1317-1325.
Rosengarth, A., J. Rosgen, H. J. Hinz and V. Gerke (2001). "Folding energetics of ligand binding proteins II. Cooperative binding of Ca2+ to annexin I." J Mol Biol **306**(4): 825-835.
Roviezzo, F., S. J. Getting, M. J. Paul-Clark, S. Yona, F. N. Gavins, M. Perretti, R. Hannon, J. D. Croxtall, J. C. Buckingham and R. J. Flower (2002). "The annexin-1 knockout mouse: what it tells us about the inflammatory response." J Physiol Pharmacol **53**(4 Pt 1): 541-553.
Ruiz-Gomez, M., N. Coutts, A. Price, M. V. Taylor and M. Bate (2000). "Drosophila dumbfounded: a myoblast attractant essential for fusion." Cell **102**(2): 189-198.
Runkler, N., E. Dietzel, M. Moll, H. D. Klenk and A. Maisner (2008). "Glycoprotein targeting signals influence the distribution of measles virus envelope proteins and virus spread in lymphocytes." J Gen Virol **89**(Pt 3): 687-696.
Russell, C. J., T. S. Jardetzky and R. A. Lamb (2001). "Membrane fusion machines of paramyxoviruses: capture of intermediates of fusion." EMBO J **20**(15): 4024-4034.
Ryzhova, E. V., R. M. Vos, A. V. Albright, A. V. Harrist, T. Harvey and F. Gonzalez-Scarano (2006). "Annexin 2: a novel human immunodeficiency virus type 1 Gag binding

protein involved in replication in monocyte-derived macrophages." J Virol **80**(6): 2694-2704.
Sakaguchi, M., H. Murata, H. Sonegawa, Y. Sakaguchi, J. Futami, M. Kitazoe, H. Yamada and N. H. Huh (2007). "Truncation of annexin A1 is a regulatory lever for linking epidermal growth factor signaling with cytosolic phospholipase A2 in normal and malignant squamous epithelial cells." J Biol Chem **282**(49): 35679-35686.
Salsman, J., D. Top, C. Barry and R. Duncan (2008). "A virus-encoded cell-cell fusion machine dependent on surrogate adhesins." PLoS Pathog **4**(3): e1000016.
Salsman, J., D. Top, J. Boutilier and R. Duncan (2005). "Extensive syncytium formation mediated by the reovirus FAST proteins triggers apoptosis-induced membrane instability." J Virol **79**(13): 8090-8100.
Sanes, J. R. (2003). "The basement membrane/basal lamina of skeletal muscle." J Biol Chem **278**(15): 12601-12604.
Sapir, A., O. Avinoam, B. Podbilewicz and L. V. Chernomordik (2008). "Viral and developmental cell fusion mechanisms: conservation and divergence." Dev Cell **14**(1): 11-21.
Sapir, A., J. Choi, E. Leikina, O. Avinoam, C. Valansi, L. V. Chernomordik, A. P. Newman and B. Podbilewicz (2007). "AFF-1, a FOS-1-regulated fusogen, mediates fusion of the anchor cell in C. elegans." Dev Cell **12**(5): 683-698.
Savina, A., M. Furlan, M. Vidal and M. I. Colombo (2003). "Exosome release is regulated by a calcium-dependent mechanism in K562 cells." J Biol Chem **278**(22): 20083-20090.
Scepek, S., J. R. Coorssen and M. Lindau (1998). "Fusion pore expansion in horse eosinophils is modulated by Ca2+ and protein kinase C via distinct mechanisms." EMBO J **17**(15): 4340-4345.
Schultz, E., D. L. Jaryszak, M. C. Gibson and D. J. Albright (1986). "Absence of exogenous satellite cell contribution to regeneration of frozen skeletal muscle." J Muscle Res Cell Motil **7**(4): 361-367.
Seemann, J., K. Weber, M. Osborn, R. G. Parton and V. Gerke (1996). "The association of annexin I with early endosomes is regulated by Ca2+ and requires an intact N-terminal domain." Mol Biol Cell **7**(9): 1359-1374.
Sens, K. L., S. Zhang, P. Jin, R. Duan, G. Zhang, F. Luo, L. Parachini and E. H. Chen (2010). "An invasive podosome-like structure promotes fusion pore formation during myoblast fusion." J Cell Biol **191**(5): 1013-1027.
Shmulevitz, M., J. Corcoran, J. Salsman and R. Duncan (2004). "Cell-cell fusion induced by the avian reovirus membrane fusion protein is regulated by protein degradation." J Virol **78**(11): 5996-6004.
Shmulevitz, M. and R. Duncan (2000). "A new class of fusion-associated small transmembrane (FAST) proteins encoded by the non-enveloped fusogenic reoviruses." EMBO J **19**(5): 902-912.
Shmulevitz, M., J. Salsman and R. Duncan (2003). "Palmitoylation, membrane-proximal basic residues, and transmembrane glycine residues in the reovirus p10 protein are essential for syncytium formation." J Virol **77**(18): 9769-9779.
Skehel, J. J. and D. C. Wiley (2000). "Receptor binding and membrane fusion in virus entry: the influenza hemagglutinin." Annu Rev Biochem **69**: 531-569.

Soe, K., T. L. Andersen, A. S. Hobolt-Pedersen, B. Bjerregaard, L. I. Larsson and J. M. Delaisse (2011). "Involvement of human endogenous retroviral syncytin-1 in human osteoclast fusion." Bone **48**(4): 837-846.
Sohn, R. L., P. Huang, G. Kawahara, M. Mitchell, J. Guyon, R. Kalluri, L. M. Kunkel and E. Gussoni (2009). "A role for nephrin, a renal protein, in vertebrate skeletal muscle cell fusion." Proc Natl Acad Sci U S A **106**(23): 9274-9279.
Solito, E., C. de Coupade, S. Canaider, N. J. Goulding and M. Perretti (2001). "Transfection of annexin 1 in monocytic cells produces a high degree of spontaneous and stimulated apoptosis associated with caspase-3 activation." Br J Pharmacol **133**(2): 217-228.
Solito, E., A. Mulla, J. F. Morris, H. C. Christian, R. J. Flower and J. C. Buckingham (2003). "Dexamethasone induces rapid serine-phosphorylation and membrane translocation of annexin 1 in a human folliculostellate cell line via a novel nongenomic mechanism involving the glucocorticoid receptor, protein kinase C, phosphatidylinositol 3-kinase, and mitogen-activated protein kinase." Endocrinology **144**(4): 1164-1174.
Sollner, T., M. K. Bennett, S. W. Whiteheart, R. H. Scheller and J. E. Rothman (1993). "A protein assembly-disassembly pathway in vitro that may correspond to sequential steps of synaptic vesicle docking, activation, and fusion." Cell **75**(3): 409-418.
Sollner, T. H. (2004). "Intracellular and viral membrane fusion: a uniting mechanism." Curr Opin Cell Biol **16**(4): 429-435.
Sprong, H., P. van der Sluijs and G. van Meer (2001). "How proteins move lipids and lipids move proteins." Nat Rev Mol Cell Biol **2**(7): 504-513.
Stiasny, K. and F. X. Heinz (2004). "Effect of membrane curvature-modifying lipids on membrane fusion by tick-borne encephalitis virus." J Virol **78**(16): 8536-8542.
Strunkelnberg, M., B. Bonengel, L. M. Moda, A. Hertenstein, H. G. de Couet, R. G. Ramos and K. F. Fischbach (2001). "rst and its paralogue kirre act redundantly during embryonic muscle development in Drosophila." Development **128**(21): 4229-4239.
Sugimoto, J., M. Sugimoto, H. Bernstein, Y. Jinno and D. Schust (2013). "A novel human endogenous retroviral protein inhibits cell-cell fusion." Sci Rep **3**: 1462.
Tamm, L. K. (2003). "Hypothesis: spring-loaded boomerang mechanism of influenza hemagglutinin-mediated membrane fusion." Biochim Biophys Acta **1614**(1): 14-23.
Tamm, L. K., J. Crane and V. Kiessling (2003). "Membrane fusion: a structural perspective on the interplay of lipids and proteins." Curr Opin Struct Biol **13**(4): 453-466.
Tannu, N. S., V. K. Rao, R. M. Chaudhary, F. Giorgianni, A. E. Saeed, Y. Gao and R. Raghow (2004). "Comparative proteomes of the proliferating C(2)C(12) myoblasts and fully differentiated myotubes reveal the complexity of the skeletal muscle differentiation program." Mol Cell Proteomics **3**(11): 1065-1082.
Tatsuo, H., N. Ono, K. Tanaka and Y. Yanagi (2000). "SLAM (CDw150) is a cellular receptor for measles virus." Nature **406**(6798): 893-897.
Tcatchoff, L., S. Andersson, A. Utskarpen, T. I. Klokk, S. S. Skanland, S. Pust, V. Gerke and K. Sandvig (2012). "Annexin A1 and A2: roles in retrograde trafficking of Shiga toxin." PLoS One **7**(7): e40429.
Thalmann, C. M., D. M. Cummins, M. Yu, R. Lunt, L. I. Pritchard, E. Hansson, S. Crameri, A. Hyatt and L. F. Wang (2010). "Broome virus, a new fusogenic Orthoreovirus species isolated from an Australian fruit bat." Virology **402**(1): 26-40.

Top, D., C. Barry, T. Racine, C. L. Ellis and R. Duncan (2009). "Enhanced fusion pore expansion mediated by the trans-acting Endodomain of the reovirus FAST proteins." PLoS Pathog **5**(3): e1000331.
Top, D., R. de Antueno, J. Salsman, J. Corcoran, J. Mader, D. Hoskin, A. Touhami, M. H. Jericho and R. Duncan (2005). "Liposome reconstitution of a minimal protein-mediated membrane fusion machine." EMBO J **24**(17): 2980-2988.
Top, D., J. A. Read, S. J. Dawe, R. T. Syvitski and R. Duncan (2012). "Cell-cell membrane fusion induced by p15 fusion-associated small transmembrane (FAST) protein requires a novel fusion peptide motif containing a myristoylated polyproline type II helix." J Biol Chem **287**(5): 3403-3414.
Uversky, V. N. (2011). "Intrinsically disordered proteins from A to Z." Int J Biochem Cell Biol **43**(8): 1090-1103.
van den Eijnde, S. M., M. J. van den Hoff, C. P. Reutelingsperger, W. L. van Heerde, M. E. Henfling, C. Vermeij-Keers, B. Schutte, M. Borgers and F. C. Ramaekers (2001). "Transient expression of phosphatidylserine at cell-cell contact areas is required for myotube formation." J Cell Sci **114**(Pt 20): 3631-3642.
Vyleta, N. P. and S. M. Smith (2011). "Spontaneous glutamate release is independent of calcium influx and tonically activated by the calcium-sensing receptor." J Neurosci **31**(12): 4593-4606.
Walther, A., K. Riehemann and V. Gerke (2000). "A novel ligand of the formyl peptide receptor: annexin I regulates neutrophil extravasation by interacting with the FPR." Mol Cell **5**(5): 831-840.
Wang, P., N. R. Chintagari, D. Gou, L. Su and L. Liu (2007). "Physical and functional interactions of SNAP-23 with annexin A2." Am J Respir Cell Mol Biol **37**(4): 467-476.
Wang, W. and C. E. Creutz (1994). "Role of the amino-terminal domain in regulating interactions of annexin I with membranes: effects of amino-terminal truncation and mutagenesis of the phosphorylation sites." Biochemistry **33**(1): 275-282.
Washington, N. L. and S. Ward (2006). "FER-1 regulates Ca2+ -mediated membrane fusion during C. elegans spermatogenesis." J Cell Sci **119**(Pt 12): 2552-2562.
Weber, T., B. V. Zemelman, J. A. McNew, B. Westermann, M. Gmachl, F. Parlati, T. H. Sollner and J. E. Rothman (1998). "SNAREpins: minimal machinery for membrane fusion." Cell **92**(6): 759-772.
White, I. J., L. M. Bailey, M. R. Aghakhani, S. E. Moss and C. E. Futter (2006). "EGF stimulates annexin 1-dependent inward vesiculation in a multivesicular endosome subpopulation." EMBO J **25**(1): 1-12.
White, J. M., S. E. Delos, M. Brecher and K. Schornberg (2008). "Structures and mechanisms of viral membrane fusion proteins: multiple variations on a common theme." Crit Rev Biochem Mol Biol **43**(3): 189-219.
Wild, T. F., E. Malvoisin and R. Buckland (1991). "Measles virus: both the haemagglutinin and fusion glycoproteins are required for fusion." J Gen Virol **72 (Pt 2)**: 439-442.
Wilson, I. A., J. J. Skehel and D. C. Wiley (1981). "Structure of the haemagglutinin membrane glycoprotein of influenza virus at 3 A resolution." Nature **289**(5796): 366-373.
Woodham, A. W., D. M. Da Silva, J. G. Skeate, A. B. Raff, M. R. Ambroso, H. E. Brand, J. M. Isas, R. Langen and W. M. Kast (2012). "The S100A10 subunit of the annexin A2

heterotetramer facilitates L2-mediated human papillomavirus infection." PLoS One **7**(8): e43519.
Worrall, D. S. and J. M. Olefsky (2002). "The effects of intracellular calcium depletion on insulin signaling in 3T3-L1 adipocytes." Mol Endocrinol **16**(2): 378-389.
Wouters, F. S., P. J. Verveer and P. I. Bastiaens (2001). "Imaging biochemistry inside cells." Trends Cell Biol **11**(5): 203-211.
Wright, J. F., A. Kurosky and S. Wasi (1994). "An endothelial cell-surface form of annexin II binds human cytomegalovirus." Biochem Biophys Res Commun **198**(3): 983-989.
Wurth, M. A., R. M. Schowalter, E. C. Smith, C. L. Moncman, R. E. Dutch and R. O. McCann (2010). "The actin cytoskeleton inhibits pore expansion during PIV5 fusion protein-promoted cell-cell fusion." Virology **404**(1): 117-126.
Xu, Y., F. Zhang, Z. Su, J. A. McNew and Y. K. Shin (2005). "Hemifusion in SNARE-mediated membrane fusion." Nat Struct Mol Biol **12**(5): 417-422.
Yang, L. and H. W. Huang (2002). "Observation of a membrane fusion intermediate structure." Science **297**(5588): 1877-1879.
Yang, S. L., Y. T. Chou, C. N. Wu and M. S. Ho (2011). "Annexin II binds to capsid protein VP1 of enterovirus 71 and enhances viral infectivity." J Virol **85**(22): 11809-11820.
Yeung, T., G. E. Gilbert, J. Shi, J. Silvius, A. Kapus and S. Grinstein (2008). "Membrane phosphatidylserine regulates surface charge and protein localization." Science **319**(5860): 210-213.
Zaitseva, E., A. Mittal, D. E. Griffin and L. V. Chernomordik (2005). "Class II fusion protein of alphaviruses drives membrane fusion through the same pathway as class I proteins." J Cell Biol **169**(1): 167-177.
Zeschnigk, M., D. Kozian, C. Kuch, M. Schmoll and A. Starzinski-Powitz (1995). "Involvement of M-cadherin in terminal differentiation of skeletal muscle cells." J Cell Sci **108 (Pt 9)**: 2973-2981.
Zimmerberg, J., R. Blumenthal, D. P. Sarkar, M. Curran and S. J. Morris (1994). "Restricted movement of lipid and aqueous dyes through pores formed by influenza hemagglutinin during cell fusion." J Cell Biol **127**(6 Pt 2): 1885-1894.
Zobiack, N., U. Rescher, S. Laarmann, S. Michgehl, M. A. Schmidt and V. Gerke (2002). "Cell-surface attachment of pedestal-forming enteropathogenic E. coli induces a clustering of raft components and a recruitment of annexin 2." J Cell Sci **115**(Pt 1): 91-98.

APPENDIX A Sample Copyright Permission Letter

NATURE PUBLISHING GROUP LICENSE TERMS AND CONDITIONS

Aug 20, 2013

This is a License Agreement between Marta Ciechonska ("You") and Nature Publishing Group ("Nature Publishing Group") provided by Copyright Clearance Center ("CCC"). The license consists of your order details, the terms and conditions provided by Nature Publishing Group, and the payment terms and conditions.

All payments must be made in full to CCC. For payment instructions, please see information listed at the bottom of this form.

License Number	3213140312312
License date	Aug 20, 2013
Licensed content publisher	Nature Publishing Group
Licensed content publication	Nature Reviews Molecular Cell Biology
Licensed content title	Annexins: linking Ca2 signalling to membrane dynamics
Licensed content author	Volker Gerke,Carl E. CreutzandStephen E. Moss
Licensed content date	Jun 1, 2005
Volume number	6
Issue number	6
Type of Use	reuse in a thesis/dissertation
Requestor type	academic/educational
Format	electronic
Portion	figures/tables/illustrations
Number of figures/tables/illustrations	1
High-res required	no
Figures	Figure 1
Author of this NPG article	no
Your reference number	None
Title of your thesis / dissertation	FAST-Mediated Pore Expansion: Novel Roles For Annexin A1 And Plasma Membrane Architecture
Expected completion date	Aug 2013
Estimated size (number of pages)	160
Total	0.00 USD
Terms and Conditions	

Terms and Conditions for Permissions

Nature Publishing Group hereby grants you a non-exclusive license to reproduce this material for this

purpose, and for no other use,subject to the conditions below:

1. NPG warrants that it has, to the best of its knowledge, the rights to license reuse of this material. However, you should ensure that the material you are requesting is original to Nature Publishing Group and does not carry the copyright of another entity (as credited in the published version). If the credit line on any part of the material you have requested indicates that it was reprinted or adapted by NPG with permission from another source, then you should also seek permission from that source to reuse the material.

2. Permission granted free of charge for material in print is also usually granted for any electronic version of that work, provided that the material is incidental to the work as a whole and that the electronic version is essentially equivalent to, or substitutes for, the print version.Where print permission has been granted for a fee, separate permission must be obtained for any additional, electronic re-use (unless, as in the case of a full paper, this has already been accounted for during your initial request in the calculation of a print run).NB: In all cases, web-based use of full-text articles must be authorized separately through the 'Use on a Web Site' option when requesting permission.

3. Permission granted for a first edition does not apply to second and subsequent editions and for editions in other languages (except for signatories to the STM Permissions Guidelines, or where the first edition permission was granted for free).

4. Nature Publishing Group's permission must be acknowledged next to the figure, table or abstract in print. In electronic form, this acknowledgement must be visible at the same time as the figure/table/abstract, and must be hyperlinked to the journal's homepage.

5. The credit line should read:
   Reprinted by permission from Macmillan Publishers Ltd: [JOURNAL NAME] (reference citation), copyright (year of publication)
   For AOP papers, the credit line should read:
   Reprinted by permission from Macmillan Publishers Ltd: [JOURNAL NAME], advance online publication, day month year (doi: 10.1038/sj.[JOURNAL ACRONYM].XXXXX)

   Note: For republication from the *British Journal of Cancer*, the following credit lines apply.
   Reprinted by permission from Macmillan Publishers Ltd on behalf of Cancer Research UK: [JOURNAL NAME] (reference citation), copyright (year of publication)For AOP papers, the credit line should read:
   Reprinted by permission from Macmillan Publishers Ltd on behalf of Cancer

Research UK: [JOURNAL NAME], advance online publication, day month year (doi: 10.1038/sj.[JOURNAL ACRONYM].XXXXX)

6. Adaptations of single figures do not require NPG approval. However, the adaptation should be credited as follows:

   Adapted by permission from Macmillan Publishers Ltd: [JOURNAL NAME] (reference citation), copyright (year of publication)

   Note: For adaptation from the *British Journal of Cancer*, the following credit line applies.
   Adapted by permission from Macmillan Publishers Ltd on behalf of Cancer Research UK: [JOURNAL NAME] (reference citation), copyright (year of publication)

7. Translations of 401 words up to a whole article require NPG approval. Please visit http://www.macmillanmedicalcommunications.com for more information.Translations of up to a 400 words do not require NPG approval. The translation should be credited as follows:

   Translated by permission from Macmillan Publishers Ltd: [JOURNAL NAME] (reference citation), copyright (year of publication).

   Note: For translation from the *British Journal of Cancer*, the following credit line applies.
   Translated by permission from Macmillan Publishers Ltd on behalf of Cancer Research UK: [JOURNAL NAME] (reference citation), copyright (year of publication)

We are certain that all parties will benefit from this agreement and wish you the best in the use of this material. Thank you.

Special Terms:

v1.1

If you would like to pay for this license now, please remit this license along with your payment made payable to "COPYRIGHT CLEARANCE CENTER" otherwise you will be invoiced within 48 hours of the license date. Payment should be in the form of a check or money order referencing your account number and this invoice number RLNK501094462.
Once you receive your invoice for this order, you may pay your invoice by credit card. Please follow instructions provided at that time.

Make Payment To:
Copyright Clearance Center
Dept 001
P.O. Box 843006
Boston, MA 02284-3006

ELSEVIER LICENSE
TERMS AND CONDITIONS

Aug 20, 2013

This is a License Agreement between Marta Ciechonska ("You") and Elsevier ("Elsevier") provided by Copyright Clearance Center ("CCC"). The license consists of your order details, the terms and conditions provided by Elsevier, and the payment terms and conditions.

All payments must be made in full to CCC. For payment instructions, please see information listed at the bottom of this form.

Supplier	Elsevier Limited The Boulevard,Langford Lane Kidlington,Oxford,OX5 1GB,UK
Registered Company Number	1982084
Customer name	Marta Ciechonska
Customer address	2579 Creighton St. Halifax, NS B3K3S3
License number	3213140488538
License date	Aug 20, 2013
Licensed content publisher	Elsevier
Licensed content publication	Virology
Licensed content title	Different activities of the reovirus FAST proteins and influenza hemagglutinin in cell–cell fusion assays and in response to membrane curvature agents
Licensed content author	Eileen K. Clancy,Chris Barry,Marta Ciechonska,Roy Duncan
Licensed content date	5 February 2010
Licensed content volume number	397
Licensed content issue number	1
Number of pages	11
Start Page	119
End Page	129
Type of Use	reuse in a thesis/dissertation
Intended publisher of new work	other
Portion	figures/tables/illustrations
Number of figures/tables/illustrations	4
Format	electronic
Are you the author of this Elsevier article?	Yes
Will you be translating?	No
Order reference number	None
Title of your thesis/dissertation	FAST-Mediated Pore Expansion: Novel Roles For Annexin A1 And Plasma Membrane Architecture

Expected completion date	Aug 2013
Estimated size (number of pages)	160
Elsevier VAT number	GB 494 6272 12
Permissions price	0.00 USD
VAT/Local Sales Tax	0.0 USD / 0.0 GBP
Total	0.00 USD

Terms and Conditions

INTRODUCTION

1. The publisher for this copyrighted material is Elsevier. By clicking "accept" in connection with completing this licensing transaction, you agree that the following terms and conditions apply to this transaction (along with the Billing and Payment terms and conditions established by Copyright Clearance Center, Inc. ("CCC"), at the time that you opened your Rightslink account and that are available at any time at http://myaccount.copyright.com).

GENERAL TERMS

2. Elsevier hereby grants you permission to reproduce the aforementioned material subject to the terms and conditions indicated.

3. Acknowledgement: If any part of the material to be used (for example, figures) has appeared in our publication with credit or acknowledgement to another source, permission must also be sought from that source. If such permission is not obtained then that material may not be included in your publication/copies. Suitable acknowledgement to the source must be made, either as a footnote or in a reference list at the end of your publication, as follows:

"Reprinted from Publication title, Vol /edition number, Author(s), Title of article / title of chapter, Pages No., Copyright (Year), with permission from Elsevier [OR APPLICABLE SOCIETY COPYRIGHT OWNER]." Also Lancet special credit - "Reprinted from The Lancet, Vol. number, Author(s), Title of article, Pages No., Copyright (Year), with permission from Elsevier."

4. Reproduction of this material is confined to the purpose and/or media for which permission is hereby given.

5. Altering/Modifying Material: Not Permitted. However figures and illustrations may be altered/adapted minimally to serve your work. Any other abbreviations, additions, deletions and/or any other alterations shall be made only with prior written authorization of Elsevier Ltd. (Please contact Elsevier at permissions@elsevier.com)

6. If the permission fee for the requested use of our material is waived in this instance, please be advised that your future requests for Elsevier materials may attract a fee.

7. Reservation of Rights: Publisher reserves all rights not specifically granted in the combination of (i) the license details provided by you and accepted in the course of this licensing transaction, (ii) these terms and conditions and (iii) CCC's Billing and Payment terms and conditions.

8. License Contingent Upon Payment: While you may exercise the rights licensed immediately upon issuance of the license at the end of the licensing process for the transaction, provided that you have disclosed complete and accurate details of your proposed use, no license is finally effective unless and until full payment is received from you (either by publisher or by CCC) as provided in CCC's Billing and Payment terms and conditions. If full payment is not received on a timely basis, then any license

preliminarily granted shall be deemed automatically revoked and shall be void as if never granted. Further, in the event that you breach any of these terms and conditions or any of CCC's Billing and Payment terms and conditions, the license is automatically revoked and shall be void as if never granted. Use of materials as described in a revoked license, as well as any use of the materials beyond the scope of an unrevoked license, may constitute copyright infringement and publisher reserves the right to take any and all action to protect its copyright in the materials.

9. Warranties: Publisher makes no representations or warranties with respect to the licensed material.

10. Indemnity: You hereby indemnify and agree to hold harmless publisher and CCC, and their respective officers, directors, employees and agents, from and against any and all claims arising out of your use of the licensed material other than as specifically authorized pursuant to this license.

11. No Transfer of License: This license is personal to you and may not be sublicensed, assigned, or transferred by you to any other person without publisher's written permission.

12. No Amendment Except in Writing: This license may not be amended except in a writing signed by both parties (or, in the case of publisher, by CCC on publisher's behalf).

13. Objection to Contrary Terms: Publisher hereby objects to any terms contained in any purchase order, acknowledgment, check endorsement or other writing prepared by you, which terms are inconsistent with these terms and conditions or CCC's Billing and Payment terms and conditions. These terms and conditions, together with CCC's Billing and Payment terms and conditions (which are incorporated herein), comprise the entire agreement between you and publisher (and CCC) concerning this licensing transaction. In the event of any conflict between your obligations established by these terms and conditions and those established by CCC's Billing and Payment terms and conditions, these terms and conditions shall control.

14. Revocation: Elsevier or Copyright Clearance Center may deny the permissions described in this License at their sole discretion, for any reason or no reason, with a full refund payable to you. Notice of such denial will be made using the contact information provided by you. Failure to receive such notice will not alter or invalidate the denial. In no event will Elsevier or Copyright Clearance Center be responsible or liable for any costs, expenses or damage incurred by you as a result of a denial of your permission request, other than a refund of the amount(s) paid by you to Elsevier and/or Copyright Clearance Center for denied permissions.

LIMITED LICENSE

The following terms and conditions apply only to specific license types:

15. **Translation**: This permission is granted for non-exclusive world **English** rights only unless your license was granted for translation rights. If you licensed translation rights you may only translate this content into the languages you requested. A professional translator must perform all translations and reproduce the content word for word preserving the integrity of the article. If this license is to re-use 1 or 2 figures then permission is granted for non-exclusive world rights in all languages.

16. **Website**: The following terms and conditions apply to electronic reserve and author websites:
Electronic reserve: If licensed material is to be posted to website, the web site is to be password-protected and made available only to bona fide students registered on a relevant course if:
This license was made in connection with a course,
This permission is granted for 1 year only. You may obtain a license for future website posting,
All content posted to the web site must maintain the copyright information line on the bottom of each image,

A hyper-text must be included to the Homepage of the journal from which you are licensing at http://www.sciencedirect.com/science/journal/xxxxx or the Elsevier homepage for books at http://www.elsevier.com , and
Central Storage: This license does not include permission for a scanned version of the material to be stored in a central repository such as that provided by Heron/XanEdu.

17. **Author website** for journals with the following additional clauses:

All content posted to the web site must maintain the copyright information line on the bottom of each image, and the permission granted is limited to the personal version of your paper. You are not allowed to download and post the published electronic version of your article (whether PDF or HTML, proof or final version), nor may you scan the printed edition to create an electronic version. A hyper-text must be included to the Homepage of the journal from which you are licensing at http://www.sciencedirect.com/science/journal/xxxxx . As part of our normal production process, you will receive an e-mail notice when your article appears on Elsevier's online service ScienceDirect (www.sciencedirect.com). That e-mail will include the article's Digital Object Identifier (DOI). This number provides the electronic link to the published article and should be included in the posting of your personal version. We ask that you wait until you receive this e-mail and have the DOI to do any posting.

Central Storage: This license does not include permission for a scanned version of the material to be stored in a central repository such as that provided by Heron/XanEdu.

18. **Author website** for books with the following additional clauses:
Authors are permitted to place a brief summary of their work online only.
A hyper-text must be included to the Elsevier homepage at http://www.elsevier.com . All content posted to the web site must maintain the copyright information line on the bottom of each image. You are not allowed to download and post the published electronic version of your chapter, nor may you scan the printed edition to create an electronic version.

Central Storage: This license does not include permission for a scanned version of the material to be stored in a central repository such as that provided by Heron/XanEdu.

19. **Website** (regular and for author): A hyper-text must be included to the Homepage of the journal from which you are licensing at http://www.sciencedirect.com/science/journal/xxxxx. or for books to the Elsevier homepage at http://www.elsevier.com

20. **Thesis/Dissertation**: If your license is for use in a thesis/dissertation your thesis may be submitted to your institution in either print or electronic form. Should your thesis be published commercially, please reapply for permission. These requirements include permission for the Library and Archives of Canada to supply single copies, on demand, of the complete thesis and include permission for UMI to supply single copies, on demand, of the complete thesis. Should your thesis be published commercially, please reapply for permission.

21. **Other Conditions**:

v1.6

If you would like to pay for this license now, please remit this license along with your payment made payable to "COPYRIGHT CLEARANCE CENTER" otherwise you will be invoiced within 48 hours of the license date. Payment should be in the form of a check or money order referencing your account number and this invoice number RLNK501094465.
Once you receive your invoice for this order, you may pay your invoice by credit card. Please follow

instructions provided at that time.

Make Payment To:
Copyright Clearance Center
Dept 001
P.O. Box 843006
Boston, MA 02284-3006

For suggestions or comments regarding this order, contact RightsLink Customer Support: customercare@copyright.com or +1-877-622-5543 (toll free in the US) or +1-978-646-2777.

Gratis licenses (referencing $0 in the Total field) are free. Please retain this printable license for your reference. No payment is required.

NATURE PUBLISHING GROUP LICENSE TERMS AND CONDITIONS

Aug 20, 2013

This is a License Agreement between Marta Ciechonska ("You") and Nature Publishing Group ("Nature Publishing Group") provided by Copyright Clearance Center ("CCC"). The license consists of your order details, the terms and conditions provided by Nature Publishing Group, and the payment terms and conditions.

All payments must be made in full to CCC. For payment instructions, please see information listed at the bottom of this form.

License Number	3213140046341
License date	Aug 20, 2013
Licensed content publisher	Nature Publishing Group
Licensed content publication	Nature Structural and Molecular Biology
Licensed content title	Mechanics of membrane fusion
Licensed content author	Leonid V Chernomordik and Michael M Kozlov
Licensed content date	Jul 3, 2008
Volume number	15
Issue number	7
Type of Use	reuse in a thesis/dissertation
Requestor type	academic/educational
Format	electronic
Portion	figures/tables/illustrations
Number of figures/tables/illustrations	1
High-res required	no
Figures	Figure 1
Author of this NPG article	no
Your reference number	None
Title of your thesis / dissertation	FAST-Mediated Pore Expansion: Novel Roles For Annexin A1 And Plasma Membrane Architecture
Expected completion date	Aug 2013
Estimated size (number of pages)	160
Total	0.00 USD

Terms and Conditions

Terms and Conditions for Permissions

Nature Publishing Group hereby grants you a non-exclusive license to reproduce this material for this purpose, and for no other use,subject to the conditions below:

1. NPG warrants that it has, to the best of its knowledge, the rights to license reuse of this material. However, you should ensure that the material you are requesting is original to Nature Publishing Group and does not carry the copyright of

another entity (as credited in the published version). If the credit line on any part of the material you have requested indicates that it was reprinted or adapted by NPG with permission from another source, then you should also seek permission from that source to reuse the material.

2. Permission granted free of charge for material in print is also usually granted for any electronic version of that work, provided that the material is incidental to the work as a whole and that the electronic version is essentially equivalent to, or substitutes for, the print version.Where print permission has been granted for a fee, separate permission must be obtained for any additional, electronic re-use (unless, as in the case of a full paper, this has already been accounted for during your initial request in the calculation of a print run).NB: In all cases, web-based use of full-text articles must be authorized separately through the 'Use on a Web Site' option when requesting permission.

3. Permission granted for a first edition does not apply to second and subsequent editions and for editions in other languages (except for signatories to the STM Permissions Guidelines, or where the first edition permission was granted for free).

4. Nature Publishing Group's permission must be acknowledged next to the figure, table or abstract in print. In electronic form, this acknowledgement must be visible at the same time as the figure/table/abstract, and must be hyperlinked to the journal's homepage.

5. The credit line should read:
   Reprinted by permission from Macmillan Publishers Ltd: [JOURNAL NAME] (reference citation), copyright (year of publication)
   For AOP papers, the credit line should read:
   Reprinted by permission from Macmillan Publishers Ltd: [JOURNAL NAME], advance online publication, day month year (doi: 10.1038/sj.[JOURNAL ACRONYM].XXXXX)

   Note: For republication from the *British Journal of Cancer,* the following credit lines apply.
   Reprinted by permission from Macmillan Publishers Ltd on behalf of Cancer Research UK: [JOURNAL NAME] (reference citation), copyright (year of publication)For AOP papers, the credit line should read:
   Reprinted by permission from Macmillan Publishers Ltd on behalf of Cancer Research UK: [JOURNAL NAME], advance online publication, day month year (doi: 10.1038/sj.[JOURNAL ACRONYM].XXXXX)

6. Adaptations of single figures do not require NPG approval. However, the

adaptation should be credited as follows:

Adapted by permission from Macmillan Publishers Ltd: [JOURNAL NAME] (reference citation), copyright (year of publication)

Note: For adaptation from the *British Journal of Cancer*, the following credit line applies.
Adapted by permission from Macmillan Publishers Ltd on behalf of Cancer Research UK: [JOURNAL NAME] (reference citation), copyright (year of publication)

7. Translations of 401 words up to a whole article require NPG approval. Please visit http://www.macmillanmedicalcommunications.com for more information.Translations of up to a 400 words do not require NPG approval. The translation should be credited as follows:

   Translated by permission from Macmillan Publishers Ltd: [JOURNAL NAME] (reference citation), copyright (year of publication).

   Note: For translation from the *British Journal of Cancer*, the following credit line applies.
   Translated by permission from Macmillan Publishers Ltd on behalf of Cancer Research UK: [JOURNAL NAME] (reference citation), copyright (year of publication)

We are certain that all parties will benefit from this agreement and wish you the best in the use of this material. Thank you.

Special Terms:

v1.1

If you would like to pay for this license now, please remit this license along with your payment made payable to "COPYRIGHT CLEARANCE CENTER" otherwise you will be invoiced within 48 hours of the license date. Payment should be in the form of a check or money order referencing your account number and this invoice number RLNK501094458.
Once you receive your invoice for this order, you may pay your invoice by credit card. Please follow instructions provided at that time.

Make Payment To:
Copyright Clearance Center
Dept 001
P.O. Box 843006
Boston, MA 02284-3006

For suggestions or comments regarding this order, contact RightsLink Customer Support: customercare@copyright.com or +1-877-622-5543 (toll free in the US) or +1-978-646-2777.

Gratis licenses (referencing $0 in the Total field) are free. Please retain this printable license for your reference. No payment is required.

ELSEVIER LICENSE
TERMS AND CONDITIONS

Aug 20, 2013

This is a License Agreement between Marta Ciechonska ("You") and Elsevier ("Elsevier") provided by Copyright Clearance Center ("CCC"). The license consists of your order details, the terms and conditions provided by Elsevier, and the payment terms and conditions.

All payments must be made in full to CCC. For payment instructions, please see information listed at the bottom of this form.

Supplier	Elsevier Limited The Boulevard,Langford Lane Kidlington,Oxford,OX5 1GB,UK
Registered Company Number	1982084
Customer name	Marta Ciechonska
Customer address	2579 Creighton St. Halifax, NS B3K3S3
License number	3213131039816
License date	Aug 20, 2013
Licensed content publisher	Elsevier
Licensed content publication	Developmental Cell
Licensed content title	Viral and Developmental Cell Fusion Mechanisms: Conservation and Divergence
Licensed content author	Amir Sapir,Ori Avinoam,Benjamin Podbilewicz,Leonid V. Chernomordik
Licensed content date	January 2008
Licensed content volume number	14
Licensed content issue number	1
Number of pages	11
Start Page	11
End Page	21
Type of Use	reuse in a thesis/dissertation
Portion	figures/tables/illustrations
Number of figures/tables/illustrations	1
Format	electronic
Are you the author of this Elsevier article?	No
Will you be translating?	No
Order reference number	None
Title of your thesis/dissertation	FAST-Mediated Pore Expansion: Novel Roles For Annexin A1 And Plasma Membrane Architecture
Expected completion date	Aug 2013
Estimated size (number of pages)	160

Elsevier VAT number	GB 494 6272 12
Permissions price	0.00 USD
VAT/Local Sales Tax	0.0 USD / 0.0 GBP
Total	0.00 USD

Terms and Conditions

INTRODUCTION

1. The publisher for this copyrighted material is Elsevier. By clicking "accept" in connection with completing this licensing transaction, you agree that the following terms and conditions apply to this transaction (along with the Billing and Payment terms and conditions established by Copyright Clearance Center, Inc. ("CCC"), at the time that you opened your Rightslink account and that are available at any time at http://myaccount.copyright.com).

GENERAL TERMS

2. Elsevier hereby grants you permission to reproduce the aforementioned material subject to the terms and conditions indicated.

3. Acknowledgement: If any part of the material to be used (for example, figures) has appeared in our publication with credit or acknowledgement to another source, permission must also be sought from that source. If such permission is not obtained then that material may not be included in your publication/copies. Suitable acknowledgement to the source must be made, either as a footnote or in a reference list at the end of your publication, as follows:

"Reprinted from Publication title, Vol /edition number, Author(s), Title of article / title of chapter, Pages No., Copyright (Year), with permission from Elsevier [OR APPLICABLE SOCIETY COPYRIGHT OWNER]." Also Lancet special credit - "Reprinted from The Lancet, Vol. number, Author(s), Title of article, Pages No., Copyright (Year), with permission from Elsevier."

4. Reproduction of this material is confined to the purpose and/or media for which permission is hereby given.

5. Altering/Modifying Material: Not Permitted. However figures and illustrations may be altered/adapted minimally to serve your work. Any other abbreviations, additions, deletions and/or any other alterations shall be made only with prior written authorization of Elsevier Ltd. (Please contact Elsevier at permissions@elsevier.com)

6. If the permission fee for the requested use of our material is waived in this instance, please be advised that your future requests for Elsevier materials may attract a fee.

7. Reservation of Rights: Publisher reserves all rights not specifically granted in the combination of (i) the license details provided by you and accepted in the course of this licensing transaction, (ii) these terms and conditions and (iii) CCC's Billing and Payment terms and conditions.

8. License Contingent Upon Payment: While you may exercise the rights licensed immediately upon issuance of the license at the end of the licensing process for the transaction, provided that you have disclosed complete and accurate details of your proposed use, no license is finally effective unless and until full payment is received from you (either by publisher or by CCC) as provided in CCC's Billing and Payment terms and conditions. If full payment is not received on a timely basis, then any license preliminarily granted shall be deemed automatically revoked and shall be void as if never granted. Further, in the event that you breach any of these terms and conditions or any of CCC's Billing and Payment terms and conditions, the license is automatically revoked and shall be void as if never

granted. Use of materials as described in a revoked license, as well as any use of the materials beyond the scope of an unrevoked license, may constitute copyright infringement and publisher reserves the right to take any and all action to protect its copyright in the materials.

9. Warranties: Publisher makes no representations or warranties with respect to the licensed material.

10. Indemnity: You hereby indemnify and agree to hold harmless publisher and CCC, and their respective officers, directors, employees and agents, from and against any and all claims arising out of your use of the licensed material other than as specifically authorized pursuant to this license.

11. No Transfer of License: This license is personal to you and may not be sublicensed, assigned, or transferred by you to any other person without publisher's written permission.

12. No Amendment Except in Writing: This license may not be amended except in a writing signed by both parties (or, in the case of publisher, by CCC on publisher's behalf).

13. Objection to Contrary Terms: Publisher hereby objects to any terms contained in any purchase order, acknowledgment, check endorsement or other writing prepared by you, which terms are inconsistent with these terms and conditions or CCC's Billing and Payment terms and conditions. These terms and conditions, together with CCC's Billing and Payment terms and conditions (which are incorporated herein), comprise the entire agreement between you and publisher (and CCC) concerning this licensing transaction. In the event of any conflict between your obligations established by these terms and conditions and those established by CCC's Billing and Payment terms and conditions, these terms and conditions shall control.

14. Revocation: Elsevier or Copyright Clearance Center may deny the permissions described in this License at their sole discretion, for any reason or no reason, with a full refund payable to you. Notice of such denial will be made using the contact information provided by you. Failure to receive such notice will not alter or invalidate the denial. In no event will Elsevier or Copyright Clearance Center be responsible or liable for any costs, expenses or damage incurred by you as a result of a denial of your permission request, other than a refund of the amount(s) paid by you to Elsevier and/or Copyright Clearance Center for denied permissions.

LIMITED LICENSE

The following terms and conditions apply only to specific license types:

15. **Translation**: This permission is granted for non-exclusive world **English** rights only unless your license was granted for translation rights. If you licensed translation rights you may only translate this content into the languages you requested. A professional translator must perform all translations and reproduce the content word for word preserving the integrity of the article. If this license is to re-use 1 or 2 figures then permission is granted for non-exclusive world rights in all languages.

16. **Website**: The following terms and conditions apply to electronic reserve and author websites:
Electronic reserve: If licensed material is to be posted to website, the web site is to be password-protected and made available only to bona fide students registered on a relevant course if:
This license was made in connection with a course,
This permission is granted for 1 year only. You may obtain a license for future website posting,
All content posted to the web site must maintain the copyright information line on the bottom of each image,
A hyper-text must be included to the Homepage of the journal from which you are licensing at http://www.sciencedirect.com/science/journal/xxxxx or the Elsevier homepage for books at http://www.elsevier.com , and

Central Storage: This license does not include permission for a scanned version of the material to be stored in a central repository such as that provided by Heron/XanEdu.

17. **Author website** for journals with the following additional clauses:

All content posted to the web site must maintain the copyright information line on the bottom of each image, and the permission granted is limited to the personal version of your paper. You are not allowed to download and post the published electronic version of your article (whether PDF or HTML, proof or final version), nor may you scan the printed edition to create an electronic version. A hyper-text must be included to the Homepage of the journal from which you are licensing at http://www.sciencedirect.com/science/journal/xxxxx . As part of our normal production process, you will receive an e-mail notice when your article appears on Elsevier's online service ScienceDirect (www.sciencedirect.com). That e-mail will include the article's Digital Object Identifier (DOI). This number provides the electronic link to the published article and should be included in the posting of your personal version. We ask that you wait until you receive this e-mail and have the DOI to do any posting.

Central Storage: This license does not include permission for a scanned version of the material to be stored in a central repository such as that provided by Heron/XanEdu.

18. **Author website** for books with the following additional clauses:
Authors are permitted to place a brief summary of their work online only.
A hyper-text must be included to the Elsevier homepage at http://www.elsevier.com . All content posted to the web site must maintain the copyright information line on the bottom of each image. You are not allowed to download and post the published electronic version of your chapter, nor may you scan the printed edition to create an electronic version.

Central Storage: This license does not include permission for a scanned version of the material to be stored in a central repository such as that provided by Heron/XanEdu.

19. **Website** (regular and for author): A hyper-text must be included to the Homepage of the journal from which you are licensing at http://www.sciencedirect.com/science/journal/xxxxx. or for books to the Elsevier homepage at http://www.elsevier.com

20. **Thesis/Dissertation**: If your license is for use in a thesis/dissertation your thesis may be submitted to your institution in either print or electronic form. Should your thesis be published commercially, please reapply for permission. These requirements include permission for the Library and Archives of Canada to supply single copies, on demand, of the complete thesis and include permission for UMI to supply single copies, on demand, of the complete thesis. Should your thesis be published commercially, please reapply for permission.

21. **Other Conditions**:

v1.6

If you would like to pay for this license now, please remit this license along with your payment made payable to "COPYRIGHT CLEARANCE CENTER" otherwise you will be invoiced within 48 hours of the license date. Payment should be in the form of a check or money order referencing your account number and this invoice number RLNK501094449.
Once you receive your invoice for this order, you may pay your invoice by credit card. Please follow instructions provided at that time.

Make Payment To: